Structural relaxation and electrical conduction in PdVSi metallic glasses

Hygate, Graham

Award date:
1988

Awarding institution:
University of Bath

STRUCTURAL RELAXATION AND ELECTRICAL CONDUCTION

IN PdVSi METALLIC GLASSES

submitted by Graham Hygate

for the degree of PhD

of the University of Bath

1988

ProQuest LLC
789 East Eisenhower Parkway
P.O. Box 1346
Ann Arbor, MI 48106-1346

COPY A
Vol 1

People and Places

This work would not have been begun, and could not have been completed, without the forethought, imagination and encouragement of Dr. Mike Gibbs, my supervisor, whom it is a pleasure for me to thank. The metallic glass ribbons were kindly supplied by Dr. H.A. Davies of the University of Sheffield. This research was funded by the Science and Engineering Research Council, who also provided funds allowing me to present some of it at an international conference. Discussions with many members of Bath University physics department have been very useful, especially some in my first year with Dr. David Bird. Miss Tracy Marshall has eased the job of writing this thesis by taking good care of the typing. This work is my own apart from the frontispiece, by Ms. Jenny Williamson.

Parts of this work have been presented at the following conferences and in the following papers:

Institute of Physics Solid State Conference, Southampton, December 1984

Informal Rapid Solidification Conference, Oxford, July 1985

Informal Rapid Solidification Conference, Surrey, September 1986

International Conference on Metallic and Semiconducting Glasses, Hyderabad (India), December 1986

Institute of Physics Solid State Conference, Bristol, December 1987

M.R.J. Gibbs and G. Hygate (1986) J. Phys. F 16, 809

G. Hygate and M.R.J. Gibbs (1987) J. Phys. F 17, 815

G. Hygate and M.R.J. Gibbs (1987) Key Engineering Materials 13-15, 187

ABSTRACT

The nature of structural relaxation in metallic glasses has been investigated by studying experimentally the effects of reversible and irreversible relaxation on the electrical resistance of the $Pd_{82-x}V_xSi_{18}$ glasses (x = 0, 1, 2), by comparing these effects with the effects of hydrostatic pressure and changes in temperature, by analysing the kinetics of the changes observed and by reviewing the many relevant results in the literature.

A novel experimental technique is described; this allows spot-welded contacts to be made to a length of ribbon without heating the part under test.

A much-simplified form of the extended Ziman theory of conduction in amorphous metals, used in the literature to relate structural change to changes in resistance, has been shown to be inapplicable to the PdVSi glasses. The results of structural relaxation experiments alone show that different electron scattering mechanisms dominate at low temperature and at high temperatures in some metallic glasses. Densification is an important component of irreversible structural relaxation in the PdVSi glasses. This is shown by comparing the effects of compression and structural relaxation. The pressure coefficient of resistance of $Pd_{82}Si_{18}$ is reduced significantly by irreversible structural relaxation.

The AES model of the kinetics of structural relaxation has been developed in two new directions. Firstly, the chemical rate theory of Eyring has been applied to the activated state involved in AES, producing a correction in the attempt frequency. Secondly, a serious limitation in the mathematical basis of AES has been removed, unifying the model's treatment of reversible and irreversible changes. In addition to these two developments, a method of correcting for the inevitably non-isothermal nature of the initial period of each anneal has been introduced. A test of the model's consistency has been devised; it passes the test when applied to the irreversible structural relaxation of $Pd_{82}Si_{18}$.

CONTENTS

1. INTRODUCTION

Chapter 1 Introduction

A metallic glass is an alloy in a metastable, amorphous state. The only stable states of a metallic glass (or 'amorphous alloy' - the terms are used interchangeably) are its crystalline phases but the glass itself exists in one of a range of more or less stable phases, according to the conditions prevalent during production and the thermal and mechanical history of the glass since production. Thermal treatments, at temperatures well below the crystallisation temperature of the metallic glass but high enough to mobilise its constituent atoms significantly, cause changes in the atomic structure which give rise to corresponding changes in physical properties of the metallic glass and in its neutron and x-ray diffraction patterns. Such treatments are known as annealing treatments and the rearrangements they cause are collectively termed 'structural relaxation'.

Structural relaxation is a different phenomenon from crystallisation, and cannot be explained as the first step towards reversion to the crystalline phase. Direct evidence for this assertion is provided by resistometric data presented in this thesis: in amorphous $Pd_{80}V_2Si_{18}$, crystallisation in its earliest stages causes a decrease in electrical resistance (figure 3.4.1) but structural relaxation causes a small monotonic increase in resistance (figure 3.4.2).

The nature of structural relaxation has been the subject of many recent investigations, both experimental and theoretical. This thesis describes a study of the effects of structural relaxation on the electrical properties of metallic glasses, with special attention being paid to the set with compositions $Pd_{82-x}Y_xSi_{18}$, x = 0, 1, 2.

1.1 Local Order in Metallic Glasses

The structure of a metallic glass owes its metastability to the method of production. The ribbons used in the experiments described here were produced by rapid solidification of the molten alloy. This is a popular method of producing metallic glasses commercially. The melt is forced, in an inert atmosphere, onto a spinning metal disc which conducts heat away from it rapidly, causing solidification at a cooling rate of order 10^6K/s. Some of the randomness of the liquid state is frozen-in to the atomic structure of the solid ribbon formed; more specifically, there is no long-range order in the metallic glass ribbon. X-ray diffraction experiments find diffuse peaks in the structure factor, in contrast to the sharp Bragg peaks characteristic of crystalline metals. These diffuse peaks are evidence of local order; the immediate surroundings of each atom resemble to some degree the surroundings of a similar atom in the corresponding crystalline phase, but at increasing

separations correlations between the exact positions of atoms disappear.

The nature and extent of this local ordering in metallic glasses, and in particular in transition metal-metalloid (TM) compositions such as $Pd_{82}Si_{18}$, has been the subject of several theoretical models. The successes and failures of some of these models in attempting to explain the experimentally determined partial distribution functions of a variety of TM glasses have been summarised by Gaskell (1987). The metalloid atoms tend to be surrounded by a cage of transition metal atoms, probably with the symmetry of a distorted trigonal prism, and are rarely one another's nearest neighbours. These cage. units are not randomly arranged, however; there is more medium-range order than would be implied by a random arrangement of such units. Gaskell reports that the notion of extensive medium range order involving interconnected trigonal prisms can be used to model experimental results with some success.

Such a description of local order necessarily comprises both topological and compositional elements. The tendency, mentioned above, for metalloid atoms to be surrounded by transition metal nearest neighbour atoms rather than by other metalloids is an example of compositional (or chemical) short range order. The geometrical structure of the distorted trigonal prism with a single atom at its centre, in contrast, can be

described without reference to the composition of its constituent atoms; this is a description of topological short range order. Changes in local compositional order will be referred to in this study as chemical short range (dis-)ordering (CSRO); changes in the geometrical arrangement of the mean positions of the atoms, without reference to their chemical identity, will be called topological short range (dis-)ordering (TSRO).

An example of the theoretical distinction between CSRO and TSRO is provided by the free volume model of structural relaxation (van den Beukel and Radelaar 1983), which will be described in detail in chapter 7. In this model, in its original form, it is proposed that any annealing of a newly-spun metallic glass causes densification, a form of TSRO. The metallic glass densifies, and continues to densify, whatever the annealing temperature. In addition to TSRO, there will be CSRO, which can be regarded as taking place without changing the density significantly. The rate and the direction of CSRO will depend strongly on the annealing temperature, according to van den Beukel and Radelaar.

It must be borne in mind though that the distinction between CSRO and TSRO is macroscopic, and has no analogue in microscopic terms. The migration of a single atom from one mean position to another, considered independently of any simultaneous migrations by other atoms close to it, necessarily causes changes both in

chemical order and in topological order. A macroscopic change, however, is the sum of many such small migratory steps. Densification, for example, is the collective effect of migrations towards the centre of the piece of metallic glass by all the atoms.

1.2 Monitoring Structural Relaxation

The ideal apparatus for studying structural relaxation would somehow allow us to follow the movements of individual atoms within the metallic glass during an anneal. No such apparatus exists, however, and we are restricted primarily by the limited resolution of instruments, but ultimately by quantum mechanical uncertainty, to studying the effects of structural relaxation on bulk properties of the metallic glass.

These bulk effects can be divided into two types: irreversible changes and changes which can be reversed by a careful choice of annealing programme. One theme of this thesis is the distinctness of reversible and irreversible structural changes. A sample of metallic glass which has not been annealed since production is said to be in the 'as-received' state (a more accurate term than the loosely synonymous 'as-quenched', because any period of storage at room temperature must be considered as a very cool, but not necessarily negligible, annealing treatment). Irreversible structural changes manifest themselves most clearly when

an as-received metallic glass is annealed isothermally. A proportion of the disorder frozen-in to the structure during production is annealed out, leaving the annealed glass locally better-ordered. When this irreversible property change is complete, by which it is meant that its rate has become undetectably low, further annealing of the stabilised glass at different annealing temperatures may produce further reversible property changes indicative of a long-term temperature dependence of the degree of local order. Whether or not a reversible change will be seen depends on the composition of the metallic glass and the physical property being measured. Some physical properties have not been observed to change reversibly: these are (Huizer 1987) the heights of the peaks in the atomic radial distribution function, the internal friction, the viscosity, the self-diffusivity and arguably (see the second paragraph of chapter 7) the density.

What microscopic rearrangements underlie these reversible and irreversible property changes? This question is central to the research described in this thesis; it has been approached here by paying particular attention to the effects of reversible and irreversible structural relaxation on electrical conduction in metallic glasses. Because the theory of electron transport in amorphous metals is poorly understood compared with the corresponding theory of crystalline metals, it is not a straightforward matter to identify structural changes

from measurements of the corresponding changes in electrical properties.

The arguments presented here are therefore of two sorts. One approach has been to gather, from the literature and by experiment, results showing how the electrical resistance is affected by structural relaxation, and hence to attempt to identify the microscopic changes occurring. The link between the observations and their cause is provided by theories of conduction in amorphous metals and by comparing the observations with results of experiments in which structural change has been brought about in a more predictable manner, especially by compression and by changing the temperature quickly, avoiding structural relaxation. Arguments of this type are to be found in chapters 3-6 of this thesis.

The second approach is the reverse of the first, in the sense that it begins with the causes of structural relaxation and attempts to predict its effects. Models of the kinetics of structural relaxation and the temperature-dependence of the structural state attained after a long isothermal anneal are reviewed in chapter 7. These models are based on thermodynamic arguments and theories of diffusive and fluid movement of atoms in solids. One of these models is developed further in chapter 8 and applied in its extended form to experimental results in chapter 9. It is assumed, in this second sort of argument, that the kinetics of the

change in some structural parameter in the model will be reflected in the kinetics of the isothermal property change observed experimentally. The implicit assumption therefore is that the relation between physical property and structural parameter is close to proportionality. The two approaches described therefore complement each other; the latter deals with the causes of microscopic change, while the former attempts to relate microscopic change to observable change in macroscopic physical quantities.

It is hoped that, by contributing something to each line of argument, this work will have helped advance the study of structural relaxation towards a point where these two approaches no longer have to be considered as separate.

2. PRECISE RESISTANCE MEASUREMENTS

Chapter 2 Precise Resistance Measurements

Central to the annealing and compression experiments described in chapters 3 and 4 respectively was the construction of a fast and reliable resistance measurement apparatus, capable of resolving resistance changes of fractional magnitude 10^{-5} (1 part in 10^5). A detailed description of the manner in which resistance changes in metallic glass samples were monitored is given in this preliminary chapter. Accounts of the measurement of temperature and pressure, of the provision of suitably controlled sample environments and of the characterisation of samples are given in chapters 3 and 4.

The purpose of this chapter is three-fold; to allow the measurements to be repeated and extended easily, to promote confidence in the experimental results obtained in this study and to record how some principles of experimental physics have been applied.

No attempt has been made to deduce the resistivity of any samples, because of the difficulty in measuring mean cross sectional area of a ribbon about 20μ thick. Likewise, no precise calibration of absolute resistance values was attempted; changes were measured relative to the initial resistance, as it is fractional property change which is of interest for the modelling of structural changes.

In order to achieve the required fractional resolution of 10^{-5}, it was necessary to eliminate the effects of thermal voltages, drifts in the standard voltage and current supplies and variations in these standard supplies due to laboratory temperature fluctuations.

The experiment in its final form was semi-automated in that many of the tasks necessary for the generation of each data set were carried out by a microcomputer, under manual control. The automation of control and of data logging is described in section (2.4) and the extra problems of instrumentation due to automation are discussed there also.

Specifications of the items of electrical equipment referred to in the text and the names of the suppliers are given in appendix 1.

(2.1) Summary of method of measuring resistance

Metallic glasses have room temperature resistivity of order 100$\mu\Omega$cm ($10^{-6}\Omega$m) (Mooij, 1973). The resistance per unit length of the ribbons used was about 50Ω/m. In order to obtain a uniform temperature distribution along the ribbon in the annealing experiments, short samples, length about 5 cm, were used with resistances of between 1 and 2 ohms. These sample resistances are comparable with typical contact and lead resistances, so a four probe method of resistance measurement was employed in order to eliminate the effect of lead and contact

resistances on the measured value of sample resistance within the resolution obtainable.

The four probe technique is well documented, eg by Squires (1985). A known current i_o is passed along the sample (of unknown resistance R), entering and leaving via two current contacts at the ends of the sample (figure 2.1). Two potential leads are attached to the sample, well within the region through which the current i_o is flowing. The current Δi drawn through the potential contacts and through the potential leads by the apparatus used to measure the potential is small. For the voltage drop across the potential contacts and leads to be negligible, we require that

$$\Delta i R_c << i_o R$$

where R_c is the total resistance of the potential leads and contacts. Since the current drawn by the voltage measurement circuit is given by

$$\Delta i = i_o R/Z$$

where Z is the impedance of the voltage measurement circuit, we require

$$R_c << Z.$$

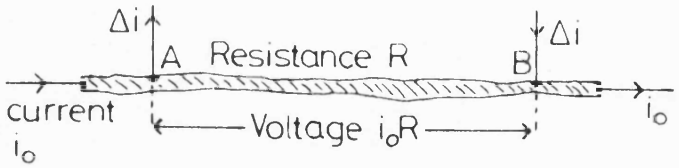

Figure 2.1: principle of the four-point resistance measurement

Since Z = 1MΩ(appendix 1), we require $R_c \ll 1M\Omega$. This is clearly satisfied by any good electrical contact or lead. R_c was estimated experimentally by connecting a variable resistance R_L across the potential contacts and measuring the effect of the introduction of this finite resistance on the voltage in the potential circuit (figure 2.2). The voltage across R_L is given by

$$V = i_o R_L \times (R/(R + R_L + R_C))$$

This can usefully be rearranged

$$\frac{1}{V} = \frac{1}{i_o R} + \frac{R_C + R}{i_o R} \quad \frac{1}{R_L}$$

so that a graph of 1/V vs. $1/R_L$ is expected to be a straight line with gradient $(R+R_C)/(i_o R)$ and intercept $1/(i_o R)$, from which two numbers the contact resistance R_C can be deduced. A good linear relationship between (1/V) and $(1/R_L)$ was obtained for several samples; the combined resistance of contacts and samples was always less than 1Ω.

Resistometric studies of metallic glasses previously reported have employed either d.c. or a.c. methods of measurement. A direct current was used in the present

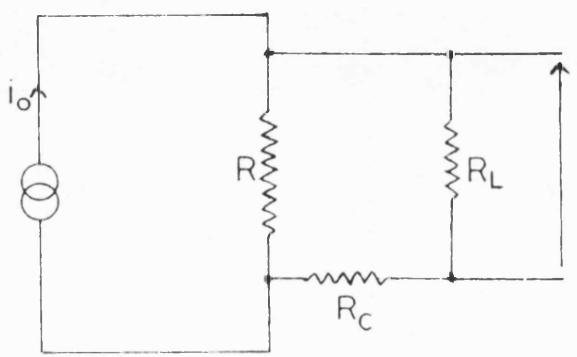

Figure 2.2: measurement of contact resistances R_c

study, following Balanzat (1980), Cost and Stanley (1981) and Woldt and Leake (1985). An a.c. circuit using a lockin amplifier is described by Marcus (1979), and is also the basis of the experimental apparatus of Kelton and Spaepen (1982) and Lin, Bevk and Turnbull (1979). Mulder, Drivjer and Radelaar (1981) use an a.c. resistance bridge circuit designed by Gaefvert (1976). The accuracies of the relative resistance measurements quoted by these workers vary from 3.10^{-3} (Lin et al. 1979), which is not fine enough to allow resolution of small reversible resistance changes as required in the present work, to roughly 10^{-6} (Cost and Stanley 1981). In this latter case though the resolution was estimated after statistical analysis of the data, so the scatter in the original data points was presumably worse than 1 part in 10^6.

Direct current apparatus is cheap and in principle simple to construct. The steady voltage i_oR can easily be measured precisely using a null technique; figure 2.3 is a circuit diagram illustrating the principle of a simple null method of measuring resistance using a current source and a voltage source.

Clearly, drifts in i_o or V_o produce proportionate drifts in the apparent resistance since

$$R = fV_o/i_o$$

where f is the fraction by which the reference voltage V_o is divided down by the potential divider in figure 2.3. The alternatives to the circuit shown in figure 2.3 are direct measurement of i_oR using a voltmeter, and the Kelvin bridge (Marton 1973) which uses a resistance standard. An improved form of the method illustrated in figure 2.3 was employed in favour of both these alternatives because apparatus suitable for making a very precise null measurement was readily available. The improved method, described in section 2.3, produced results with resolution as good as any reported in the comparable studies already mentioned.

The main disadvantage of a d.c. measurement of resistance is that the presence of any parasitic e.m.f in the potential circuit must be allowed for explicitly by reversing the current i_o each time a measurement is made and taking the mean of the calculated resistances in the cases of forward and reverse currents. In a.c. experiments, any slowly varying offset voltage is automatically excluded because in the frequency domain it lies well to the low frequency side of the narrow window through which the lock-in amplifier accepts signals. It is always good practice to allow for any offset voltage in a d.c. potential circuit, but in experiments like the present one, involving high temperature gradients in regions where dissimilar metals join, the accurate elimination of thermovoltages is particularly important.

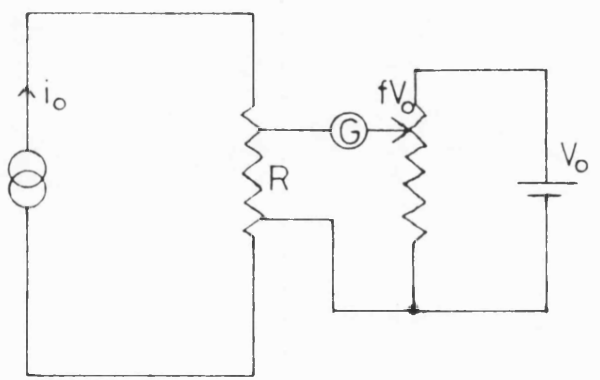

Figure 2.3: null voltage measurement

Figure 2.4 is a simplified diagram of the potential circuit, showing where the thermal offset voltages appear. We suppose that the sample is at a temperature T, and that the difference in temperature between the two ends is ΔT. Let $V(T)$ be the thermoelectric voltage generated between the copper leads and the metallic glass in question; then the upper hot junction in figure 2.4 creates a voltage $V(T_h)$ in the potential circuit; the lower of the two hot junctions inserts a voltage $V(T_h + \Delta T)$ into the potential circuit, but with the opposite sign. The thermal offset V_T experienced by the voltage measurement system is therefore given by

$$V_T = V(T_h + \Delta T) - V(T_h)$$

The magnitude of V_T was typically 10^{-4} in the experiments; the magnitude of i_0R was about 0.1V. The fractional thermal voltage correction is therefore of magnitude 10^{-3}, 2 orders of magnitude greater than the resolution of the experiment and big enough to obscure all small structural effects.

Accurate reversal of the current i_0 is easy to arrange using a double pole, double throw relay, as shown in figure 2.5; to make a single resistance measurement, i_0 is passed forward and then backward, producing voltages $(V_T + i_0R)$ and $(V_T - i_0R)$ respectively across the

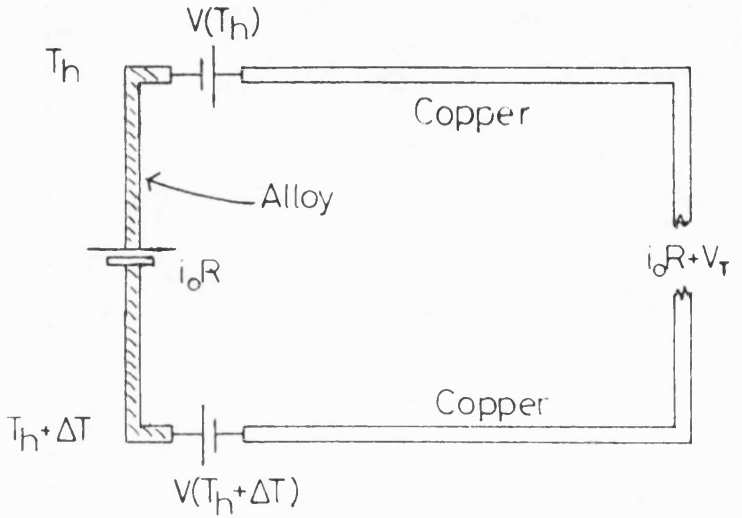

Figure 2.4: thermal e.m.f. in the potential circuit
$V_T = V(T_h+\Delta T) - V(T_h) \approx \Delta T(dV(T)/dT)$

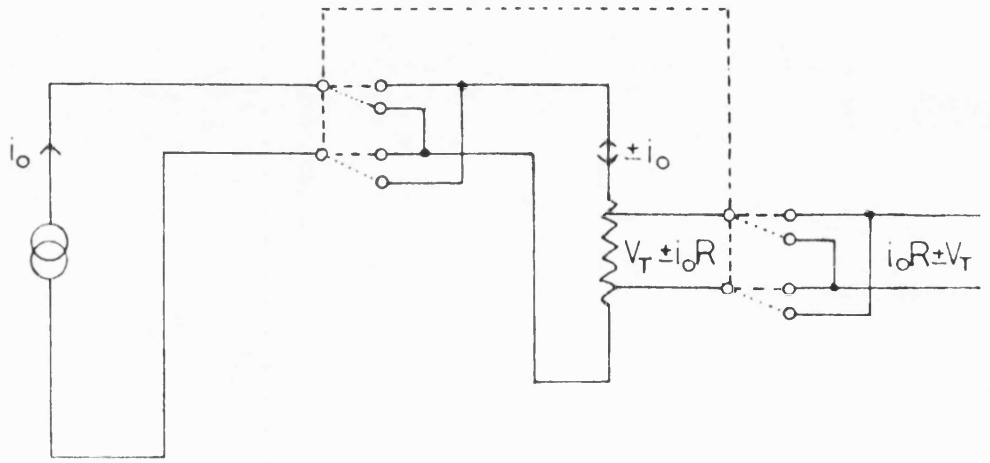

Figure 2.5: reversal of current

potential leads. A similar pair of double throw relays is used to cross over the potential leads when the current is reversed. The voltages thus generated by forward and reverse currents are $(i_0R + V_T)$ and $(i_0R - V_T)$ respectively.

In principle, the simplest way to deduce the value of R is to measure $(i_0R \pm V_T)$ and then to take their mean. Direct measurement of these voltages using an analogue to digital converter proved to be insufficiently precise; the stability of the analogue to digital converter with respect to fluctuations in temperature is poor (see appendix 1). Typically, laboratory temperature changes through about 5K during one daily cycle; this would limit the resolution of the analogue to digital converter to about 0.05%, or 35μV, taking 70mV as a typical value for i_0R. The voltage measurements were therefore made using instead a vernier potentiometer. However, during heating and cooling of the sample, both R and V_T vary rapidly, and the delay between making two precise potentiometric measurements therefore introduces an error into the estimate of R. A better method for separating the thermal contribution from the required voltage i_0R was devised and is illustrated in figure 2.6.

With the current flowing forwards, a null is obtained (figure 2.6a) using a nulling microvoltmeter in place of

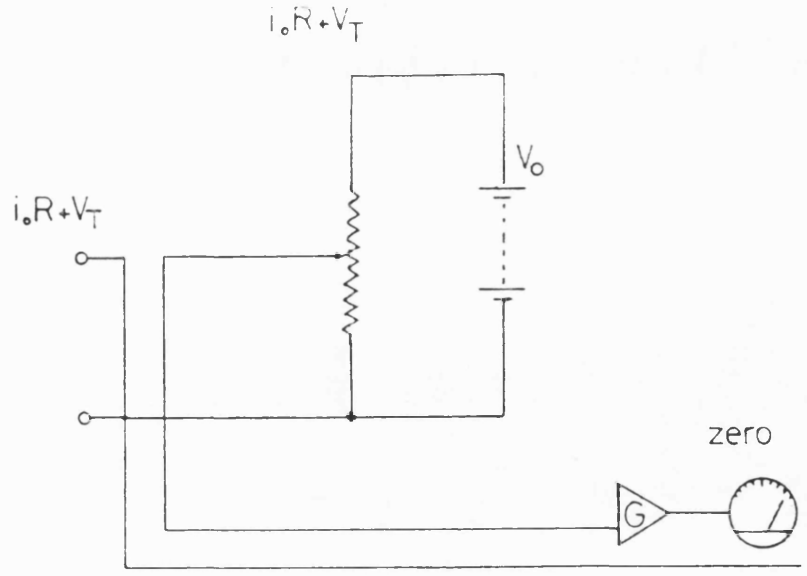

(a)

Figure 2.6: elimination of thermal voltage

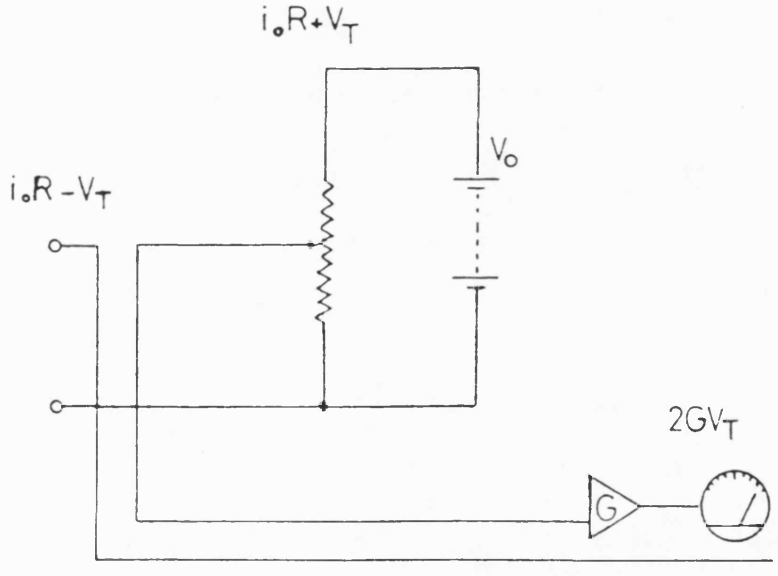

(b)

the conventional galvanometer, on a sensitive range, typically with a full scale deflection of 10μV. This nulling voltage is then given by

$$fV_o = i_oR + V_T$$

The current is then quickly reversed (figure 2.6b), and the nulling microvoltmeter, on a less sensitive range, is used to measure the difference between the old nulling voltage still being produced by the potentiometer, and the voltage $(i_0R - V_T)$ produced by the reversed potential circuit. The nulling microvoltmeter has an analogue output; the voltage at this output is given by

$$V_{OUT} = G((i_oR + V_T) - (i_oR - V_T))$$

$$= 2GV_T$$

where G is the gain of the analogue output with respect to the input of the microvoltmeter, which is at this point being used simply as a d.c. amplifier. The resistance is therefore given by

$$R = (fV_o - V_{OUT}/2G)/i_o$$

The advantage of this configuration for the measurement of rapidly varying resistances is speed. The potentiometer can be set in advance; as the micro-

voltmeter passes through the null point, the current and sample voltage are reversed simultaneously using computer control and the voltage at the output of the microvoltmeter is immediately logged. The delay between registering the null and making a digitally averaged reading of $2GV_{OUT}$ is about 2 seconds. The accuracy of this method of eliminating parasitic e.m.f.s was tested by inserting artificial offset voltages into the potential circuit, using a calibrated voltage source, with the sample at room temperature and therefore producing negligible thermal offset voltages itself. It was found that by varying the artificial offset voltage through a range of 0.1mV, a fractional change of magnitude less than 10^{-5} was induced in the apparent resistance. This error, which arises from non-linearity in the amplification of the thermal voltage by the nulling microvoltmeter, is the main limit on the resolution of the voltage measurement system.

2.2 Compensating for drifts

The nulling voltage was generated by a 64 amp-hour, 2V battery and a potentiometer with resolution 1μV. The battery, of the lead-acid type, produces a voltage which is very stable over short periods of time of the order of 1s, but which drifts over periods of a few hours. The current drawn by the potentiometer from the battery is small, of order 10mA, so the battery needs recharging only very infrequently (every few months). The best way to recharge the battery is on a trickle current of about

0.5A over a weekend; it can be charged at a higher rate but a settling time of a few hours at a discharge rate of order 100mA is then needed. The battery was monitored before the beginning of each experiment by continually calibrating the potentiometer, as described in detail below, to make sure that any fast voltage drift associated with settling had finished. The magnitude of the rate of battery voltage drift needs to be 0.1 microvolt per second or less for the standardisation technique described here to be of use.

The potentiometer is fitted with a standardisation circuit (figure 2.7); the battery e.m.f. is divided down to a standard voltage V_0 by moving the slider of the rheostat marked "standardise" until a null is obtained between the reference voltage and some external standard. The designers of the potentiometer intended that a Weston cell or similar be used as a standard. Instead, in the present experiment, the voltage across a standard resistor R_0 connected into the current circuit, in series with the sample, provided the reference voltage (figure 2.8).

We are therefore using a potentiometer to compare the resistance of the sample with that of a standard resistor. This design eliminates the effects of long term drifts in the current i_0 and the battery voltage, as we will now demonstrate.

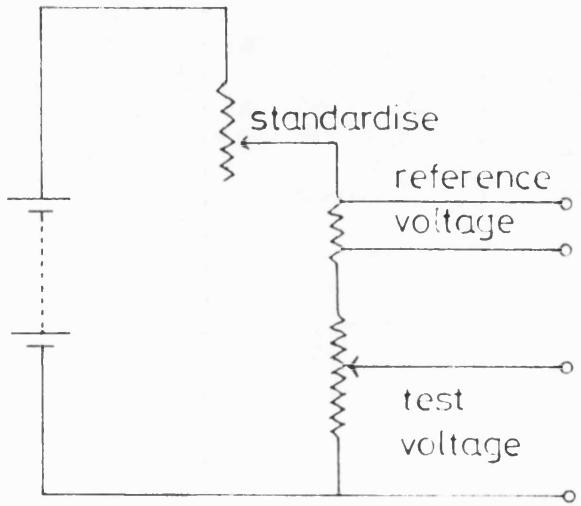

Figure 2.7: standardisation of potentiometer

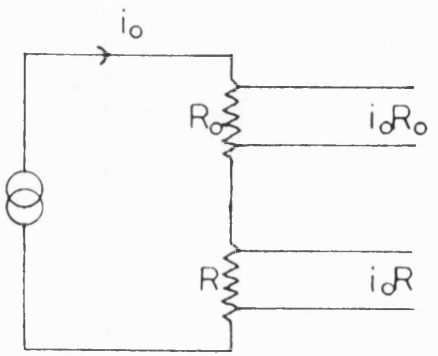

Figure 2.8: compensation for drifts in current

Suppose a fluctuation di_0 occurs in the current i_0. The new reference voltage seen by the potentiometer standardisation circuit is then

$$V_{ref.} + dV_{ref.} = (i_0 + di_0)R_0$$

Therefore

$$dVref. = diR_0$$

$$\frac{dV_{ref.}}{V_{ref.}} = \frac{di_0}{i_0}$$

The potentiometer is then recalibrated such that

$$\frac{dV}{V_0} = \frac{di_0}{i_0}$$

The voltage at the test terminals of the potentiometer has therefore changed from fV to fV $(1 + di/i_0)$, while the sample voltage has increased from i_0R to $i_0R(1 + di_0/i_0)$. The two voltages to be nulled have therefore increased by the same fraction, so no change in f is necessary; the fluctuation in current has not affected the measured value of the sample resistance.

A similar argument applies to fluctuations in the battery voltage; in this case the action of the standardisation circuit is to maintain a steady voltage V_0 throughout.

We have removed the effects of slow drifts in i_0 and in battery voltage, but introduced in their place errors due to any fluctuations in R_o, the standard resistance. A wire wound resistor was used in a four terminal configuration; the temperature coefficient of R_o was specified to lie in the range 0 ± 3 ppm/K. The temperature of the standard resistor was maintained to within ± 1K by immersing it in a reservoir of liquid nitrogen. Fractional fluctuations in R_o were therefore of magnitude less than 10^{-5}.

This estimate of the long term stability of the measurement system was tested by changing i_0 in a controlled manner, recalibrating the potentiometer as usual and remeasuring the resistance of the sample. It was found that very large artificial fluctuations (magnitude 1%) in the current i_0 produced no detectable error in the result to within 1 part in 10^5. Fluctuations in the current are expected to be at worst one hundredth of this size (appendix 1), so the contribution of fluctuations in current and in battery voltage had clearly been eliminated, as expected. This reduction of the effects of drift to much less than 1 part in 10^5 compares favourably with estimates of drifts

quoted by other experimenters. Kelton and Spaepen (1982) for example measure a drift of 2.10^{-4} over 24 hours on their a.c. experiment; this introduces a large uncertainty into the results which has been avoided here.

The values of i_0 and R_0 were chosen such that their product was a typical Weston cell e.m.f. Typical values were

R_o = 15 ohms (nominal)

i_o = 61.354 mA

giving a reference voltage of 920.31 mV (nominal) which was chosen because it allowed the standardisation rheostat to operate around the centre of its range. The self-heating of the sample due to the current i_0 was negligibly small. This fact was ascertained by monitoring the sample temperature for a period of several minutes after switching off the current; there was no detectable temperature change.

It was necessary to isolate the standardisation circuit while measuring the voltage across the sample and vice versa, in order to avoid making a connection between the two circuits via the sample itself. This was achieved by switching the test voltage selector to an unconnected pair of terminals during standardisation and by physically disconnecting one of the standard voltage

leads from the potentiometer when measuring the voltage at the sample. These points of connection and disconnection are represented by switches marked "std" in the overall circuit diagram, figure 2.9; they are shown in the position appropriate to resistance measurement rather than to standardisation.

2.3 Contacts

The four leads to the sample need to make good electrical contact with the sample and remain fixed in position throughout the experiment. A fractional change $\Delta l/l$ in the separation l of the potential contacts will cause a change $R\Delta l/l$ in the resistance R of the sample. Since the resolution required is 10^{-5}, and the sample length is of order 0.1m, the positions of the potential contacts on the ribbon must be maintained to within an accuracy Δl given by

$$\Delta l/l = 10^{-5}$$

$$\Delta l = 10^{-6}m = 1\mu m$$

Spot welding is usually the best way of making fixed electrical contacts between metal wires and a metallic ribbon and this is the method of Balanzat (1980), Lin et al. (1979), Marcus (1979) and Mulder et al. (1981). However, spot welded contacts to a current-carrying metallic glass sample are of questionable value as resistance probes.

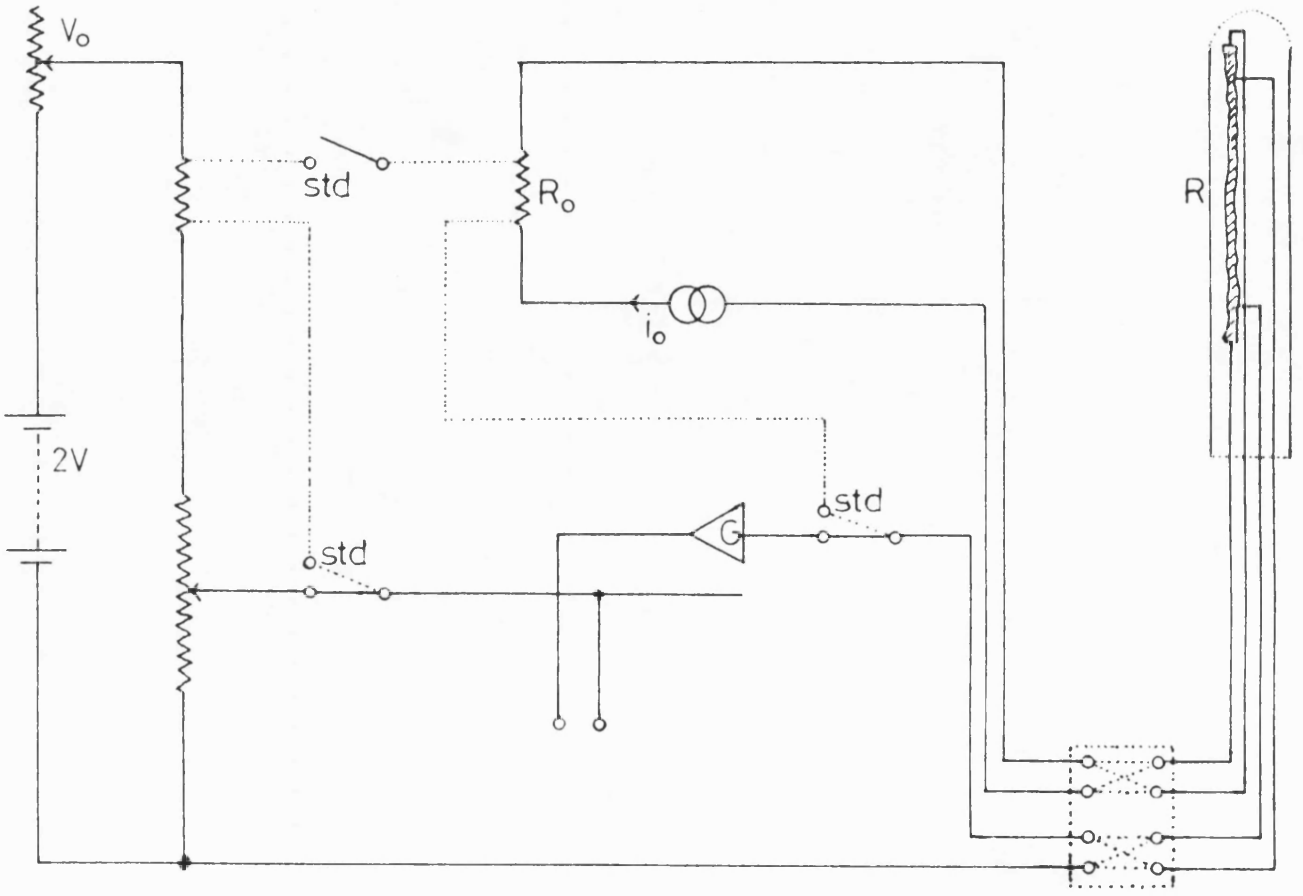

Figure 2.9: circuit diagram

Spot welding involves the melting and resolidification of small regions of both the sample and the lead itself. Since the contact is thermally isolated from any good heat sink as it cools, solidification cannot be very rapid and we must expect crystallisation around the contacts. While crystallinity around the current contacts is quite unimportant (figure 2.1), the presence of microcrystallites around the potential contacts will affect the absolute measured resistance value. More importantly in our investigation, the presence of microcrystallites increases the likelihood of further crystal growth, such that it might occur during high temperature anneals and give rise to a spurious extra resistance change.

Mogro-Campero and Walter (1980) have warned that the presence of a few percent crystallinity in a metallic glass can double the temperature coefficient of electrical resistance. No attempt has been made here to quantify the effects of any crystallinity or crystal growth around a spot weld. The fact that the results presented in this thesis, which definitely lack any such spurious contributions as will be shown below, agree well with similar results obtained using a conventionally spot welded sample (Kelton and Spaepen 1982, who refer to the experimental method of Marcus 1979) suggests that these effects are negligibly small. In view of the precision required of the results however, spot welding was avoided in any region of the sample contributing to the resistance measured.

As an alternative to spot welding, pressure contacts were tried. Pressure was applied firstly by trapping the ribbon between pairs of 2mm nuts on studding and secondly by using the leads themselves, bent over, as springs. Both types of contact suffered from unacceptably large sudden readjustments in position, causing sudden jumps in the resistance of the sample, as can be seen marked by vertical arrows in figure 2.10 for example.

The problem of making good contacts was solved by employing a novel sample geometry. Longitudinal cuts of approximate length 2cm were made at the ends of the ribbon samples (figure 2.11). The four arms thus formed were pulled out from the long axis of the sample to form potential and current contacts. Spot welds were used to make contact at the free ends of the arms; any crystallisation introduced locally by the potential lead welds is too far from the current carrying part of the sample to affect the resistance.

All results were free from artefacts of the type illustrated in figure 2.10 after this new method of making contacts had been introduced.

This unconventional sample geometry would not be suitable for absolute resistivity measurements because of the non-uniformity which we must expect in the equipotential lines around the ends of the longitudinal cuts. For the present purposes, no estimates of the sample dimensions

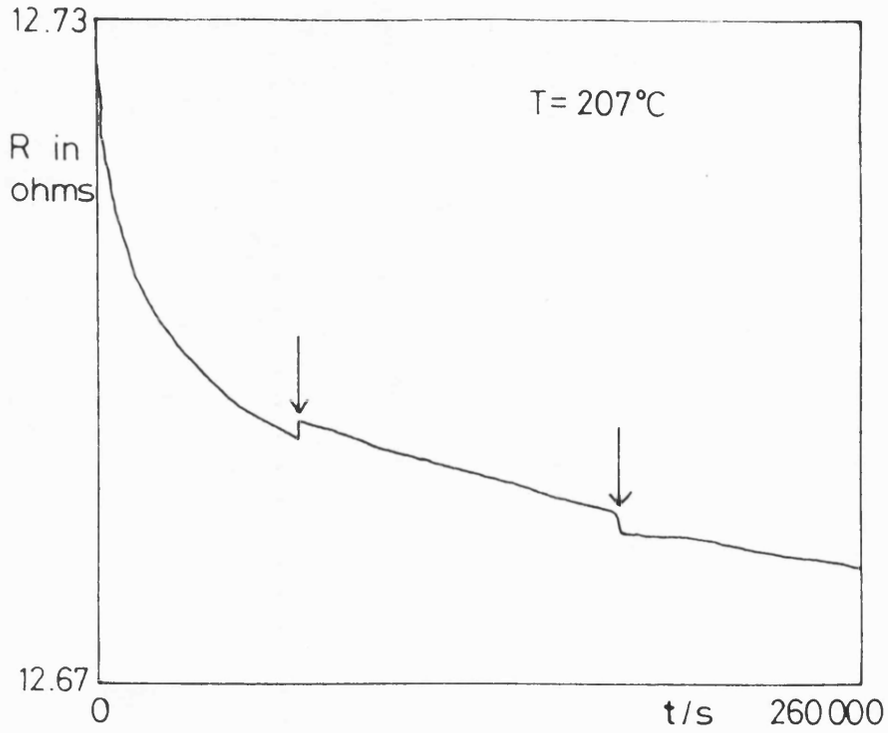

Figure 2.10: $R_T(t)$ for $Pd_{82}Si_{18}$ showing artefacts which indicate slipping of contacts along ribbon

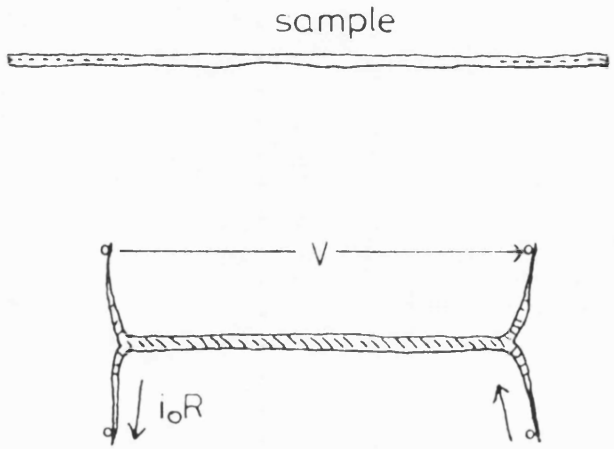

Figure 2.11: sample geometry

are necessary; the relative resistance change is independent of the shape of the sample.

2.4 Control

As a null is detected, the following tasks need to be performed:

(a) reverse the current and voltage leads to the sample,
(b) record the time at which the measurement has been made,
(c) measure the voltage at the nulling microvoltmeter,
(d) measure the temperature and in compression experiments the pressure,
(e) record the potentiometer setting,
(f) return the current and voltage leads to their original polarity.

In addition

(g) display and storage of data, and
(h) frequent standardisation of the potentiometer

are necessary. The connections necessary for (h), standardisation of the potentiometer, were made and undone manually before and after each standardisation; all the other tasks, (a) to (g) were performed using a microcomputer as the controller and as the data logger.

A block diagram of the arrangement is shown in figure 2.12. A control program is kept on flexible disc and loaded into the microcomputer at the beginning of the experiment. The microcomputer, together with a standard interface and an analogue to digital converter, then responds to controls from the keyboard and controls the opening and closing of relays and the measurement of the analogue output from the nulling microvoltmeter. The computer interrogates the operator (dashed lines in figure 2.12) whenever information from the temperature and pressure displays and the nominal potentiometer voltage are needed, and it then carries out the calculations necessary to determine the resistance R and records on the printer, reading by reading, the time, temperature, resistance, pressure (in compression experiments) and thermal offset voltage appropriate to each measurement made. A separate record is kept, reading by reading, of time, temperature, (pressure), and resistance, on flexible disc. The control program was written in BASIC and run on a BBC microcomputer with a disc filing system supplied by Watford Electronics.

The voltage at the output of the nulling microvoltmeter is measured fifty times in quick succession each time a reading is taken in order to reduce the effects of random digital noise in the analogue to digital converter. A simple arithmetic mean of the fifty readings is calculated. Each reading is digitally filtered to reduce the effects of high frequency noise; the time between each of the fifty successive digitally filtered

Figure 2.12: block diagram of control of experiment

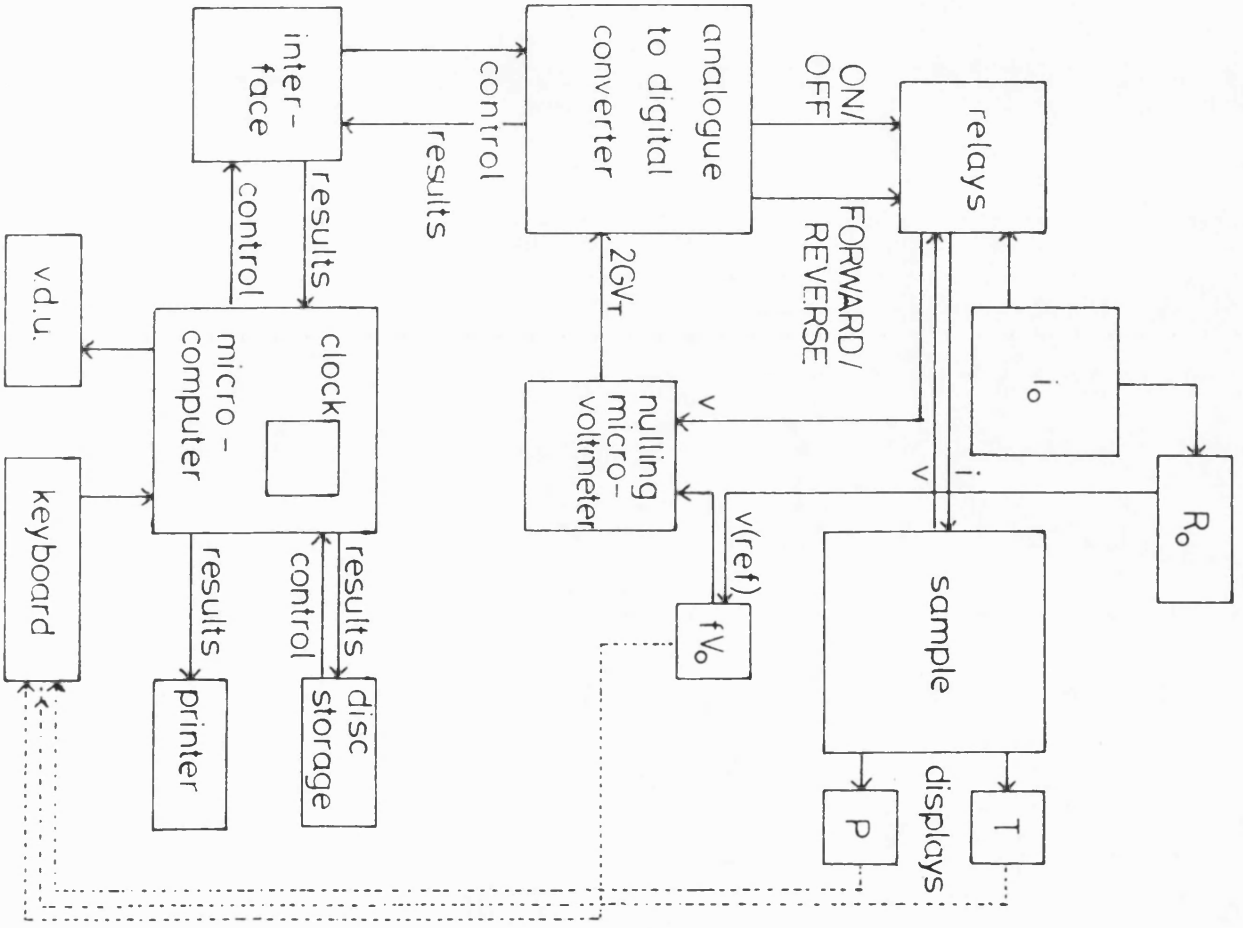

measurements is 13ms, the minimum delay possible with the analogue to digital converter used. This estimate of maximum possible sampling rate was made by timing with a stopwatch the execution of a large number of successive measurements. The control program provides for the display on a television monitor screen of a graph of the fifty successive voltage readings versus time as they are read back from the analogue to digital converter. This provides a useful check for the experimenter that the scatter of the points is not excessive, as might be the case if a connection were working loose at the vacuum seal or at the sample itself.

The computer used (BBC microcomputer) was liable to fail, especially when the ambient temperature was high. The probability of failure was reduced by increasing the ventilation of the circuitry, but more importantly, care was taken to avoid relying on memory from one complete measurement to the next by building the following measures into the control program.

(1) Data sets were stored on flexible disc as they were generated, not as elements of a matrix in the computer's random access memory.

(2) A quick and convenient restart subroutine allowed all the necessary parameters to be reset in the event of failure, allowing the experiment to continue without loss of too much time.

(3) Files on flexible disc were not kept open continuously. Disc errors occurred when files were kept open for periods of several days and this problem was eliminated when instead the data file was closed after each data set had been stored and reopened for the input of the next data set.

The advantages of automatic control are its speed and the ease with which results can be presented on a printed graph. Speed is important because for kinetic analysis good resolution in time is essential, but also because the number of individual voltage measurements (fifty in this case) which can be used to generate each datum point is limited by the speed at which successive measurements can be made.

A problem with automation which was avoided rather than overcome was the loading effects of the nominally independent input channels of the analogue to digital converter on one another. It was found that plugging the output of the digital thermometer into one input I_1 of the analogue to digital converter while another of the inputs I_0 was connected to the sample via the voltage measurement circuitry consistently caused unacceptably large changes in the voltage detected at I_0. This unexpected behaviour was due to the electrical contact between thermocouple and sample and the fact that the ground connections of the two inputs I_0 and I_1 were

effectively joined by a large but finite impedance, of magnitude a few megaohms. This finite inter-channel impedance loads the sample, which can be regarded as a poor voltage source, between one of the potential leads and the point of contact of the thermocouple; because the "voltage source" has an impedance of only a few ohms, its output is depressed slightly.

This problem was avoided by using only one input of the analogue to digital converter (to measure the microvoltmeter output) and by entering the displayed pressure (in compression experiments) and temperature readings manually at the keyboard. It was the time taken to enter numbers at the keyboard which limited the frequency of taking readings to one every 20s so this is clearly a feature which can be usefully improved on. A simple solution to the ground loop problem is to optically isolate all the inputs to the analogue to digital converter, so that all voltages can be read automatically. This improvement would be inexpensive and would increase the resolution of the experiment in time, though not of course in resistance or in temperature.

3. THE EFFECTS OF STRUCTURAL RELAXATION ON CONDUCTION

Chapter 3 The Effects of Structural Relaxation on Conduction

Measurements of electrical resistance provide a sensitive probe of structural change. Experimental studies of the effects of structural relaxation on electrical resistance are reviewed in section 3.2 below. In section 3.1 we consider the nature of electrical conduction in metals and in section 3.3 we show how a simple theoretical approach (Ziman theory) to the difficult problem of predicting the resistivity of amorphous metals has been invoked in the interpretation of the results.

One set of amorphous alloys to which the Ziman theory has been applied is that with stoichiometry $Pd_{82-x}V_xSi_{18}$, with x between 0 and 6. Further experimental results showing the effects of structural relaxation on electrical resistance in three of these alloys are presented in section 3.4.

(3.1) The Nature of Electrical Conduction in Crystalline and Amorphous Metals

In metals, electric current is carried by the conduction electrons, whose number is not a strong function of temperature. In the presence of an externally applied electric field, the conduction electrons acquire a net linear acceleration and a current begins to flow. The current, rather than increasing indefinitely, rapidly attains a steady value because of electron scattering.

Scattering is always taking place in real metals, but in the absence of any applied electric field, its net effect on the total momentum of the conduction electrons is zero, because scattering is random and therefore centrosymmetric. When an electric field is applied, however, the randomising effect of scattering tends to reduce the net momentum of the conduction electrons and it therefore opposes the applied field. Electron scattering acts as a restoring force on the accelerated electrons and it is the number and efficacy of scattering processes which determines the steady current density attained in a given electric field. Our understanding of the effects of structural change on resistance is therefore based on our knowledge of electron scattering mechanisms and how they depend on atomic structure.

In an idealised, perfectly crystalline metal at zero temperature, the eigenstates of the conduction electrons are Bloch waves (Bloch's Theorem); in a real crystalline metal, we picture the conduction electrons being scattered between these perfect-crystal eigenstates. The sources of electron scattering are deviations from perfect periodicity due to thermal motion of the atoms and the presence of static imperfections in the crystalline lattice. At room temperature, deviations from periodicity due to thermal motions dominate; resistance is therefore a strong function of temperature in crystalline metals, and the resistance at low temperature, known as the residual resistance, can be very low in crystals prepared with a low concentration of

imperfections. In figure 3.1.1, the curve labelled 'c' shows the strong temperature dependence and low residual value of the resistance of a crystalline ribbon of composition $Fe_{40}Ni_{40}P_{14}B_6$ determined by Rayne and Levy (1977).

In amorphous metals, no state of perfect long-range order exists even at zero temperature; Bloch's Theorem does not apply and we cannot write down a set of single-electron eigenstates for some idealised amorphous state. The residual resistance of a length of amorphous alloy ribbon is accordingly much higher than that of its crystalline counterpart because the conduction electrons are scattered frequently even at zero temperature. This fact is illustrated by a comparison of curve 'a' (amorphous $Fe_{40}Ni_{40}P_{14}B_6$) with curve 'c' in figure 3.1.1. The two curves converge at higher temperatures because the temperature dependence of the resistance of the amorphous alloy is lower than that of the crystalline alloy.

The disorder of the arrangement of the atoms in a hot metallic glass is high, so the effects of thermal disruption of this arrangement are less significant than the effects of thermal disruption of a crystalline lattice. The magnitude E of the electric field applied to a metal is related to the resulting current density j by

$$j = \sigma E$$

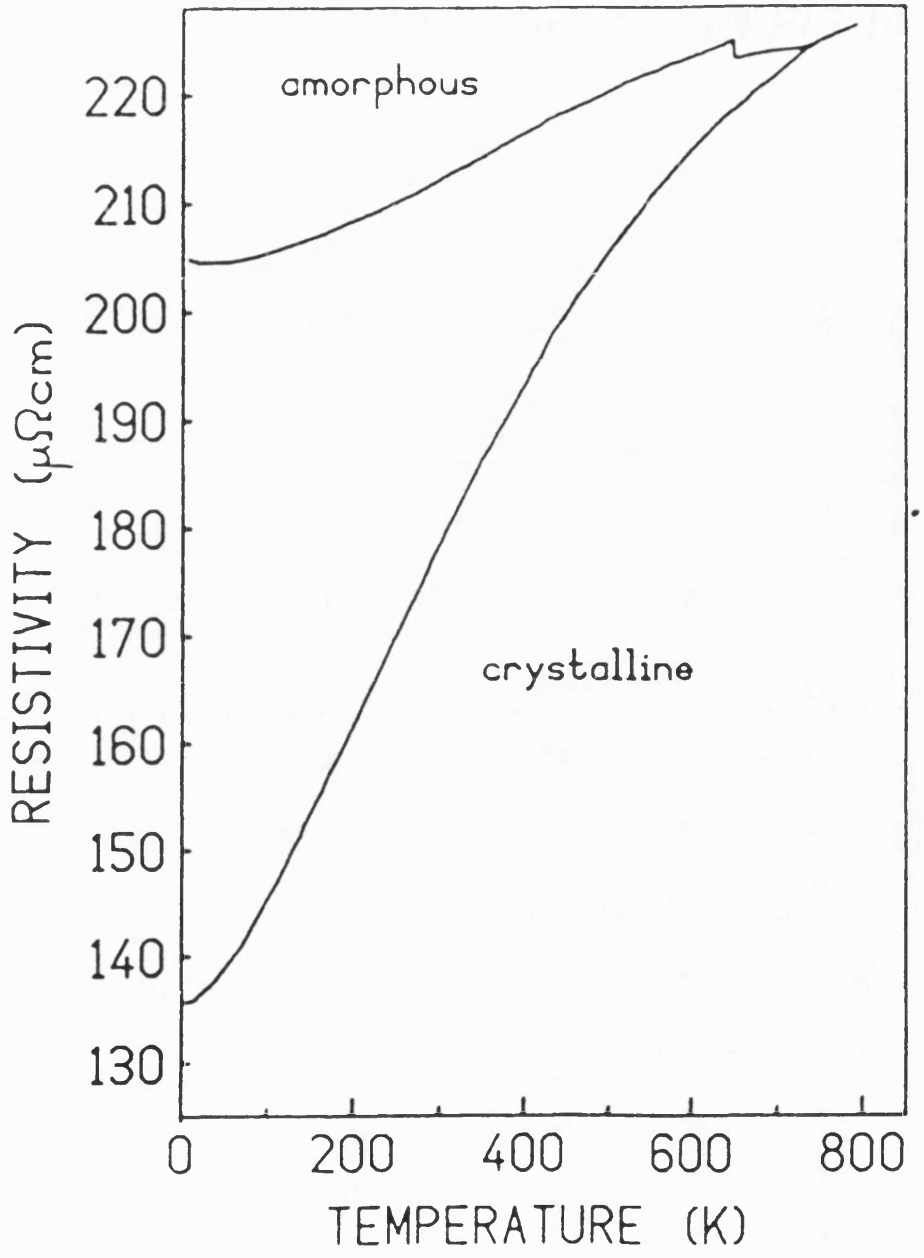

Figure 3.1.1: the resistivity of $Fe_{40}Ni_{40}P_{14}B_6$ as a function of temperature in the amorphous and crystalline states (Rayne and Levy 1977)

where σ is the conductivity. The relation between conductivity and electron scattering is expressed by the relaxation - time - approximation equation

$$\sigma = \frac{ne^2\tau}{m^*} \qquad \text{(3.1.1)}$$

where

n is the number of conduction electrons per unit volume,

e is the magnitude of the electronic charge,

τ is the relaxation time and

m* is the effective mass of a conduction electron at the Fermi level.

The relaxation time τ is defined as the mean time between scattering events for each conduction electron, assuming that electrons are always scattered into a state of zero momentum. τ is really an effective scattering time; each conduction electron spends less time than τ between scattering events on average, but the average reduction in forward momentum is less than 100%.

According to equation (3.1.1), structural changes cause changes in conductivity through changes in n, the number density of conduction electrons, τ, the relaxation time and m*, the effective mass of a conduction electron as it is accelerated by the electric field, in between scattering events. Since our aim in chapters 3-6 is to

interpret observed changes in electrical properties in terms of specific underlying structural changes, we require a model which allows us to predict the small changes in n, τ and m* which would accompany small changes in specific structural parameters.

The simplest such model is the nearly free electron (NFE) model, in which the conduction electrons are treated independently and in which the single-electron scattering potential is taken to be zero between collisions and small during collisions. Because it is simple and because it is the basis of Ziman theory, which is described in section 3.3, the NFE model is outlined here.

We begin with the free-electron model, in which the conduction electrons, considered independent, experience no external potential. Free-electron eigenstates are plane waves of the form $e^{i\underline{k}\cdot\underline{r}}$. The occupied single-electron states form a sphere in k-space. The radius K_f of this fermi sphere is determined by the number density of electrons in real space; this can be shown by considering some arbitrary volume V within a region of free space in which the number density of electrons is n. We apply periodic boundary conditions to the plane wave eigenfunctions within this volume to ensure that it is typical of its surroundings, and find (eg Ashcroft and Mermin 1976, p. 136) that the density in k-space of the allowed eigenstates is $(V/4\pi^3)$. The number N of states

contained by the fermi sphere, radius K_f, is therefore given by

$$N = \frac{VK_f^3}{3\pi^2}$$

Since $N = Vn$, we have

$$n = \frac{1}{3\pi^2} K_f^3$$

$$K_f = (3\pi^2 n)^{1/3}$$

showing that K_f is a function of n only.

In the NFE model of metallic conduction, the fermi sphere remains undistorted and is displaced along a k-vector during conduction. Figure 3.1.2 shows the NFE fermi sphere displaced along k_x as a result of an electric field applied in the negative x direction. The applied field accelerates the conduction electrons in the x-direction, tending to cause a steady increase in k_x, but scattering events (curved arrows in figure 3.1.2) keep the displaced sphere in equilibrium. The broken line represents the fermi sphere in the absence of any electric field; no net current flows because the total electronic momentum is zero.

The NFE theory is developed in many textbooks on solid state physics and applied to crystalline metals. The NFE treatment of amorphous metals relies on two important facts. Firstly, the existence of a spherical fermi

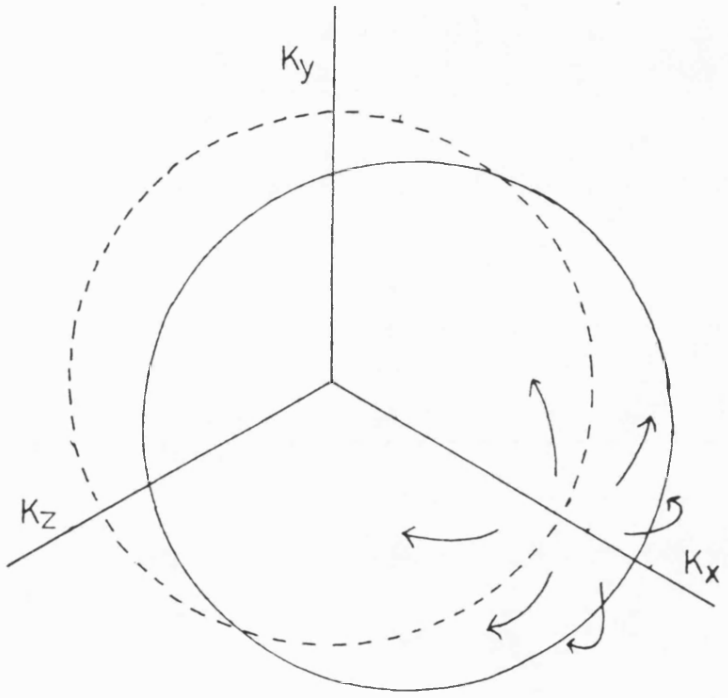

Figure 3.1.2: nearly-free-electron model of conduction; section of Fermi sphere in K-space

surface in electronic k-space depends on the weakness of the scattering potential and not on any periodicity of that scattering potential. Secondly, the pseudopotential approach, which is used to justify the assumption that the scattering potential is weak, can be used in amorphous alloys as well as in their crystalline counterparts; this fact will become apparent in section 3.3 where the pseudopotential is defined. The NFE model can therefore be used to calculate the conductivity of an amorphous metal in a weak-scattering approximation.

There are many other theories of conduction in amorphous metals (see Naugle 1984). They are all more realistic than NFE theory, but accordingly more complicated, and none has been invoked to interpret a set of structural relaxation measurements specifically, as the Ziman theory has.

The Mott s-d scattering model, like NFE theory, is based on the Boltzmann transport equation and therefore on the assumption that multiple scattering events are unimportant. Mott (1972) proposed that, when the mean free path of the conduction electrons is approximately equal to the interatomic spacing, scattering of electrons in the sp-band into vacant states in the d-band dominates. Morgan, Howson and Paja (1987) argue that hybridisation of the sp- and d-bands is important because it modifies the wave functions representing the conduction electrons and introduces conduction by the modified d-bands.

Conduction by d-electrons is usually ignored in the Mott model because their effective mass is high (Naugle 1984).

In contrast to the above weak-scattering treatments, the onset of localisation of the conduction electrons has been invoked (Naugle 1984) to account for some observed features of the temperature-dependence of conductivity in metallic glasses, eg the Mooij correlation (see section 3.2).

The theory of electron transport in amorphous metals is a busy area of research characterised by exciting developments (e.g. Mott 1987, Morgan et al. 1987); at present no single theory can explain all the current experimental facts. For the present purpose, we will use the simplest (NFE) approach to model the effects of specific structural changes on resistivity.

(3.2) Resistometric Studies of Structural Relaxation

Many experiments have examined the effects of thermal treatments on the electrical resistance R(T) of metallic glasses of various compositions. The temperatures of the treatments are chosen to be high enough to allow structural changes to take place over periods of order one hour, but low enough to ensure that no appreciable amount of crystallisation occurs during the anneal. The latter constraint limits anneal temperatures to well below the temperature of the onset of crystallisation as measured at a low, constant heating rate. We first

outline a method of interpreting results of such experiments and then survey the experimental literature.

Interpretation of Resistometric Data

Changes in the degree of short range atomic order are reflected in changes in the temperature-dependent electrical resistivity $\rho(T)$. The resistance of a piece of metallic glass is related to the resistivity by the equation

$$R(T) = \rho(T) \frac{l(T)}{A(T)}$$

where $l(T)$ is its length and $A(T)$ its mean cross-sectional area; the temperature-dependent quantities $\rho(T)$, $l(T)$, $A(T)$ and $R(T)$ are all in general affected by changes in short range order. Structural change therefore causes a change $\Delta R(T)$ in resistance given by

$$\frac{\Delta R(T)}{R(T)} = \frac{\Delta \rho(T)}{\rho(T)} + \frac{\Delta l(T)}{l(T)} - \frac{\Delta A(T)}{A(T)}$$

If metallic glass ribbons contracted isotropically during structural relaxation, we could write

$$\frac{\Delta A}{A} = 2 \frac{\Delta l}{L}$$

yielding for ΔR the simpler expression

$$\frac{\Delta R(T)}{R(T)} = \frac{\Delta \rho(T)}{\rho(T)} - \frac{\Delta l(T)}{l(T)}$$

and this is indeed the method of Lin et al. (1979), equation (1) and Kelton and Spaepen (1984), equation (11). But length changes in amorphous $Fe_{40}Ni_{40}B_{20}$ have been found (Cahn, Pratten, Scott, Sinning and Leonardsson 1984) to be strongly anisotropic, contraction along the ribbon being significantly greater than across it. This result on a single composition shows that we cannot justifiably expect isotropic changes in size in general during relaxation.

Many authors (Marcus 1979, Komatsu and Matusita 1986, Allia, Andreone, Sato Turtelli, Vinai and Riontino 1982) assume that the fractional changes in dimension which do occur are negligible beside the fractional change in resistivity; accordingly, they write

$$\frac{\Delta \rho}{\rho} = \frac{\Delta R}{R}$$

However, a comparison of the effects of structural relaxation on resistance and length changes in $Fe_{40}Ni_{40}B_{20}$ shows that contraction during structural relaxation can be significant. The effect of an anneal of duration 3.10^4s at a temperature of 526K was found (Woldt 1986) to cause a relative resistance change

$$\frac{\Delta R}{R_0} = -5.10^{-4}$$

The virtually identical thermal treatment of 3.10^4s at a temperature of 523K was found (Gibbs and Sinning 1985) to cause a relative length change

$$\frac{\Delta l}{l} = - 1.10^{-4}$$

The fractional change in dimension is of a similar order of magnitude to the fractional resistance change in this case. From here on, we will discuss experimental results as changes in the resistance of the sample, rather than attempting to quote the underlying resistivity change.

The use of electrical resistance as a probe of structural change is complicated by the fact that, even in the absence of any structural change, resistance depends strongly on temperature in many metallic glasses. This temperature-dependence of resistance is easy to measure at low temperatures (below about 100°C) where it is the only effect, but it is also present in the region of useful annealing temperatures (above about 100°C). We refer from here on to the dependence of R on T in the absence of any structural change as the isostructural temperature-dependence of resistance, R(T).

Figure 3.2.1 shows schematically the isostructural temperature-dependence of R in two different structural states. $R_1(T)$ refers to the structural state which we will suppose is attained after a long anneal at temperature T_1 and $R_2(T)$ to the state attained after a

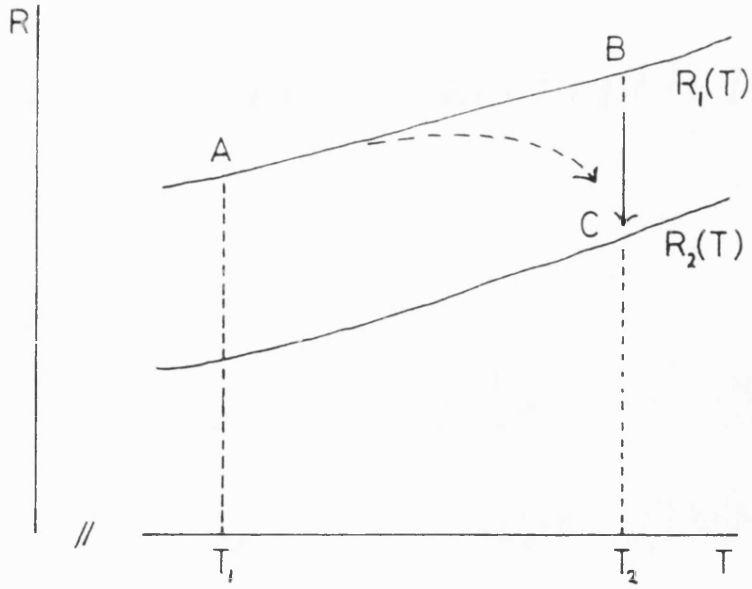

Figure 3.2.1: isostructural temperature dependence of resistance in two different structural states (schematic)

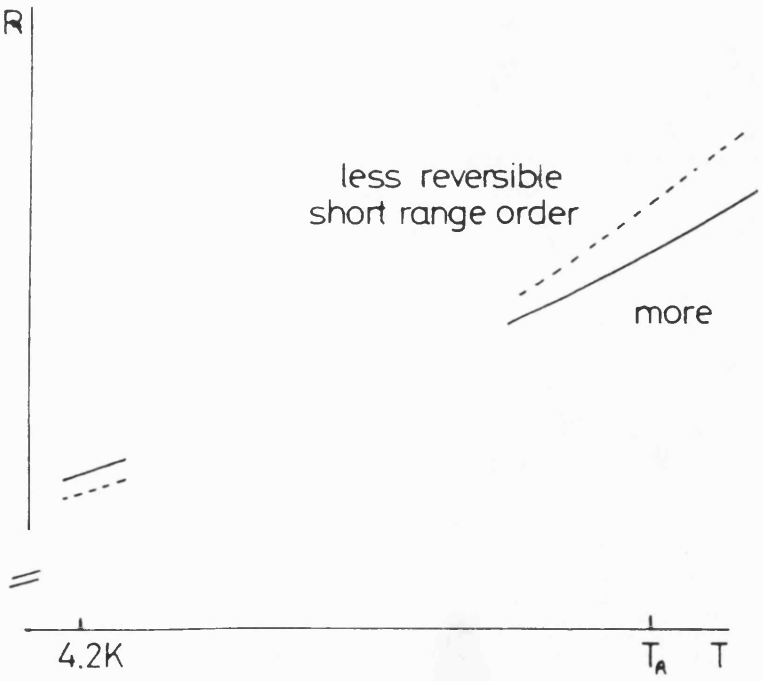

Figure 3.2.2: isostructural temperature dependence of resistance in two structural states (schematic-based on $Fe_{40}Ni_{40}P_{14}B_6$)

long anneal at T_2. Consider an idealised experiment in which the metallic glass has been annealed at temperature T_1 for such a long time that the perceptible resistance change is complete. The resistance is given by $R_1(T_1)$ (point A in figure 3.2.1). Now let the temperature be changed rapidly to T_2. Before any appreciable degree of structural relaxation takes place at the new temperature, the resistance will change, isostructurally, to $R_1(T_2)$ (point B) because of instantaneous changes in length (thermal expansion) and in dynamic properties of the atoms. As structural change occurs, the resistance will gradually approach the value $R_2(T_2)$, following the vertical arrow on the figure to point C. In a real experiment, because of the finite time needed to effect any temperature change, structural relaxation will begin as the temperature is still increasing (dashed arrow in figure 3.2.1); the distinction between structural and thermal (isostructural) effects will be blurred.

The curves $R_1(T)$ and $R_2(T)$ are shown parallel in figure 3.2.1. This is often a good approximation over a narrow temperature range, and it is a convenient one because it allows us to interpret the effect of structural change simply as the vertical offset BC of the two curves. Over the temperature range OK to T_A, though, $R(T)$ does not change by a constant term as a result of structural ordering and disordering. This fact is illustrated by

measurements of the reversible effects of alternate annealing treatments at different temperatures on R(T) in $Fe_{40}Ni_{40}P_{14}B_6$. The differential coefficient $(1/R)d\Delta R/d\Delta T_A$ of the height of the R(T) curve with respect to variations in the temperature T_A of long anneals is

$$\left.\frac{1}{R}\frac{d(\Delta R)}{d\Delta T_A}\right|_{T_A} = +3.5 \times 10^{-5}K^{-1} \text{ (Cost and Stanley 1982)}$$

$$\left.\frac{1}{R}\frac{d\ (\Delta R)}{d\Delta T_A}\right|_{4.2K} = -3 \times 10^{-5}K^{-1} \text{ (Balanzat 1980)}$$

This apparent discrepancy, noted and described as curious by Balanzat et al. (1985), indicates that the effect of prestabilising a piece of $Fe_{40}Ni_{40}P_{14}B_6$ at one temperature and subsequently annealing it at a lower temperature is to decrease its resistance *measured at high temperature* and to increase its resistance *measured at low temperature*. Figure 3.2.2 shows schematically how R(T) depends on the degree of reversible structural order in this case. We need not be surprised that a given structural change sometimes affects R(4.2K) and $R(T_A)$ oppositely since the dominant scattering mechanisms are likely to be different at the two ends of the accessible temperature scale.

Sonius et al. (1983) have described this complication as an indication of the inapplicability of Matthiessen's

rule in this alloy. This terminology is easy to understand if we imagine that structural change takes place at zero temperature. It would then cause a change in the intrinsic resistivity ρ_0 of the alloy. Matthiessen's rule states that the resistivity of the alloy is given by

$$\rho(T) = \rho_0 + f(T)$$

where only ρ_0, and not $f(T)$, depends on structural state. In reality though, at least in the case of $Fe_{40}Ni_{40}P_{14}B_6$, $f(T)$ is also affected by structural change and Matthiessen's rule is invalid.

Structural relaxation is in general the sum of simultaneous changes in more than one type of order. (The large body of experimental evidence for this assertion is considered in chapter 7.) Therefore, we cannot expect to be able to represent relaxation effects by changes in a single order parameter. In particular, reversible and irreversible ordering may affect $R(T)$ in opposite senses, as will be demonstrated below; the two effects must therefore be described by at least two different order parameters.

In the as-received state, the atomic structure of a metallic glass is likely to be very different from the

structure it will adopt after a long anneal at a high temperature because the disorder of the melt from which the glass is quenched will be in part frozen-in to the solid. Annealing a glass in its as-received state is therefore expected to give rise to relatively large changes in its physical properties; these changes are expected to be irreversible in the main since the glass cannot be annealed at a temperature high enough to create reversibly the degree of disorder present in the as-received state without undergoing crystallisation. If the irreversible resistance change expected during thermal treatment of an as-received metallic glass at temperature T_A is small or absent, we can conclude that either

(a) the resistance is only very weakly coupled to the order parameter which is changing during the anneal, or

(b) the degree of structural order is approximately equal in the as-received state and the state of equilibrium at T_A.

The sign of the irreversible resistance change, when it exists, is the sign of the differential coefficient $dR(T)/d\alpha_I$ where α_I represents an order parameter which increases irreversibly during structural relaxation of glasses initially in the as-received state. We have

assumed here for the sake of brevity that one order parameter alone is sufficient to describe irreversible structural change. In general we should expect to need more than one such parameter.

Once the irreversible resistance changes characteristic of the as-received state are complete (i.e. when $(1/R)(dR/dt)$ has fallen to some small fraction of its initial value) the long term temperature dependence of structural state can be investigated by annealing at each of a series of temperatures, in the manner illustrated in figure 3.2.1. Most experimenters choose a preannealing temperature higher than the highest of this series in order to hasten the completion of irreversible ordering so that the prestabilisation can be both thorough and brief.

The results of resistometric investigations of reversible structural changes are often summarised by drawing a graph of resistance, at some fixed temperature of measurement, versus annealing temperature T_A, where the glass has been left at temperature T_A until the rate of resistance change has become negligibly small. Figure 3.2.3 is such a graph, taken from the work of Balanzat et al. (1985) on prestabilised $Fe_{40}Ni_{40}B_{20}$. Each point on the graph represents a ten minute anneal. The first anneal was at the highest temperature and the interval between successive anneals was 25K. The detailed interpretation of the graph by Balanzat et al. is

described below; we observe here that its gradient is negative. We emphasize that the property measured by Balanzat is low-temperature resistance.

We can define, along the lines of the irreversible order parameter introduced above, a reversible order parameter α_R, such that α_R decreases during anneals at temperatures higher than that of prestabilisation and increases at lower temperatures. The gradient of the curve in figure 3.2.3 is then opposite in sign to the differential coefficient $dR(T)/d\alpha_R$ of $R(T)$ with respect to changes in α_R. For $Fe_{40}Ni_{40}B_{20}$ we can therefore conclude that

$$\left.\frac{dR}{d\alpha_R}\right|_{4.2K} > 0 \qquad \text{(3.2.1)}$$

The importance of the distinction between reversible and irreversible ordering now emerges; in the same study, Balanzat et al. observed an irreversible decrease in the low temperature resistance of $Fe_{40}Ni_{40}B_{20}$ when it was annealed from its as-received state. Therefore

$$\left.\frac{dR}{d\alpha_I}\right|_{4.2K} < 0 \qquad \text{(3.2.2)}$$

in sharp contrast to equation (3.2.1). Here is firm evidence that reversible and irreversible ordering can be quite distinct in their effects on a single physical property.

Survey of Published Experimental Work

Table 3.2.1 summarises values of resistivity, temperature coefficient of resistance $(1/R)dR/dT$ measured at room temperature, and the signs and magnitudes of the effects of irreversible and reversible structural change on resistance and on t.c.r. for melt-spun amorphous alloys of various compositions. A dash (---) in table 3.2.1 indicates that the value was not measured; measurement temperatures are in brackets where they differ from that specified at the top of the column.

Balanzat et al. (1985) summarise some earlier work and present new results. They annealed samples of metallic glass at each of a series of temperatures, usually for 10 minutes and sometimes for 30 minutes, and measured the low temperature resistance R(4.2K) by quenching the sample in a liquid helium cryostat at the end of each anneal. This technique is known as isochronal annealing because equal time is spent at each temperature.

Balanzat et al. (1985) are concerned primarily with reversible changes and figure 3.2.3 typifies their results. We have observed above that the sign of the gradient of this graph implies that the quantity $(d\Delta R/d\Delta T_A)_{4.2K}$ is negative but we have not yet attempted to interpret the form of the curve. Balanzat et al. explain the form of the curve as follows.

TABLE 3.2.1

Composition	Reference	RESISTIVITY $\rho/\mu\Omega$cm (as-rec. state)	tcr/10^{-4} K^{-1}	$\Delta R/R$ (irrev) (10^{-3})	Δ(tcr) (irrev) (10^{-4} K^{-1})	$\frac{1}{R}\left(\frac{d\Delta R}{d\Delta T}\right)_{REV.}$ (10^{-5} K^{-1})
$Cu_{50}Ti_{50}$	Balanzat et al (1985)	190	-1.0	-	-	-9(4.2K) -4(T_A)
$Ni_{35}Ti_{65}$		290	-2.8	-	-	-5(4.2K) (x1 1/2(T))
$Ti_{50}Be_{40}Zr_{10}$		290	-1.7	-	-	-4(4.2K0 -2(T)
$Cu_{40}Zr_{60}$		170	-0.9	-	-	-4(4.2K) (x1 1/2(T))
$Fe_{40}Ni_{40}B_{20}$		130	+3.6	-	-	-2.3(4.2K)
$Fe_{40}Ni_{38}Mo_4B_{18}$		155	+2.3	-	-	-4(4.2K)
$Co_{58}Ni_{10}Fe_5Si_{11}B_{16}$		130	+1.6	-	-	-10(4.2K)
$Fe_{41}Co_{31}Si_{10}B_{12}$		-	+1.8	-	-	-1(4.2K)
$Fe_{81.5}B_{14.5}Si_4$		-	+1.2	-	-	+1.1(4.2K)
$Ni_{24}Zr_{76}$	Hillairet et al (1984)	165	-1.1	-ve(4.2K)	-	≈-2(4.2K)
$Fe_{40}Ni_{40}P_{14}B_6$	Balanzat (1980)	185	+2.1	-ve(4.2K)	-	-3(4.2K)

TABLE 3.2.1 (cont.)

Composition	Reference	$\rho/\mu\Omega$cm	tcr/10^{-4} K^{-1}	$\Delta R/R$ (irrev) (10^{-3})	Δ(tcr) (irrev) ($10^{-4}K^{-1}$)	$\frac{1}{R}\left(\frac{d\Delta R}{d\Delta T_A}\right)_{REV}$ (10 K)
$Pd_{80}Si_{20}$	Balanzat et al (1985)	80	+0.9	-	-	0(4.2K)
$Pd_{78}Ge_{22}$		-	+0.8	-	-	≈-2(4.2K)
$Fe_{80}B_{20}$		130	+1.6	-	-	0(4.2K)
$Fe_{40}Ni_{40}P_{14}B_6$	Cost and Stanley (1982)	-	+2	-	-	+3.5(T)
$Fe_{80}B_{20}$		-	+1.5	-ve(T)	-	0(T)
$Pd_{82}Si_{18}$	Kelton and Spaepen (1982, 1984)	74	+1.53	-3.8(T)	+0.08	≤-1(40°C)
$Pd_{81}V_1Si_{18}$		78	+0.72	-0.9(T)	≈0	-
$Pd_{80}V_2Si_{18}$		108	+0.30	+1.5(T)	-0.04	-
$Pd_{76}V_6Si_{18}$		166	-0.36	+4.3(T)	-0.03	-
$Pd_{74}Au_8Si_{18}$		103	+0.79	-5.1(T)	+0.06	-
$Pd_{70}Fe_{12}Si_{18}$		144	+0.37	+0.9(T)	-0.03	-
$Pd_{69}Fe_{13}Si_{18}$		153	+0.48	-0.9(T)	~0	-
$Pd_{77.5}Cu_6Si_{16.5}$		82	+1.23	-5.8(T)	+0.05	-
$Co_{90}Zr_{10}$		105	+0.89	-8.3(T)	+0.10	-
$Ni_{30}Zr_{70}$		172	-1.21	+14.2(T)	-0.05	-
$Ni_{39}Fe_3Zr_{58}$		178	-1.14	+8.0(T)	-0.05	-
$Pd_{79}V_3Si_{18}$	Lin et al. (1979)	-	qualitative agreement with above results on $Pd_{82-x}V_xSi_{18}$			
$Pd_{78}V_2Si_{18}$		-				
$Pd_{80.54}Sb_{1.41}Si_{17.75}$	Marcus (1979)	-	+0.945	-10(T)	-	-

TABLE 3.2.1 (cont.)

Composition	Reference	$\rho/\mu\Omega$cm	tcr/$10^{-4}K^{-1}$	$\Delta R/R$ (irrev) (10^{-3})	Δ(tcr) (irrev) ($10^{-4}K^{-1}$)	$\frac{1}{R}\left(\frac{d\Delta R}{d\Delta T_A}\right)_{Rev.}$ ($10^{-5}K^{-1}$)
$Fe_{40}Ni_{40}B_{20}$	Woldt (1986) Woldt & Leake (1985)	-	+ 4 (annealed state)	$-5(T_A)$	-	$-1.1(T_A)$
$Fe_{40}Ni_{40}B_{20}$	van den Beukel (1986)	104*	+4.3	$\approx-3(T_A)$		$\approx+1(T_A)$
$Fe_{40}Ni_{40}B_{20}$	Kokmeijer et al. (1987)	-	-	-	-	$-3.5(T_A)$ $+1.2(77K)$
$Fe_{40}Ni_{40}P_{14}B_6$	Sonius et al. (1983)	154*	+1.9*	+ve(T_A)	-	$+2(T_A)$
$Fe_{40}Ni_{40}P_{20}$	Majewska-Glabus and Thijjse (1975)	162 (*Mizutani 1983)	+1	$+7(T_A)$	-	$\approx0(T_A)$
$Fe_{67}Ni_{19}B_{14}$	Allia et al. (1982)	-	+3.33	$-5(T_A)$	+0.52	-
$Fe_{60}Ni_{24}Mo_2B_{14}$		-	+0.80	$-1.5(T_A)$	+0.14	-
$Fe_{59}Ni_{23}Mo_4B_{14}$		-	+0.73	$-1.5(T_A)$	+0.24	-
$Fe_{54.5}Ni_{21.5}Mo_{8.5}B_{14.5}$		-	+0.31	$-1(T_A)$	+0.19	-
$Fe_{75}Ti_5B_{20}$	Riontino & Marino (1984)	-	+0.8	+0.8	-	-
$Fe_{75}V_5B_{20}$		-	+0.5	+0.2	-	-
$Fe_{75}Cr_5B_{20}$		-	+0.5	+0.3	-	-
$Fe_{75}Mn_5B_{20}$		-	+0.6	+0.6	-	-
$Fe_{80}B_{20}$		-	+1.6	-1.5	-	-
$Fe_{75}Co_5B_{20}$		-	+1.8	-0.8	-	-
$Fe_{75}Ni_5B_{20}$		-	+1.7	-0.4	-	-

TABLE 3.2.1 (cont.)

Composition	Reference	$\rho/\mu\Omega$cm	tcr/10^{-4} K^{-1}	$\Delta R/R$ (irrev) (10^{-3})	Δ(tcr) (irrev) ($10^{-4}K^{-1}$)	$\frac{1}{R}\left(\frac{d\Delta R}{d\Delta T}\right)_{rev.}$ ($10^{-5}K^{-1}$)
$Fe_{86}B_{14}$	Riontino et al. (1984)	-	-	-1	-	-
$Fe_{30}Ni_{36}Cr_{14}P_{14}B_6$	Riontino et al. (1984)	-	-	-1	-	-
$Ni_{36}Fe_{32}Cr_{14}P_{12}B_6$	Mulder et al. (1981)	-	+0.2	-2	-	-ve
$(Fe_xNi_{1-x})_{78}Si_8B_{14}$	Komatsu et al (1984)	-	-	-	-	>0 ($x \geq 30$) (77K) <0 ($x \leq 30$) (77K)
$(Co_{75}Fe_{25})_{75}Si_{10}B_{15}$	Komatsu et al (1986)	-	-	-	-	-7
$Ni_{72}(Si_{0.25}B_{0.75})_{28}$	Yokota et al. (1985)	103	+0.9	-1.2(77K)	+0.01	-
$Ni_{70}(Si_{0.25}B_{0.75})_{30}$		120	+0.5	+0.6(77K)	0	-
$Ni_{68}(Si_{0.25}B_{0.75})_{32}$		125	+0.1	+2.0(77K)	-0.01	-
$Ni_{66}(Si_{0.25}B_{0.75})_{34}$		150	-0.2	+3.2(77K)	-0.03	-
$Cu_{30}Zr_{70}$	Chen, Croxon & Gr g (1986)	-	-0.8	+11(T)	~0	-
$Cu_{60}Zr_{40}$		-	-0.9	+44(T)	~0	-
$Fe_{40}Ni_{38}Mo_4B_{18}$	Keupers et al (1985)	-	+1.6	-5(300K)	~0	-1.6(300K)
$(Mo_{0.6}Ru_{0.4})_{100-x}B_x$ ($x < 14, 18, 22$)	Schulz et al. (1985)	-	-0.9	+10(T_A)	-	-

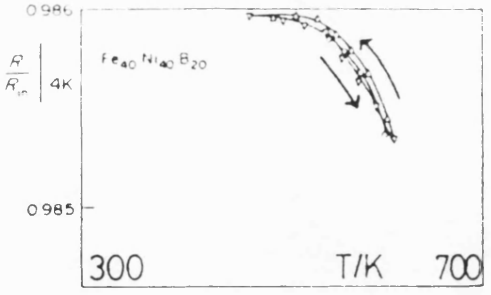

Figure 3.2.3: R(4.2K), normalised to its as-received value, as a function of the temperature of successive ten-minute anneals (Balanzat et al. 1985, $Fe_{40}Ni_{40}B_{20}$)
∧ sequence of increasing annealing temperatures
∨ decreasing

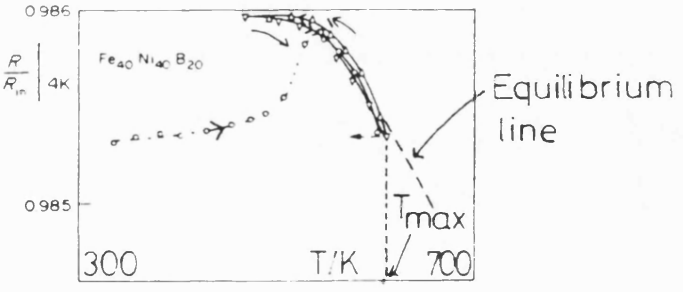

Figure 3.2.4: as figure 3.2.3 with extra annealing sequence

The high temperature region of the curve is a straight line called the 'equilibrium line' because 10 minute anneals at these temperatures are sufficiently long for the structure to reach its equilibrium state. The use of the word 'equilibrium' by Balanzat et al. and by others might seem to suggest that the atoms are arranged in their most stable state. This is not so. The true equilibrium state is the crystalline phase in which the collective free energy of the atoms is minimised. However, the idea of a temperature-dependent local equilibrium state in a region isolated kinetically from the true equilibrium (crystalline) state is a useful one which we will define more carefully in the course of kinetic analysis in chapter 8.

At lower temperatures, the 10 minute anneals are too short to allow local equilibration. The curve starts to depart from the equilibrium line and becomes flat where the temperature is too low to allow appreciable structural change within a 10 minute anneal. Figure 3.2.4 illustrates this point.

The dotted line in figure 3.2.4 shows a variation on the experimental regime outlined above. The sample is preannealed for 30 minutes at temperature T_{MAX} and then annealed at each of a series of lower, increasing temperatures. The line starts to curve up towards the extrapolated equilibrium line (shown dashed) as mobility increases. Only when mobility is high enough for local

equilibrium to be attained within 10 minutes does the curve join the equilibrium line.

Balanzat et al. also examine the effects of irreversible structural relaxation, seen in as-received samples, on electrical resistance. Figure 3.2.5 shows their results for $Cu_{50}Ti_{50}$. The part of the curve labelled 1 represents reversible structural change and is interpreted in the same way as the dashed line of figure 3.2.4. The reversible contribution to structural change is simliar to that seen in a sample preannealed at a high temperature, because disorder characteristic of the molten alloy is frozen-in, partly reversibly, to the as-received sample. The curve reaches a maximum point and then drops sharply due to the onset of irreversible structural ordering which, in this alloy, appears to affect the 4.2K resistance in the opposite sense to the effect of reversible ordering, as it did in $Fe_{40}Ni_{40}B_{20}$ also. The decrease in resistance due to irreversible structural relaxation continues beyond the bottom of the graph; meanwhile, reversible effects can be seen by reversing the progression of anneal temperatures. Sections 2 and 3 of the curve of figure 3.2.5, which interrupt the continuing irreversible decrease in resistance, are similar to the equilibrium line of figure 3.2.3. Section 4 of the curve represents the same thermal treatment as the dashed curve of figure 3.2.4 and they are of the same form.

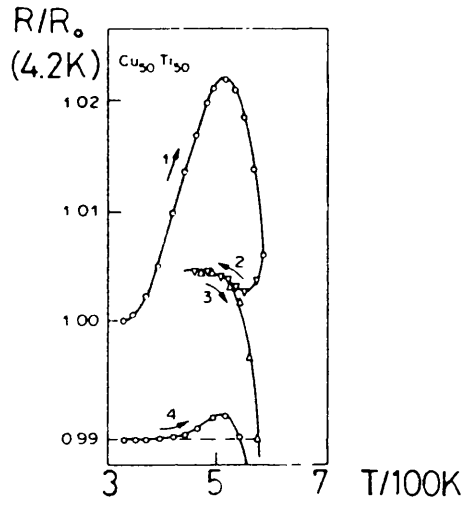

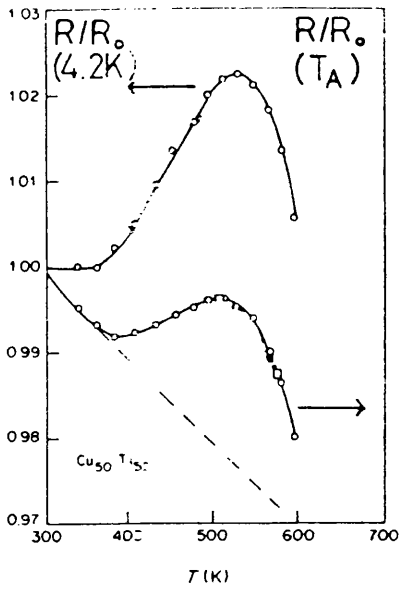

3.2.5 3.2.6

Figure 3.2.5: effect of irreversible structural relaxation in as-received $Cu_{50}Ti_{50}$ on electrical resistance (Balanzat et al. 1985)

Figure 3.2.6: comparison of the effects of structural relaxation or resistance measured at low temperature and at the annealing temperature of $Cu_{50}Ti_{50}$ in the as-received condition (Balanzat et al. 1985)

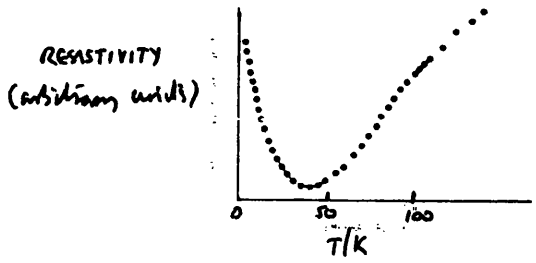

Figure 3.2.7: the highly non-linear dependence of resistivity on temperature in $(Fe_{0.2}Ni_{0.8})_{75}P_{16}B_6Al_3$ (Gudmundsson et al. 1983)

Not all of the measurements made by Balanzat et al. (1985) were at low temperature. They also investigated the effects of identical treatments on the resistance measured at the anneal temperature. Figure 3.2.6 shows a set of results, again for $Cu_{50}Ti_{50}$. In this case the form of the two sets of curves is similar; the high temperature resistance change appears to be the sum of a component similar in its temperature-dependence to that seen at low temperature and a linear correction for measurement temperature, shown as a dashed line in the figure. The effect of structural change (the difference between the full curve and the dashed straight line in figure 3.2.6) is smaller though, when expressed as a fractional resistance change per unit change in annealing temperature, than the effect at low temperatures; the differences between low and high temperature measurements are summarised in more detail immediately below. Balanzat et al. do not report the effect of thermal treatments on the resistance of $Fe_{40}Ni_{40}P_{14}B_6$ at the anneal temperature; we would expect, in the light of the result of Cost and Stanley (1982) quoted above, to see a difference in sign between the gradient of the equilibrium line determined at low temperature and that of the equilibrium line determined at the anneal temperature.

We now summarise the findings of Balanzat et al. (1985). They studied binary metal alloys (e.g. $Cu_{50}Ti_{50}$),

multimetal-metalloid alloys (e.g. $Fe_{40}Ni_{40}B_{20}$) and monometal-metalloid alloys (e.g. $Pd_{80}Si_{20}$, $Fe_{81.5}B_{14.5}Si_4$) and found that in alloys containing more than one metallic species, the equilibrium line, determined at 4.2K, always had a negative gradient. This conclusion, which appears to apply whether metalloids are present or not, implies that reversible ordering increases the resistance measured at 4.2K in these multimetal alloys. In the glasses $Pd_{80}Si_{20}$ and $Fe_{80}B_{20}$, no reversible effects can be seen. In amorphous $Fe_{81.5}B_{14.5}Si_4$, the reversible effect is of opposite sign to that in the multimetal alloys; the equilibrium line has a positive gradient, implying that the reversible ordering decreases the resistance, measured at 4.2K. In $Pd_{80}Ge_{20}$ however, the reversible effect is of the same sign as that in the multimetal alloys, with reversible ordering causing a decrease in resistance as measured at low temperature. Balanzat et al. compare these results with the effect of reversible chemical short range ordering on the 4.2K resistance of crystalline disordered alloys. These alloys, like crystalline metallic elements, have long range topological order; above a critical temperature, they lack long range chemical order and show a temperature-dependent degree of chemical short range order. The effect of chemical short range ordering (CSRO) on low temperature electrical resistance in crystalline alloys is somewhat larger in magnitude than the effect of reversible short range ordering on the low

temperature resistance of the metallic glasses studied by Balanzat et al. and can be of either sign. The results on crystalline disordered alloys were obtained in experiments similar to those of Balanzat et al. (1985) by Balanzat and Hillairet (1981), Balanzat, Halbwachs, Hillairet, Mairy, Guyot and Simon (1983) and Pierron-Bohnes, Mirabeau, Balanzat and Cadeville (1984).

The magnitude of the effect of reversible ordering on the resistance measured at the annealing temperature was found to be about half that of the effect on resistance measured at 4.2K in the amorphous alloys $Cu_{50}Ti_{50}$ and $Ti_{50}Be_{40}Zr_{10}$. 'Similar results' were obtained for $Ni_{35}Ti_{65}$ and for $Cu_{40}Zr_{60}$; i.e. in all four metalloid-free compositions, the effect of a reversible increase in order is to increase the resistance measured at 4.2K and to increase, but by a smaller fraction, the resistance measured at the annealing temperature.

The comparable result for $Fe_{40}Ni_{40}B_{20}$, already quoted above, is that the effects of a reversible increase in order are to increase the resistance measured at 4.2K but to decrease the resistance measured at the annealing temperature. Balanzat et al. do not indicate how the measurements made at the annealing temperature compared with the measurements made at 4.2K in the other compositions they studied.

Balanzat et al. interpret the measurements made at the annealing temperature as follows. Write the resistance $R(T_A)$ at the annealing temperature as

$$R(T_A) = R(4.2K\ (1 + \bar{\alpha}(T_A - 4.2K)))$$

where $\bar{\alpha}$ is the average temperature coefficient of resistance over the range of temperature between 4.2K and T_A. The effect of a reversible increase in order is then to increase R(4.2K) and to decrease $\bar{\alpha}$, according to Balanzat et al. This interpretation provides a valuable mnemonic for the results in the five alloys studied but the average temperature coefficient of resistance $\bar{\alpha}$ is not related obviously to any fundamental parameter. In general R is not a linear function of T over this wide temperature range so the temperature coefficient of resistance, (1/R)dR/dT varies with temperature, changing sign at temperatures of a few K in many magnetic metallic glasses. Figure 3.2.7 for example shows the minimum point in the resistivity of $(Fe_{0.2}Ni_{0.8})_{65}P_{16}B_6Al_3$ at about 40K as measured by Gudmundson, Rao, Astrom and Chen (1983).

The effect of reversible ordering on the resistance of $Fe_{40}Ni_{40}P_{14}B_6$ at 250°C is the subject of an experimental study by Cost and Stanley (1981, 1982). They pre-

annealed each sample at a 'quench temperature' in the range 230°C to 270°C until no further resistance change was detectable and then quenched rapidly to 250°C and monitored the isothermal resistance change. A typical result is shown in figure 3.2.8; the graph is of the type sketched in figure 3.2.1, but with $R_1(T)$ in figure 3.2.1 lying below $R_2(T)$ instead of above it. The straight lines labelled $R_{ISOSTRUCTURAL}$ by Cost and Stanley in figure 3.2.8 correspond to lines such as AB in figure 3.2.1. The line labelled $R_{EQUILIBRIUM}$ corresponds to a straight line drawn through AC in figure 3.2.1.

Figure 3.2.8 shows the effect of quenching to 250°C after preannealing at each of two different 'quench temperatures'. The effect of annealing 20K above the quench temperature (reversible disordering) is an increase in R(250°C) of .070%; the effect of annealing 10K below the quench temperature is a decrease in R(250°C) of .035%. Cost and Stanley note that the magnitude of the total reversible isothermal resistance change at 250°C is proportional to the difference between the anneal temperature and the quench temperature. This fact will be of importance in one of the arguments put forward in chapter 8.

Quenching to a low measurement temperature, in the manner of Balanzat et al. (1985) is the method used by Kelton and Spaepen (1984) to investigate the effects on

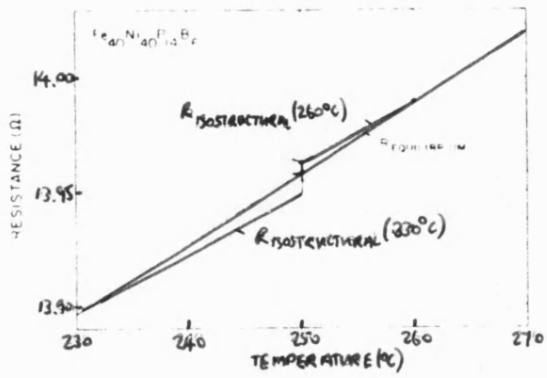

Figure 3.2.8: the effect of reversible ordering on the electrical resistance of $Fe_{40}Ni_{40}P_{14}B_6$, measured at the anneal temperature by Cost and Stanley (1982)

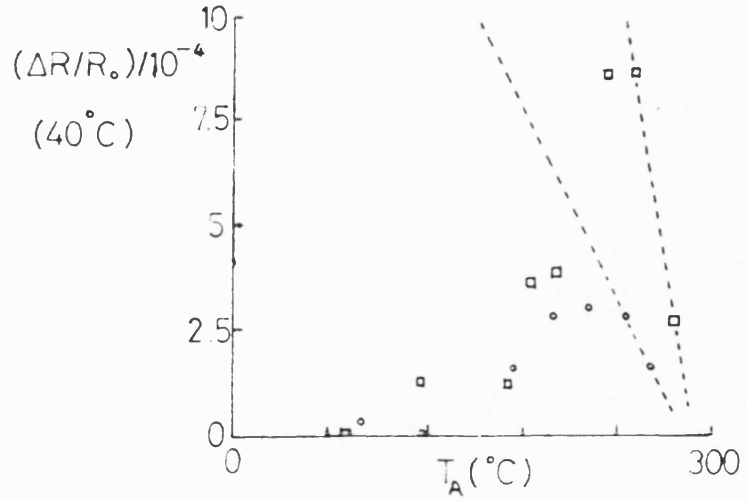

Figure 3.2.9: preannealed $Pd_{82}Si_{18}$; the effect of isochronal annealing on resistance as measured at 40°C (Kelton and Spaepen 1982)
o 15-minute anneals
□ 30-minute anneals

resistance of reversible ordering in $Pd_{82}Si_{18}$. Their measurement temperature is 40°C and their isochronal annealing programme comprises successive 15 or 30 minute anneals at increasing temperatures. The results are shown in figure 3.2.9. The original label '$\Delta\rho$' on the vertical axis has been changed to '$\Delta R/R_0$' for the reasons set out in the preamble to this review.

The extrapolated dashed lines in figure 3.2.9 are similar in form to the dashed equilibrium line in figure 3.2.4 but the random errors in relative resistance change appear to be too large (of order 2.10^{-4}) to allow any reliable estimate of the gradient of the equilibrium line to be made. We can estimate that its order of magnitude is $-10^{-5}K^{-1}$.

Kelton and Spaepen (1982, 1984) also investigated the effects of irreversible structural relaxation on the resistance of various metallic glasses at the annealing temperature. Their results are comprehensive; they record the resistivity and temperature coefficient of resistance (t.c.r) of the alloys, both properties being measured at room temperature, and they determine the effect of isothermal anneals on the resistance at the annealing temperature and on the room temperature t.c.r.

These results are all summarised in table 3.2.1; those for the PdVSi glasses are shown graphically in figure 3.2.10 because of their special relevance to the

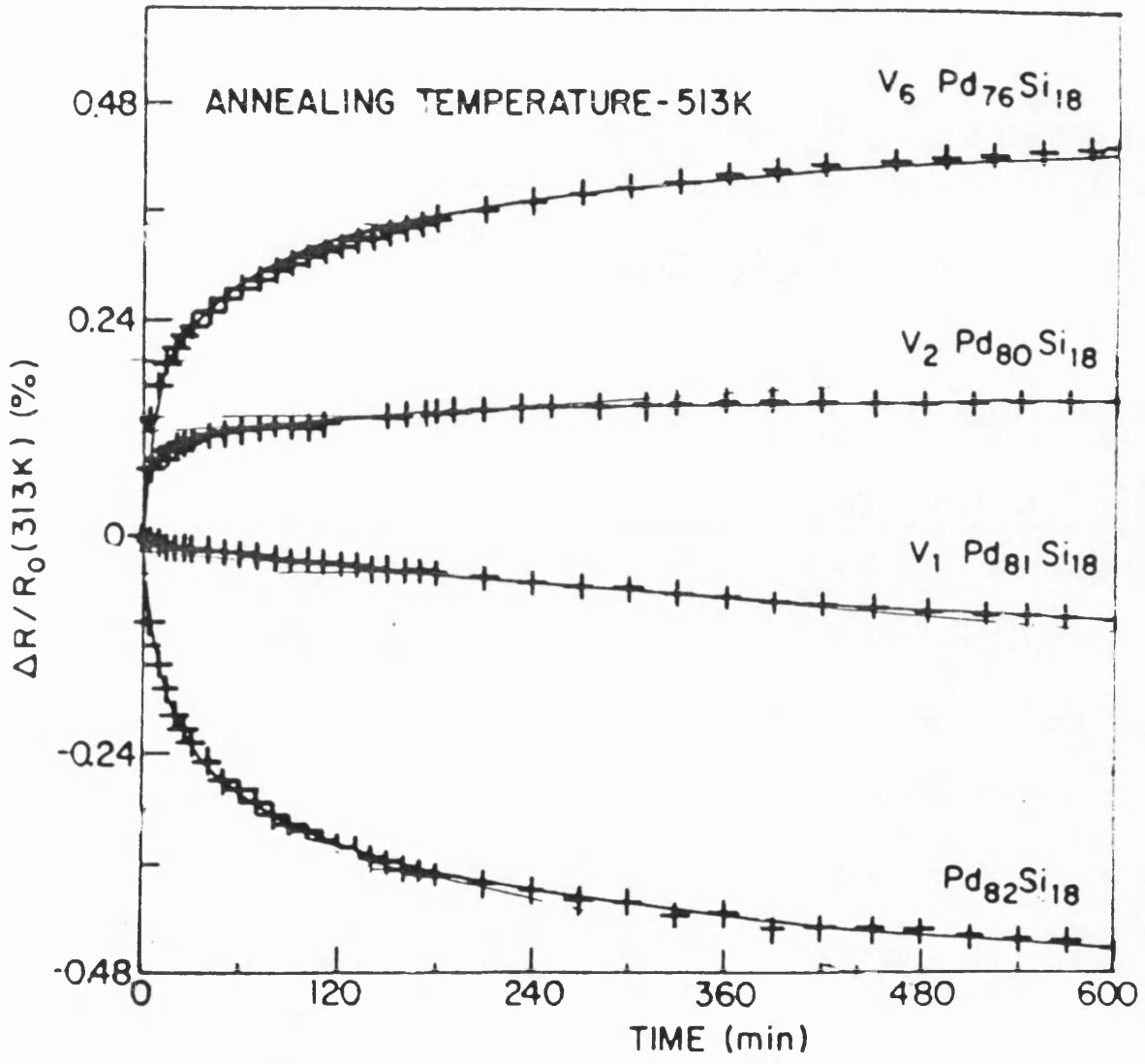

Figure 3.2.10: PdVSi glasses; irreversible resistance changes measured at the annealing temperature, 513K, and normalised to the initial resistance at 313K (from Kelton and Spaepen 1984)

experimental results presented in section 3.4. This set of results illustrates how sensitively the relation between structural change and resistance change can depend on composition. The glasses are of composition $Pd_{82-x}V_xSi_{18}$ with x = 0, 1, 2, 6. Between x = 1 and x = 2, the sign of the irreversible change in resistance seen in as-received samples changes from negative to positive; between x = 2 and x = 6, the t.c.r. changes sign from positive to negative.

Kelton and Spaepen found that the effects of irreversible ordering caused resistance to increase for some compositions and to decrease for others. The t.c.r., they found, could also either increase or decrease. In all compositions showing a measurable change in t.c.r. due to irreversible ordering, this change was found by Kelton and Spaepen to be opposite in sign to the associated irreversible resistance change. Moreover, those compositions showing an increase in resistance on annealing from the as-received state (and therefore showing a decrease, if measurable, in t.c.r.) have values of t.c.r. less than about $5.10^{-5}K^{-1}$ at room temperature in their as-received states. These correlations noted by Kelton and Spaepen are summarised in table 3.2.2. The eleven compositions they studied can also be divided into a group with t.c.r. positive in the as-received state and a second group with t.c.r. negative in the as-received state. Those with negative t.c.r. have room temperature resistivity greater than 160$\mu\Omega$cm; those with positive t.c.r. have room temperature resistivity less than

Table 3.2.2

Correlations in some properties of eleven metallic glasses studied by Kelton and Spaepen (1984)

Room temperature t.c.r. in as-received state	change in resistance at the anneal temperature due to irreversible ordering	change in room temperature t.c.r. due to irreversible ordering
$\lesssim 5.10^{-5}K^{-1}$	< 0	$\gtrsim 0$
$\gtrsim 5.10^{-5}K^{-1}$	> 0	$\lesssim 0$

160μΩcm. This is an example of the Mooij correlation. Mooij (1973) established, in experiments on fifteen bulk crystalline disordered binary alloys, one hundred thin-film crystalline disordered binary alloys and eleven amorphous binary alloys, that a correlation exists between resistivity and t.c.r. in disordered metallic systems, especially concentrated disordered alloys, containing at least one transition metal. They show a low t.c.r., resistivity of order 100μΩcm and a tendency for relatively high resistivity (> 200μΩcm) to be associated with negative t.c.r. and for low resistivity (< 100μΩcm) to be associated with positive t.c.r. Mooij attributed this phenomenon to the strength of electron scattering, and suggested that the electronic mean free paths might be close to a lower limit in these alloys.

Kelton and Spaepen (1984) were following up the work of Lin, Bevk and Turnbull (1979) in choosing the $Pd_{82-x}V_xSi_{18}$ series of compositions as the backbone of their study. Lin et al. had showed that $Pd_{79}V_3Si_{18}$ and $Pd_{78}V_4Si_{18}$ fitted qualitatively into the pattern of results described above for x = 0, 1, 2, 6. Both these groups based their experimental designs on the methods of Marcus (1979) who investigated a PdSbSi alloy with positive t.c.r. and found that its resistance, monitored at the anneal temperature, decreased by about 1% during isothermal annealing starting in the as-received state. The decrease in the resistance of amorphous $Fe_{40}Ni_{40}B_{20}$ when annealed from the as-received state was studied by

Woldt (1986) at eight different isothermal annealing temperatures, all measurements being made at the annealing temperature. These results are reproduced in figure 3.2.11.

Woldt also observed a reversible effect at the annealing temperature. An 'equilibrium line' like that of Balanzat et al. (1985) was obtained by referring all resistance measurements to a single temperature, using an empirical estimate of the isostructural t.c.r. The gradient of the equilibrium line is negative but smaller in magnitude than that derived by Balanzat et al. (1985) for the resistance of the same alloy measured at 4.2K.

$$\left.\frac{1}{R}\frac{d\Delta R}{d\Delta T_A}\right|_{T_A} = -1.1 \times 10^{-5}K^{-1} \text{ (Woldt 1986)} \text{----------} \quad (3.2.3)$$

$$\left.\frac{1}{R}\frac{d\Delta R}{d\Delta TA}\right|_{4.2K} = -2.3 \times 10^{-5}K^{-1} \text{ (Balanzat et al. 1985)} \quad (3.2.4)$$

Sonius et al. (1983) observe both reversible and irreversible isothermal resistance changes in amorphous $Fe_{40}Ni_{40}P_{14}B_6$. Their experiments on preannealed samples show that an increase in annealing temperature produces an increase in resistance, as Cost and Stanley (1982) found. This is more evidence for our earlier finding that Mattheissen's rule does not apply.

Sonius et al. interpret the irreversible resistance change associated with the as-received state as the

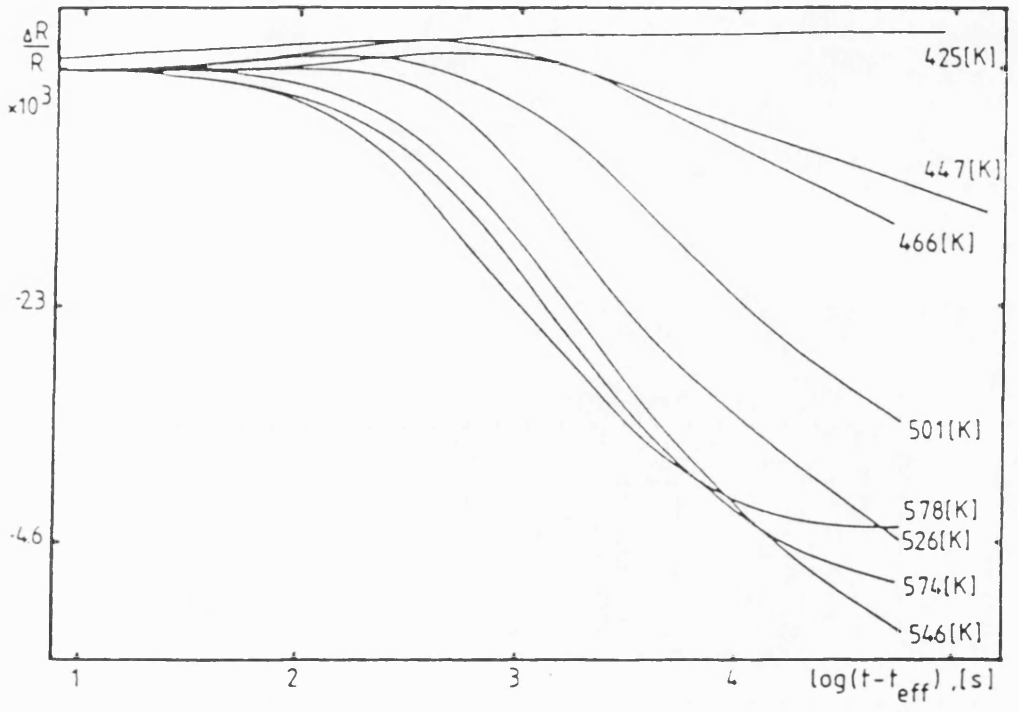

Figure 3.2.11: change in resistance, measured at the anneal temperature, of as-received $Fe_{40}Ni_{40}B_{20}$ during isothermal anneals at each of a series of temperatures (Woldt 1986)

effect of densification of the atomic structure. This interpretation of structural relaxation, known as the free volume model, will be described in detail in chapter 7 below; we outline here some of its elements in order to record an important feature of it pointed out by Sonius et al. (1983).

Associated with each atom in the alloy is an atomic volume; the mean atomic volume is the reciprocal of the atomic number density. The difference between the mean atomic volume and the minimum value of the mean atomic volume when the structure is in its most dense amorphous state is known as the free volume; v_f is defined as the ratio of this free volume to the minimum value of the mean atomic volume and is therefore dimensionless and smaller than one. By fitting a model of the kinetics of the decay of free volume to their observed resistance isotherms, Sonius et al. (1983) were able to estimate how strongly a given change in v_f affects the resistivity in their model. They found that in $Fe_{40}Ni_{40}P_{14}B_6$

$$-3000\mu\Omega cm < \frac{d\rho}{dv_f} < -2000\mu\Omega cm \qquad (3.2.5)$$

This means that a decrease in v_f, the ratio of free volume to minimum volume, of 0.01, say from 10% to 9%, causes an increase in resistivity of between 20 and $30\mu\Omega cm$. The room temperature resistivity of the alloy

in question ($Fe_{40}Ni_{40}P_{14}B_6$) was found (Balanzat 1980) to be about 180μΩcm. We can therefore write

$$-17 < -\frac{1}{\rho}\frac{d\rho}{dv_f} < -11 \qquad (3.2.6)$$

Equation (3.2.6) is important because it provides an estimate of the magnitude of resistivity change which can be explained by densification alone in this model.

Sonius et al. compare their results with those of Mulder, Drijver and Radelaar (1981) who conducted a variety of experiments on $Ni_{36}Fe_{32}Cr_{14}P_{12}B_6$ including isothermal anneals of as-received samples. One of their graphs is reproduced in figure 3.2.12. It shows the resistance, measured continuously at the anneal temperature, normalised to the initial room-temperature resistance value, during an isothermal anneal at 492K of a sample in the as-received state. The dashed line represents measurements taken before the anneal temperature was reached. At the anneal temperature (full line) the resistance at first rises and then starts to fall. Mulder et al. interpret the fall in resistance as the effect of densification. Sonius et al. note that this interpretation implies that a decrease in free volume causes a decrease in resistivity, opposite to what their experiments on $Fe_{40}Ni_{40}P_{14}B_6$ appeared to indicate. If both the fall in resistance of $Ni_{36}Fe_{32}Cr_{14}P_{12}B_6$ and the

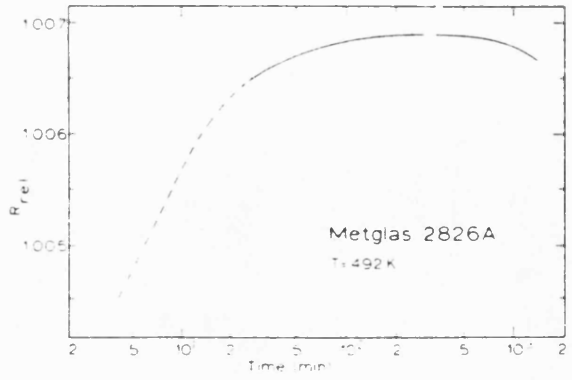

Figure 3.2.12: change in resistance, measured at the anneal temperature, of as-received $Ni_{36}Fe_{32}Cr_{14}P_{12}B_6$ at 492K (Mulder et al. 1980)

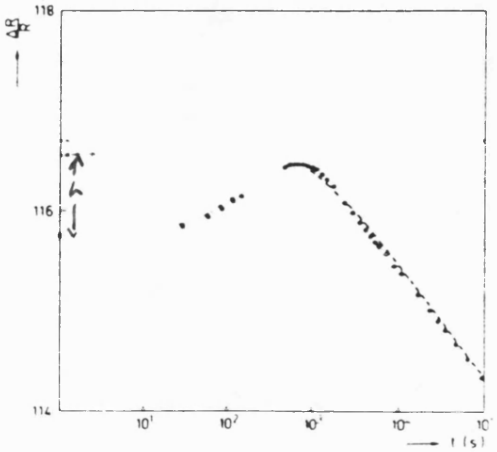

Figure 3.2.13: reversible increase, followed by irreversible decrease in resistance at 578K as reported by van den Beukel (1986) in $Fe_{40}Ni_{40}P_{14}B_6$ after a pre-anneal at 503K.

rise in resistance of $Fe_{40}Ni_{40}P_{14}B_6$ are to be ascribed to the annealing-out of free volume then coupling between free volume change and resistance change in the two alloys must be of different signs. Sonius et al. prefer to ascribe the fall in resistance of $Ni_{36}Fe_{32}Cr_{14}P_{12}B_6$ to clustering of chromium atoms; the initial rise in resistance can then be regarded as the effect of densification. This interpretation is consistent with their own results on $Fe_{40}Ni_{40}P_{14}B_6$ but it does imply that the clustering process is slower than the densification process. The kinetic predictions of the free volume model (chapter 7) rely on the relatively fast completion of compositional ordering compared with densification. If clustering is the cause of the slow decrease in resistance in figure 3.2.12, then it must be quite distinct kinetically from chemical short range ordering.

Mulder et al. (1981) explain the initial rise in resistance which they observe as the effect of reversible ordering. This interpretation is supported by thermal cycling experiments and by experiments on prestabilised samples. They ascribe reversible structural change to chemical short range ordering; this is a theoretical model of structural change in which pairs of chemically unlike atoms swap places leaving the topological structure of the solid unchanged. The resistance changes ascribed to reversible ordering by Mulder et al. (1981) are again, as in the case of irreversible change, opposite in sign to those ascribed to reversible change

by Sonius et al. (1983). The differences between the results of Sonius et al. and those of Mulder et al., the latter as interpreted by Mulder et al. themselves, are summarised in table 3.2.3.

Van den Beukel (1987) reports measurements of changes in resistance of $Fe_{40}Ni_{40}B_{20}$ during annealing, made by H. Melissant. The effect of irreversible structural relaxation is a large decrease in resistance measured at the anneal temperature, of approximate magnitude 0.3%. Reversible ordering appears to lower the resistance (i.e. $d\Delta R(T_A)/d\Delta T_A$ is positive) but the magnitude of the effect is difficult to estimate from the account given by van den Beukel (1987) because only one set of results of measurements on a preannealed sample are included. This one graph is reproduced in figure 3.2.13. It shows the behaviour during an isothermal anneal at 578K of a sample of $Fe_{40}Ni_{40}B_{20}$ preannealed at 503K for 10^6s. The resistance, measured at the anneal temperature, first rises as a result of reversible ordering, then starts to fall as a result of further irreversible ordering. Assuming that the later contributions to the reversible increase in resistance are swamped by the start of the irreversible decrease in resistance, then the height h of the peak as marked on figure 3.2.13 can be used in an estimate of a lower bound on $(1/R)\,d\Delta R/d\Delta T_A$.

$$\frac{1}{R}\frac{d\Delta R}{d\Delta T_A}\bigg|_{T_A} \geq \frac{h}{\Delta T_A} = \frac{7.3 \times 10^{-4}}{75K} = 1.10^{-5}K^{-1}$$

Table 3.2.3

Difference between the effects of reversible and irreversible ordering on resistance, measured at the anneal temperature in two Fe-based amorphous alloys

Composition	Reference	Effect of reversible ordering on resistance at T_A	Effect of irreversible ordering on resistance at T_A
$Ni_{36}Fe_{32}Cr_{14}P_{12}B_6$	Mulder et al. (1981)	↑	↓
$Fe_{40}Ni_{40}P_{14}B_6$	Sonius et al. (1983)	↓	↑

This is an important manipulation because it shows that these measurements disagree with those of Woldt (1986) on the same alloy over the same temperature range (equation 3.2.3). Recent work by Kokmeijer, Huizer, Thijsse and van den Beukel (1987) estimates a value of $-3.5.10^{-5}k^{-1}$ for $(1/R)(d\Delta R/d\Delta T_A)_{TA}$, in approximate agreement with Woldt.

Majewska-Glabus and Thijsse (1985) found that $Fe_{40}Ni_{40}B_{20}$ showed no appreciable reversible change in resistance, measured at the annealing temperature. They saw irreversible resistance changes of about +0.7%. In this study, Majewska-Glabus and Thijsse collected some results on the three metallic glasses $Fe_{40}Ni_{40}B_{20}$, $Fe_{40}Ni_{40}P_{14}B_6$, and $Fe_{40}Ni_{40}P_{20}$ with a view to establishing what effect changes in the ratio of the concentration of the two metalloids have on electrical properties. They found (table 3.2.1) that as the phosphorus concentration increases, the t.c.r. falls and the resistivity increases. This is another example of the Mooij correlation.

At this point, we should emphasize that the presence of a maximum or minimum point in the graph of resistance change versus time for an isothermal anneal of an as-received sample does not necessarily imply the existence of a reversible effect. The initial rise in resistance seen in figure 3.2.12 was identified by Mulder

et al. (1981) as a reversible component by comparison with the results of complementary studies of preannealed samples of the same alloy. In general though, all we can conclude from a graph like figure 3.2.12 alone is that at least two competing effects are present, the faster one being an increase in resistance, the slower one a decrease.

Allia et al. (1982) investigated the effects of isothermal anneals on the resistance, measured at the anneal temperature, of as-received amorphous alloys with compositions $Fe_{67}Ni_{19}B_{14}$, $Fe_{60}Ni_{24}Mo_2B_{14}$, $Fe_{59}Ni_{23}Mo_4B_{14}$ and $Fe_{54.5}Ni_{21.5}Mo_{8.5}B_{14.5}$. One of their aims was to elucidate the effect of the substitution of molybdenum for the other transition metals. They found that the resistance of the alloy containing no molybdenum decreased at each isothermal annealing temperature they tried, the magnitude of the effect being of order 0.5%. On addition of molybdenum though, more complicated behaviour was observed. Figure 3.2.14 for example shows the evolution of the resistance of the alloy containing 4 atom percent molybdenum at a variety of isothermal annealing temperatures.

After long anneals at temperatures higher than 570K, the resistance was found to have decreased in all the alloys containing molybdenum. At temperatures much higher than 570K, this decrease was monotonic, but during anneals at temperatures close to 570K, the resistance increased

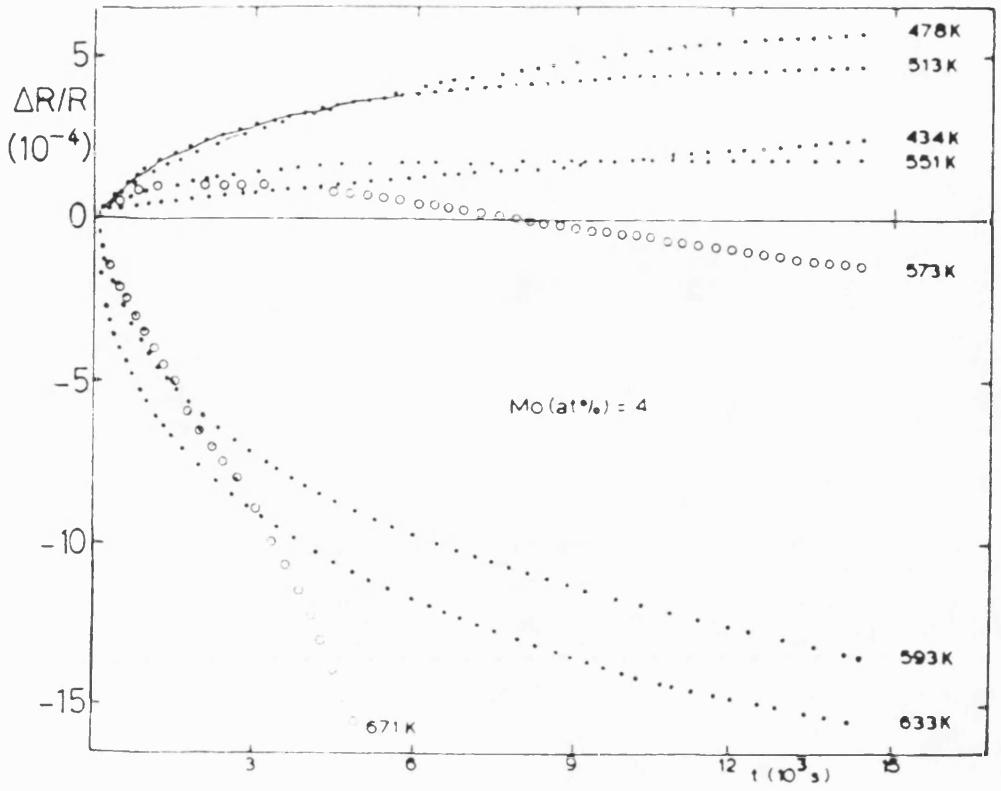

Figure 3.2.14: fractional change in resistance, measured at the annealing temperature, of $Fe_{59}Ni_{23}Mo_4B_{14}$ starting in the as-received state (Allia et al. 1982)

initially and then started to decrease. The curve representing the anneal at 573K in figure 3.2.14 is an example. It is comparable with figure 3.2.12 and the interpretation given by Allia et al. is similar to the interpretation of figure 3.2.12 given by Mulder et al. (1981). The initial increase in resistance is ascribed to irreversible ordering. However, Allia et al. present no results on preannealed samples, so this interpretation is not necessarily correct.

Riontino, Allia and Vinai (1984) conducted a similar study of the metallic glasses $Fe_{86}B_{14}$ and $Fe_{30}Ni_{36}Cr_{14}P_{14}B_6$. The as-received alloy containing nickel, chromium and phosphorus atoms experienced an initial increase in resistance during isothermal anneals, followed by an eventual decrease. The resistance of the $Fe_{86}B_{14}$ alloy decreased monotonically at all temperatures. The substitution of nickel, chromium and phosphorus atoms, largely for iron atoms, therefore appears to be analogous to the substitution, in the $Fe_{67}Ni_{19}B_{14}$ alloy of Allia et al. (1982), of molybdenum atoms for iron atoms. Riontino et al. interpret the initial rise in resistance as evidence of reversible ordering, as Allia et al. did in their similar study, but again no experiments on preannealed samples are reported to support this conclusion.

A systematic study of the effects of the presence of transition metal atoms on structural relaxation, as detected by resistometry, was made by Riontino and Marino (1984). They prepared amorphous alloys of nominal composition $Fe_{75}TM_5B_{20}$ wherein TM represents one of the seven transition metals between and including titanium and nickel in the periodic table of the elements, including iron itself. Figure 3.2.15 shows the effect of isothermal annealing at 72% of the absolute crystallisation temperature on the resistance, measured at the anneal temperature, of as-received samples of each of the seven alloys. Figure 3.2.16 shows the position in the periodic table of these seven transition metals and two of their neighbours.

Riontino and Marino (1984) observe a correlation between the position in the periodic table of the transition metal and the sign of the change in resistance during isothermal annealing at 72% of the absolute crystallisation temperature. Elements lying to the left of the vertical dashed line in figure 3.2.16 all produce alloys which show an increase in resistance in figure 3.2.15. Elements lying to the right of the vertical dashed line correspond to the decreasing curves.

This generalisation is valid also for the results of Allia et al. (1982) on the substitution of molybdenum atoms into an iron- and nickel-based alloy. The results of Riontino et al. (1984) do not lend themselves to a generalisation of this type; nickel, chromium and

phosphorus atoms were used to replace both iron and boron atoms in this work, so no one-for-one substitution can be identified.

Riontino and Marino (1984) interpret the correlation they have observed between position in the periodic table and sign of resistance change by postulating that the increases in resistance they saw are due to 'clustering' of substituent atoms and that clustering is more likely in elements to the left of iron in the periodic table. Riontino et al. (1984) similarly attribute the rise in resistance of $Fe_{30}Ni_{36}Cr_{14}P_{14}B_6$ to clustering of chromium atoms.

Riontino and Marino (1984) suggest that 'clustering' might correspond to chemical short range ordering similar to that seen in crystalline mixed borides containing iron, another transition metal and boron.

In all three of the above papers on the presence of transition metal atoms, the authors identify a decrease in resistance during isothermal annealing with irreversible structural change due to densification and they identify an increase in resistance with reversible chemical short range ordering or clustering. Allia et al. have made this distinction by comparing their results with those of Mulder et al. (1982) but Allia et al. do not prove by experiment that the increases they see are reversible, whereas Mulder et al. do. The increase in resistance seen in alloys containing titanium, manganese,

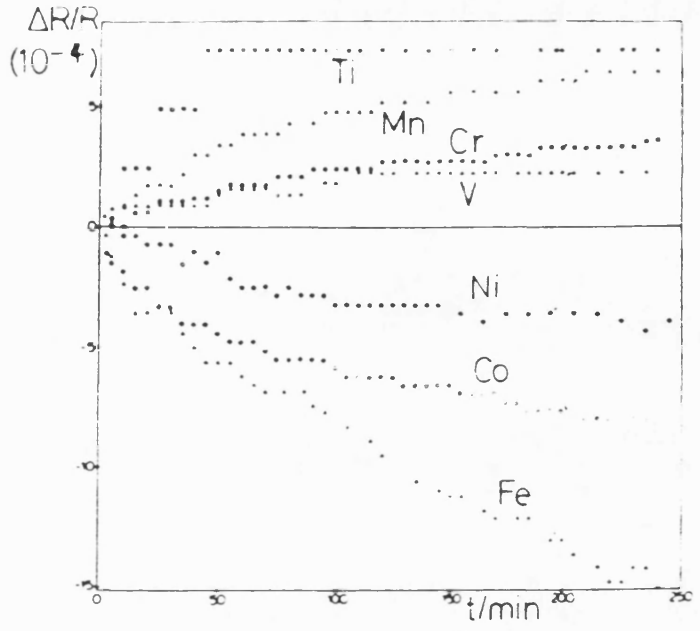

Figure 3.2.15: evolution of electrical resistance of amorphous alloys of nominal composition $Fe_{75}TM_5B_{20}$ in the as-received state during isothermal anneals at 72% of the absolute crystallisation temperature of each alloy (Riontino and Marino 1984)

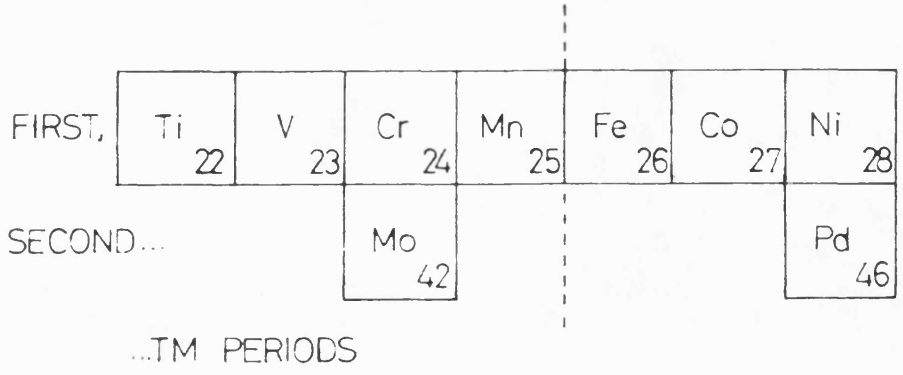

Figure 3.2.16: iron and its adjacent elements in the periodic table, with atomic numbers

chromium and vanadium may be irreversible, and the underlying structural change may be densification rather than chemical short range ordering. The results of Sonius et al. (1983) (table 3.2.3) on amorphous $Fe_{40}Ni_{40}P_{14}B_6$ are witness to this possibility.

The results of Kelton and Spaepen (1982) also suggest caution in labelling as reversible increases in resistance due to the substitution of transition metals in alloys whose resistance otherwise decreases during anneals. Figure 3.2.10 shows how the substitution of vanadium atoms for palladium atoms in $Pd_{82}Si_{18}$ converts the decrease in resistance seen in isothermal anneals of as-received $Pd_{82}Si_{18}$ to an increase. Reference to figure 3.2.16 will show that this substitution produces a composition like those studied by Riontino and Marino (1984), vanadium being to the left, in the "d" block of the periodic table, of palladium, the major metallic constituent. The resistance change results also fit the pattern. Kelton and Spaepen (1982, 1984) do not indicate whether a reversible effect is present in the vanadium-substituted alloys but results to be presented in section 3.4 demonstrate that the reversible effects in $Pd_{80}V_2Si_{18}$ and in $Pd_{81}V_1Si_{18}$ are very small.

Riontino and Marino (1984) measured the room temperature t.c.r. of the $Fe_{75}TM_5B_{20}$ series of alloys, in their as-received states. The values obtained (table 3.2.1)

also demonstrate a marked difference between transition metals on the two sides of the dashed line in figure 3.2.16. The alloys in which TM is to the left of the dashed line (TM=Ti, V, Cr, Mn) each have a small positive t.c.r. of magnitude about 0.8 $.10^{-4}K^{-1}$ or less. In contrast, the alloys in which TM is iron, cobalt or nickel each have a large positive t.c.r. of magnitude 1.5 $.10^{-4}K^{-1}$ or greater. The alloys containing molybdenum (Allia et al. 1982) are in line with this observation (table 3.2.4). Addition of 4 atom percent molybdenum to amorphous $Fe_{67}Ni_{19}B_{14}$ brings down the t.c.r. in the as-received state from 3.3 $.10^{-4}K^{-1}$ to 0.7 $.10^{-4}K^{-1}$. There appears to be a correlation between a small positive t.c.r. and a resistance increase on annealing in the as-received state (TM=Ti, V, Cr, Mn, Mo) and between a large positive t.c.r. and a resistance decrease (TM=Fe, Co, Ni).

Again, comparison with the results of Kelton and Spaepen (1984) confirm this trend (table 3.2.2, first two columns).

Allia et al. (1982) also measured the effect of annealing on the room temperature t.c.r. (table 3.2.4). These results do not fit into the pattern observed above; although t.c.r. varies from +3 $.10^{-5}K^{-1}$ to +33 $.10^{-5}K^{-1}$, the change in t.c.r. on annealing is always positive. Further detailed studies of the effects of changes in composition on structural relaxation have been made by

Table 3.2.4

T.c.r. for annealed and as-received metallic glass ribbons (Allia et al. 1982)

Composition	t.c.r./$10^{-5}K^{-1}$ (as-received)	t.c.r./$10^{-5}K^{-1}$ (annealed)	Δ(t.c.r.)/ $10^{-5}K^{-1}$
$Fe_{67}Ni_{19}B_{14}$	33	39	5.2
$Fe_{60}Ni_{24}Mo_2B_{14}$	8	9	1.4
$Fe_{59}Ni_{23}Mo_4B_{14}$	7	10	2.4
$Fe_{54.5}Ni_{21.5}Mo_{8.5}B_{14.5}$	3	5	1.8

Komatsu, Yokota, Shindo, and Matusita (1984). They make all resistance measurements at a low reference temperature of 77K, and their thermal treatments are isochronal, typically for 30 minutes at each of a series of annealing temperatures 25K apart.

Komatsu et al. (1984) investigate reversible structural changes in a series of alloys of composition $(Fe_xNi_{1-x})_{76}Si_{10}B_{14}$ and find that the gradient $(1/R)d\Delta R/d\Delta T_A$ of the equilibrium line changes sign from negative to positive as x increases through the value 0.3. Komatsu, Sato and Matusita (1986) followed up this work by studying reversible resistance changes in a series $(Co_{1-x}Fe_x)_{75}Si_{10}B_{15}$ of alloys. They found that the equilibrium line is always negative in gradient and that its magnitude takes a maximum value ($(1/R)d\Delta R/d\Delta T_A = -7 .10^{-5}K^{-1}$) as x passes through the value 0.25. Komatsu et al. believe that this fact can be explained by postulating that a structural unit with composition Co_3Fe is responsible for reversible structural change; they calculate the probability of formation of a Co_3Fe unit and show that it takes its maximum value when x = 0.25.

Komatsu and Matusita (1986) develop this theory in more detail in an attempt to explain their observation of a minimum in the irreversible change in length of the series $(Fe_xNi_{1-x})_{78}Si_8B_{14}$ of glasses at the value 0.19 of

x. In alloys containing 25% metalloid, they ascribe reversible structural change characterised by short relaxation times to movements of iron and nickel atoms within a trigonal prism of composition $(Ni_{0.75}Fe_{0.25})_3Me$, where Me represents any metalloid. Reversible structural changes characterised by longer relaxation times they explain as the rearrangements of the trigonal prisms themselves. The minimum observed in an irreversible property change near to x = 0.25 is accounted for, in this model, as follows. The Ni_3Fe trigonal prism is the stable state of short range order toward which irreversible structural relaxation leads. Such units are already prevalent in the as-received alloy with x = 0.25 because of its overall stoichiometry, so there is comparatively little scope for irreversible formation of these structural units in this glass.

Yokota, Tanaka, Komatsu and Matusita (1985) substantiate the Mooij correlation by measuring both the resistivity and the t.c.r. of a series of alloys containing nickel, silicon and boron. This study also provides more evidence that the resistance change upon isothermal annealing is opposite in sign to the change in t.c.r., in as-received samples (table 3.2.2).

In a more wide-ranging study, Komatsu, Matusita and Yokota (1985) found that in $Fe_{27}Ni_{53}P_{14}B_6$, reversible changes in Curie temperature, T_c, were directly

proportional to reversible changes in resistance during isochronal annealing programs. Irreversible changes in T_c and in R were not proportional. Contraction along the length of the ribbons was found, in contrast to ΔR and ΔT_c, to be monotonic and therefore irreversible.

Chen, Croxon and Greig (1986) observed increases in resistance in two copper-zirconium alloys, each having a negative t.c.r., upon annealing in their as-received states. Keupers, De Schepper, Knuyt and Stals (1985) observed an irreversible decrease in the resistance, measured at 300K, of as-received $Fe_{40}Ni_{38}Mo_4B_{18}$ on annealing. The magnitude of the irreversible effect is about 0.5%. A smaller reversible effect, also detected at 300K, was such that annealing at a temperature higher than the prestabilisation temperature caused a decrease in resistance, with $(1/R)d\Delta R/d\Delta T_A = -1.6 \times 10^{-5}K^{-1}$.

Schulz, Mehra and Johnson (1985) found that the metallic glasses $(Mo_{0.6}Rn_{0.4})_{100-x}B_x$ with x = 14, 18, 22 all have negative t.c.r. of approximate magnitude $-9.10^{-5}K^{-1}$ and show an increase in resistance, measured at the anneal temperature, of about 1% on being annealed starting from the as-received state.

Summary of Experimental Findings

1. Changes of dimension during structural relaxation are not negligible. We cannot simply write $\Delta R/R_0 = \Delta\rho/\rho_0$.

2. Reversible and irreversible short range ordering are distinct, in that they can change a single physical property of a particular metallic glass in opposite senses (e.g. resistance measured at 4.2K in $Fe_{40}Ni_{40}B_{20}$ by Balanzat et al. (1985)).

3. Reversible structural change can cause resistance of a metallic glass measured at 4.2K and resistance of the same metallic glass measured at the anneal temperature to change in opposite senses (e.g. in $Fe_{40}Ni_{40}P_{14}B_6$ (Cost and Stanley 1982, Balanzat 1980)). In amorphous alloys containing more than one metallic species, Balanzat et al. (1985) found that reversible ordering always caused an increase in the low temperature resistance. The effect on resistance measured at the anneal temperature was always either a smaller increase or a decrease. The rule of thumb derived by Balanzat et al. is

R(4.2K) increases
average t.c.r. decreases
} with reversible ordering

4. Irreversible structural change can cause resistance of a metallic glass measured at 4.2K and resistance of the same metallic glass measured at the anneal temperature to change in opposite senses (e.g. in $Fe_{40}Ni_{40}P_{14}B_6$ (Sonius et al. 1983, Balanzat 1980)).

5. The irreversible resistance change seen when a metallic glass is annealed from its as-received state appears to be correlated with the room temperature t.c.r. of the same glass in its as-received state (Kelton and Spaepen 1984, Riontino and Marino 1984, Allia et al. 1982, Yokota et al. 1985). When the t.c.r. is less than about $5.10^{-5}K^{-1}$, resistance increases during the anneal; otherwise it decreases (see table 3.2.2). The temperature of measurement ranged from 77K to the anneal temperature in these studies.

   The sign of the irreversible resistance change was also found to be opposite in sign to the associated irreversible change in t.c.r. in these studies. The results of Allia et al. (1982) on alloys containing molybdenum conflict with this generalisation however.

6. Sonius et al. (1983) have interpreted irreversible structural ordering as the annealing out of free volume. They calculated how strongly the fractional resistance change would have to be

coupled to the change in reduced free volume in this model; the result was:

$$-17 \quad < \quad \frac{1}{R}\frac{dR}{dV_f} \quad < -11$$

7. The results of van den Beukel (1987) on reversible resistance changes, detected at the anneal temperature, in $Fe_{40}Ni_{40}B_{20}$ conflict with those of Woldt (1986) and those of Kokmeijer et al. (1987) on the same material; this needs to be resolved. We emphasize that discrepancies such as this in results on prestabilised glasses cannot be ascribed to differences in the production conditions between the two samples of material. The presence of impurities, differences in stoichiometry and the possibility of crystallisation during the anneal could all give rise to such a conflict of results.

8. The substitution for Fe, Co or Ni of one of the d block metals to the left of Fe, Co and Ni in the periodic table appears to reduce the t.c.r. and to change the effect on resistance of annealing from the as-received state. In alloys which would otherwise show a monotonic decrease in resistance on annealing in the as-received state, the effect of such a substitution is to cause the resistance to increase instead, sometimes temporarily, giving way to a slower decrease in resistance after a long time

and sometimes monotonically. This increase can be a reversible effect (Mulder et al. 1981) but need not be (Kelton and Spaepen 1984, together with the results in section 3.4 of this thesis).

9. In metallic glasses containing both Fe and Co and in those containing both Fe and Ni, the approximate stoichiometry

$$(Fe_{0.3}Tm_{0.7})_{75}(Me(1)Me(2)\ldots)_{25}$$

where TM represents Co or Ni and Me(1), Me(2) ... represent different metalloids, is associated with maximum reversible resistance change (Komatsu et al. 1986) and with minimum irreversible resistance change (Komatsu and Matusita 1986). In the latter reference, the authors suggest that a trigonal prism containing Fe and TM in the stoichiometric ratio 1:3 is an important stable structural unit.

3.3 Ziman Theory and Structural Change

According to equation (3.1.1), we need to know the effective scattering time or relaxation time τ in order to calculate the conductivity σ of a metal. Ziman theory obtains an expression for τ in the NFE approximation. For the present purpose of linking structural change to changes in resistance we note that the effective mass m*

of a conduction electron in equation 3.1.1 is equal to the free-electron mass m in the NFE approximation, because the electrons are considered free except during the (instantaneous) collisions. We therefore need to consider only changes in n and in τ when modelling the effects of specific structural changes.

Ziman (1961), in a theory of conduction in simple metallic liquids, derives an expression for the mean free path λ of the electrons

$$\frac{1}{\lambda} = \frac{3\pi}{2\sqrt{2}} E_f^{-3/2} \left(\frac{1}{4k_f}\right)^4 \int_0^{2K_f} |c(K)|^2 \, a(K) \, K^3 dK \quad \text{----------} \quad (3.3.1)$$

where E_f represents the fermi energy, K_f the fermi wave-vector, a(K) the atomic structure factor and c(K) the fourier transform of the total scattering potential. The integration is over K, the magnitude of the scattering vector, related to θ, the angle through which the conduction electron is scattered, by

$$K = 2K_f \sin (1/2)\theta.$$

Ziman assumes, in the derivation of equation (3.3.1), that multiple scattering effects are negligibly small and that each scattering centre scatters elastically and weakly, such that only a small fraction of the incident intensity is scattered (Born approximation).

The form of $|c(K)|^2$ predicted by Ziman for a monovalent liquid metal is sketched in figure (3.3.1). The height $|c(0)|^2$ of the curve at K = 0 is determined according to Ziman by 'plasma scattering'. The pure 'plasma' potential is the dashed curve in figure 3.1.3 and it falls virtually to zero at $K = 2K_f$. The height $|c(2K_f)|^2$ of the curve at $K = 2K_f$ is determined by 'pseudopotential scattering'. These two terms require some explanation.

'Plasma scattering' of electrons is due to fluctuations in the density of atoms throughout the solid. Ziman pictures a 'hole' in a liquid metal, in thermal equilibrium with its surroundings like a vacancy in a crystalline metal; the 'hole' is a region deficient in positive change and it is therefore itself a scattering site. We do not need to consider plasma scattering further, as will be established below.

Resistance due to pseudopotential scattering is the sum of the effects of scattering at each of the atom cores considered independently of the others. We might expect each atom core to be a strong scatterer because each provides a strongly attractive potential well and the conduction electron wave function oscillates rapidly in its vicinity; overall, the conduction electron wave functions resemble the plane waves of NFE theory very little. Pseudopotential theory is a justification of the use of the NFE model in these circumstances. We note that in the Swiss-cheese shaped region between the atom

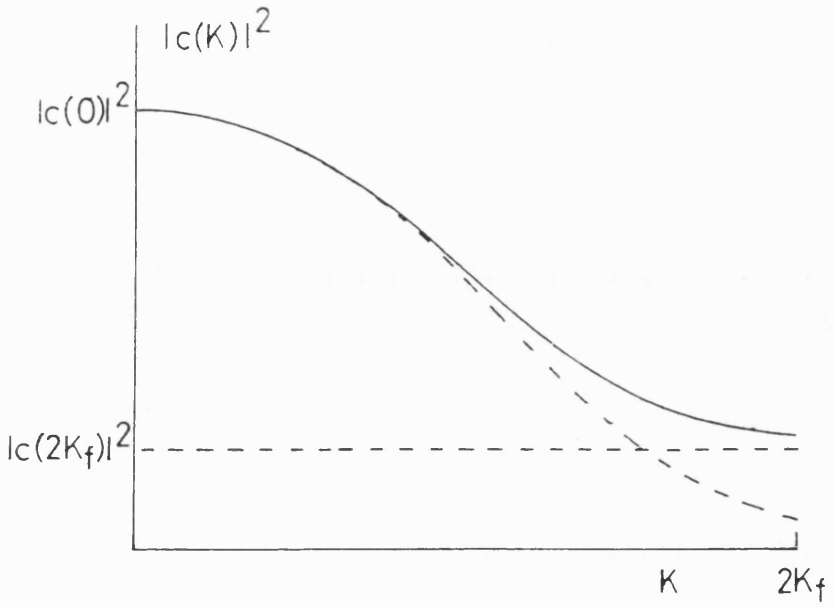

Figure 3.3.1: square of the fourier transform of the scattering potential $|c(K)|^2$ according to Ziman (1961) for a monovalent liquid metal

cores, the wave functions are similar to plane waves because of the screening of the attractive nuclear potential by the core electrons. An electron in a plane-wave state incident on an atom core is therefore scattered by it into some different plane-wave state. Despite the numerous oscillations which the conduction electron wave function in fact undergoes in the vicinity of the atom core, seen from without it appears simply to have changed the phase of the plane wave and its direction. The deeply attractive scattering potential can therefore be represented by a much shallower potential having the same asymptotic effect on an incident plane wave. This weaker potential is the pseudopotential and the magnitude of the pseudopotential determines the term $|c(2K_f)|^2$ in Ziman's theory.

An important feature of the integral in equation (3.3.1) is a strong weighting towards the top limit due to the presence of the term K^3. Any small change in the amount of plasma scattering as a result of structural change therefore affects the conductivity by a negligible amount, compared with the effect of changes in $a(2K_f)$, the value of the structure factor when $K = 2K_f$. Changes in K_f itself and in E_f will also be important and will likewise swamp the effect of any small change in plasma scattering. This insensitivity of σ to changes in plasma scattering explains why the published interpretations of resistometric investigations of structural relaxation

discussed below ignore the effect of plasma scattering altogether.

Ziman's theory has been extended in various directions. Bradley, Faber, Wilson and Ziman (1962) extended it to polyvalent liquid metals and Faber and Ziman (1965) to binary liquid alloys. The use of partial wave theory (Schiff 1968, p. 116) to replace the pseudopotential with a form appropriate to scattering by transition metal atoms (Evans, Greenwood and Lloyd 1971) is particularly important in applying this model to metallic glasses because of the large number of metallic glass compositions which contain a transition metal.

However, Sinha (1970) pointed out that to predict the temperature-dependence of the resistivity of amorphous alloys, detailed knowledge of the atomic scattering potentials is not necessary. By assuming that the position of the first peak of the total atomic structure lies close to $2K_f$ and that this peak broadens and decreases in height with increasing temperature (as observed by Halder, North and Wagner 1969 in liquid CuSn), Sinha was able to explain qualitatively the negative temperature of resistance observed experimentally in a series of NiPtP alloys.

By making the same two assumptions and using in addition the experimentally established fact (Waseda and Egami 1979) that the effect of the large irreversible component of structural relaxation characteristic of the

as-received state is to sharpen the first peak in the structure factor and increase its height, some resistometric studies of irreversible structural relaxation can be consistently explained.

Kelton and Spaepen (1984) interpreted their results on irreversible resistance changes in $Pd_{82-x}V_xSi_{18}$ (x = 0, 1, 2, 6) in this way. They postulate that in $Pd_{82}Si_{18}$, the first peak in the structure factor is at a value of K greater than $2K_f$, and that the substitution of vanadium for palladium does not alter the atomic structure significantly but merely increases $2K_f$. The latter postulate is after a suggestion by Lin, Bevk and Turnbull (1979) that vanadium, with electron configuration $(Ar)3d^34s^2$, gives up more free electrons per atom than palladium, with configuration $(Kr)4d^{10}5s^0$. The positions of the four values of $2K_f$ (x = 0, 1, 2, 6) are shown schematically in figure 3.3.2 by vertical broken lines. The broken curve represents the structure factor in the as-received state and the full curve the structure factor in the relaxed state.

By choosing the positions of the vertical lines carefully, Kelton and Spaepen are able to explain qualitatively their results.

Firstly, they explain the change in sign of the irreversible resistance change between x = 1 (decrease)

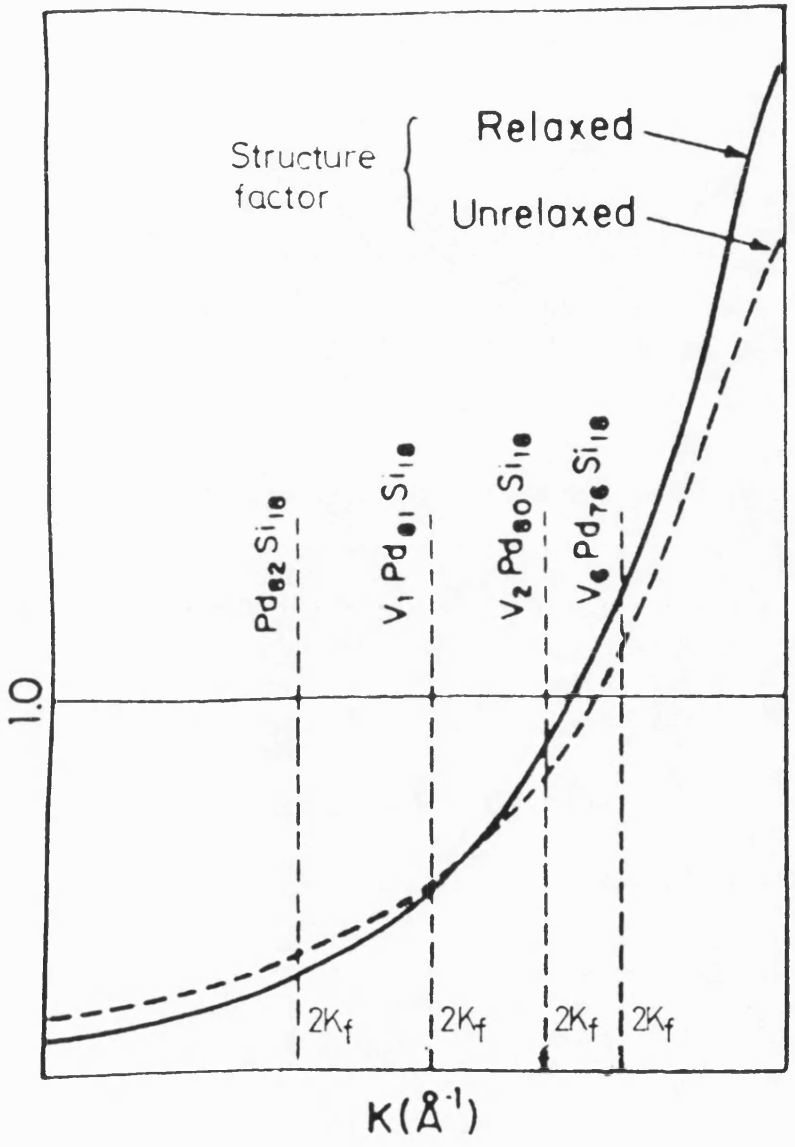

Figure 3.3.2: the structure factor a(K) and values of $2K_f$ in the alloys $Pd_{82-x}V_xSi_{18}$, x = 0, 1, 2, 6 (Kelton and Spaepen 1984)

and x = 2 (increase) by using a much simplified form of equation (3.3.1). They assume that resistivity is proportional to the value of $a(2K_f)$ in Ziman's theory. This amounts to assuming that changes in $a(2K_f)$ are the only important effect, i.e. that

$$\int_0^{2K_f} |c(K)|^2 K^3 a(K)\,dK \propto a(2K_f)$$

making use of the strong weighting of the integral towards its upper limit. Because the relaxed and as-received structure factors cross between the values of $2K_f$ corresponding to x = 1 and x = 2, the model is consistent with a change in the sign of the irreversible resistance change on annealing.

Secondly, Kelton and Spaepen show that a change in sign of the irreversible change in temperature coefficient of resistivity is expected at the same value of x. They use a simple form

$$a(K) = 1 + (a_0(K)-1)e^{-2W(T,K)} \qquad (3.3.2)$$

for the structure factor, where $a_0(K)$ is the static (zero temperature) structure factor and W(T,K) is the Debye-Waller factor. Assuming again that resistivity is proportional to $a(2K_f)$, the temperature coefficient of

resistivity is obtained by differentiating (3.3.2) with respect to T with $K = 2K_f$.

$$\frac{1}{\rho}\frac{d\rho}{dT} = \frac{1 - a(2K_f)}{a(2Kf)} \frac{2dW(T,2K_f)}{dT}$$

The change on annealing of this temperature coefficient is therefore given by

$$\Delta\left(\frac{1}{\rho}\frac{d\rho}{dT}\right) = 2 \frac{dW(T,2K_f)}{dT} \frac{\Delta(a(2K_f))}{(a(2K_f))^2}$$

$$\propto \Delta\rho$$

assuming again that resistivity is proportional to $a(2K_f)$. $\Delta\alpha$ and $\Delta\rho$ must therefore change sign at the same value of x, according to this approximate argument.

Thirdly, by choosing that the ordinate $a(K) = 1$ should pass through both structure factors between the values of $2K_f$ corresponding to $x = 2$ and $x = 6$, Kelton and Spaepen have made their model consistent with the observed change in sign of t.c.r. between $x = 2$ and $x = 6$. This follows from equation (3.3.1); the temperature coefficient of resistivity, which is the t.c.r. to within a few percent, changes sign as $a(2K_f)$ passes through 1.

Yokota, Tanaka, Komatsu and Matusita (1985) have analysed their very similar results on the glasses

$Ni_{100-x}(Si_{0.25}B_{0.75})_x$, x = 28, 30, 32, 34 almost identically.

One very important feature of this interpretation of these sets of results is the assumption that small variations in composition affect *only the electronic structure* of the alloys, and leave the *atomic structure* and its changes during structural relaxation unchanged. This contrasts with the interpretation, e.g. by Riontino and Marino (1984) of their own results on the effect of transition metal substitutions in $Fe_{80}B_{20}$; they and other authors (section 3.2) ascribed the differences in the resistance change seen on annealing to differences in type of structural change.

In conclusion, it should be noted that figure 3.3.2 is by no means a test of the applicability of Ziman's theory because so many of the unknown parameters in it have been chosen in order to fit a single set of results. It has been shown though that this simple theory is not inconsistent with a comprehensive and dramatic set of experimental results.

3.4 Experiments

The electrical resistance of short pieces of metallic glass ribbon with nominal compositions $Pd_{82-x}V_xSi_{18}$, x = 0, 1, 2 was measured during anneals in a furnace. The

ribbons of metallic glass were supplied by Dr. H. A. Davies, University of Sheffield, U.K.

Characterisation of the Ribbon

The absence of crystallinity in the as-received material was confirmed by x-ray diffractometry. Short strips from ribbons of each composition were mounted side by side in the window of an aluminium slide such that they covered an area of roughly $2cm^2$. Both shiny and dull sides were examined in each case. The slide was placed in a Philips diffractometer and a graph of intensity vs. angle of diffraction was obtained using cobalt Kα radiation. The diffraction angle was increased from zero to about 60° at a rate of (1/8)° per minute.

The graphs always comprised diffuse peaks; no sharp peak was observed in any sample other than those crystallised deliberately by heat treatment. The annealing treatments designed to bring about structural relaxation but to avoid crystallisation caused no detectable change in the graph of intensity vs. diffraction angle.

We conclude from these experiments that the ribbons supplied were amorphous, and that they remained so throughout the annealing treatments.

The concentrations of vanadium in the metallic glasses with nominal compositions $Pd_{81}V_1Si_{18}$ and $Pd_{80}V_2Si_{18}$ were

determined by atomic absorption spectrophotometry. In each case, a small known mass of ribbon was dissolved in hot aqua regia; the solution was then made up to a standard volume with distilled water. The concentration by mass of vanadium was detected by a spectrometer calibrated using standard solutions of vanadium, concentrations 1, 2 and 3 ppm. The mass concentration was converted to an atom percentage by assuming that the atom percentage of silicon present was the nominal 18% in both cases. The results are shown in table 3.4.1. Within the 10% error limits of the spectroscopic determination ($\Delta x = \pm 0.01$), the nominal values were confirmed.

The crystallisation of the three metallic glasses was investigated by differential scanning calorimetry (d.s.c.) using a Du Pont calorimeter (9900).

Samples of approximate mass 20mg were heated quickly to 200°C, then the heat flow with respect to an empty sample pan, which served as a reference, was measured during a heating ramp to 450°C at 5K per minute. The heating rate was chosen to be roughly equal to that of about 6K per minute experienced by samples in the resistometric investigations of structural relaxation described below.

The results, graphs of heat flow per unit mass of sample, are shown in figure 3.4.1. For each alloy, the trace is smooth and flat until a sharp peak sets in at between 350°C and 400°C. The peak gets sharper, and the

Table 3.4.1

Concentrations of vanadium in metallic glass ribbons

nominal composition	atomic percentage V
$Pd_{81}V_1Si_{18}$	1.1 ± 0.1
$Pd_{80}V_2Si_{18}$	2.2 ± 0.2

Figure 3.4.1: d.s.c. curves

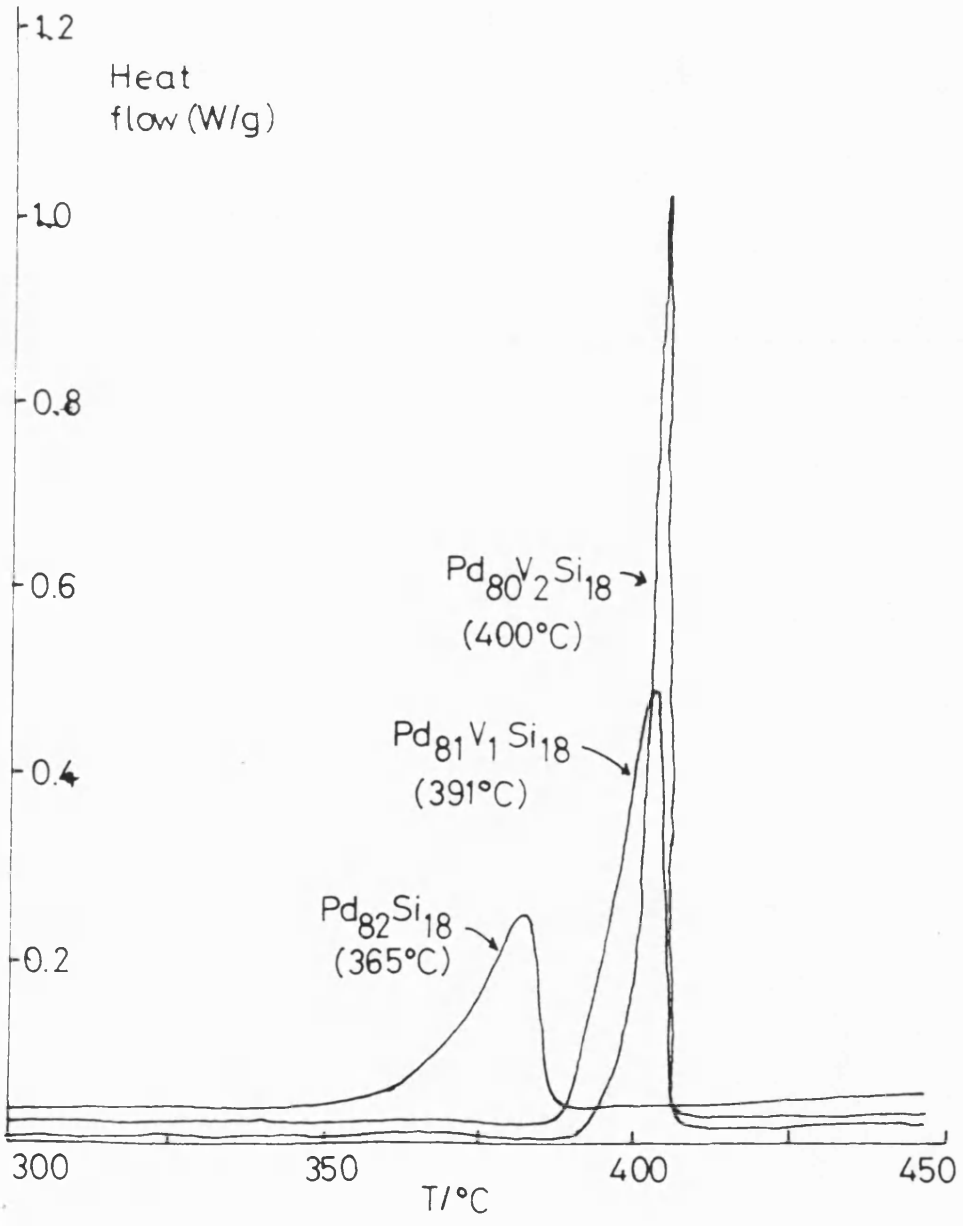

temperature of its onset gets higher, with the addition of vanadium. These peaks show the heat absorbed upon crystallisation. The area under each peak represents the heat of crystallisation and was higher in $Pd_{81}V_1Si_{18}$ and $Pd_{80}V_2Si_{18}$ (47 kJ/kg, 46kJ/kg, respectively) than in $Pd_{82}Si_{18}$ (34 kJ/kg). The temperature of onset of crystallisation (estimated as the abscissa of the intersection of the extrapolations of the leading edge of the peak and of the flat portion to the low temperature side of the peak) depends on heating rate. At 5K per minute the onset temperatures were 365°C, 391°C and 400°C respectively (x = 0, 1, 2); with a lower heating rate of 2K per minute this temperature was reduced by about 10K in $Pd_{82}Si_{18}$.

The thermocouple built in to the calorimeter was calibrated by melting lead and indium (melting points 327.5°C and 156°C respectively) at the same heating rate of 5K per minute.

From figure 3.4.1 we conclude that, in all three compositions, anneals of duration a few minutes at temperatures below about 350°C will not cause crystallisation. The isothermal annealing treatments described below were much longer than this however, and it was necessary to choose a set of annealing temperatures low enough to ensure that crystallisation did not occur, to a degree large enough to modify the

electrical resistance appreciably, for periods of order 1 day. Masumoto and Maddin (1971), in a resistometric study of the crystallisation of $Pd_{80}Si_{20}$, measured an onset time of about 10 hours during an isothermal anneal at 290°C. A pessimistic choice of 250°C for the approximate maximum annealing temperature was made. The highest isothermal annealing temperature used, 253°C, was 27K less than the highest temperature used by Kelton and Spaepen (1984). Kelton and Spaepen saw no resistometric indications of crystallisation.

The absence of any effects due to crystallisation was confirmed by the results (described below). $Pd_{80}V_2Si_{18}$ is a particularly sensitive indicator because crystallisation and structural relaxation affect its resistance oppositely. The irreversible increase in its resistance during the isothermal anneal at 253°C was monotonic throughout (figure 3.4.4) in contrast to the decrease we would expect upon crystallisation in the light of figure 3.4.1.

The crystallisation temperatures and approximate heats of crystallisation of the three alloys, as determined by d.s.c., are summarised in table 3.4.2.

Heating the Metallic Glass

An electronic furnace with high thermal mass was used to provide a high temperature environment in which to anneal

Table 3.4.2

Results of differential scanning calorimetry

Composition	Tx/°C	H(J/g)
$Pd_{82}Si_{18}$	365	34
$Pd_{81}V_1Si_{18}$	391	47
$Pd_{80}V_2Si_{18}$	400	46

the lengths of metallic glass ribbon. The furnace was fitted with a proportional-integral-derivative (p.i.d.) controller which employed a chromel-alumel thermocouple, mounted in the heating block, as its input. The p.i.d. controller is meant to be used to overcome problems with overshoot past the furnace setpoint and oscillations around it. After much experiment, p.i.d. control had to be abandoned because the input thermocouple could not be put sufficiently close to the heating element to allow proper control. Instead, the control unit was used as a simple proportional controller with proportional band 2% of setpoint, measured in degrees celsius. Overshoot was overcome instead by setting the controller to a lower temperature than that required and allowing the input to exceed the set point, causing the controller to cut off. The set point was chosen, using the experience of trial and error, such that the heating curve of the furnace levelled off at the higher, required temperature. At this point, the set point was changed to the required value, and the proportional controller then maintained the temperature at the newly set value to within 1K.

Connections to the sample were delicate and, to avoid unnecessary movement of the sample itself, the furnace was fitted with four rugged non-swivelling castors, in place of the more conventional feet, and rolled into place once the sample had been connected, the castors running in tracks made by bending up the edges of a large aluminium sheet (figure 3.4.2). The heated region was cylindrical, and the stability of the sample temperature

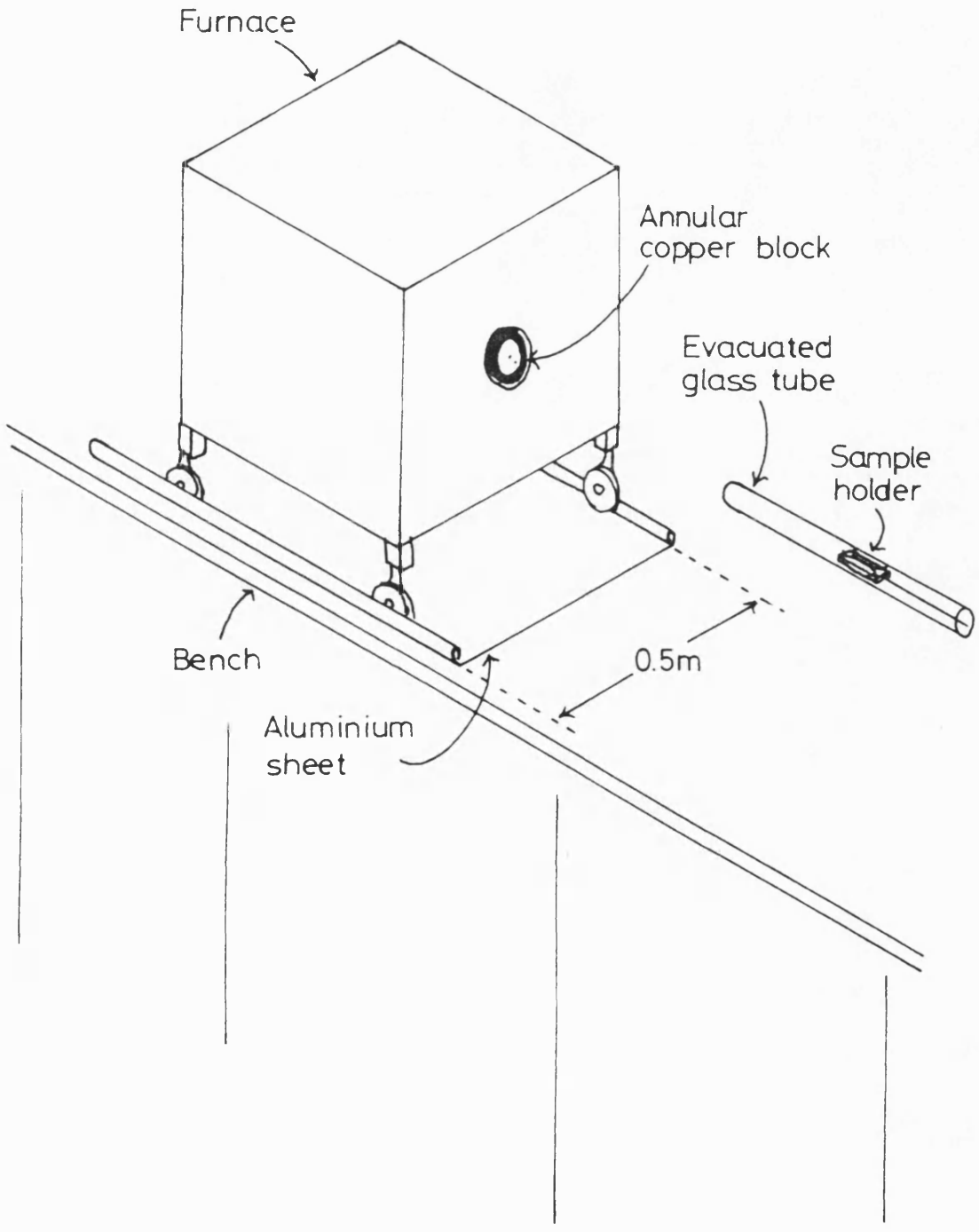

Figure 3.4.2: arrangement of the experiment

was improved by inserting an aluminium block, annular in section, into the cylindrical cavity of the furnace. This block in turn fitted over the glass tube containing the sample when the furnace was wheeled into position. The temperature profile along the inner heated cavity was determined using a thermocouple on a calibrated rod. The temperature was found to be constant, to within 1K, within 10cm of the halfway point. The furnace was always rolled into such a position that the sample and its holder were well within this constant-temperature region.

The glass tube containing the sample was evacuated to a pressure of 5.10^{-2} torr using a rotary pump. This reduction in air pressure was an attempt to prevent unwanted oxidation of the metallic glass during long anneals. This measure was successful; the erratic and unrepeatable behaviour attributed to oxidation in other resistometric annealing experiments, e.g. Marcus (1979) on a PdCuSi alloy, was not seen. Wires from the sample were brought out of the evacuated region through a sealing plug fitted with copper contacts, at the far end of the glass tube from the furnace.

The sample itself was 10 cm long and was cut into the shape required (chapter 2) such that about 6 cm of its length was used as a resistor, the remainder forming contacts. The 'legs' of the sample (figure 3.4.3) were spot-welded to stiff copper wires, held in place by being passed through holes in a ceramic mount as shown in figure 3.4.3. The forward direction of current flow and

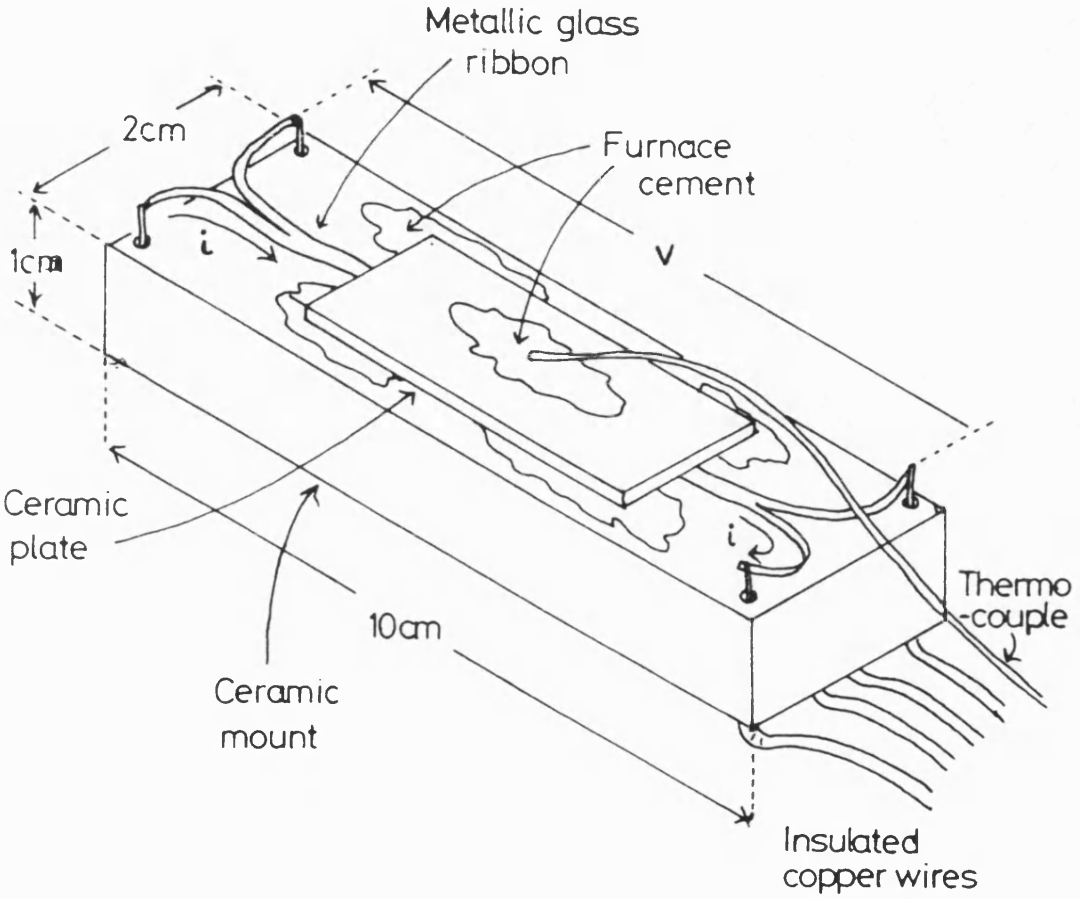

Figure 3.4.3: sample and holder

the points at which voltage was measured are shown in the drawing. The middle 6 cm of the ribbon was held down on the surface of the ceramic mount by a ceramic plate, secured with high temperature furnace cement which had to be dried out under a desk lamp before evacuation of the surroundings of the sample. The ceramic used is pyrophyllite, supplied by Ceramic Substrates and Components, Stag Works, Broadway, Farnham Common, Bucks, SL2 3PQ. The pyrophyllite parts were machined before firing. After firing at 1200°C, pyrophyllite is very hard but rather brittle.

Temperature was measured using a chromel-alumel thermocouple in intimate contact with the metallic glass halfway along the ribbon. The thermocouple was calibrated by replacing the metallic glass ribbon with lead wire; the temperature registered by the thermometer as the wire suddenly became open-circuit during heating corresponds to a true temperature of 327.5°C, the melting point of lead. It passed through a hole in the ceramic plate and was secured using furnace cement. The electrical contact between thermocouple and resistometric apparatus caused some instrumental problems, but these were overcome (chapter 2). A lag, during heating, of the temperature registered by the thermocouple behind the temperature of the metallic glass ribbon, deduced from its resistance, was reduced considerably when the thermocouple was brought into contact with the ribbon. The chromel and alumel wires were passed through the

vacuum seal without a break, in order to avoid introducing contact voltages unnecessarily.

Mostly, samples were heated from room temperature by preheating the furnace before sliding it into place. When a change of temperature was required during an anneal, the furnace was left in place and its temperature was changed as described above. The sample temperature was typically 10K lower than the steady furnace temperature. The sample took about 2500s to get within 1K of its steady temperature, the average heating rate being about 6K/min.

Results

We present here results showing the marked effect of changes in x on isothermal resistance changes in the $Pd_{82-x}V_xSi_{18}$ series of glasses. Some of these experiments are directly comparable with those of Kelton and Spaepen (1982, 1984), but it was necessary to repeat their work for a number of reasons. Firstly, the results of Kelton and Spaepen are incomplete in that they did not investigate reversible behaviour in those alloys containing vanadium. Secondly, Kelton and Spaepen (1984) do not describe how they estimated at what point, during the warming-up period, they considered the 'isothermal' anneal to have started. In chapter 8 of this thesis we derive a method for estimating effective isothermal annealing time in a real experiment with non-zero warming-up time; this method is used here and allows us

to compare with confidence the effects on different alloys of thermal treatments in which the alloys were warmed at slightly different rates to the same final constant temperature. Thirdly, because all the properties of the $Pd_{82-x}V_xSi_{18}$ alloys measured depend strongly on x, we prefer to compare the behaviour of alloys with analytically determined values of x, rather than relying on the nominal value, as Kelton and Spaepen (1982, 1984) appear to do.

Some experiments were performed with kinetic modelling in mind. The results of these are presented and discussed in chapter 9 of this thesis; here we examine the results of a series of experiments designed to elucidate the effect of composition on the signs and magnitudes of reversible and irreversible structural effects.

Irreversible Structural Relaxation

For all three compositions, the same set of experiments was performed on lengths of ribbon cut consecutively from the same end of the reel. We first follow through the analysis of results on $Pd_{80}V_2Si_{18}$ because it has a relatively small t.c.r., making structural effects more obvious. We then compare the graphs derived in this analysis with those pertaining to $Pd_{82}Si_{18}$ and to $Pd_{81}V_1Si_{18}$, derived in the same way.

The first thermal treatment was rapid heating ($dT/dt \approx 0.4Ks^{-1}$) to about 400°C in order to induce crystallisation. Figure 3.4.4 shows clearly the effect of crystallisation both on resistance and on t.c.r. in as-received $Pd_{80}V_2Si_{18}$. The temperature was maintained at 395°C for about 18 hours before cooling to room temperature. From this graph we can estimate the change $\Delta R(0°C)$ in the resistance at 0°C by extrapolating the heating and cooling lines to 0°C. We can also estimate the t.c.r. of the crystallised alloy. The calculations are as follows.

$$\left.\begin{aligned} R_A(0°C) &= 2.53\ \Omega \\ R_C(0°C) &= 1.49\ \Omega \end{aligned}\right\} \qquad \Delta R(0°C) = 1.04\ \Omega$$

$$\frac{\Delta R(0°C)}{R_A(0°C)} = 0.41$$

$$\frac{1}{R_C(0°C)} \left.\frac{dR_C}{dT}\right|_{0°C} = \frac{1}{1.49\ \Omega} \frac{0.285\ \Omega}{200K} = 9.6 \times 10^{-4}K^{-1}$$

where the subscripts A and C stand for amorphous and crystalline respectively.

The temperature of the onset of crystallisation T_x we define as the abscissa of the intersection of the two dashed lines on figure 3.4.4. They are extrapolations of $R_A(T)$ and of the straight portion of the R(T) curve representing crystallisation. For $Pd_{80}V_2Si_{18}$, T_x = 394°C, slightly lower than the value of 400°C found by d.s.c.

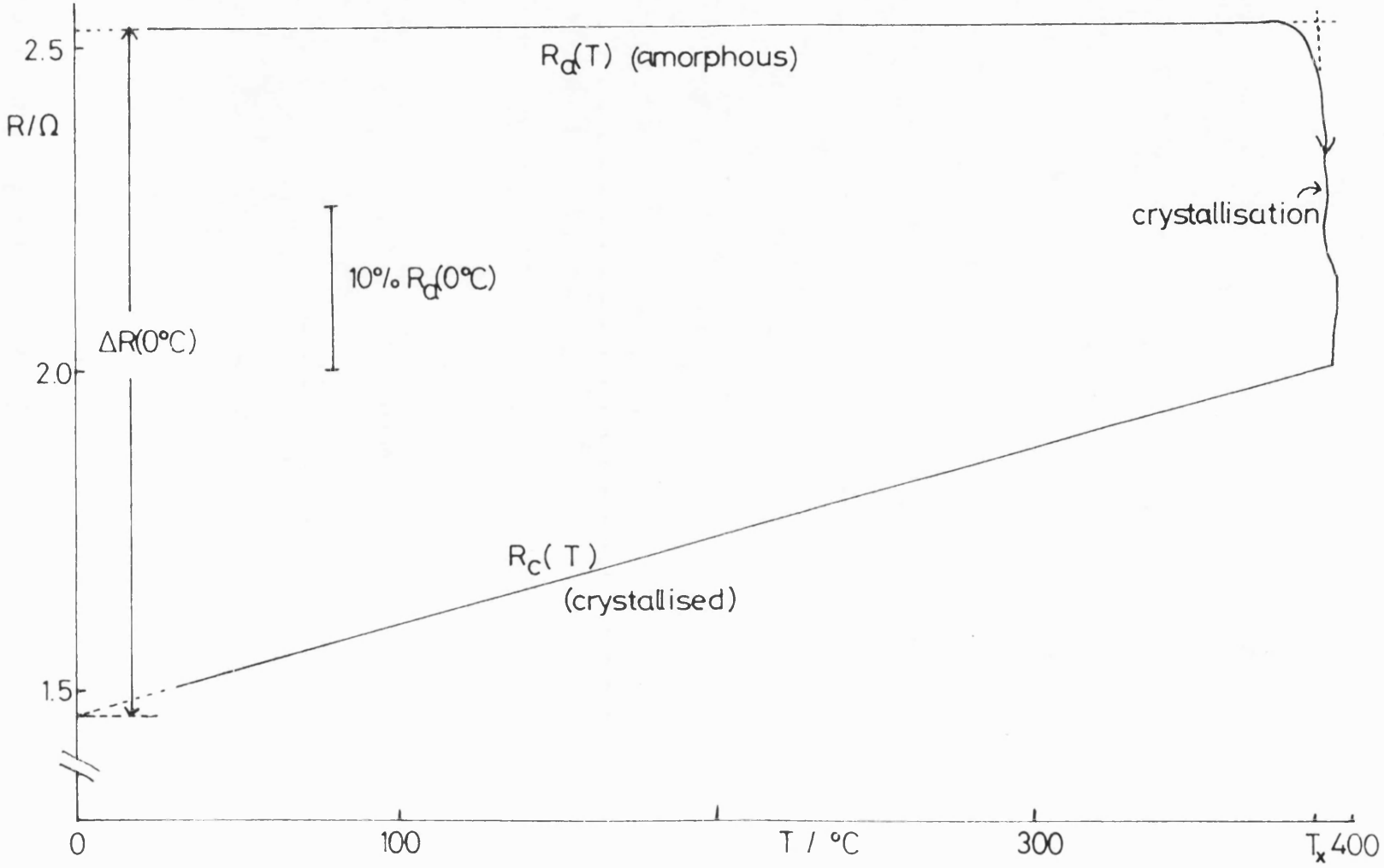

Figure 3.4.4: crystallisation of $Pd_{80}V_2Si_{18}$; effect on electrical resistance

The vertical section of the curve of figure 3.4.4, corresponding to crystallisation, shows some small irregularities in temperature control. The decrease in resistance due to crystallisation was very rapid, so small fluctuations in T as proportional control was being established are visible here.

The t.c.r. of the amorphous alloy can in principle be deduced by replotting the graph of figure 3.4.4 with a much finer vertical scale and measuring the gradient of the line $R_A(T)$. However, the heating rate in the crystallisation experiment is very high and the accuracy with which the null resistance measurements can be made is proportionately low. We therefore prefer to use the heating curve obtained in the experiment described next, in estimating $(1/R_A(0^\circ C))\ dR_A/dT$.

The next thermal treatment was a long isothermal anneal of a fresh, as-received sample at 253°C. This is well below the crystallisation temperature so structural relaxation is the only effect present; it can be seen clearly as an upturn at the high temperature end of the $R_A(T)$ line in figure 3.4.5, which shows resistance as a function of temperature during this experiment. The effect of structural relaxation on resistance is positive, opposite in sign to the effect of crystallisation and two orders of magnitude smaller (compare the vertical bars showing percentages of $R_A(0^\circ C)$ in figures

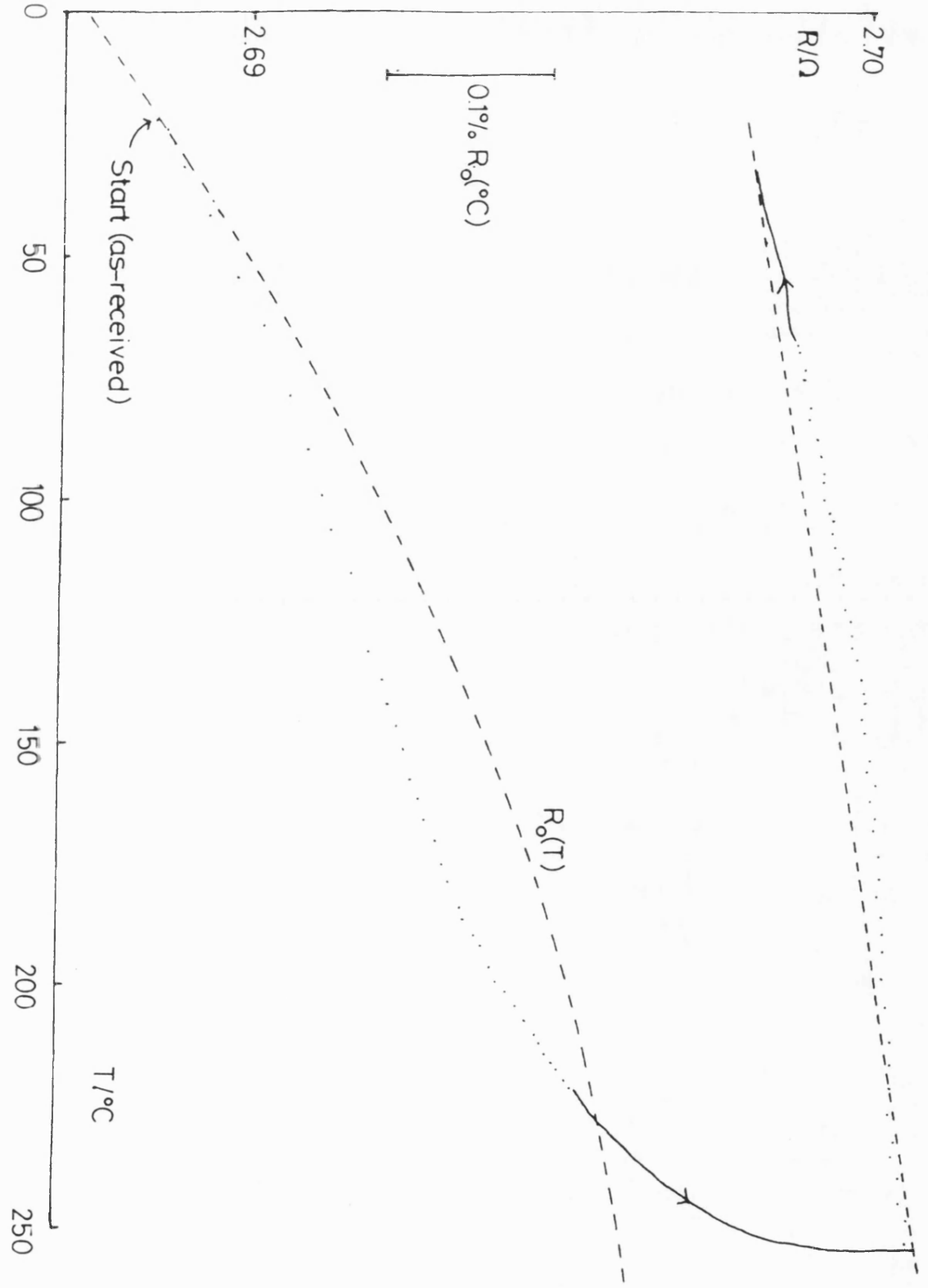

Figure 3.4.5: resistance of as-received $Pd_{80}V_2Si_{18}$ during an isothermal anneal at 253°C. Dots represent individual data points, replaced by a solid line when very close together. For dashed lines, see text.

3.4.4 and 3.4.5). This qualitative difference between the effects of crystallisation and structural relaxation reinforces the point made in chapter 1 that structural relaxation, rather than being the beginning of crystallisation, is in fact a qualitatively different kind of ordering of the atomic structure.

The dots represent individually gathered data points; where they would be very close together a bold line is used instead. The upper dashed line is drawn through two points: the highest point reached during structural relaxation and the steady point reached once the sample was in equilibrium at room temperature. Because the structure of the alloy has been well prestabilised by the anneal, we can assume that very little structural change will take place during cooling; the gradient of this dashed line is therefore the average value of the isostructural temperature-dependence of resistance between room temperature and 250°C.

The lower dashed line, representing isostructural temperature dependence of resistance in the as-received state, is not so easy to construct, however, because there is not a reliable reference point at a high temperature. The two points used to draw the upper dashed line represent states of thermal equilibrium; any datum point representing a state of relatively rapid temperature change we must interpret cautiously, because it is reasonable to expect that there will be some lag of the temperature measured by the thermocouple behind the

temperature of the metallic glass ribbon, the ribbon being thermally very light. A separate experiment was necessary for the determination of the t.c.r. of each glass in its as-received state.

The results of this subsiduary experiment on $Pd_{80}V_2Si_{18}$ are shown in figure 3.4.6. Resistance and temperature were measured in boiling liquid nitrogen and at three temperatures in the range 0°C - 150°C. The curve is especially non-linear in this alloy because of the unusually low value of the linear component $(1/R)dR/dT$, of order $10^{-5}K^{-1}$ (c.f. $(1/R)dR/dT \approx 10^{-4}K^{-1}$ in $Pd_{82}Si_{18}$). A curve was drawn by hand through the four points (figure 3.4.6); in addition, the four points were fitted, using a least-squares computer algorithm, to the equation

$$R_0(T) = R_0(0°C)\ \{1 + \alpha(T - 0°C) + ß(T - 0°C)^2\} \quad -- \quad (3.4.1)$$

and the best values of α and ß were found to be

$$\alpha = 2.116 \times 10^{-5}\ K^{-1}$$

$$ß = -3.206 \times 10^{-8}\ K^{-2}$$

The fractional errors in the estimation of $R_0(T)$ introduced by this quadratic fit are very small (better than ± 0.1%) because of the weak dependence of resistance on temperature, relative to the residual resistance, in these metallic glasses. A fast thermal effect (see

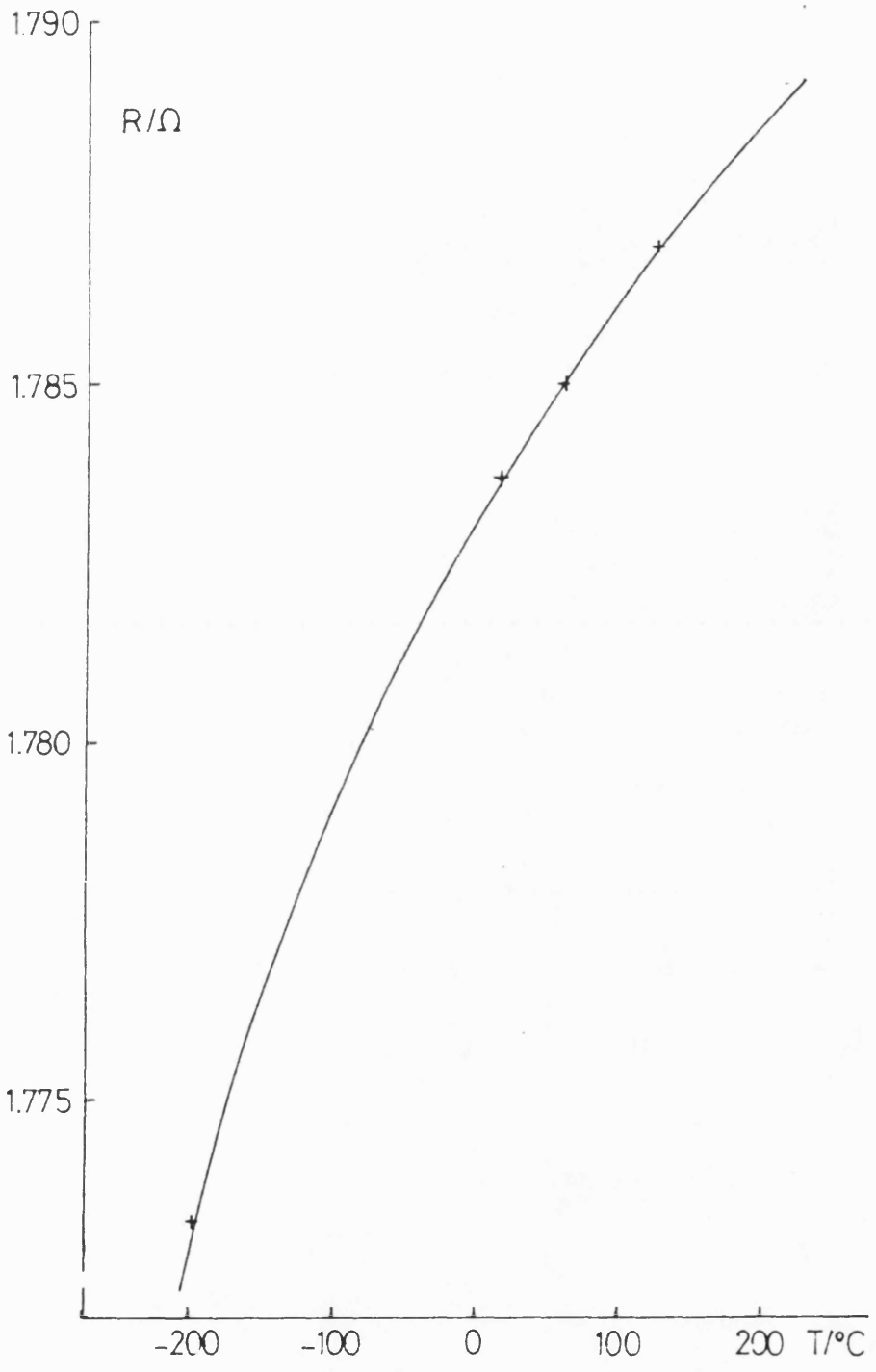

Figure 3.4.6: temperature dependence of resistance of a length of as-received $Pd_{80}V_2Si_{18}$ ribbon

description of figure 3.4.7 below) in the resistance-time curve, corrected using the above quadratic form, was ascribed to the errors introduced in this estimation of isostructural temperature-dependence of resistance.

The lower dashed line in figure (3.4.5) therefore represents equation (3.4.1), with the above values of α and ß and with the value 2.6873Ω of R(0°C), obtained by fitting (3.4.1) to the pair of values (R,T) measured in the as-received state before wheeling the furnace into place (point labelled 'start' on figure 3.4.5). The isostructural t.c.r. decreases as a result of irreversible structural relaxation.

We now define the fractional departure of the observed R(T) curve from its isostructural form $R_0(T)$.

$$\frac{\Delta R}{R_0} = \frac{R(T) - R_0(T)}{R_0(T)}$$

$\Delta R/R_0$ is plotted as a function of time in figure 3.4.7. The parameter t_0 is the effective starting time of the anneal, assuming that the anneal is perfectly isothermal at 253°C. Part of the $(\Delta R/R_0)(t)$ curve is drawn full; this indicates that the temperature was within 1K of the anneal temperature, 253°C. The dashed part of the curve shows the resistance change before isothermal conditions

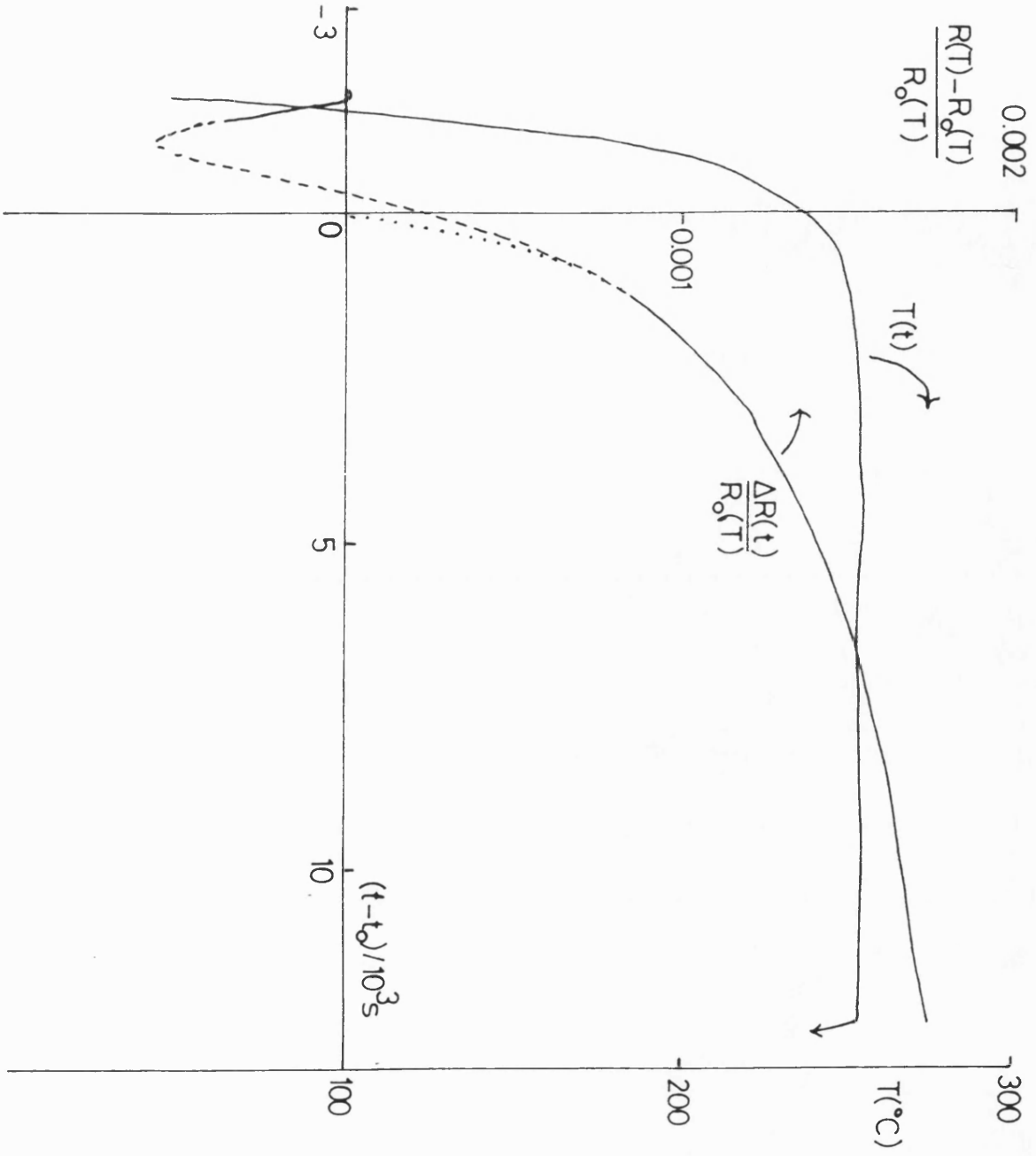

Figure 3.4.7: evolution of fractional resistance change in as-received $Pd_{80}V_2Si_{18}$ during an isothermal anneal at 253°C

were attained. The curve $(\Delta R/R_0)(t)$ which would result from a perfectly isothermal anneal must therefore begin at the origin of figure 3.4.7 and join the observed curve where it becomes fully drawn-in (dotted line in figure 3.4.7).

The value of t_0 used was obtained by evaluating numerically the integral

$$t_0 = \int_0^{t_H} \{1 - \exp \frac{-E_1}{kT_A} (x + x^2 + x^3)\} \, dt$$

where $x = (T_A - T(t))/T_A$,

T_A is the annealing temperature 253°C,

t_H is the time at which $T(t)$ reaches T_A,

$E_1 = 1.5$eV.

The reasons for calculating t_0 this way are set out in chapter 8.

The trough in the dashed portion of figure 3.4.7 shows that the quadratic function of temperature used to describe the isostructural temperature dependence of the as-received state is in error by about 0.06% over the temperature range 20°C - 200°C, as discussed above. Since it is the isothermal resistance changes and the difference between room temperature and high temperature values of resistance which are of interest, this

inaccuracy, which affects strongly only the intermediate part of the resistance-temperature curve, is not important for the present purpose.

From the graph, figure 3.4.7, we extract two pieces of information in order to characterise the effect of irreversible structural relaxation on the resistance of $Pd_{80}V_2Si_{18}$. Firstly, the value of $\Delta R/R_0$ at t_0 + 10000s is 1.67×10^{-3}; secondly, the rate of change of $\Delta R/R_0$ at t_0 + 10000s is

$$\frac{1}{R_0}\frac{dR}{dt} = 3.9 \times 10^{-8}\ s^{-1}$$

or, expressed as a function of log-time,

$$\frac{1}{R_0}\frac{dR}{d\ln t} = \frac{t}{R_0}\frac{dR}{dt}$$

$$= 3.9 \times 10^{-4} \quad (253^{\circ}C)$$

Identical sets of experiments were carried out on as-received samples of $Pd_{82}Si_{18}$ and $Pd_{81}V_1Si_{18}$; the results for all three compositions are compared in table 3.4.3

The small quadratic term ß in the expression for the isostructural temperature-dependence of resistance in the as-received state does not change much with vanadium concentration x, but α, which is positive in all three

Table 3.4.3:

$Pd_{82-x}V_xSi_{18}$: comparison of results. For definitions of symbols see text. Figures in parentheses are from Kelton and Spaepen (1984) who used a lower annealing temperature

Composition:		$Pd_{82}Si_{18}$	$Pd_{81}V_1Si_{18}$	$Pd_{80}V_2Si_{18}$
α /10^{-4} K^{-1}		1.243	0.400	0.212
β /10^{-8} K^{-2}		-1.56	-1.14	-3.21
[Errors:		less than 0.1% between 0°C and 250°C]		
Crystallisation				
Tx/°C		373	388	394
$(1/R_c)(dRc/dT)/10^{-3}$ K^{-1}		1.43	1.10	0.96
Irreversible Structural Relaxation				
$(\Delta R(10\ 000s)/R_0)/10^{-3}$		-8.70 (-4.16)	-2.06(-0.42)	+1.67(+1.32)
$(1/R)(dR/dt)$ /10 s		-8.6(-6.7)	~0(-2.9)	+3.9(+2.2)
$\left(\frac{1}{R}\frac{dR}{dT}\right)/10^{-4}$ 0°-250°C	as-received (= α + 250β)	1.20	0.37	0.13
	after irreversible struct relaxation	1.26	0.28	0.05
	change on structural relaxation	+(+)	-(~0)	-(-)
Reversible Structural Relaxation				
$(1/R)(d\Delta R/d\Delta T_A)_{T_A}$ /10^{-6} K^{-1}		-10	-5	-8

cases, increases with decreasing x, sc the curvature of R(T) is less pronounced when x = 1 (figure 3.4.8) and when x = 2 (figure 3.4.9).

Graphs showing crystallisation in $Pd_{82}Si_{18}$ and in $Pd_{81}V_1Si_{18}$ are not reproduced here; the value of t.c.r. in the crystallised state increases with decreasing x.

The effects of irreversible structural relaxation are shown in figures 3.4.10 (x = 0) and 3.4.11 (x = 1). Both graphs show transient spikes during heating, similar to that seen in figure 3.4.7, though in $Pd_{81}V_1Si_{18}$ the effect is very small. The values of $\Delta R/R_0$ and its time-derivative after 10000s of annealing at 253°C are compared in table 3.4.2, together with the change in t.c.r., evaluated at 0°C, as a result of irreversible structural relaxation. The bracketed entries are taken from the graphs of Kelton and Spaepen (1984) (figure 3.2.13); these are not directly comparable with our results because we used an annealing temperature of (253°C), 13K higher than theirs. The magnitudes of the resistance changes they measure are consistently smaller than ours because structural relaxation proceeds more slowly at lower temperatures.

Our results are consistent with those of Kelton and Spaepen, except for the estimate of the rate of change of resistance after 10000s in $Pd_{81}V_1Si_{18}$. Figure 3.4.9

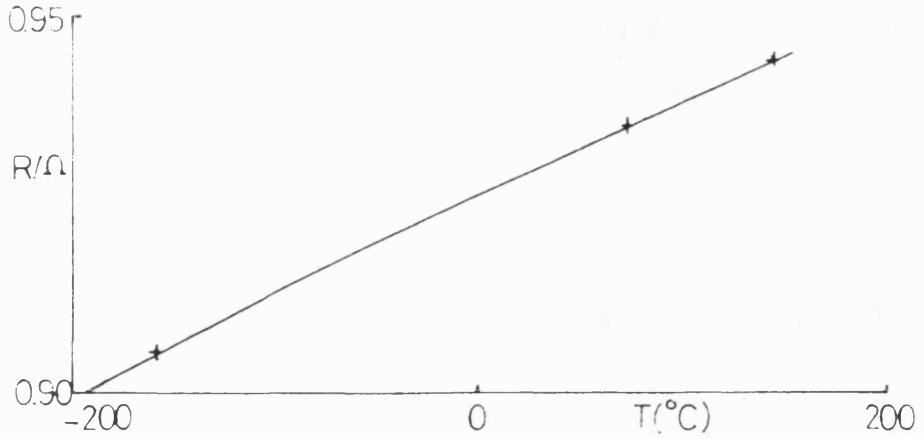

Figure 3.4.8: temperature dependence of resistance: $Pd_{82}Si_{18}$

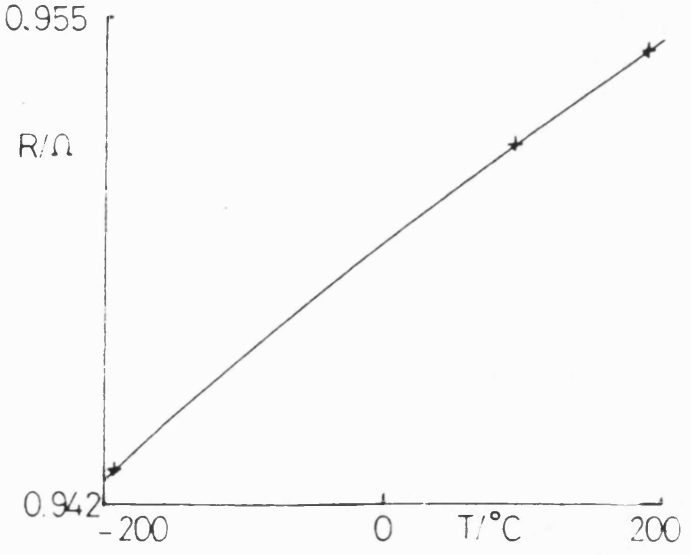

Figure 3.4.9: temperature dependence of resistance: $Pd_{81}V_1Si_{18}$

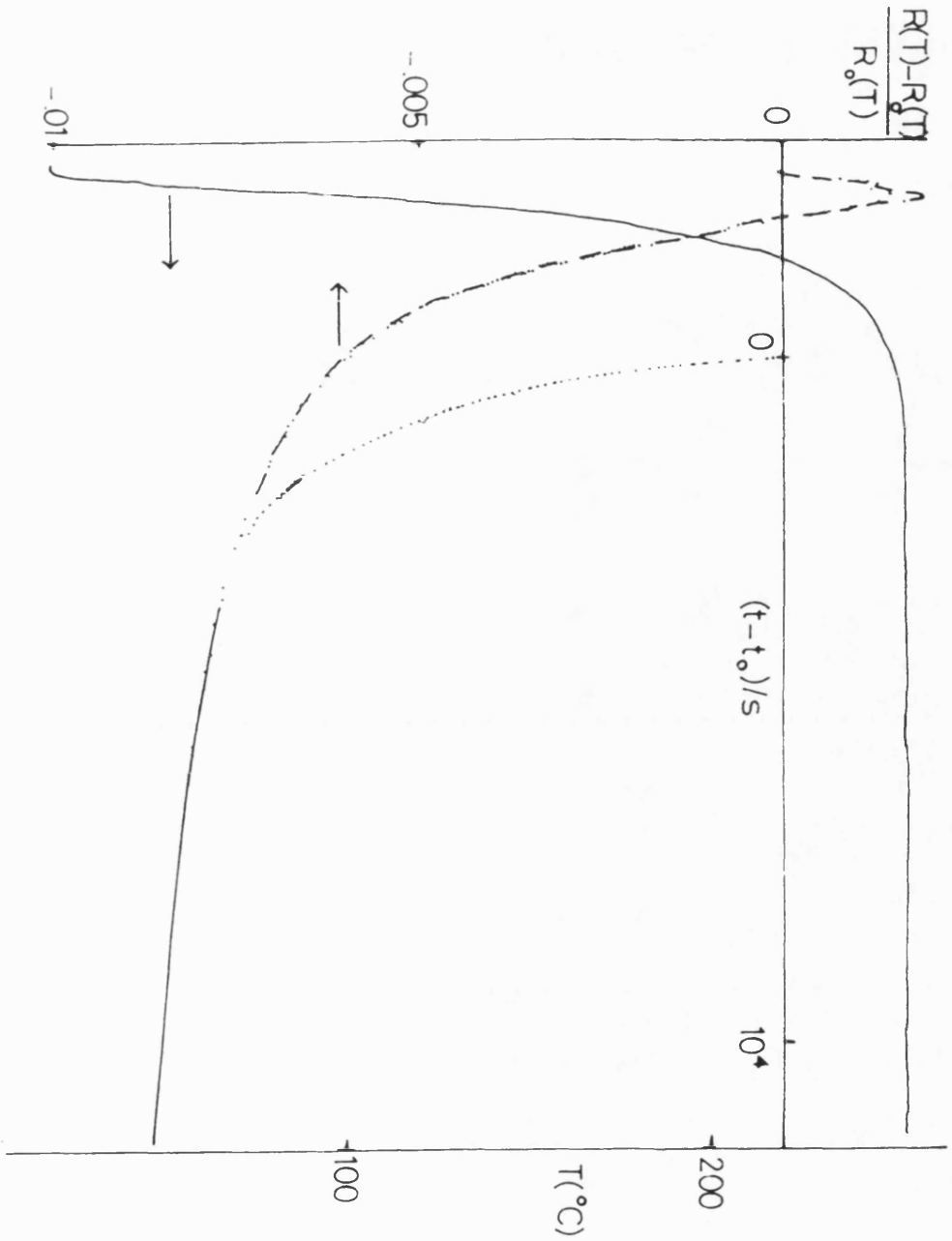

Figure 3.4.10: evolution of fractional resistance change in as-received $Pd_{82}Si_{18}$ during an isothermal anneal at 253°C

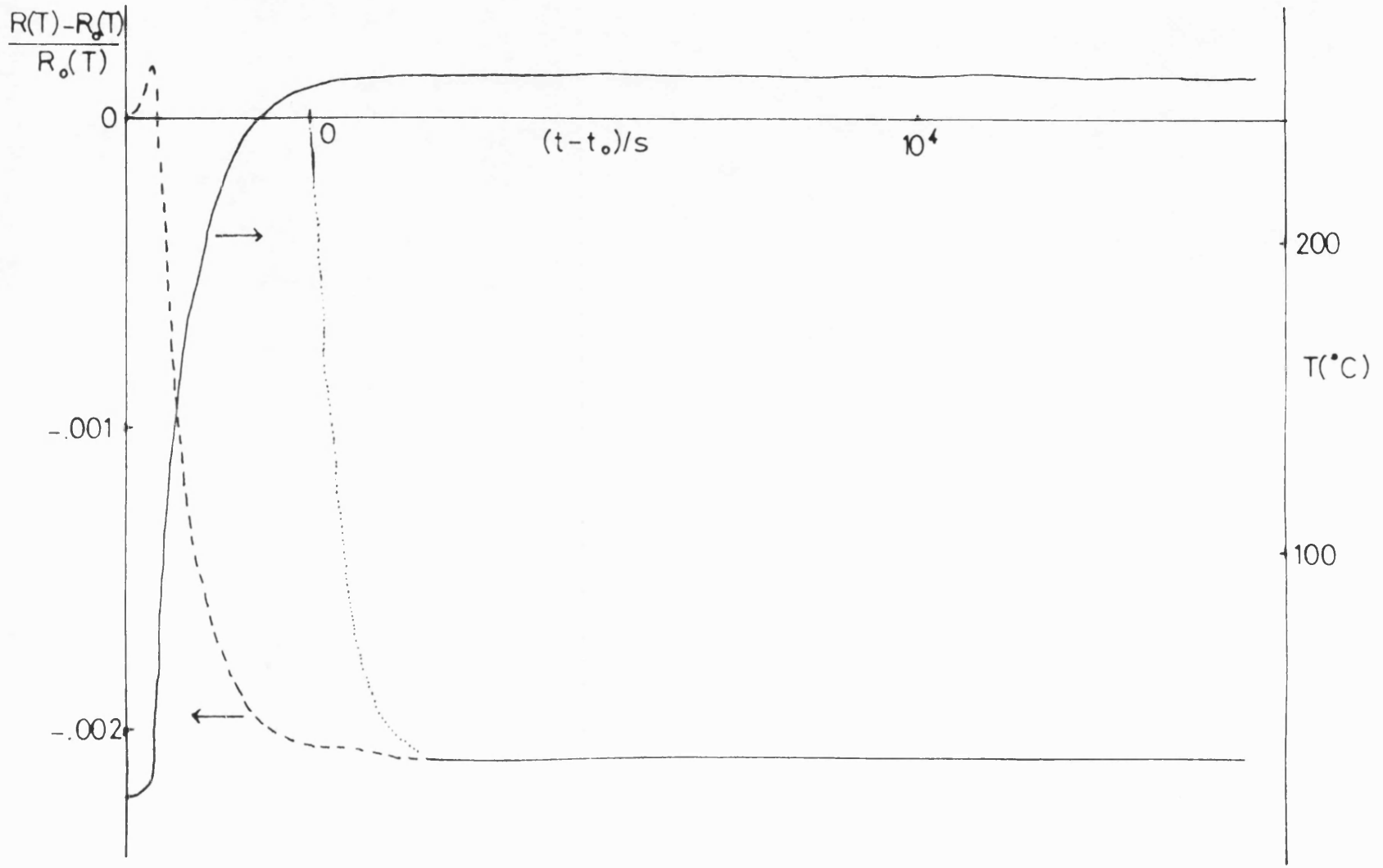

Figure 3.4.11: evolution of fractional resistance change in as-received $Pd_{81}V_1Si_{18}$ during an isothermal anneal at 253°C

shows conclusively a levelling-off of $\Delta R(t)$ for t > 3000s, whereas Kelton and Spaepen (figure 3.2.10) see no levelling off even when t has reached 36000s. This discrepancy cannot be attributed to differences in the procedures used to estimate t_0 and to correct for isostructural temperature change because the rate of change of resistance well into the isothermal region is independent of both of these. The underlying difference is likely to be one of composition.

Our ribbon with nominal composition $Pd_{81}V_1Si_{18}$ appears, from the behaviour of its resistance during the anneal, to contain more vanadium than that of Kelton and Spaepen; this is not inconsistent with our finding, reported earlier in this section, that $x = 1.1 \pm 0.1$, slightly higher than the nominal value of 1.

It is interesting to compare the curve $\Delta R/R_0(t)$ of figure 3.4.11 with those of figures 3.4.7 and 3.4.10 in the light of the explanation offered by Kelton and Spaepen (1984) of the effects of changing x in $Pd_{82-x}V_xSi_{18}$ (section 3.3). They postulate that the structural changes are not significantly different in the three alloys, but that the addition of vanadium alters the coupling between resistance and structure by increasing K_f (figure 3.3.2). Figure 3.4.11 however indicates that in the alloy showing almost zero resistance change, the kinetics of the change is relatively fast. This

experimental fact suggests that the relatively small degree of structural relaxation remaining is caused by fast relaxation processes, and therefore that varying x changes the structural relaxation processes themselves as well as their coupling to the electrical resistance. The model of Kelton and Spaepen could be made consistent with figure 3.4.11 by postulating that the structure factor changes more quickly on annealing around the value of K equal to $2K_f$ for $Pd_{81}V_1Si_{18}$, but neither the arguments of Kelton and Spaepen and of Yokota et al. (1985) nor diffraction experiments (Waseda and Egami 1979) suggest that this is the case. More work on $Pd_{81}V_1Si_{18}$ is needed to resolve this conflict.

Reversible Structural Relaxation

After anneals of 2-4 days at 253°C, irreversible resistance change had become imperceptibly slow, within the resolution of the experiment, in all three compositions. In each case, the sample was then cooled rapidly by about 18K and annealed isothermally at a lower temperature, around 235°C. A small increase in resistance was seen in each case. This is a reversible effect as was demonstrated by raising the temperature again, once the resistance had stopped changing at the lower temperature, and isothermally annealing close to the original anneal temperature of 253°C.

These reversible effects are shown graphically for x = 0, 1, 2 in figures 3.4.12, 3.4.13 and 3.4.14 respectively. The horizontal axis represents annealing temperature; the vertical axis shows fractional resistance change, defined by

$$\frac{\Delta R}{R_0} = \frac{R(T) - R_0(T)}{R_0(T)}$$

and using for $R_0(T)$ a simple linear expression with the gradient as given in table 3.4.2 ('t.c.r. after irreversible structural relaxation'). In each of these three figures, the circles represent a state of structural equilibrium having been reached and the arrows show the direction of cooling and heating. The two linear portions of the graphs (drawn in dashed) do not represent structural change. Ideally, these portions of the curves would be flat; their non-zero gradient arises from the inadequacy of the simple linear expression used for isostructural temperature-dependence in the relaxed state to match the true $R_0(T)$ curve over the range 0°C - 250°C. A similar problem caused the transient spikes in figures 3.4.7, 3.4.10 and 3.4.11.

The reversible effect can be seen in the curved portions of the R(T) graphs; as the rate of temperature change tends to zero, structural effects become visible. We define $(\Delta R)_{rev.}$ as the vertical displacement of the two straight portions of each graph from one another and

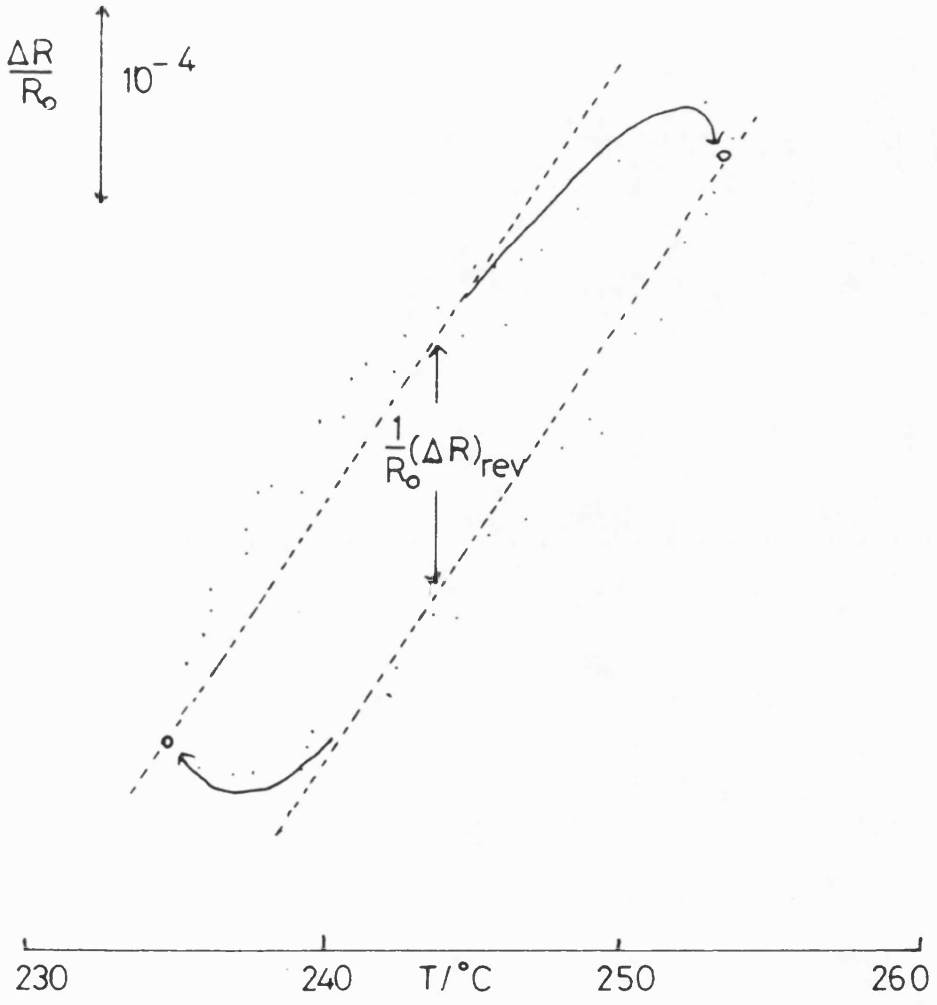

Figure 3.4.12: $Pd_{82}Si_{18}$: reversible resistance changes

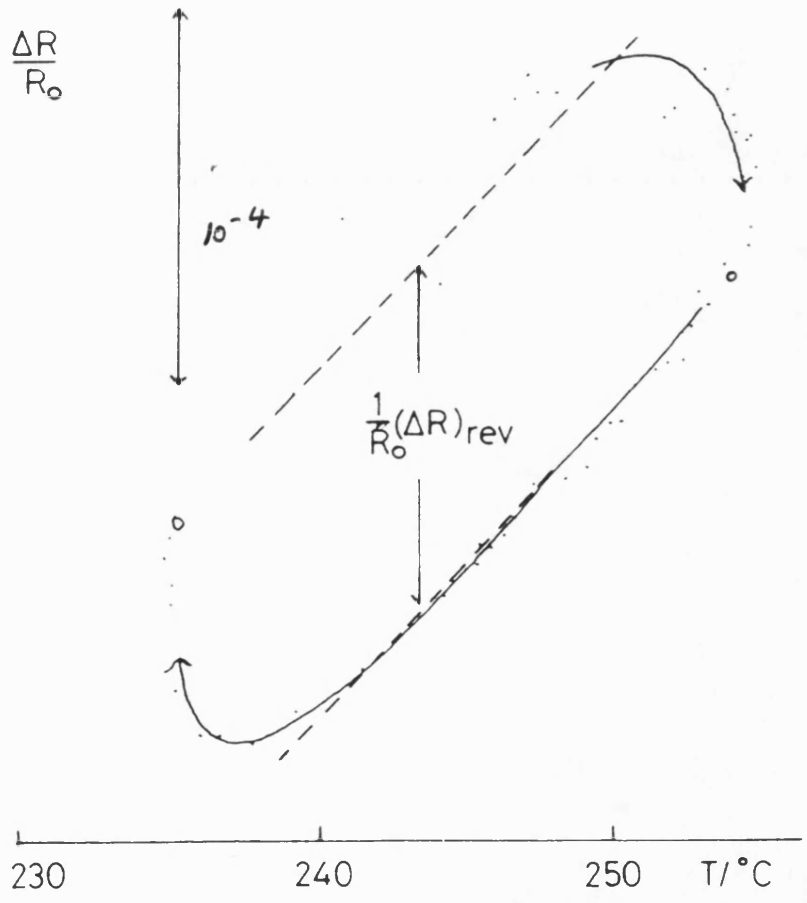

Figure 3.4.13: $Pd_{81}V_1Si_{18}$: reversible resistance changes

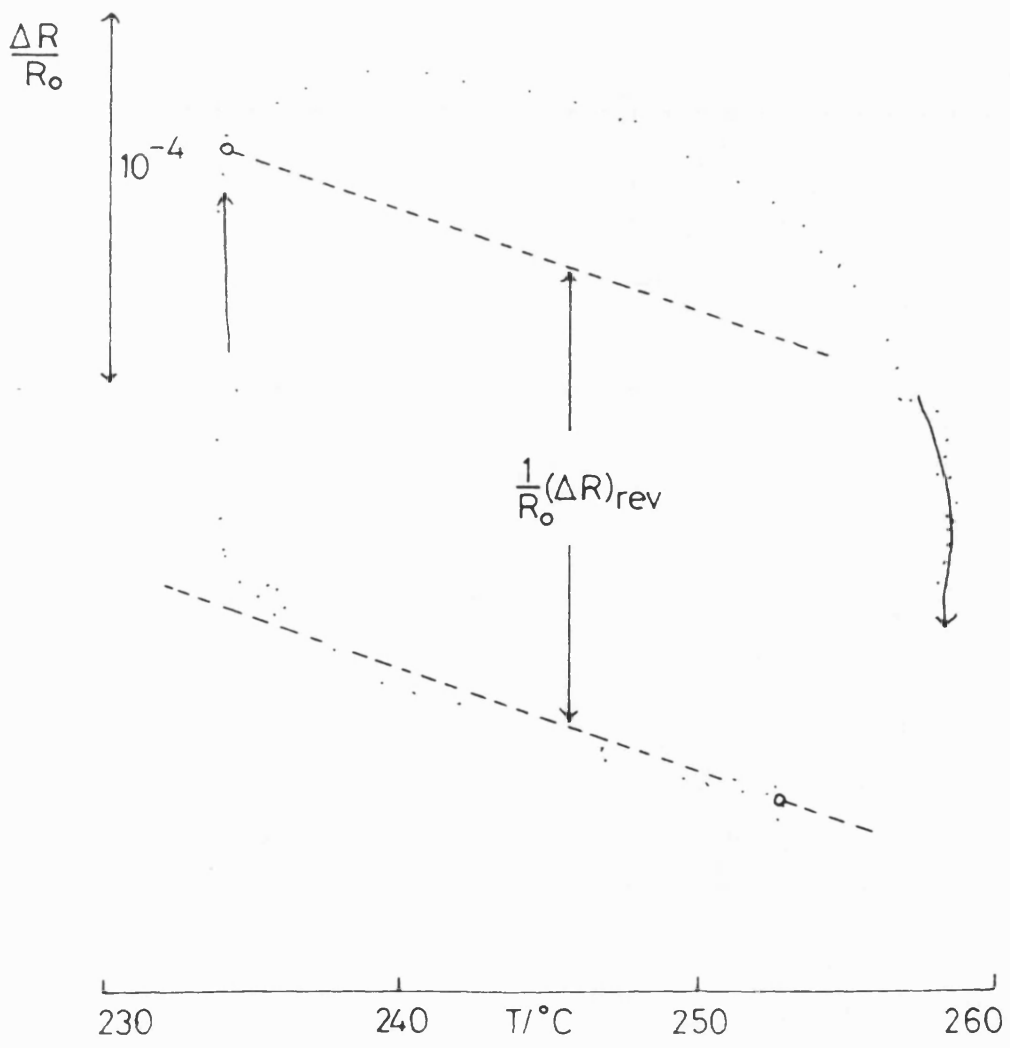

Figure 3.4.14: $Pd_{80}V_2Si_{18}$: reversible resistance changes

hence arrive at a quantitative estimate of the effects of reversible structural relaxation or electrical resistance:

$$\frac{1}{R(T_A)} \quad \frac{(\Delta R)_{rev.}}{\Delta T_A}$$

where T_A represents annealing temperature. The values of this parameter are given in table 3.4.2; in all three alloys, the effect is small, with magnitude $10^{-5}K^{-1}$ or less, and it is always negative in sign. These measurements are not sufficiently precise to allow any trend with changes in x to be identified. These results are consistent with those of Kelton and Spaepen (1982) on $Pd_{82}Si_{18}$; they found (section 3.2) that the irreversible ordering associated with an increase in annealing temperature causes a decrease in the resistance, as measured at 40°C. Their results do not allow a numerical estimate of the magnitude of $(1/R)d\Delta R/d\Delta T_A$ to be made, however.

These experiments therefore provide further evidence for the point made in paragraph 2 of the Summary of Experimental Findings, section 3.2. Reversible and irreversible ordering in amorphous $Pd_{82}Si_{18}$ affects the electrical resistance, measured at temperatures around 250°C, oppositely.

4. A CORRESPONDENCE BETWEEN STRUCTURAL RELAXATION AND COMPRESSION

Chapter 4 A Correspondence between Structural Relaxation and Compression

The results presented in chapter 3 show the effects of isothermal structural relaxation on resistance, of isostructural temperature change on resistance, and of irreversible structural relaxation on temperature coefficient of resistance in the $Pd_{82-x}V_xSi_{18}$ alloys where x = 0, 1, 2. Densification is an important component of irreversible structural relaxation, as pointed out in section 3.2 and in chapter 7. An experimental study of the effects of hydrostatic pressure on the electrical resistance of the PdVSi metallic glasses was therefore carried out with a view to comparing directly the effects of structural relaxation with the effects of compression. These experiments are described, and their results are presented, in section 4.1 below. A correspondence was found between the behaviour of room-temperature electrical resistance under compression and the behaviour of the resistance, measured at 253°C, during irreversible structural relaxation. In addition it was found that the effect of structural relaxation on the pressure coefficient of resistance (p.c.r.) of $Pd_{82}Si_{18}$ is to reduce its magnitude appreciably. This latter finding appears to be the first of its kind for any metallic glass.

The interpretation of these results will clearly be aided by an understanding of the mechanisms whereby hyrostatic compression brings about changes in the resistance of

amorphous alloys. With the aim of establishing how much this is understood, the results of some experimental studies of the effects of compression and tension on resistance are surveyed and discussed in section 4.2; in section 4.3, the results presented here are discussed and compared with the results of the annealing experiments presented above.

4.1 Experiments

Hydrostatic pressure was applied to sections of metallic glass ribbon of approximate length 15 cm by immersing each in a cylindrical oil-filled cavity in a large steel cylinder. The sample was passed through holes in a rigid ceramic mount fastened to the end of a piston (figure 4.1.1). The ceramic used, pyrophyllite, is soft and easily machined before firing and very hard after firing. The mount was cylindrical (length 30 mm, diameter 15 mm) with four tunnels of diameter 3 mm drilled through it at right angles to its axis. The tunnels were at regular intervals along the length of the cylinder, each at right angles to the next. A hollow threaded brass stud, cut from a conventional 8 mm gas pipe fitting, was glued to the top of the mount using cyanoacrylate adhesive; it fitted into a tapped brass cylindrical neck-piece, cut from the other half of the same fitting, which was attached to the piston. The ribbon passed through the holes in a spiral pattern; this geometry was chosen to maximise the length of the ribbon and thereby to maximise the voltage generated across it. The screw fastening allowed the mount to be removed easily in between compression

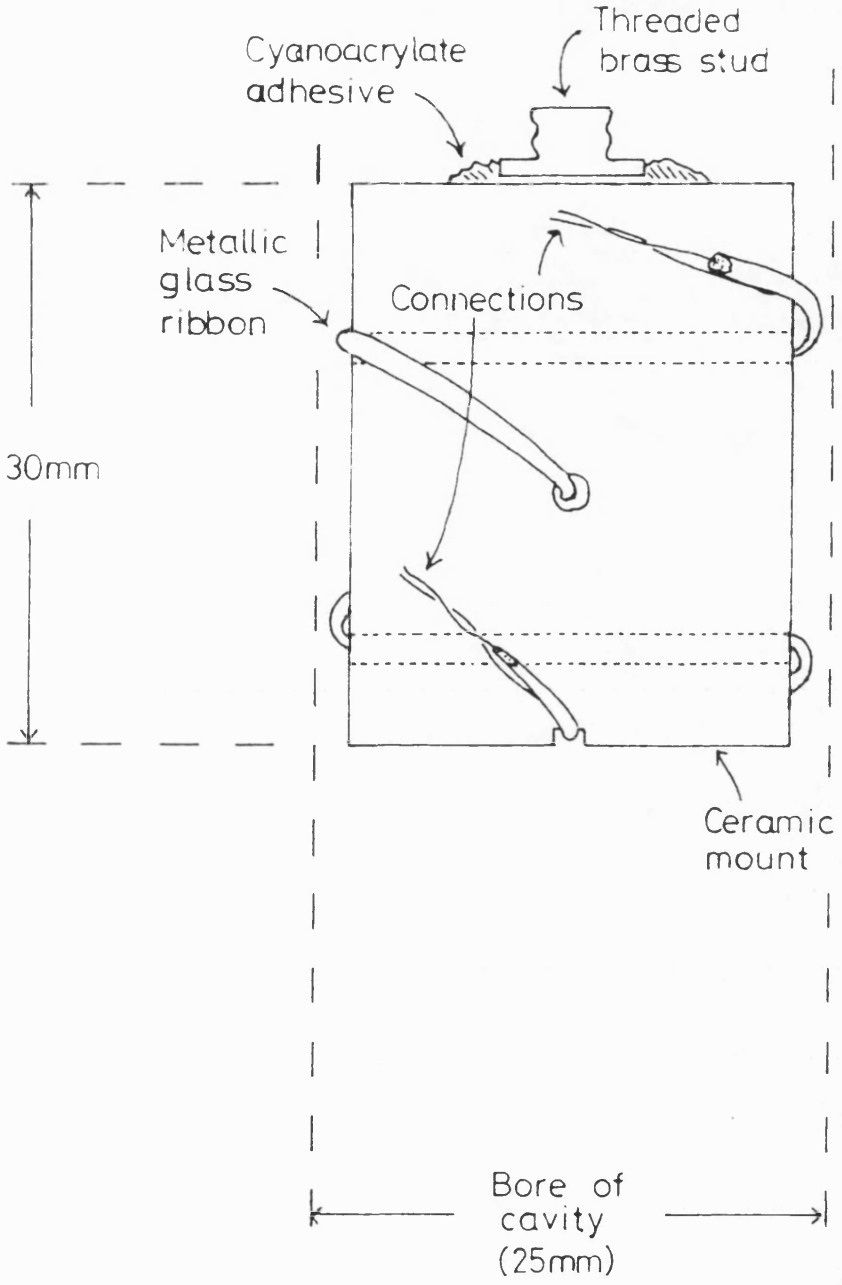

Figure 4.1.1: ceramic mount

experiments so that it could be cleaned and the sample replaced.

The resistance was measured as described in chapter 2. At first contacts were attached in the manner described in section 3.4, as in the annealing experiments. However, this resulted in unsteadiness of the resistance value during compression and poor repeatability between cycles of compression and release of pressure. This problem was overcome by adopting instead the arrangement shown in figure 4.1.2. Leads supplying the constant current i_0 were soldered to the ends of the ribbon. Insulated copper leads were soldered to the ribbon a few centimetres from each end such that their short bared portions were well distanced from the current lead contacts. This inner pair was used to measure the potential difference along the ribbon. The soldering iron was applied only to the copper wire and to the solder itself and not to the ribbon, in order to minimise the increase in temperature of the metallic glass during soldering. Solder joins metals by surface adhesion without melting them (Brady 1963); they melt at temperatures below 200°C and their use is therefore greatly preferable to spot welding in an instance, such as this compression experiment, where the novel geometry employed in the annealing experiments is unsuitable. Soldered joints could not be used in the annealing experiments because they would have melted.

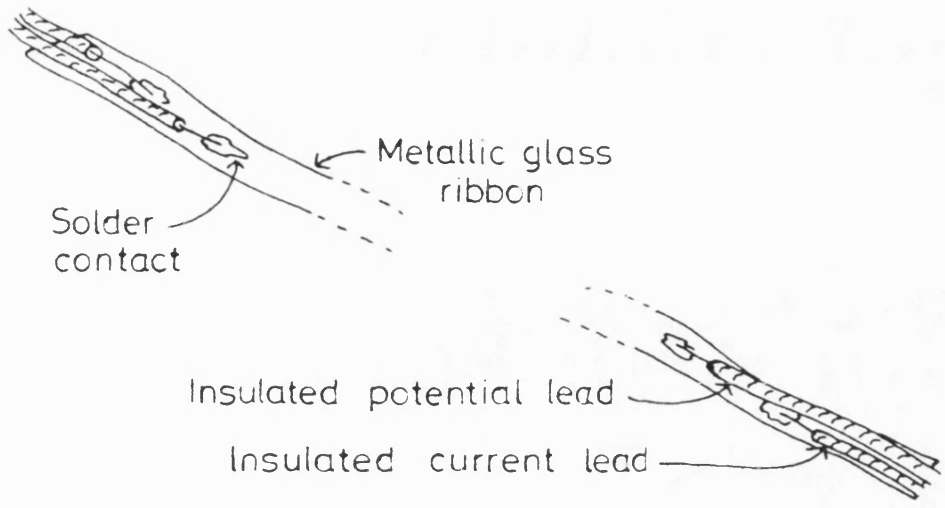

Figure 4.1.2: geometrical arrangement of ribbon and contacts before threading ribbon through mount

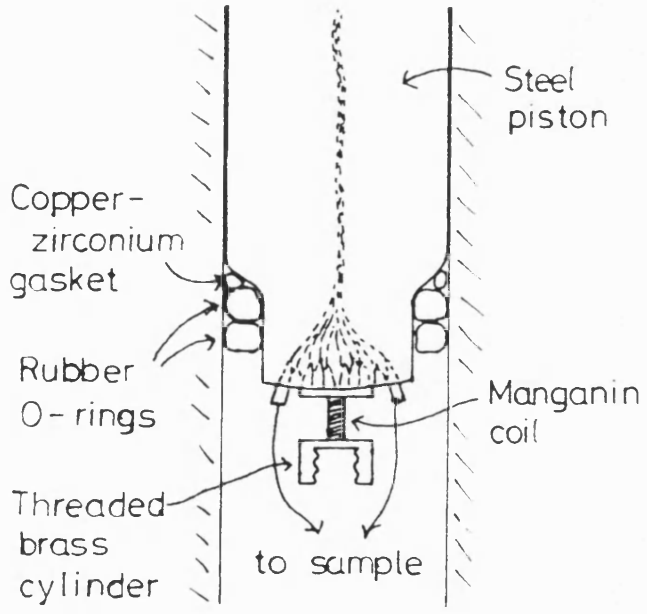

Figure 4.1.3: measuring and containing the pressure

Each fresh sample of ribbon was threaded through the holes in the mount before the mount was screwed into place on the end of the piston. The four insulated copper wires were soldered to contacts at the end of the steel part of the piston (figure 4.1.3). These eight contacts, sealed with epoxy adhesive into eight holes in the end of the hollow steel part of the piston, joined the current contacts, the voltage contacts, the leads to a manganin coil and the leads of a thermocouple to wires inside the piston at atmospheric pressure. The manganin coil, used to measure pressure, was wound on a ceramic former and glued, using cyanoacrylate adhesive, to the end of the steel part of the piston. The chromel-alumel thermocouple was put close to the metallic glass ribbon in the oil.

Bridgman (1958) used a manganin gauge to measure hydrostatic pressure. Subsequent calibration studies by Samara and Giardini (1964) and by Wang (1967) show that manganin wire, after seasoning at 200°C for several days, is a linear, reproducible gauge of hydrostatic pressure with pressure coefficient of resistance at room temperature given by

$$\frac{1}{R}\frac{dR}{dp} = (2.4 \pm 0.1) \times 10^{-3}\ (\text{kbar})^{-1}$$

The manganin wire was seasoned before being wound on to its former; the same coil was then used throughout the series of experiments to be described below.

A gasket, made from an alloy of copper and zirconium, and two rubber 'o'-rings sealed the piston as it entered the cavity.

The cavity, of diameter 25 mm and depth 10 cm, had been drilled into a fat steel cylinder of depth 15 cm and of diameter 15 cm (figure 4.1.4). Pressure was built-up in the cavity by applying an external force to the top of the piston; the oil used was silicone fluid, manufactured by Dow Corning.

The applied force was provided by a hand-pumped, secondary, hydraulic pressure system. The maximum pressure attained in the cavity was 3.2 kbar. The entire apparatus, apart from the hand-pump, was enclosed in a steel box in case the cylinder should crack during compression. The eight insulated wires from the cavity were led to instruments outside this box through a small hole in its side.

The resistance of metallic glasses depends weakly on pressure and strongly on temperature. For example, $Pd_{82}Si_{18}$ in its as-received state has a t.c.r. of about $+1.5 \times 10^{-4}\ K^{-1}$ (chapter 3) and a pressure coefficient of resistance (p.c.r.) of about $-1.3 \times 10^{-4}\ (kbar)^{-1}$ (table 4.1.1). The effect on the resistance of an increase in pressure of 0.1 kbar is therefore equal to the effect of a decrease in temperature of about 0.1K. Since 0.1 kbar was typical of the difference in pressure between successive measurements, it was necessary to monitor the

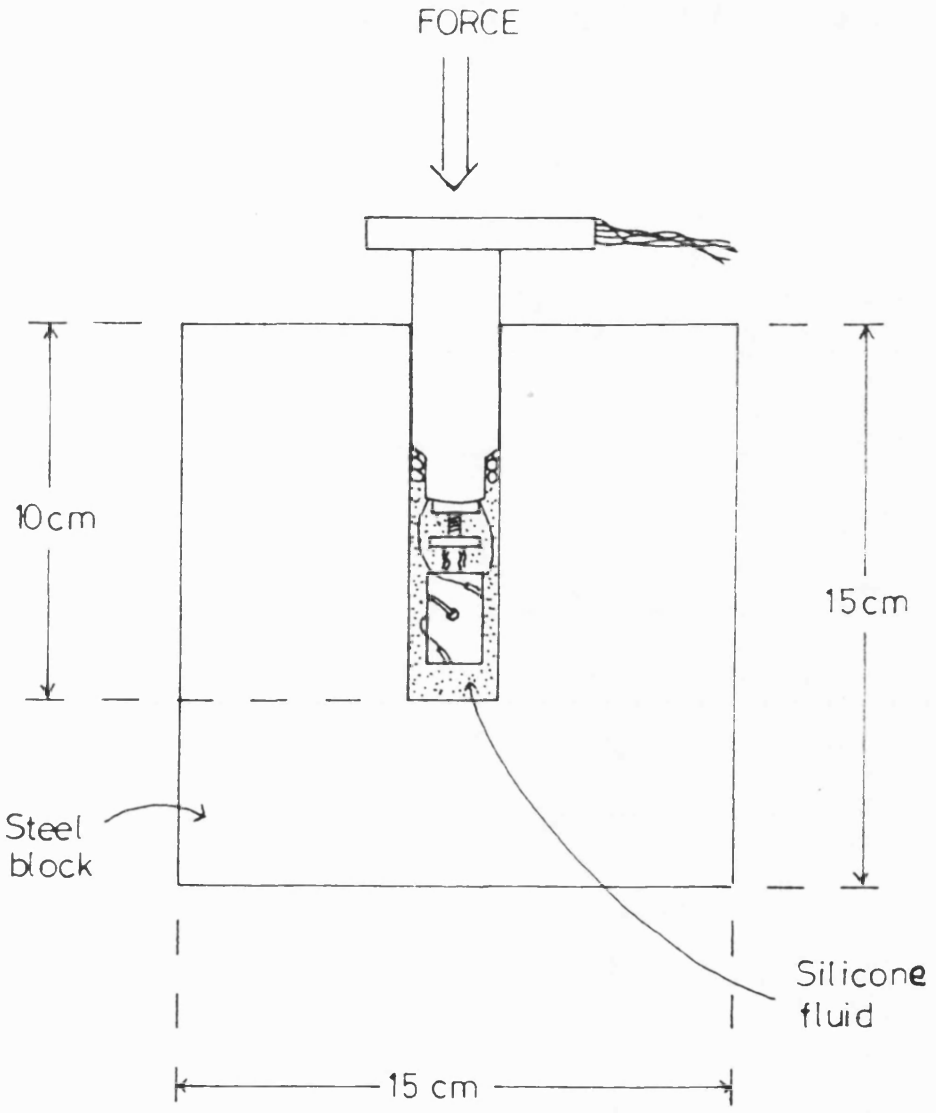

Figure 4.1.4: application of pressure

temperature of the sample of metallic glass with a resolution of 0.1K. Each time more pressure is applied, the sample and the oil around it are warmed by the heat evolved during compression. The temperature then decays exponentially towards that of the surroundings. The regular input of heat provided by each step in the compression causes fluctuations of a few K in the temperature inside the cavity.

Since temperature could not be kept constant, it would seem necessary to record the temperature measured by the thermocouple each time resistance and pressure were measured and to use this information, together with the known t.c.r. of the alloy in question, to correct for fluctuations in temperature. However, it was found that this procedure caused large amounts of scatter in the corrected resistance measurements when plotted against temperature. The reason for this was elucidated as follows.

The thermocouple was close to the metallic glass ribbon but was not in contact with it. Each time the pressure was increased, the temperatures of the metallic glass ribbon and of the surrounding oil both rose rapidly and then fell slowly, but the changes in the two temperatures were not proportional to one another. Instead, the temperature of the metallic glass ribbon appeared to lag behind that of the oil. This fact was ascertained by monitoring continuously the temperature of the oil and the resistance of the metallic glass (proportional to temperature for small changes at constant pressure) after

a sharp increase in pressure. Such a lag is to be expected, as it is the oil which, because of its relatively high compressibility, is heated during compression; heat then passes by conduction to the metallic glass.

Since the temperature inevitably fluctuates and since the temperature of the metallic glass ribbon itself was not known with the resolution required, neither continuous temperature control nor temperature-compensation could be used to overcome this difficulty. Instead, each measurement was taken several minutes after the application of extra pressure, when the temperature at the thermocouple, having risen by a few K upon compression, had fallen to a precisely measured value T_0, about 0.5K above ambient temperature. After several minutes of cooling, any difference in temperature between oil and metallic glass, it was thought, was likely to be very small and constant between readings. This argument was borne out by the results which showed very little scatter in resistance.

Figures 4.1.5 to 4.1.7 show how the resistance of $Pd_{82-x}V_xSi_{18}$ glasses (x = 0, 1, 2) changes due to the application of hydrostatic pressure at a constant temperature T_0, approximately equal to 20°C in each case. Each composition was studied in its as-received state and in a relaxed state, attained by preannealing for 22 hours at 230°C in a vacuum of 5×10^{-2} torr. It was not

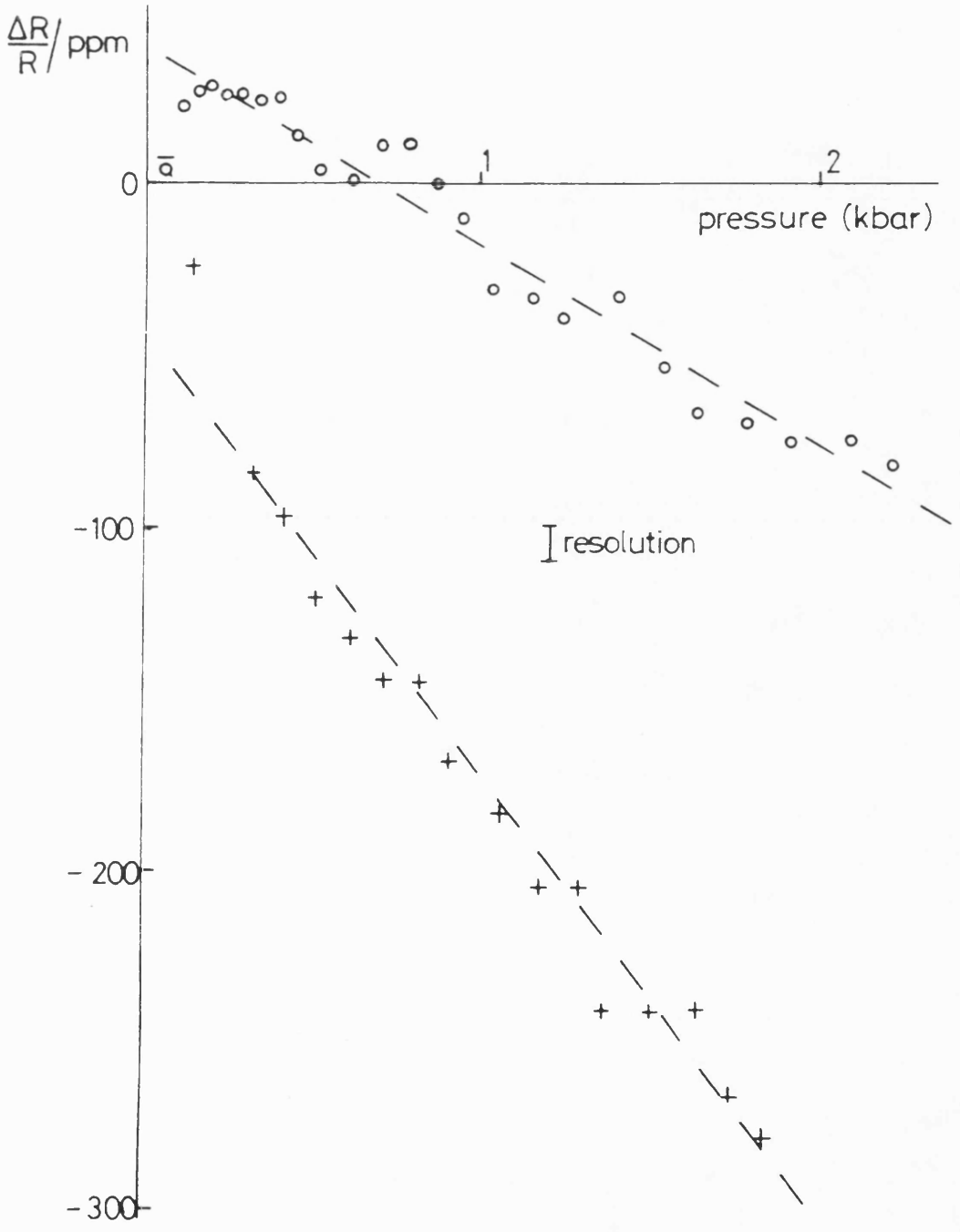

Figure 4.1.5: $Pd_{82}Si_{18}$ - effect of pressure on resistance
+ as-received
0 after anneal (22 hours at 230°C)

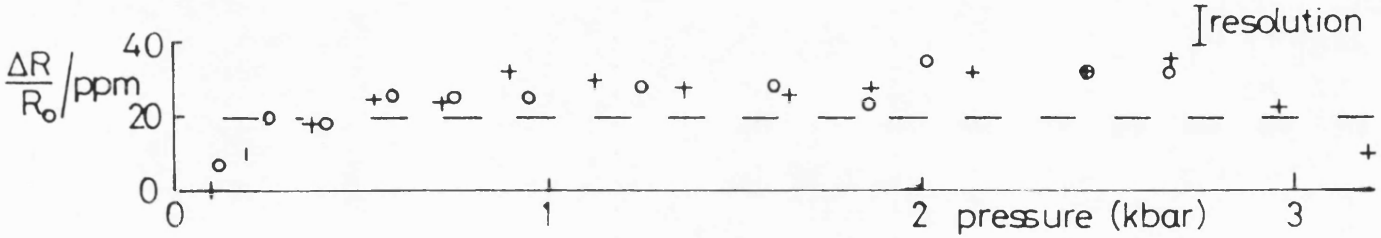

Figure 4.1.6: $Pd_{81}V_1Si_{18}$ - effect of pressure on resistance
+ as-received
0 after anneal (22 hours at 230°C)

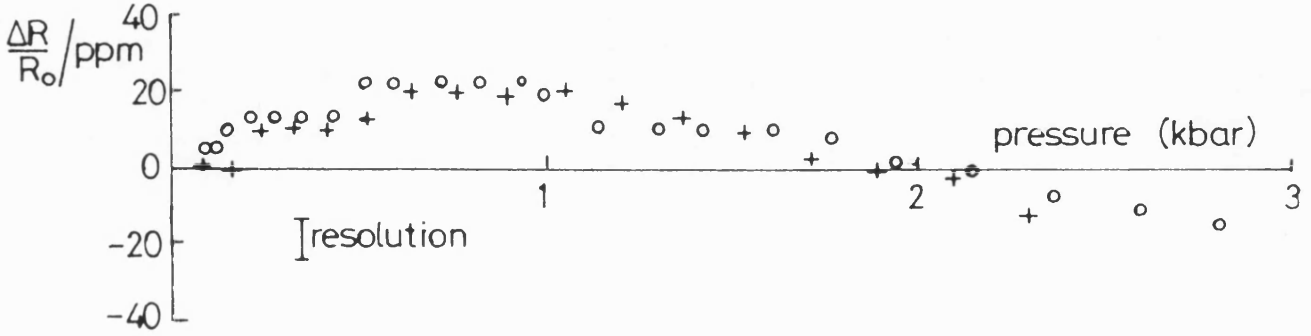

Figure 4.1.7: $Pd_{80}V_2Si_{18}$ - effect of pressure on resistance
+ as-received
0 after preanneal (22 hours at 230°C)

possible to compare as-received and preannealed p.c.r. directly by using the same length of ribbon with the same contacts because the solder would have melted, and the contacts come loose, during preannealing. Fresh samples were used for each of the compositions in both states and the effect of pressure on resistance is recorded as a fractional resistance change in figures 4.1.5 to 4.1.7, so that all six curves can be compared.

In each of these three graphs, crosses represent measurements made in the as-received state and circles refer to the pre-annealed state. The vertical axis represents the difference between the resistance at elevated pressure and at atmospheric pressure, normalised to the atmospheric pressure value. The broken straight lines were fitted, by eye, to each set of points, excluding in each case the point (0.001 kbar, 0) through which all the lines would pass ideally. This point, very close to the origin, is unreliable because the resistance R_0 at atmospheric pressure and at temperature T_0 could not be measured directly but had to be calculated from a measurement at atmospheric pressure and at ambient temperature, which was slightly less than T_0. The non-zero intercepts of the straight lines of figures 4.1.5 to 4.1.7 are therefore not significant; they indicate that the value of R_0 used was in error. This error was always of a magnitude less than 1 part in 10^4 and therefore its effect on the normalisation of the gradients of the straight lines can be ignored. The

vertical bar, height 10 ppm, on each graph represents the limit of resolution of the resistance measurement.

The pressure coefficient of resistance of $Pd_{82}Si_{18}$ is $(-1.3 \pm 0.2) \times 10^{-4}$ $Kbar^{-1}$ in the as-received state and $(-0.6 \pm 0.1) \times 10^{-4}$ $Kbar^{-1}$ in the preannealed state. In $Pd_{81}V_1Si_{18}$ and in $Pd_{80}V_2Si_{18}$, any linear term in the dependence of resistance or pressure is zero, to within the experimental resolution of 0.1×10^{-4} $Kbar^{-1}$, both before and after the annealing treatments, which were comparable to those giving significant resistance changes in the same glasses (chapter 3). The negative curvature in figure 4.1.7, both as-received and preannealed, was repeatable but is too close to the limit of resolution to justify any quantitative analysis.

The pressure coefficient of as-received $Pd_{82}Si_{18}$ is approximately halved upon preannealing, and is reduced in magnitude, approximately to zero, by the substitution of vanadium atoms for palladium atoms.

These results are summarised in table 4.1.1.

Table 4.1.1

Pressure coefficients of resistance in $Pd_{82-x}V_xSi_{18}$ alloys

Composition	Pressure Coefficient of Resistance (10-4 Kbar-1)	
	As-received	Pre-annealed (230°C, 22 Hours)
$Pd_{82}Si_{18}$	-1.3 ± 0.2	-0.6 ± 0.1
$Pd_{81}V_1Si_{18}$	0.0 ± 0.1	0.0 ± 0.1
$Pd_{80}V_2Si_{18}$	0.0 ± 0.1	0.0 ± 0.1

4.2 Survey of Published Experimental Results

The effect of hydrostatic pressure on the resistance of $Pd_{82-x}V_xSi_{18}$ glasses (x = 0, 1, 2, 3, 4, 5, 6) was investigated by Lazarus (1979), who found that the pressure coefficient of resistance (p.c.r.) was zero at room temperature, with error limits given by

$$\left|\frac{1}{R}\frac{dR}{dp}\right| < 10^{-4} \quad (\text{kbar})^{-1}$$

More precise work by McNeil (1983) estimates the p.c.r. of $Pd_{82}Si_{18}$, measured between 0 and 5 kbar, to be

$$\frac{1}{R}\frac{dR}{dp} = (-1.3 \pm 0.1) \times 10^{-4} \quad (\text{kbar})^{-1}$$

Although these two results do not quite agree within their own error limits, McNeil's precise value is close to the range of values estimated by Lazarus.

Fortuitously, the p.c.r. of $Pd_{82}Si_{18}$ obtained in the present experiment (table 4.1.1) agrees exactly with that of McNeil. In fact the agreement is only as good as the worse of the two error limits, i.e. ± 0.2 $(\text{kbar})^{-1}$.

McNeil also studied four other metallic glasses; the results are presented by McNeil as values of pressure coefficient of resistivity at various temperatures. The conversion from p.c.r. to pressure coefficient of

resistivity is effected by McNeil using the following relation:

$$\frac{d\ln\rho}{d\rho} = \frac{d\ln R}{d\rho} - \beta \qquad (4.2.1)$$

wherein ρ represents the resistivity and β the linear compressibility. Equation (4.2.1) rests on the assumption that contraction under pressure is isotropic. Since metallic glass ribbons are highly anistropic as argued in section 3.2 above, the use of equation (4.2.1) introduces an error of unknown magnitude into the result obtained. Correction for the effects of contraction, however approximately, is clearly desirable if a value of the fundamental derivative $d\ln\rho/dp$ is required for comparison with theory; however, this attempt to make such a correction decreases the value of a simple empirical comparison of the pressure coefficients obtained in various metallic glasses because it is likely that the errors introduced will be different in each case. From here on we compare values of p.c.r., uncorrected for dimensional change. Working back to the measured p.c.r. from the quoted $d\ln\rho/dp$ is easy in the above case, since McNeil reports the values of β used for each conversion. The work on $Fe_{80}B_{20}$, $Fe_{19}Ni_{61}P_{14}B_6$, $Fe_{32}Ni_{36}C_{14}P_{12}B_6$ and $Cu_{42}Zr_{58}$ can be summarised as follows: p.c.r. is always negative, as is the case in $Pd_{82}Si_{18}$. The numerical values of p.c.r. are summarised, together

with values found in the studies discussed below, in table 4.2.1.

Ast and Krenitsky (1976) found that amorphous $Fe_{40}Ni_{40}P_{14}B_6$ has a negative p.c.r. in the pressure range from 0 to 7 kbar, magnitude -3.9×10^{-4} $(kbar)^{-1}$; in addition they found that uniaxial tension increased the resistance. The temperature to which these results pertain is not given by Ast and Krenitsky.

Cote and Meisel (1982) measured the room-temperature resistance of five amorphous alloys at pressures up to 8 kbar. The p.c.r. of a NiCrSiFe alloy was found to be approximately zero, but no error limits are given. The other four alloys ($Ni_{77}P_{23}$, $Fe_{78}P_{22}$, a NiBSiCrFe alloy and $Fe_{32}Ni_{36}Cr_{14}P_6B_{12}$) each showed a negative p.c.r.

Cochrane, Strom-Olsen, Rebouillat and Blanchard (1980) investigated $Be_{40}Ti_{50}Zr_{10}$, $Fe_{78}Mo_2B_{20}$, $Fe_{40}Ni_{40}P_{14}B_6$ and an YNi alloy in the pressure range 0 - 5.2 kbar and found negative p.c.r. at room temperature. Their p.c.r. value for $Fe_{80}B_{20}$ at room temperature is -4.5×10^{-4} $(kbar)^{-1}$, in good agreement with the value -5×10^{-4} $(kbar)^{-1}$ obtained by McNeil (1983). Their estimate of the p.c.r. of $Fe_{32}Ni_{36}Cr_{14}P_6B_{12}$ is -5.5×10^{-4} $(kbar)^{-1}$ which is in good agreement with the value -5.0×10^{-4} $(kbar)^{-1}$ obtained by Cote and Meisel (1982); McNeil's value though is -3.8×10^{-4} $(kbar)^{-1}$. On this alloy therefore the agreement is

Table 4.2.1

Summary of experimentally determined values of p.c.r. at room temperature, at pressures between atmospheric and 10 Kbar, in metallic glasses.

Composition	P.C.R./ 10^{-4}kbar^{-1}		Reference
$Fe_{80}B_{20}$	-5.0 ± 0.2	}	
$Fe_{19}Ni_{61}P_{14}B_6$	-1.6 ± 0.1	}	
$Fe_{32}Ni_{36}Cr_{14}P_6B_{12}$	-3.8 ± 0.1	}	McNeil (1983)
$Pd_{82}Si_{18}$	-1.3 ± 0.1	}	
$Cu_{42}Sr_{58}$	-8.0 ± 0.1	}	
$Fe_{40}Ni_{40}P_{14}B_6$	-3.9 ± 10%		Ast and Krenitsky (1976)
$Ni_{77}P_{23}$	-0.44	}	
$Fe_{78}P_{26}$	-5.8	}	
$Ni_{69}B_{14}Si_8Cr_6Fe_4$	-1.2	} ± 5%*	Cote and Meisel
$Ni_{63}Cr_{12}Si_8Fe_4$	0	}	(1982)
$Fe_{32}Ni_{36}Cr_{14}P_6B_{12}$	-5.0	}	
YNi	-2.8	}	
$Be_{40}Ti_{50}Zr_{10}$	-5.7	}	
$Fe_{80}B_{20}$	-4.5	} ± 0.1	Cochrane et al.
$Fe_{78}Mo_2B_{20}$	-11.7	}	(1980)
$Fe_{40}Ni_{40}P_{14}B_6$	-4.2	}	
$Fe_{32}Ni_{36}Cr_{14}P_6B_{12}$	-5.5	}	

* error estimated by present author from scatter in published data

poor. Cochrane et al. (1980) also measured p.c.r. at the lower temperature of 77K. The values were positive for the YNi and FeB alloys and negative for the others.

The results mentioned above all indicate that p.c.r. is negative at room temperature. However, Vassilou (1986) has shown that amorphous $Mg_{70}Zn_{30}$ has a p.c.r. of about $+50 \times 10^{-4}$ $(kbar)^{-1}$ at room temperature, up to 6 kbar. This value contrasts both in its large magnitude and in its positive sign with the other results.

More significant than the absolute value of the p.c.r. is the lack of correlation between p.c.r. and temperature coefficient of resistance (t.c.r.) in amorphous alloys.

Nearly all pure crystalline metals have a negative p.c.r. (Bridgman 1958) and a positive t.c.r. (Ashcroft and Mermin 1976) at room temperature. This correlation is an example of the law of corresponding states (McNeil 1983). Both compression and cooling reduce the mean square displacement of the ions of a crystalline lattice from their mean positions; the ratio of p.c.r. to t.c.r. depends on mechanical factors (compressibility, degree of anharmonicity and heat capacity) but not on the relation between this mean square atomic displacement and the resistance. This argument is built on the assumption that the dominant electron scattering mechanism is the thermal vibrations of the ions, i.e. electron-phonon scattering.

This assumption is good at room temperature for *crystalline* metals (Ashcroft and Mermin 1976) but poor for metallic glasses. The dominant electron-scattering mechanism in *amorphous* metals is the disorder of the mean atomic structure, as is demonstrated by their relatively small t.c.r. values (section 3.1)

A more general model of the effects of pressure, and of changes in temperature, is therefore needed in these materials. Any structural change, resulting from compression, heating, structural relaxation or some combination of the three, can be regarded as the superposition of a change in the dynamics of the ions on a change in their mean (time-averaged) positions. In crystalline metals, p.c.r. and t.c.r. can be modelled to a first approximation by neglecting the latter (static) effect entirely and ascribing all resistance changes to changes in mean square amplitude of the thermal vibrations of the ions. In amorphous metals, changes in the mean atomic structure contribute significantly to p.c.r., to t.c.r. and to structural relaxation itself.

A comparison of p.c.r. and t.c.r. at room temperature for a number of the metallic glasses mentioned above (McNeil 1983) bears out this conclusion. Some examples quoted by McNeil are sufficient demonstration. Both the p.c.r. and the t.c.r. of $Cu_{42}Zr_{58}$ are negative; the p.c.r. of $Fe_{32}Ni_{36}Cr_{14}P_{12}B_6$ is large and negative ($-3.8 \times 10^{-4}(\text{kbar})^{-1}$) whereas its t.c.r. is very small ($+0.2 \times 10^{-4}\ K^{-1}$). By comparing the values of t.c.r. in table

3.2.1 with p.c.r., where it has been measured, we can lengthen by one the list of those amorphous alloys exhibiting negative t.c.r. and negative p.c.r. $Ti_{50}Be_{40}Zr_{10}$ has a room temperature t.c.r. of -1.7×10^{-4} K^{-1} (Balanzat et al. 1985), to be compared with a p.c.r. of -5.7×10^{-4} $(kbar)^{-1}$ (Cochrane et al. 1980). McNeil's value of -1.2×10^{-4} K^{-1} for the t.c.r. of $Cu_{42}Zr_{58}$ is confirmed by the value (-0.9×10^{-4} K^{-1}) obtained by Balanzat et al. (1985) for the chemically very similar alloy $Cu_{40}Zr_{60}$. These comparisons are summarised in table 4.2.2. They show that compression and cooling are not corresponding states, and this confirms that the effect of pressure on the time-averaged atomic structure, as well as its effect on the mean square amplitude of thermal vibrations, must be considered in any theory of the p.c.r. of metallic glasses.

However, the $Pd_{82-x}V_xSi_{18}$ alloys studied experimentally as part of the present work, when considered separately, resemble crystalline metals in so far as their temperature and pressure coefficients of resistance are of opposite sign and are approximately proportionate. These results are discussed in detail, in the light of the conclusions of this review of compression measurements, in section 4.3 below. Before this, we give a qualitative argument for omitting from this review some results obtained at very high pressures.

Table 4.2.2

Examples refuting the law of corresponding states in the effect of cooling and compression on the resistance of metallic glasses at room temperature.

Composition	P.C.R./10^{-4}(Kbar)$^{-1}$	T.C.R./$10^{-4}K^{-1}$	Reference
$Cu_{42}Zr_{58}$	-8.0	-1.2	McNeil (1983)
		-0.9	Balanzat et al. (1985)
$Fe_{32}Ni_{36}Cr_{14}P_{12}B_6$	-3.8	+0.2	McNeil (1983)
			Cochrane et al. (1980)
$Ti_{50}Be_{40}Zr_{10}$	-5.7	-1.7	Balanzat et al. (1985)

Fritsch, Dyckhoff, Pollich and Lüscher (1985) studied the dependence of the resistance of $Pd_{80}Si_{20}$ on temperature (0 - 300K) and on pressure (0 - 115 kbar). At room temperature, the resistance decreased sharply with increasing pressure between 0 and 35 kbar, but increased again steadily with further increases in pressure, passing through its original zero pressure value again at about 70 kbar. Since this high pressure dependence of resistance is more complicated than the relatively low pressure effects described above, we must establish what range of pressures is relevant to this comparison of compression with structural relaxation.

Gibbs and Hygate (1985) estimated the order of magnitude of the hydrostatic pressure which must be applied to a metallic glass to cause as much densification as takes place during structural relaxation as follows. A typical value for the fractional densification of metallic glasses during irreversible structural relaxation is 0.3% (based on measured values of 0.25% (Cahn, Pratten, Scott, Sinning and Leonardsson 1984) and 0.3% in $Pd_{82}Si_{18}$ (Chason et al. 1985)). The bulk modulus, B, of metallic glasses is typically about 150 GPa (based on a value of 141 GPa in $Fe_{80}B_{20}$, measured by Chou, Davis and Hasegawa 1979). Since B is defined by

$$B = -V \frac{dp}{dV}$$

we can write, for small changes in V,

$$\Delta p = -B \ (\Delta V/V)$$

which yields, on insertion of the typical values given above, an estimate of the increase in pressure, above atmospheric, required to cause as much densification as occurs during irreversible structural relaxation:

$$\Delta p = -(150\text{GPa})(-3.10^{-3})$$
$$= 4.5 \text{ kbar}$$

The effect of pressures greater than about 10 kbar on electrical resistance are therefore of little interest for a direct comparison of structural relaxation with compression. The experiments of Fritsch et al. (1985), along with other very high pressure studies, tell us little about the dependence of resistance on pressure in the range of pressures of interest; they cannot therefore be used in the present direct comparison with structural relaxation experiments.

4.3 $Pd_{82-x}V_xSi_{18}$: Interpretation of Experimental Results

Amorphous $Pd_{82}Si_{18}$ has, at room temperature, a negative pressure coefficient of resistance of magnitude 1.3×10^{-4} $Kbar^{-1}$ and a positive temperature coefficient of resistance of magnitude 1.3×10^{-4} K^{-1}. The substitution of vanadium for 1 at % of the palladium reduces the

magnitude of t.c.r. by a factor of 5 and renders the p.c.r. unobservably small. With 2 at % vanadium, t.c.r. is lower still (2×10^{-5} K^{-1}) and p.c.r. is again zero, within the experimental resolution of $\pm 10^{-5}$ $Kbar^{-1}$.

These trends are summarised graphically in figure 4.3.1. They show that compression and cooling are corresponding states with respect to resistance measurements in this set of alloys. The $Pd_{82-x}V_xSi_{18}$ glasses are therefore a special case; metallic glasses in general fail to show this correlation of p.c.r. with t.c.r.

With this important finding in mind, we move on to a comparison of the effects of irreversible structural relaxation and compression in these glasses. As a measure of the effect of structural relaxation on resistance we take, from table 3.4.2, the normalised resistance change $\Delta R/R_0$ after an anneal of length 10^4s at 253°C, starting in the as-received state; here both ΔR and R_0 refer to measurements made at, or extrapolated to, the annealing temperature. Figure 4.3.2 shows $(\Delta R/R_0)$ and p.c.r. as functions of x, the concentration of vanadium in at %. This comparison shows clearly that the substitution of vanadium atoms for palladium atoms in $Pd_{82}Si_{18}$ reduces both the magnitude of the (negative) change in electrical resistance seen during irreversible structural relaxation and the magnitude of the (negative)

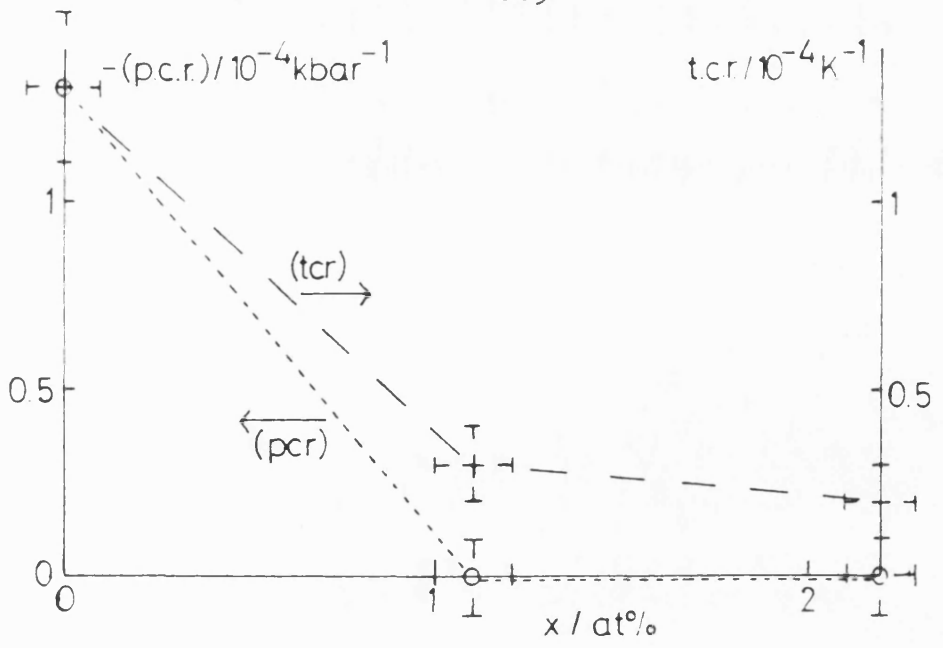

Figure 4.3.1: p.c.r. and t.c.r. of $Pd_{82-x}V_xSi_{18}$ alloys, at room temperature, as a function of x

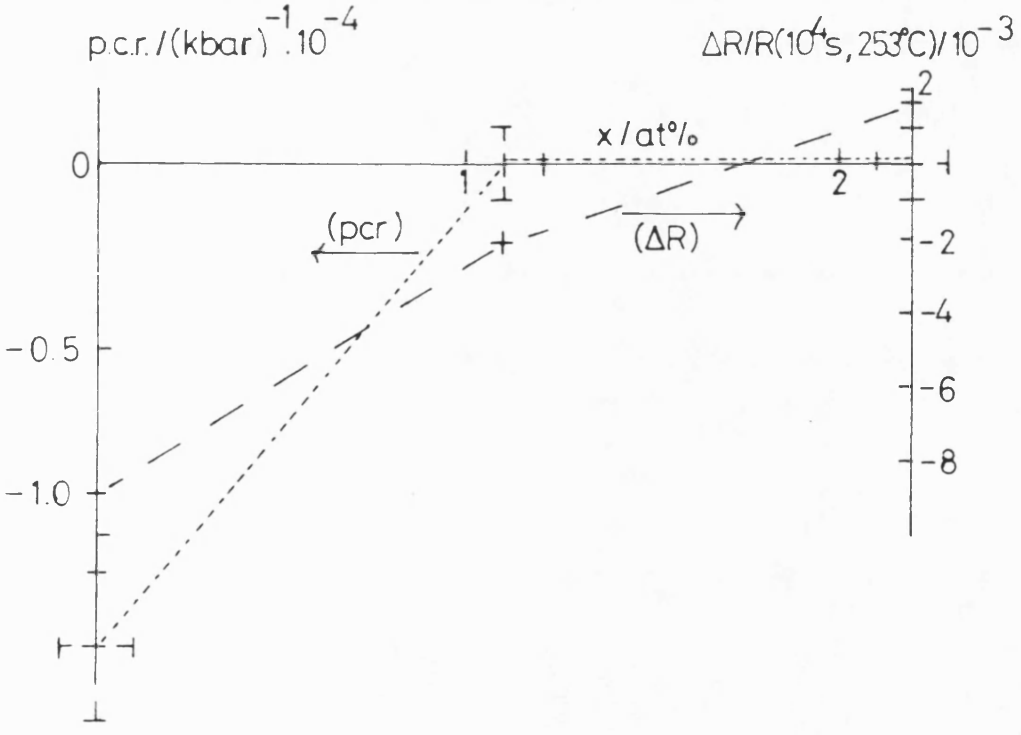

Figure 4.3.2: comparison of the effects of irreversible structural relaxation and hydrostatic compression on the electrical resistance of the $Pd_{82-x}V_xSi_{18}$ glasses (10^4s at 253°C; 0-3Kbar)

p.c.r. There is an approximate correlation between p.c.r. and $\Delta R/R_0$ as composition varies.

Table 4.3.1 extends this comparison of the effects of pressure and structural relaxation to those other metallic glasses for which both have been studied. In both $Fe_{80}B_{20}$ and $Fe_{32}Ni_{36}Cr_{14}P_6B_{12}$, all the measurements cited indicate that both p.c.r. and the change in resistance upon annealing are negative.

In $Fe_{40}Ni_{40}P_{14}B_6$, however, p.c.r. is negative, according to both Ast and Krenitsky and Cochrane et al., and the change in resistance upon isothermal annealing is positive, according to Sonius et al. (1983).

This comparison with other metallic glasses shows that the approximate correspondence between p.c.r. and $\Delta R/R_0$ seen in the PdVSi glasses is not exceptional. Neither is it universal; in $Fe_{40}Ni_{40}P_{14}B_6$ at least, densification is not the dominant mechanism by which irreversible structural relaxation affects electrical resistance.

In the case of $Pd_{82}Si_{18}$ alone, we know also that irreversible structural relaxation approximately halves the p.c.r. This experimental result is, to the best of the author's knowledge, the first of its kind for any metallic glass. The interpretation of this result must

Table 4.3.1

Comparison of the effects of compression and irreversible structural relaxation on electrical resistance in several metallic glasses.

Composition	P.C.R./10^{-4}(Kbar)$^{-1}$	$(\Delta R/R_0)/10^{-3}$
$Fe_{80}B_{20}$	-5.0 (McNeil 1983)	-1.5 (Rio Tinto & Marine 1984) -ve (Cost and Stanley 1982)
$Fe_{32}Ni_{36}Cr_{14}P_6B_{12}$	-3.8 (McNeil 1983) -5.0 (Cote & Meisel 1982) -5.5 (Cochrane et al. 1980)	-2 (Mulder et al. 1981)
$Pd_{82}Si_{18}$	-1.3 (McNeil 1983) -1.3 (present work)	-8.7 (present work)
$Pd_{81}V_1Si_{18}$	0 } (present work)	-2.1 } (present work)
$Pd_{80}V_2Si_{18}$	0 }	+1.7 }
Fe40Ni40P14B6	-3.9 (Ast & Krenitsky 1976) -4.2 (Cochrane et al. 1980)	+ve (Sonius et al. 1983)

be based on an understanding of the mechanism whereby compression alters electrical resistance in $Pd_{82}Si_{18}$.

It was pointed out in section 4.2 that it is necessary in general to allow for changes in both the dynamic behaviour and the average positions of the ions of a metallic glass when considering the effect on its resistance of changes in structure such as those caused by hydrostatic compression. In crystalline metals the effect of pressure on the mean square amplitude of thermal ionic vibration dominates the p.c.r. (McNeil 1983). To what extent does this contribution also dominate in $Pd_{82}Si_{18}$?

In order to answer this question, let us begin by noting that the fractional change, -0.5, in the p.c.r. of $Pd_{82}Si_{18}$ due to irreversible structural relaxation is large, being of order unity, unlike the corresponding small fractional changes in resistance reported above. This result is inconsistent with the notion that changes, during compression, in the mean (time-averaged) atomic structure are dominant in their effects on resistance over changes in dynamics of the ions; this inconsistency can be demonstrated by a simple argument.

Suppose that an applied hydrostatic pressure of 1 kbar causes a change in the *mean* atomic structure of as-received $Pd_{82}Si_{18}$ large enough to reduce its room temperature resistance by 130 parts per million. After

irreversible structural relaxation, application of the same hydrostatic pressure changes the room temperature resistance by only half that fraction: this would imply that the change in mean atomic structure with unit applied pressure is halved upon irreversible structural relaxation. The effect of structural relaxation on the stiffness of the metallic bonding would be to reduce it by 50%; this would imply that such physical properties as Young's modulus and speed of sound must be reduced by a similar degree during structural relaxation. Such dramatic changes have not been observed in any metallic glass.

Let us suppose instead that changes in the dynamics of the ions are the dominant mechanism whereby pressure affects resistance in $Pd_{82}Si_{18}$. For a small applied pressure to change the potential well in which an ion finds itself, and hence to change the dynamic properties of that ion, the potential well must be anharmonic, as is demonstrated in appendix 2. It is also shown there that any component of p.c.r. which can be ascribed to the effect of pressure on the dynamics of the ions is proportional to the anharmonicity of the interionic potential well, provided that the anharmonity is not too great. The halving of p.c.r. can therefore be attributed, on the basis of our last assumption, to a halving of the anharmonicity of the interionic potential well during irreversible structural relaxation.

This explanation is not in conflict with the relatively small changes in resistance observed during irreversible structural relaxation because changes in anharmonicity alone have no direct effect on either the dynamics or the mean structure of the atoms at atmospheric pressure.

However, if the dominant contribution to p.c.r. in $Pd_{82}Si_{18}$ is the change in the dynamics of the ions with pressure, then we would expect that t.c.r. would be dominated by the same effect and would therefore show the same dramatic sensitivity to irreversible structural relaxation. In fact t.c.r. changes by only about 5% when as-received $Pd_{82}Si_{18}$ is given a similar annealing treatment (table 3.4.2). This conflict between observation and the idea that anharmonicity changes dramatically during structural relaxation is confirmed by the results of Leonardsson (1984) who found that irreversible structural relaxation in $Fe_{40}Ni_{40}B_{20}$ had a negligibly small effect on the coefficient of thermal expansion; this quantity is directly related to anharmonicity in metals (Ashcroft and Mermin 1976, p. 495).

In conclusion: the PdVSi glasses obey approximately a law of corresponding states with respect to compression and cooling; such a correspondence is seen in some other, but not all other metallic glasses. The p.c.r. of $Pd_{82}Si_{18}$ is approximately halved by irreversible structural relaxation; this effect has not been explained satisfactorily.

5. THE THERMOELECTRIC POWER

Chapter 5 The Thermoelectric Power

Measurements of the thermoelectric power or thermopower, S, of an amorphous alloy can be used to test the applicability of the Ziman (nearly free electron) model to the transport properties of that amorphous alloy (Cochrane, Destry, Brebner, Baibich and Muir 1981). Measurements of the room-temperature thermoelectric power of the $Pd_{82-x}V_xSi_{18}$ metallic glasses, all in the as-received state, were made with a view to applying such a test.

5.1 What is Thermoelectric Power?

When heat is driven along an electrically isolated strip of metal by an imposed temperature gradient, an electric field builds up along the strip. The following account of the origin of this thermoelectric effect is an extension of a short explanation given by Barnard (1972) and is based on the NFE model of electron transport.

Consider the metal strip of figure 5.1.1(a), which is subject to a longitudinal temperature gradient. Heat flows from the hot end to the cold end and is mostly carried, at room temperature, by electrons. (From here on, we will neglect the contribution of phonons to the thermal conductivity of metals.) Since the metal strip is an open electrical circuit, the total steady current flowing along it must be zero. The 'thermal' electric current, consisting of relatively energetic electrons

Figure 5.1.1: thermoelectric power of a NFE metal:

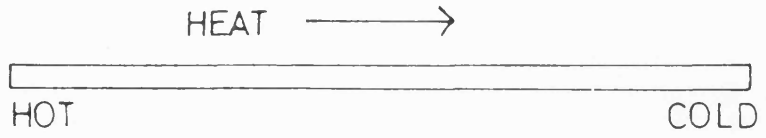

(a) metal strip in a thermal gradient

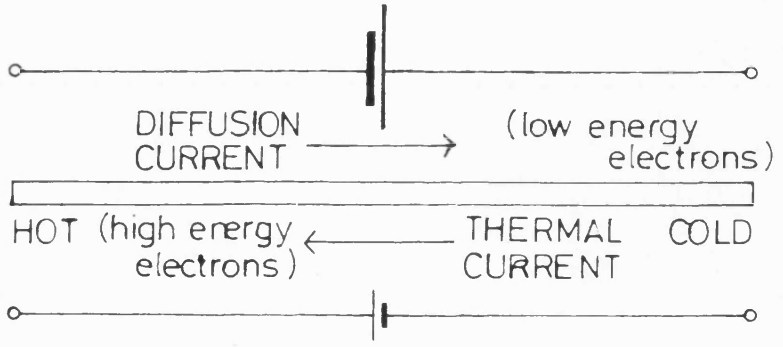

(b) negative thermopower

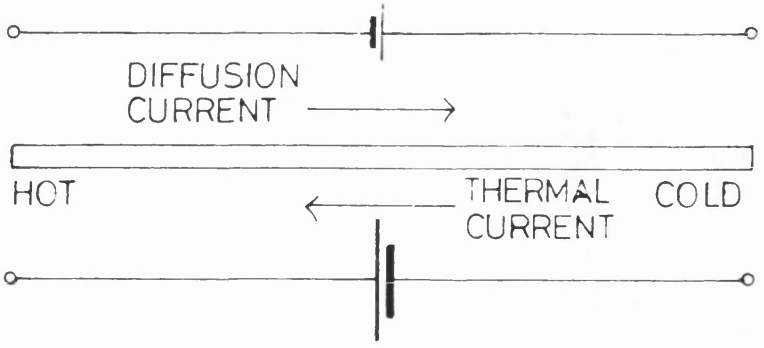

(c) positive thermopower

driven by the temperature gradient, is therefore matched by an equal and opposite 'diffusion' electric current consisting of electrons with relatively little energy driven by a chemical potential gradient. Since no net current flows, what is the origin of the thermovoltage?

Its origin is in the different resistivities which the thermal current and the diffusion current experience. Let us suppose that electrons of relatively high energy are scattered less effectively by the potentials of the ions than lower energy electrons are. Then the potential difference associated with the (higher-energy) thermal current would be smaller in magnitude than that associated with the (lower-energy) diffusion current. Figure 5.1.1(b) shows this case, in which the strip is electrically equivalent to a voltage source with its positive terminal at the cold end of the strip and the absolute thermopower of the metal is conventionally defined to be negative.

If the energy-dependence of the degree of electron scattering was opposite in sign, such that electrons with more energy were scattered more effectively by the ionic potential, then the potential difference driving the thermal current would be larger in magnitude than that driving the diffusion current and the metal strip would be equivalent to a voltage source with its positive terminal at the hot end (figure 5.1.1(c)). In this case the absolute thermopower of the metal is positive.

If the efficacy of electron scattering is independent of the energy of the current-carrying electrons, the thermopower will be zero according to this simple model.

The above argument can be summarised algebraically by defining a function $\sigma(E)$ such that the conductivity σ of the metal in question is given by

$$\sigma = \sigma(E_f)$$

where E_f is the fermi energy. The thermopower S is the differential coefficient dV/dT of the thermovoltage V with respect to the difference T in temperature between the ends of the strip. S is then proportional to the energy-derivative $\sigma'(E)$ of $\sigma(E)$ and its sign is opposite to that of $\sigma'(E)$. The rough argument is therefore in agreement with the expression

$$S(T) = - \frac{\pi^2 K^2}{3e} T \frac{d\ln\sigma(E)}{dE}$$

derived, e.g. by Ashcroft and Mermin (1976), from a semiclassical treatment of electron dynamics.

The thermopower can be measured by connecting leads to the ends of the metal strip and measuring the potential difference between the other ends of the leads at some constant temperature. The material from which the leads are made will itself have in general some non-zero

thermopower, so the voltage measured will be an indication of the strength of the thermoelectric power in one metal with respect to another, rather than an absolute determination. Only by using superconducting leads, with zero thermopower, can an absolute measurement be made.

The principle behind the experimental arrangement described in section 5.2 below is illustrated in figure 5.1.2. A nanovoltmeter of very high input impedance measures the potential difference between the end of a strip of metallic glass and a length of platinum tape, both at a temperature of 0°C. The tape and the strip are soldered together, at their other ends, at a temperature T, greater than 0°C. The nanovoltmeter is connected such that its reading is positive when the potential of the platinum joint is positive with respect to that of the metallic glass join.

The nanovoltmeter reading is approximately proportional to the difference between T and the cold junction temperature 0°C. The thermopower of platinum at 0°C is about $-4\mu VK^{-1}$ (Weiss 1963); therefore (figure 5.1.1(b)) the platinum tape will always contribute positively to the reading at the nanovoltmeter. If the reading were always zero, we could conclude that the metallic glass had the same thermopower as platinum. A positive reading indicates that the metallic glass has a thermopower greater than $-4\mu VK^{-1}$ at 0°C; a negative reading indicates that the metallic glass has a thermopower less than (i.e.

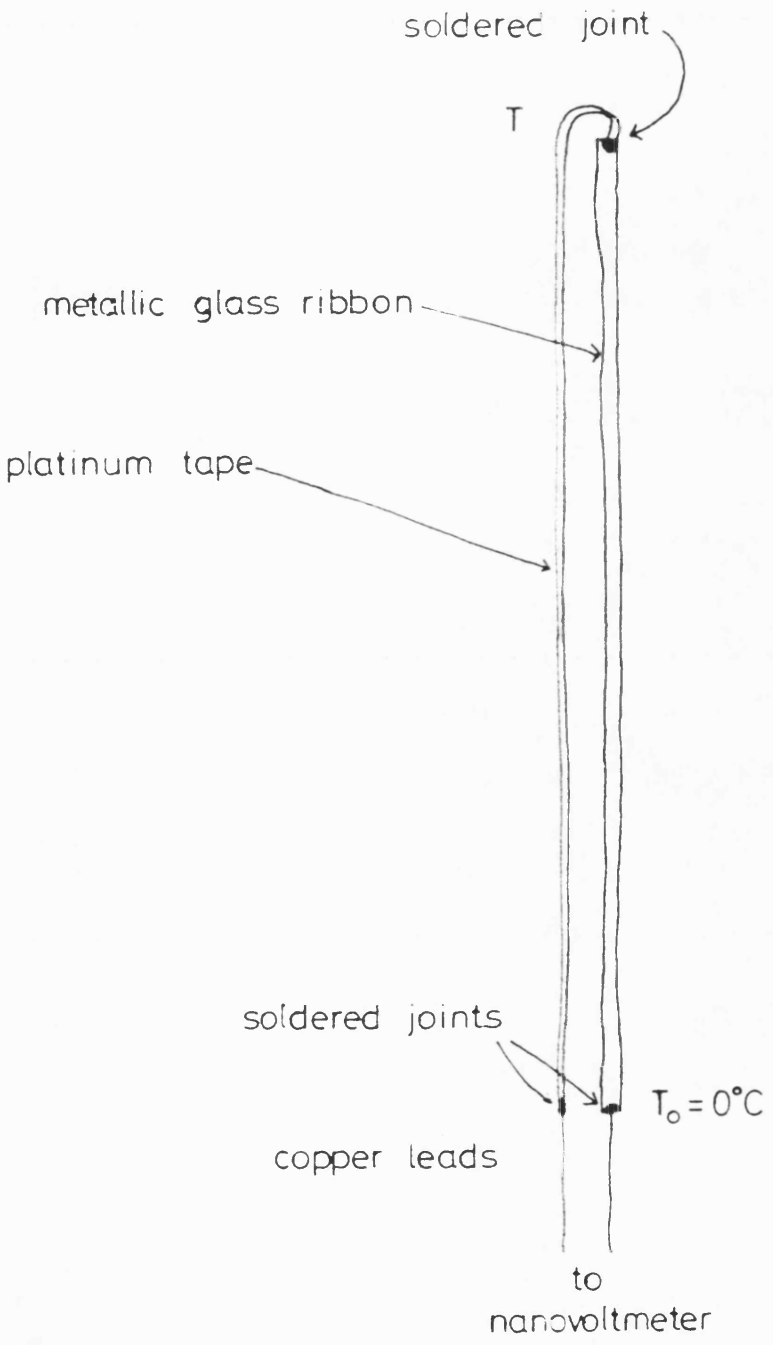

Figure 5.1.2: measurement of thermoelectric power: principle

more negative than) $-4\mu VK^{-1}$ at 0°C. Algebraically,

$$dV/dT = S - (-4\mu V/K) \quad \text{---------- (5.1.1)}$$

where V is the nanovoltmeter reading and S is the absolute thermopower of the metallic glass at 0°C.

5.2 Experiment

The principle of figure 5.1.2 was implemented physically by constructing the apparatus shown in figure 5.2.1. The cold junctions were maintained at 0°C by submerging them in melting ice. The temperature of the hot junction, measured by a calibrated thermocouple, was controlled by wrapping it in a large wad of securely clamped furnace padding material which was then heated using an air blower. T was allowed to rise steadily to 100°C; the hot junction was then allowed to cool slowly, and about twenty pairs of readings (T, V) were obtained for each metallic glass as T fell from about 100°C to room temperature.

The results V(T) are shown in figure 5.2.2. In all three cases, V is a linear function of T, indicating that a single constant S is sufficient to characterise the thermoelectric power of each alloy over the temperature range 0°C - 100°C. Application of formula (5.1.1) yields for the room temperature thermoelectric powers of the PdVSi glasses the values given in table 5.2.1. The (large) thermoelectric power of crystalline constantan was also measured in order to confirm that the values obtained for

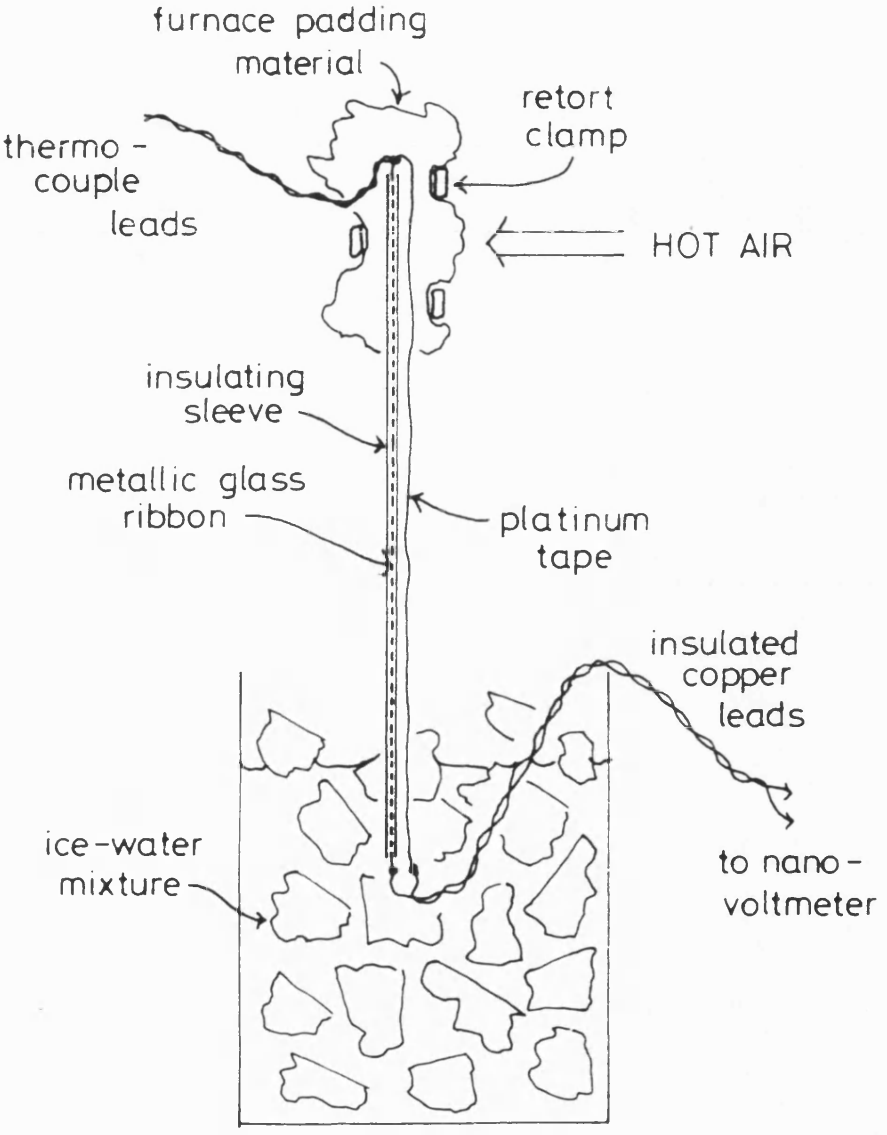

Figure 5.2.1: experimental arrangement

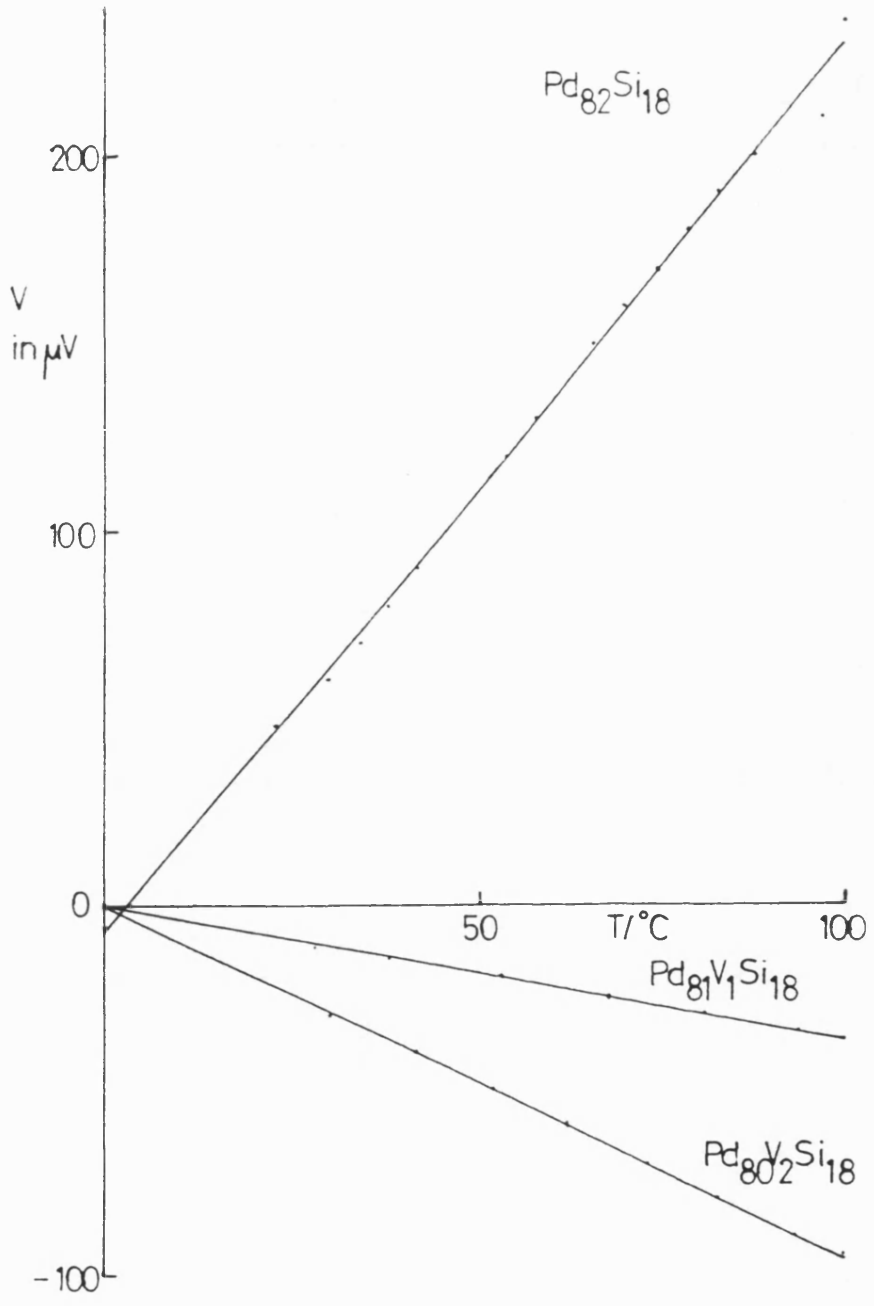

Figure 5.2.2: thermoelectric voltages of PdVSi glasses with reference to platinum. Hot junction at temperature T, cold junction at 0°C

Table 5.2.1

Absolute Thermoelectric Powers of PdVSi glasses

Composition	dV/dT (μVK^{-1})	S(μVK^{-1})
$Pd_{82}Si_{18}$	+2.2	-1.8 ± 10%
$Pd_{81}V_1Si_{18}$	-0.4	-4.4 ± 10%
$Pd_{80}V_2Si_{18}$	-1.0	-5.0 ± 10%

the PdVSi glasses were of the correct signs and order of magnitude. The experimental result was

$$S = +35\mu VK^{-1}$$

in reasonable agreement with a literature value of $+39\ \mu VK^{-1}$ (Kaye and Laby 1976). The slight disagreement suggests that systematic errors might be of order 10%.

The thermoelectric powers S of all three glasses are small and negative. Substitution of vanadium for palladium reduces S from about $-2\mu VK^{-1}$ to about $-5\mu VK^{-1}$.

5.3 Testing the NFE Model

The NFE expression for thermopower can be written

$$S = -\frac{\pi^2 K^2 T}{3eE_f}\ [3 - 2q] \qquad (5.3.1)$$

(Barnard 1972, Nagel 1978), provided that the effective scattering potential of each ion is not strongly energy-dependent. The quantity q above is given in Ziman's model by

$$q = \frac{|u(2K_f)|^2\, a(2K_f)}{\langle |u|^2 a \rangle} \qquad (5.3.2)$$

(Sinha 1970, Faber 1972), where $|u(K)|^2$ is the square of the magnitude of the effective scattering potential as a function of the length K of the scattering vector, a(K) is the structure factor and triangular brackets denote an

integration of the same form as in equation (3.3.1). The value of q is determined by the differential coefficient of $|u|^2 a$ with respect to K around $2K_f$ (Faber 1972) and would be difficult to calculate. However, q also occurs in NFE expressions for t.c.r. and p.c.r.; comparisons of S, t.c.r. and p.c.r., determined experimentally for a single composition of glass, can therefore provide a test of the applicability of the NFE model to that glass.

The relation between S, as given by 5.3.1 and 5.3.2, and t.c.r. is easy to see in the light of the models of t.c.r. used by Sinha (1970), Kelton and Spaepen (1984) and Yokota et al. (1985) and described in section 3.3. These authors assume that the dominant contribution to changes in resistivity with temperature is obtained by setting resistivity proportional to the value $a(2K_f)$ of the structure factor evaluated at $2K_f$. By assuming, on the basis of diffraction studies of liquid metals by Halder et al. (1969), that the first peak in the structure factor broadens and decreases in height with increasing temperature, Sinha, Kelton and Spaepen and Yokota et al. were able to attribute negative t.c.r. to the coincidence of $2K_f$ with the position K_p of the first peak in the structure factor. Conversely, positive t.c.r. shows that $2K_f$ lies well to one side of the peak, according to these authors.

A similar argument relating thermoelectric power Q to the relative values of $2K_f$ and K_p is given by Nagel (1978). The quantity q will be large, according to Nagel, when $2K_f \approx K_p$. A positive thermoelectric power should therefore be found when t.c.r. is negative. In the opposite case ($2K_f$ not close to K_p), the thermopower will be negative and approximately equal to $-\pi^2k^2T/eE_f$ and t.c.r. will be positive.

In order to make a numerical estimate of the quantity π^2k^2T/eE_f we need first to estimate the Fermi energy E_f. The free-electron value is

$$E_f = \frac{h^2}{2m} (3\pi^2n)^{2/3}$$

where n is the number density of free electrons, yielding a value of about 5eV for E_f if we take a typical metallic value of about $10^{28}m^{-3}$ for n (Omar 1975). Experimentally determined values of E_f in metals range from 2 to 12eV (Omar 1975); Nagel (1978) took E_f = 7.3eV in amorphous $Ti_{50}Be_{40}Zr_{10}$ and Cochrane et al. (1980) estimate that a valence of two, in three ion-based alloys, corresponds to a Fermi energy of 8eV.

We set E_f = 8eV ± 50% and T = 300K and find that

$$\frac{\pi^2 k^2 T}{eE_f} = 2.8\ \mu V/K \pm 50\% \text{ ---------- (5.3.3)}$$

Since $Pd_{82}Si_{18}$ has a positive t.c.r., we would expect on the basis of Nagel's argument that its thermopower would be given by $-\pi^2k^2T/eE_f$. The measured value, $-1.8\mu VK^{-1}$, of Q at room temperature in $Pd_{82}Si_{18}$ lies within the range of Q values predicted by equation (5.3.3) and is therefore consistent with Nagel's argument. However, the explanation of the trends in t.c.r. as vanadium is substituted for palladium in the PdVSi series given by Kelton and Spaepen (1984) is definitely inconsistent with the measured values of the thermoelectric power in $Pd_{81}V_1Si_{18}$ and in $Pd_{80}V_2Si_{18}$, as we will now demonstrate.

The account given by Kelton and Spaepen (1984) (section 3.3) rests on the assumption that $2K_f$ increases toward K_p as vanadium is substituted for palladium. This implies that both E_f and $a(2K_f)$ are greater in the alloys containing vanadium than the corresponding quantities in $Pd_{82}Si_{18}$. As $2K_f$ approaches K_p, the quantity q in equation (5.3.1) increases according to Nagel (1978); the increases in q and in E_f as vanadium is substituted for palladium have the same effect in equation (5.3.1), namely to increase the predicted value of S. Experiment has shown (table 5.2.1) that S is more negative in

$Pd_{81}V_1Si_{18}$ than in $Pd_{82}Si_{18}$, and slightly more negative still in $Pd_{80}V_2Si_{18}$. The explanation of the trends in t.c.r. with vanadium concentration in these alloys is therefore inconsistent with the experimental results presented in section 5.2, no matter whether the changes in E_f or the changes in $a(2K_f)$ are considered the dominant effect. This application of the NFE model to electron transport in the PdVSi amorphous alloys is over-simplistic and cannot be used to explain the effects of irreversible structural relaxation on the resistance of these glasses.

A further test of the NFE model has been suggested by Cochrane et al. (1980). They plot points representing five different compositions of metallic glass on a graph of the volume coefficient of resistivity versus the thermoelectric parameter ξ, defined by

$$\xi = - \frac{3|e|E_f}{\pi^2 k^2} \frac{Q}{T} \qquad \text{(5.3.4)}$$

Faber (1972) had found that the five lightest liquid alkali metals, together with liquid bismuth and liquid gallium, lie on the line

$$\frac{d\ln\rho}{d\ln V} = \frac{2}{3}\xi + 3 \qquad \text{(5.3.5)}$$

and Faber explained this within the NFE model by assuming that the combined effects of a change in atomic volume on

each scattering potential and on the structure factor do not vary much from one liquid metal to another.

Cochrane et al. (1980) estimated $d\ln\rho/d\ln V$ from each measurement of $d\ln R/dp$ using the approximate relation

$$\frac{d\ln\rho}{d\ln V} = \frac{1}{3} - K\frac{d\ln R}{dp} \qquad (5.3.6)$$

where K is the bulk modulus, for which they took the value 1600 kbar as representative of metallic glasses. Equation (5.3.6) relies on the assumption that deformation is isotropic under hydrostatic pressure; this assumption is questionable in the light of the anisotropy of metallic glass ribbon (Cahn et al. 1984) noted in the preamble to section 3.2 of this thesis. Cochrane et al. used a value of 8eV for E_f in equation (5.3.4) to derive ξ from each measurement of thermoelectric power Q. They found that all but one of the metallic glasses they studied lay well to one side of the 'Faber line' (5.3.5). Figure 5.3.1 shows the Faber line, the band within which Faber's metals fell, and the five points representing metallic glasses. Cochrane et al. noted that they were unable to add points corresponding to the PdVSi alloys because of a lack of thermopower data. Points representing amorphous $Pd_{82}Si_{18}$, $Pd_{81}V_1Si_{18}$ and $Pd_{80}V_2Si_{18}$ have been added to figure 5.3.1 by making the approximations that Cochrane et al. made. Table 5.3.1

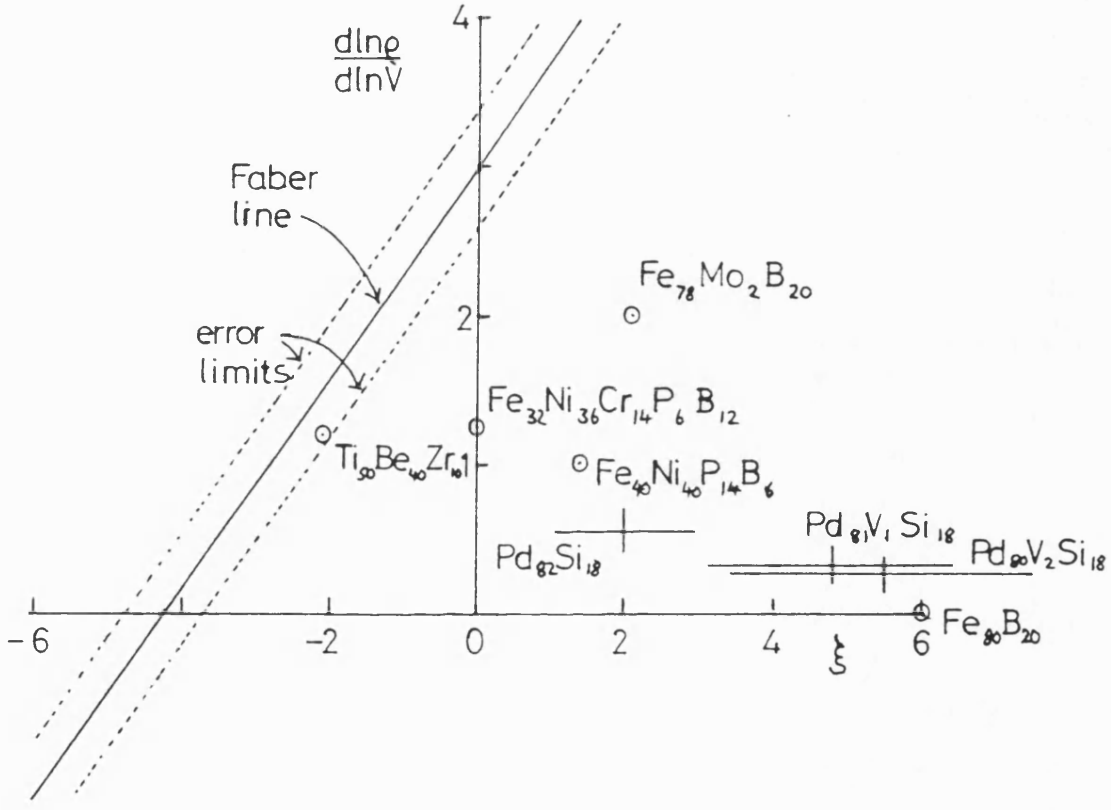

Figure 5.3.1: the Faber line

Table 5.3.1

Composition	S/ VK^{-1}	ξ	$\frac{d\ln R}{dp}$ /10^{-4}Kbar^{-1}	$\frac{d\ln\rho}{d\ln v}$
$Pd_{82}Si_{18}$	-1.8 ± 10%	2.0 ± 50%	-1.3 ± 0.2	0.54 ± 0.2
$Pd_{81}V_1Si_{18}$	-4.4 ± 10%	4.8 ± 50%	0 ± 0.1	0.33 ± 0.1
$Pd_{80}V_2Si_{18}$	-5.0 ± 10%	5.5 ± 50%	0 ± 0.1	0.33 ± 0.1

ξ calculated using E_f = 8eV T = 300K in equation (5.3.4)

$d\ln\rho/d\ln v$ calculated using K = 1600 Kbar in equation (5.3.6)

records the conversion of S to ξ and of $d\omega R/dp$ to $d\omega\rho/d\omega V$ in each case.

The PdVSi alloys lie well to the same side of the Faber line as the alloys investigated by Cochrane et al. Allowing for an error of ± 50% in ξ, due to uncertainty in E_f, the PdVSi glasses fail to fit the Faber correlation. This disagreement is in fact independent of the magnitude of our estimate of E_f; the fact that S is negative, and therefore that ξ is positive, in each glass, together with the fact that $d\ln\rho/d\ln V$ is less than unity in each case puts the PdVSi alloys at best twice as far from the Faber line than any of Faber's liquid metals.

This comparison of measurements of thermopower and the effects of pressure on resistance shows that the Ziman model, as developed by Faber (1972) for liquid alkali metals, is not applicable to conduction in the PdVSi alloys. However the assumptions made by Faber, and by Cochrane et al. in converting p.c.r. to $d\ln\rho/d\ln V$, are all questionable when applied to metallic glasses. The failure of Faber's equation (5.3.5) to describe the points representing the PdVSi alloys on figure 5.3.1 does not, therefore, imply that the NFE model itself is inapplicable.

6. SUMMARY (CHAPTERS 3 - 5)

Chapter 6 Summary (Chapters 3-5)

Without making use of any analysis of the kinetics of structural relaxation, we have been able to draw some conclusions about the effects of reversible and irreversible structural relaxation on the electrical properties of metallic glasses, and in particular of the $Pd_{82-x}V_xSi_{18}$ glasses (x = 0, 1, 2). These conclusions are set out below. All measurements of changes in electrical resistance are quoted as such rather than being transformed to changes in resistivity because no reliable method of effecting this transformation has been found, as demonstrated in section 3.1.

It was shown (Summary of Experimental Findings, section 3.2) that reversible and irreversible ordering are distinct; they can change a single property of a single metallic glass in opposite senses. This conclusion is confirmed by the results of the present experiments (table 6.1). It was also shown, from the results of structural relaxation experiments alone, that in general the electron scattering processes which dominate at the low temperature of 4.2K are distinct from those prevalent at temperatures higher than 77K; both reversible and irreversible ordering, in separate experiments, changed the low-temperature resistance in one sense and the high-temperature resistance in the other, in $Fe_{40}Ni_{40}P_{14}B_6$.

Table 6.1

PdVSi Glasses - Electrical Properties

Composition	$Pd_{82}Si_{18}$	$Pd_{81}V_1Si_{18}$	$Pd_{80}V_2Si_{18}$
t.c.r./$10^{-4}K^{-1}$ (0°C - 250°C), as-received	1.20	0.37	0.13
p.c.r./$10^{-4}Kbar^{-1}$	-1.3 ± 0.2	0 ± 0.1	0 ± 0.1
Effects of Irreversible Structural Relaxation (253°C, 10^4s)			
$\Delta R/R_0/10^{-3}$	-8.7	-2.1	+1.7
Δ(t.c.r.)/$10^{-4}K^{-1}$	+0.06	-0.09	-0.08
$\Delta\|$p.c.r.$\|10^{-4}Kbar^{-1}$	-0.7 ± 0.1	0	0
Effect of Reversible Structural Relaxation			
(1/R) $d\Delta R/d\Delta T_A/10^{-6}K^{-1}$	-10	-5	-8

Some electrical properties of the PdVSi glasses, and the effects of structural relaxation on these properties, are summarised in table 6.1. The three metallic glasses obey approximately a law of corresponding states with respect to compression and cooling, but this has not been useful in identifying the mechanism whereby changes in pressure and temperature affect electrical resistance. More interesting is the correlation of both p.c.r. and t.c.r. with the change ΔR of resistance, measured at the anneal temperature, during irreversible structural relaxation. This correlation shows that densification is an important component of irreversible structural relaxation in these metallic glasses. Irreversible structural relaxation affects p.c.r. strongly; this has not been properly understood.

The effects, both on electrical properties and on their structure-dependence, of the substitution of 1 at% and 2 at% vanadium for palladium in $Pd_{82}Si_{18}$ are dramatic. The t.c.r. and the p.c.r. are reduced in magnitude almost to zero. The effects of irreversible structural relaxation on resistance and on t.c.r. are reversed, but the reversible effects of temperature cycling on resistance show no significant change. How can such a small change in composition have such large effects?

Kelton and Spaepen (1984) assume that the vanadium atoms change the electronic structure of the metallic glass, rather than its atomic structure. They suggest that the extra conduction band elctrons introduced by the vanadium

atoms increase the Fermi level, thereby changing the sensitive dependence of electron scattering on atomic structure. They use an extended and simplified form of Ziman's nearly free electron theory to model this change in Fermi level, and hence the structure-dependence of resistivity, qualitatively.

A 2% change in stoichiometry is much smaller than those used by other experimenters to produce significant changes in the structural processes underlying any isothermal property change. It seems unlikely that the atomic rearrangements underlying structural relaxation in $Pd_{80}V_2Si_{18}$ differ greatly from those in $Pd_{82}Si_{18}$. The differences therefore seem likely to lie in the dependence of electrical properties on structural change, rather than in the structural changes themselves, as Kelton and Spaepen assumed. However, it has been shown in chapter 5 that the nearly-free-electron analysis carried out by Kelton and Spaepen, and used on a different group of metallic glasses by Yokota et al. (1985), can be extended (Faber 1972) to predict the thermoelectric powers of the three metallic glasses and is in conflict with their experimentally determined values. The Ziman model may be applicable, but the much simplified form of it used by Kelton and Spaepen is not.

Finally, we address the contrast between the reversible changes in resistance, which appear to be insensitive to the concentration of vanadium, and the highly composition-dependent irreversible resistance changes.

Here is more evidence that reversible and irreversible structural relaxation are distinguishable on non-kinetic grounds. The dominant underlying *irreversible* structural change in the PdVSi glasses is clearly linked to the irreversible resistance changes it causes by a highly composition-dependent mechanism. The *reversible* structural change is therefore different in nature, otherwise it too would give rise to widely different reversible resistance changes in the three metallic glasses studied.

7. THE KINETICS AND TEMPERATURE-DEPENDENCE OF STRUCTURAL RELAXATION

Chapter 7 The Kinetics and Temperature-Dependence of Structural Relaxation

In a review of the observed effects of structural relaxation on electrical resistance (section 3.2), we identified two distinct modes of structural change. Irreversible resistance changes were seen in as-received metallic glasses annealed well below their crystallisation temperatures; much smaller reversible changes were seen in pre-stabilised metallic glasses and seem to indicate that the equilibrium glassy structure is different at different annealing temperatures. One of the conclusions of section 3.2 was that irreversible and reversible ordering are distinct in that they can affect the electrical resistance, measured at a fixed temperature, oppositely.

We now consider the effects of structural relaxation on physical properties in general. Measurements of many properties have been used to monitor structural relaxation and all show an irreversible effect (Huizer 1987). Reversible effects are seen in Curie temperature, Young's modulus,enthalpy, ductility, hardness, magnetic after-effect and superconducting transition temperature as well as in electrical resistance (Huizer 1987). The existence of a reversible isothermal length change in $Fe_{40}Ni_{40}B_{20}$ is deduced by Huizer, only by assuming that the early stages of isothermal anneals of pre-stabilised samples are well described by the free-volume model (see below) of structural relaxation. Huizer's results

certainly show that any reversible length effect is very small in magnitude, about 1 ppm/K.

In many experimental studies, the isothermal change Δp in some physical property p has been plotted as a function of the logarithm of annealing time, t, because data points are spread over several decades in time. Such plots are often linear over some of the range of time investigated (Inque, Matsuzaki, Toyota, Chen, Masumoto and Fukase 1985; Hernando, Nielsen and Madurga 1985; Egami 1978). The occurrence of a region of "log-time kinetics" is central to one analysis of relaxation kinetics (Gibbs, Evetts and Leake 1983) but Gibbs, Stephens and Evetts (1984) point out that the occurrence of log-time kinetics arises from the limited range of annealing times and temperatures available. Annealing time is limited by thermal mass of the apparatus during the warm-up ($t \gtrsim 10^1$s) and by the economics of running very long experiments ($t \lesssim 10^7$s). Annealing temperature is limited by the need to provide enough thermal energy for relaxation to take place in the above timescale ($T \geq$ 400K) and by the onset of crystallisation ($T \lesssim T_x$ - 50K where T_x is the crystallisation temperature). The occurrence of a linear region in a log-time plot of Δp is an important feature of isothermal annealing studies of metallic glasses (Gibbs et al. 1984).

Implicit in log-time kinetics is the fact that the evolution $\Delta p(t)$ of the change in some physical property during isothermal annealing experiments cannot be

represented by a simple exponential decay curve. The main tasks of any general theory of structural relaxation in metallic glasses are to account for the non-simply-exponential form of $\Delta p(t)$ and to explain the temperature dependence of the long-term values of some physical properties. Two different mathematical approaches to these questions are considered in section 7.1. Physical interpretations of the two mathematical approaches are outlined in sections 7.2 and 7.3. In section 7.4 we review some attempts to fit experimental data using these two models.

7.1 Mathematical Analysis

The first task of a mathematical model of structural relaxation is to account for the kinetics of irreversible property changes seen during isothermal anneals of as-received metallic glasses. A universal problem with using experimental kinetic results to differentiate between mathematical models is that a significant proportion of any observed property change takes place during the warming-up period before the required anneal temperature is reached. At best, we have to try to fit models to incomplete kinetic curves. More pessimistically, we have to recognise that each approach $T(t)$ to a desired annealing temperature T_A is unique because the equilibrium glassy structural state toward which relaxation is progressing is in general temperature-dependent. Strictly, a truly isothermal anneal cannot be simulated at all in an experiment

because of the uniqueness of each experimental heating rate, but in practice it is assumed that some effective zero in time can be found such that the effects, once the desired annealing temperature has been attained, of the real experimental thermal treatment are the same as the effects of an ideal isothermal anneal beginning at this effective zero in time. This point of view becomes less reasonable the more strongly the equilibrium value of the property in question depends on temperature. A consistent and systematic method of estimating the effective zero in time is clearly required for sensitive kinetic analysis. This problem will be addressed in chapter 8.

The simplest kinetic equation is simple exponential decay

$$\Delta p(t) = (\Delta p)_{total} \ (1 - e^{-t/\tau}) \quad \text{----------} \quad (7.1.1)$$

where τ is the relaxation time. The expression (7.1.1) for $\Delta p(t)$ is the solution of the differential equation

$$dp(t)/dt = -(p(t) - p(\infty))/\tau \quad \text{----------} \quad (7.1.2)$$

which states that the rate of change of p is proportional to the difference between p and its equilibrium value. Many physical processes (e.g. radioactive decay and first-order chemical reactions) can be modelled by choosing τ and $(\Delta p)_{total}$ in (7.1.1) correctly, but for the kinetics of irreversible structural change, a more complicated model is needed.

Irreversible Relaxation Kinetics - Free Volume Model

In the "free volume" model of structural relaxation (van den Beukel and Radelaar 1983), the physical property p of interest is regarded as simply related to the mean atomic free volume $\langle v_f \rangle$. The free volume model predicts the evolution of changes in $\langle v_f \rangle$ as a result of thermal treatments. It is used to model $\Delta p(t)$ on the assumption that the kinetic features of $\langle v_f \rangle(t)$ will be identical to those of $\Delta p(t)$. The differential equation for $\langle v_f \rangle(t)$ is

$$\frac{d\langle v_f \rangle}{dt} = -C(T) \frac{\langle v_f^2 \rangle}{v^*} e^{-Q_a/kT} e^{-v^*/\langle v_f \rangle} \quad \text{---------- (7.1.3)}$$

where $C(T)$, v^* and Q_a are constants at constant temperature. The physical basis for equation (7.1.3) is discussed in section 7.2 where a rigorous definition of $\langle v_f \rangle$ is also given. For the purposes of the present comparison of mathematical descriptions of structural relaxation, we note that equation 7.1.3 is fundamentally different from equation 7.1.2 in that we would have to make τ a function of $\langle v_f \rangle$ if we wanted to write (7.1.3) in the form (7.1.2). In this seemingly obscure observation lies a fundamental difference between free volume theory and the alternative mathematical approach which we will consider below. In the free volume theory, departures from simple exponential decay can be accounted

for without invoking the presence of a variety of contributory relaxation processes with different relaxation times. Instead, by using the more complicated kinetic equation (7.1.3), departures from the simple exponential form of (7.1.1) can be attributed to a single mechanism of relaxation, characterised by a single set of constants.

Integration of (7.1.3) (van den Beukel and Radelaar 1983) yields implicitly the time-dependence of $\langle v_f \rangle$.

$$e^{v^*/\langle v_f \rangle} - e^{v^*/\langle v_f \rangle_0} = t\,C'(T) \qquad \text{(7.1.4)}$$

where $C'(T) = C(T)\, e^{-Q_a/kT}$. Plots of $\langle v_f \rangle$ as a function of $\log[tC'(T)]$ according to (7.1.4) are reproduced in figure 7.1.1 for various values of $\langle v_f \rangle_0$. The curves of figure 7.1.1 show a monotonic decrease in $\langle v_f \rangle$ from $\langle v_f \rangle_0$ towards zero. At no point are any of the curves even approximately linear in log-time; each has a point of inflection, but this is always at a knee in the curve. The claim made by van den Beukel and Radelaar (1983) that part of each curve is fairly linear in log-time seems to conflict with their graph, figure 7.1.1. Any plausible decay curve will be approximately linear in log-time for part of its range; the tails of the curves of figure 7.1.1 show a consistent upward curvature and therefore contain a definite non-zero quadratic component in log-time.

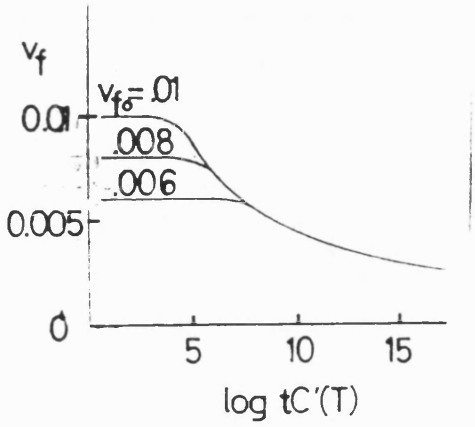

Figure 7.1.1: decay of free volume according to van den Beukel and Radelaar (1983)

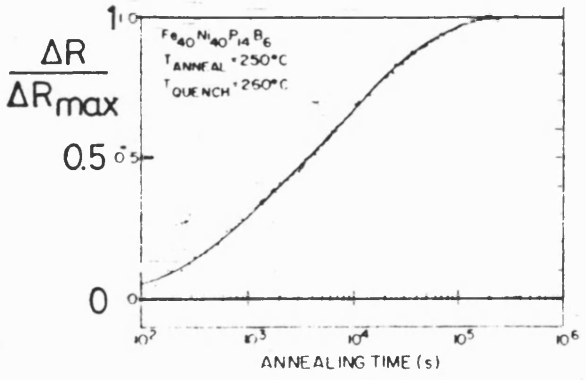

Figure 7.1.2: experimental data of Cost and Stanley (1981) on $Fe_{40}Ni_{40}P_{14}B_6$

Van den Beukel and Radelaar (1983) point out that in much of the literature, a broad spectrum of relaxation times has been invoked to account for observed relaxation kinetics. The idea of a spread of relaxation times, avoided in the free volume model, is the basis of the second mathematical approach which we will now outline.

Irreversible Relaxation Kinetics - AES Model

Complicated kinetic behaviour can be modelled by taking linear combinations of solutions of the form (7.1.1) of equation (7.1.2), each with a different relaxation time τ and a different weighting (Δp_∞).

$$\Delta p(t) = \Sigma\ (\Delta p_\infty)_i\ (1 - e^{-t/\tau_i}) \quad \text{----------} \quad (7.1.5)$$

A fundamental difference between this approach and the free volume model is that the relaxation mechanisms represented by each term in the summation act independently. Each term represents a simple exponential decay process whose relaxation time τ is unaffected by the progress of structural relaxation. This contrasts with the dependence of the effective relaxation time of equation (7.1.3) on v_f.

Cost and Stanley (1981) used equation (7.1.5) to fit an isothermal resistance change curve which shows a region of linearity with log-time (figure 7.1.2; log-time

kinetics between 10^5s and 10^6s). These results in fact refer to reversible structural change, but the analytical method of Cost and Stanley is appropriate here. They were able to fit the curve well by including four terms in the summation of (7.1.5).

Gibbs et al. (1983) see fundamental problems in relating the four relaxation times of Cost and Stanley to physical properties of the metallic glass. Cost and Stanley however have an explanation for their discovery of distinct relaxation times, rather than a broad spread; they postulate that the microscopic atomic jumps contributing to structural relaxation are distributed broadly over relaxation time τ, but that each "kinetic process" involves the cooperative occurrence of one hundred single atomic jumps or more of the same type and therefore drawn from the same distribution in τ. The averaging of relaxation times involved sharpens the distribution such that each "kinetic process" is characterised by a lognormal distribution in τ with very small width, i.e. by a single relaxation time. This explanation has not been adopted in subsequent treatments of the problem.

Starting with the same postulate, that microscopic relaxation processes are each described independently by equation (7.1.1), Gibbs et al. (1983) developed the activation energy spectrum model (AES), in which the distribution of relaxation times is described by a

continuous function rather than by a collection of narrow peaks. This method was first applied by Primak (1955) to the trapping of electrons in potential wells in phosphorus.

The summation of equation (7.1.5) is replaced by an integration in AES:

$$\Delta p(t) = \int_0^\infty f(\tau)(1 - e^{-t/\tau})d\tau \quad \text{----------} \quad (7.1.6)$$

where $f(\tau_0)d\tau$ is the contribution to $\Delta p(t)$ from those processes with a relaxation time τ within $d\tau$ of τ_0. The relaxation time of a relaxation process is expressed in terms of its energy of activation, E, in AES.

$$\frac{1}{\tau} = \nu e^{-E/kT} \quad \text{----------} \quad (7.1.7)$$

The physical origin of this equation will be discussed in section (7.3), with particular attention to the significance of ν.

Substituting the form (7.1.7) for τ into equation (7.1.6) produces

$$\Delta p(t) = \int_{-\infty}^{\infty} \tilde{f}(E)\ \{1 - \exp(\nu t e^{-E/kT})\}\left(\frac{1}{\nu kT} e^{E/kT}\right)dE$$

where $\tilde{f}(E) \equiv f(\tau)$. The lower limit of this integral can

be changed from $-\infty$ to 0, excluding processes with negative activation energy, for the following practical reason. There will be in any experiment a minimum attainable delay Δt between the effective start of the isothermal anneal and the first truly isothermal measurement. This delay will be long in experiments in which the metallic glass is heated slowly. All the relaxation processes with $E < kT\ln(\nu\Delta t)$ will occur during this period of delay and will therefore never be observed. The product $\nu\Delta t$ is a number many orders of magnitude greater than 1, as we find in the analysis presented in chapter 9. Any choice of the lower limit less than $kT\ln(\nu\Delta t)$ is therefore acceptable; we choose zero because equation (7.1.7) is derived (section 7.3) by considering processes with $E > 0$, and is therefore not valid when $E < 0$.

We now adopt the notation of Gibbs et al. (1983) by redefining the arbitrary distribution function $\tilde{f}(E)$:

$$\frac{1}{\nu kT}\, e^{E/kT}\tilde{f}(E) \equiv \overline{c(E)}\,q(E)$$

to give

$$\Delta p(t) = \int_0^\infty \overline{c(E)}\,q(E)\,\theta(E, T, t)\,dE \qquad \text{---------- (7.1.8)}$$

where

$$\theta(E, T, t) = 1 - \exp(-\nu t e^{-E/kT})$$

The form chosen for this distribution function by Gibbs et al. reflects a distinction they make between the *number* of relaxation processes $q(E)dE$ with activation energy within dE of E and the strength of *coupling* between the relaxation processes and the changes Δp in physical property.

The coupling function $\overline{c(E)}$ represents an average, over all the processes with activation energies within dE of E, of the coupling constants c(E) of each such process.

$$\overline{c(E)} = \frac{1}{n} \sum_{i=1}^{n} c_i(E)$$

where the summation is over the n processes with activation energy within dE of E.

The use of the integral in equation (7.1.8) in place of a sum of discrete contributions from processes with distinct activation energies reflects the defining characteristic of an amorphous solid: the atoms have widely different environments, unlike atoms in a crystal, whose environments are nearly identical. Comparable relaxation processes at different points in the solid have to overcome energy barriers with a wide range of heights E when they take place. In contrast, similar processes such as self-diffusion in a crystalline solid are characterised by a single activation energy.

We can therefore expect to have to use a function $\overline{c(E)}q(E)$ which is appreciable over a wide range of E, rather than one which is sharply peaked, to simulate structural relaxation in amorphous metals. The extreme case of a broad function $\overline{c(E)}q(E)$ is

$$\overline{c(E)}q(E) = \text{constant} \quad \text{---------- (7.1.9)}$$

and this trial form has been much used in applications of AES.

Inserting the trial form (7.1.9) into (7.1.8) yields

$$\Delta p(t) \; \alpha \int_0^\infty \theta(E,T,t)\, dE \quad \text{---------- (7.1.10)}$$

The function $\theta(E,T,t)$ is sketched as a function of E for a range of values of the parameter kTlnνt in figure 7.1.3a. For each value of kTlnνt, Δp is proportional to the area under the graph of $\theta(E)$, according to equation (7.1.10). This can easily be evaluated by numerical integration.

Gibbs et al. (1983) pointed out that a good approximation to the function $\theta(E,T,t)$ is the step function

$$H(E,kT\ln\nu t) = \begin{cases} 1 & E \leq kT\ln\nu t \\ 0 & E > kT\ln\nu t \end{cases}$$

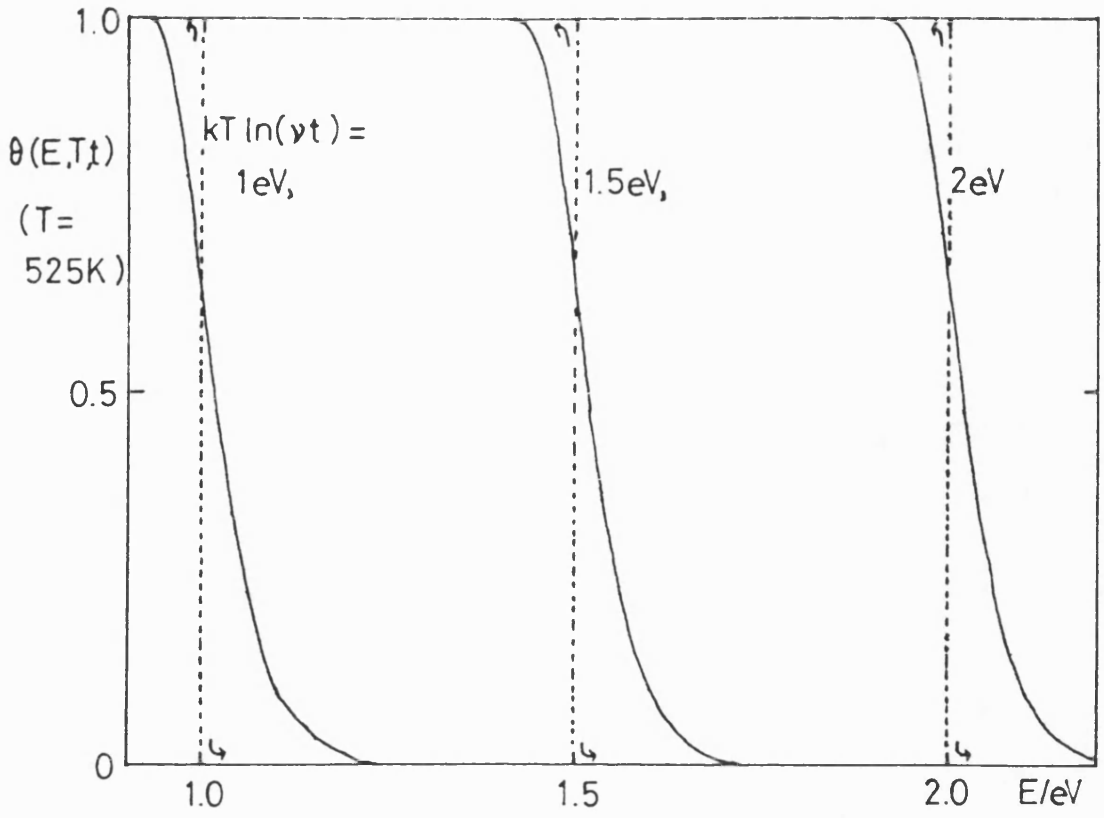

(a)

Figure 7.1.3: the function θ(E,T,t)

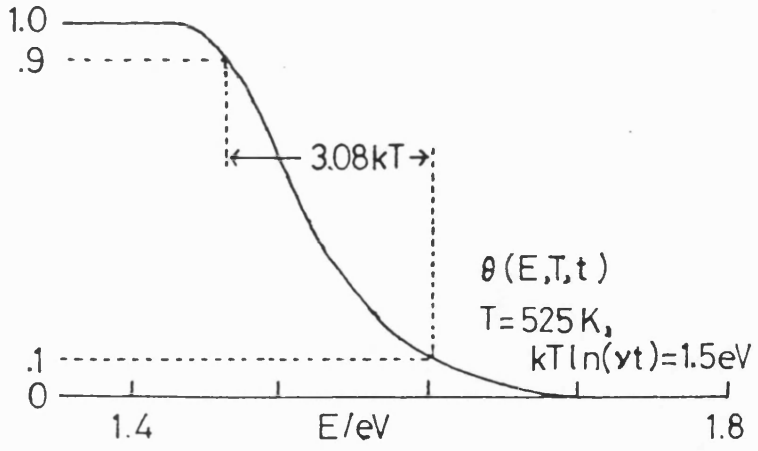

(b)

represented, for each value of kTlnνt, by broken lines in figure 7.1.3a. Because of the frequent occurrence of the parameter kTlnνt in AES it has been given the symbol E_0.

$$E_0 = kT\ln\nu t$$

$$\theta(E,T,t) \approx H(E,E_0) \qquad (7.1.11)$$

Equation (7.1.10) can now be reduced, using the approximate form (7.1.11) for θ, to

$$\Delta p(t) \alpha E_0$$

Reverting to the original notation,

$$\Delta p(t) \alpha kT\ln\nu t$$

we see that AES, in its step function approximation and with the trial form (7.1.9) for $\overline{c(E)}q(E)$, predicts linearity of $\Delta p(\ln t)$ or log-time kinetics.

The shoulder of the function $\theta(E,T,t)$ in figure 7.1.3a is very narrow as illustrated in figure 7.1.3b which shows the exact and approximate forms for θ for a typical value, 1.5eV, of kTlnνt. θ changes from 0.9 to 0.1 over

a width 3kT of E. The value of $\theta(E_0,T,t)$ is 1-1/e, or 0.632.

The characteristic isothermal-annealing function $\theta(E,T,t)$ (Primak 1955) sweeps along the E-axis such that the area under it increases approximately logarithmically with time. As well as predicting log-time kinetics in the special case of a flat function $\overline{c(E)}q(E)$, this feature of the annealing function can be used to visualise the evolution of property change for a general function $\overline{c(E)}q(E)$.

Figure 7.1.4 shows an arbitrary function $\overline{c(E)}q(E)$ and the annealing function $\theta(E,T,t)$. The shaded area is proportional to $\Delta p(t)$. The form of $\overline{c(E)}q(E)$ chosen in figure 7.1.4 is in fact a Gaussian; clearly the wider the Gaussian, the better $\overline{c(E)}q(E)$ approximates to equation (7.1.9) and the more nearly linear will a graph of Δp vs. lnt appear. Section 9.1 includes a computational study of the relation between the width of a Gaussian trial form for $\overline{c(E)}q(E)$ and the kinetic behaviour predicted by AES.

The step approximation (7.1.11) can be usefully employed in the case of an arbitrary function $\overline{c(E)}q(E)$;

substituting $H(E,E_0)$ for $\theta(E,T,t)$ in equation (7.1.8) yields

$$\Delta p(t) \approx \overline{c(E_0)}q(E_0)$$

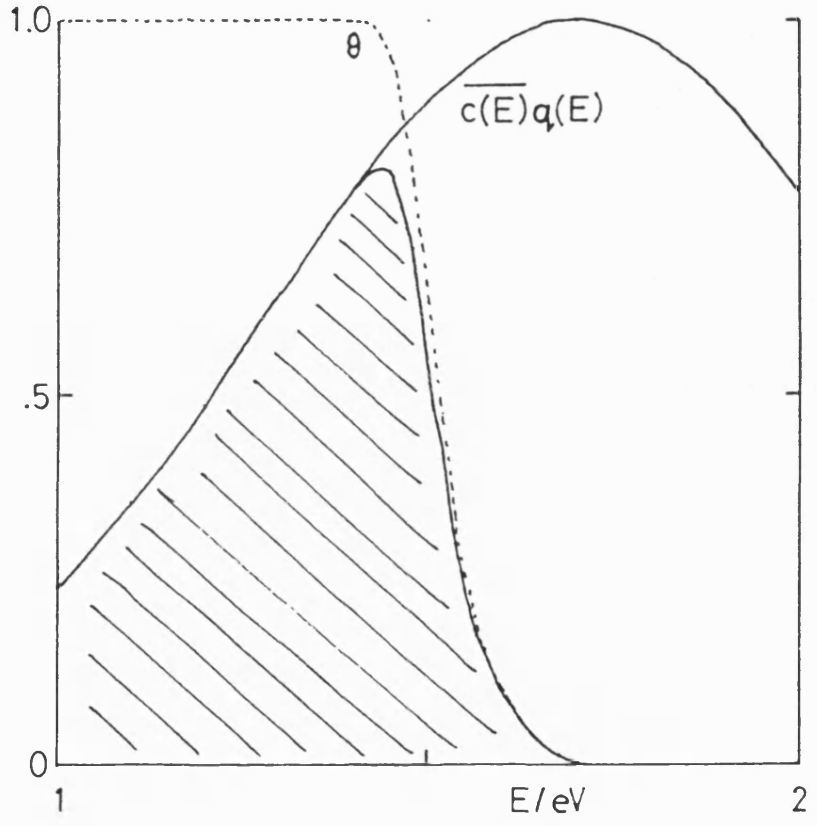

Figure 7.1.4: visualisation of the evolution of Δp for a general function $\overline{c(E)}q(E)$

In this approximation, the value of $\Delta p(t)$ is determined simply by the value of $\overline{c(E)}q(E)$ when $E = kT\ln\nu t$; using the exact form of θ, we find that the value of Δp at a particular time t is determined by the value of $\overline{c(E)}q(E)$ over a range of E of width a few kT, centred on $kT\ln\nu t$. The analysis so far has been of the kinetics of structural relaxation; we now outline the mechanisms for temperature-dependence of the equilibrium glassy state in these two models.

Reversibility

In the free volume model, as originally proposed by van den Beukel and Radelaar (1983), reversibility (temperature-dependence of the equilibrium glassy state) is attributed to chemical short-range ordering (CSRO) and disordering. The distinction between reversible CSRO and the irreversible decay of free volume is a sharp one in this model. CSRO is a simple decay process; changes in the degree of chemical short-range order α are assumed to be proportional to the physical property change being measured, and obey the first-order decay equation

$$\frac{d\alpha}{dt} = \frac{-1}{\tau_s}(\alpha - \alpha_E) \qquad (7.1.12)$$

where α_E is the temperature-dependent equilibrium value

of α and where τ_s is a relaxation time. Like free volume decay itself, CSRO slows down as less free volume becomes available; mathematically, this is evident in the dependence of τ_s on $\langle v_f \rangle$:

$$\tau_s = \tau_0 \, e^{v^*/\langle v_f \rangle} \, e^{Q_s/kT} \qquad (7.1.13)$$

where v^* and Q_s are constants.

The free-volume analysis has been adapted in order to make it fit experimental facts (section 7.4) but the features of it emphasised above remain. They are the dependence of both irreversible and reversible relaxation kinetics on the degree of irreversible structural relaxation so far attained and a sharp distinction of kind between irreversible and reversible relaxation processes.

The AES model makes no such sharp distinction. Reversibility is attributed to temperature-dependence of the number of relaxation processes which have not yet occurred when irreversible structural relaxation is complete. The term $\overline{c(E)}q(E)$ in equation (7.1.8) is regarded as the difference between a term $\overline{c(E)}q_0(E)$ which represents the initial, as-received structural state and a term $\overline{c(E)}q_s(E,T)$ which represents the temperature-dependent equilibrium structural state.

$$q(E) = q_0(E) - q_s(E,T)$$

Figure 7.1.5 shows a hypothetical form for $q_0(E)$ and for a series of functions $q_s(E,T)$. Suppose that structural relaxation from the as-received state at some temperature T_2 has become negligibly slow at time t_L and that the property change after this time t_L is represented by the area shown shaded (\) in figure 7.1.5, including the cross-hatched area. If the temperature is then increased to T_3, a fresh contribution to the total property change will begin, corresponding to the cross-hatched region of figure 7.1.5.

Conversely, an anneal at temperature T_1 after a preanneal at the higher temperature T_2 gives rise to a fresh contribution to $\Delta p(t)$ represented by the stippled area in figure 7.1.5. The figure seems to show that an anneal at a temperature higher than that of the preanneal causes a reversal in the sign of $\Delta p(t)$ upon changing the temperature and that an anneal at a temperature lower than that of the preanneal causes $\Delta p(t)$ to continue in the same direction as during the preanneal; however, this need not be the case. We expect $q_s(E,T)$ to increase, for all E, with increasing T, but $\overline{c(E)}$ may have a different sign for the processes which contribute significantly to reversible change and for all the relaxation processes on average. A comparison of the sign of irreversible

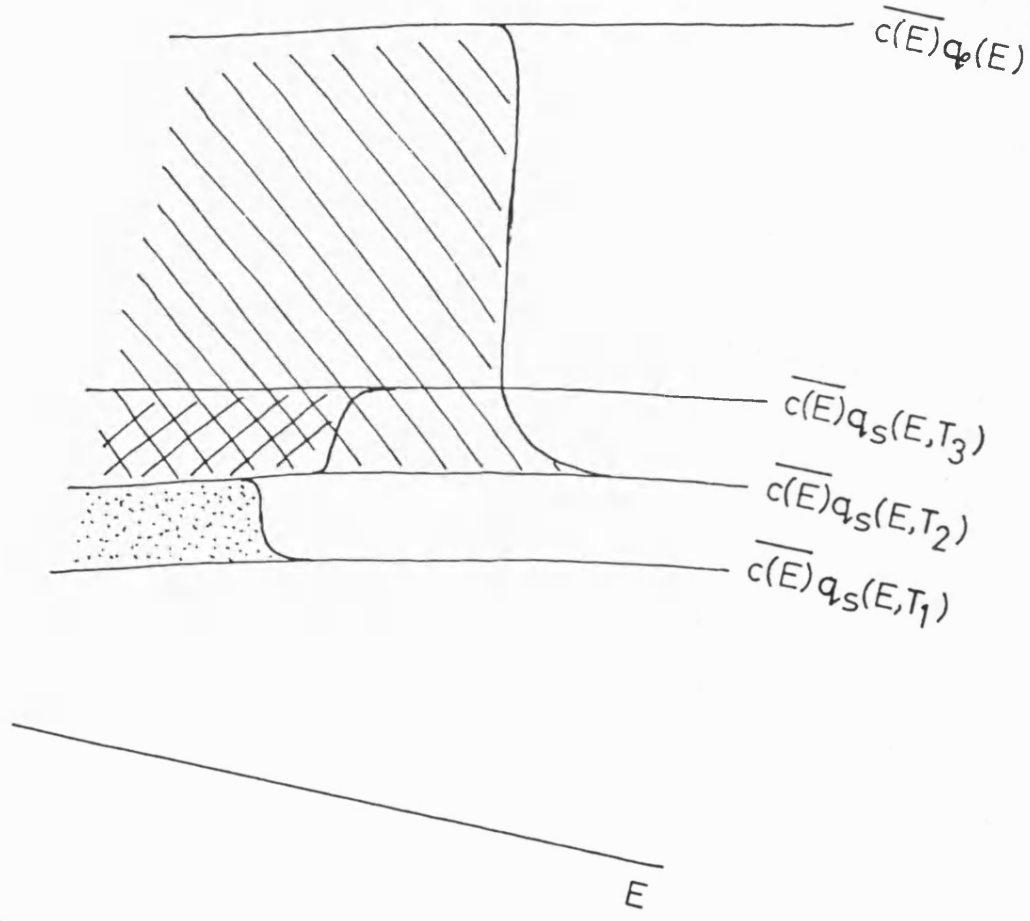

Figure 7.1.5: reversibility in the AES model

property change with the sign of the temperature dependence of the long-term value of the same property is not therefore a test of the AES model. The simple picture of a single function $\overline{c(E)}$ linking a physical property to structural change in a particular metallic glass therefore has to be sacrificed in order to account for reversibility. The average coupling function $\overline{c(E)}$ depends on which processes are being averaged and it therefore depends on the thermal history of the glass.

In chapter 8, the nature of the distinction between relaxation processes which contribute to reversibility and those which do not is examined. It is shown that this distinction can be regarded as one of degree rather than of kind. This feature of AES contrasts with the distinction between reversible CSRO and irreversible annihitation of free volume made by van den Beukel and Radelaar (1983). In AES, kinetics is independent of how much irreversible structural relaxation has occurred, and this is the other important difference between AES and the free-volume model.

Experimental studies of the effect of irreversible structural relaxation on the kinetics of reversible structural relaxation are inconclusive (Leake 1987). Sonius et al. (1983) report a decrease, during annealing from the as-received state, of the rate of reversible structural relaxation in $Fe_{40}Ni_{40}B_{20}$ as detected by resistometry. However, Balanzat et al. (1985) find that the rate of reversible relaxation in a wide variety of amorphous alloys does not change as irreversible relaxation proceeds.

In general, it must be expected that the rate of all relaxation processes will depend on the structural state of the solid. If this dependence proves to be appreciable in magnitude, then it will be necessary to introduce a structure-dependence, and therefore a time-dependence, into the spectral functions of AES, complicating the analysis considerably.

This survey of phenomenological modelling has not been exhaustive. Egami (1978) proposed that the kinetics of the changes in some general relaxation parameter x can be described by the differential equation

$$\frac{dx}{dt} = c \exp\left(\frac{-\alpha x}{kT}\right) \qquad (7.1.14)$$

where c is a constant. Egami showed that this equation, upon integration, predicts log-time behaviour in x. This model will not be pursued further in this thesis because it lacks of a physical interpretation. Egami states that equation (7.1.14) describes the kinetics of a thermally activated process with apparent activation energy proportional to x itself but this is inaccurate. Such an equation is

$$\frac{dx}{dt} = - \frac{(x - x_0)}{\tau_0} \; e^{-\alpha x/kT}$$

and equation (7.1.14) is in fact equation (7.1.2) with *relaxation time*, rather than activation energy, proportional to x.

7.2 Interpretation - The Free Volume Model

Spaepen (1977) proposed that steady state flow in metallic glasses is the result of diffusive atomic jumps. Following Cohen and Turnbull (1959), Spaepen considered an atom with effective hard-sphere volume v*, next to a gap in the atomic structure (figure 7.2.1). A potential energy barrier separates the initial (shaded) and final (dotted) positions; thermal activation is the mechanism for crossing the barrier.

The statistics of thermal activation across a potential barrier are represented in Spaepen's analysis as follows. "In order for an atom to be on a potential jump site, its free volume must be larger than v*." Spaepen defines free volume as that part of an atom's nearest neighbour cage in which it can move around without an energy change.

The probability that an atom is at a potential jump site is therefore simply the probability that its free volume exceeds v*. Cohen and Turnbull (1959) proposed that the probability $p(v_f)dv_f$ that the free volume of an atom is within dv_f of v_f is given by

$$p(v_f)dv_f = \frac{\gamma}{\langle v_f \rangle} \exp - \left(\frac{\gamma v_f}{\langle v_f \rangle}\right) dv_f \quad \text{---------- (7.2.1)}$$

where γ is a constant between 1/2 and 1 and $\langle v_f \rangle$ is the mean free volume. The probability that an atom is at a

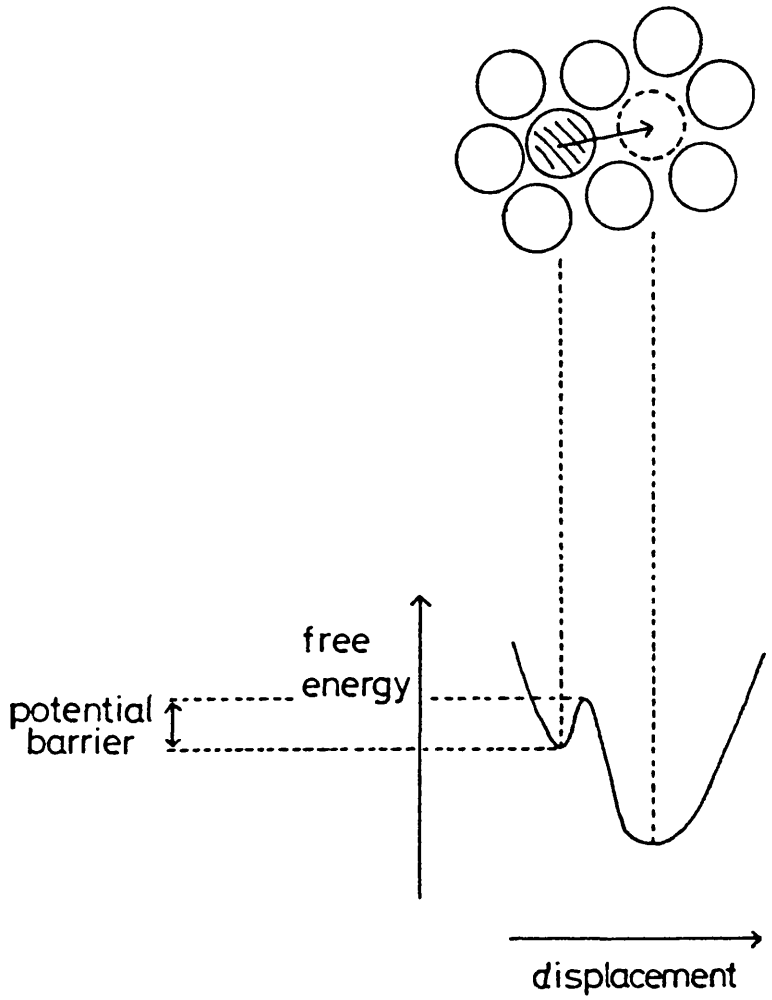

Figure 7.2.1: individual atomic jump, after Spaepen (1977)

potential jump site is therefore

$$\int_{v^*}^{\infty} \frac{\gamma}{\langle v_f \rangle} \exp\left(\frac{-\gamma v_f}{\langle v_f \rangle}\right) dv_f = \exp \frac{-\gamma v^*}{\langle v_f \rangle} \quad \text{---------- (7.2.2)}$$

At high temperatures and with low applied stresses, flow is homogeneous; i.e., all volume elements contribute to the flow. Under these conditions, all atoms at a potential jump site will jump, and the (Newtonian) viscisity, η, is given by

$$\eta = (\text{const.})\ T \exp\left(\frac{Q_a}{kT}\right) \exp\left(\frac{\gamma v^*}{\langle v_f \rangle}\right) \quad \text{---------- (7.2.3)}$$

where (const.) contains no temperature- or time-dependence and where Q_a represents the energy of activation of the jumping atom. The approach of van den Beukel and Radelaar (1983) is to use equation (7.2.3) to relate the (measurable) kinetics of viscosity change to the (unknown) kinetics of mean free volume change in metallic glasses. To this end, we differentiate equation (7.2.3) with respect to time.

$$\dot{\eta} = (\text{const.})\ T \exp\left(\frac{Q_a}{kT}\right) \exp\left(\frac{\gamma v^*}{\langle v_f \rangle}\right) \left(\frac{-\gamma v^*}{\langle v_f \rangle^2}\right) \dot{\langle v_f \rangle} \quad \text{--- (7.2.4)}$$

The experimental result is a simple and very convenient one. Taub and Spaepen (1980) found that the viscosity of amorphous $Pd_{80}Si_{20}$ in homogeneous flow increased linearly with time during isothermal annealing experiments. The rate of increase was found to vary with temperature as

$e^{-Q_a/kT}$ where Q_a = 32kJ/mol. Rewriting $\dot{\eta}$ as $\dot{\eta}(T)$ in (7.2.4), and arbitrarily condensing some of the terms, we have

$$\frac{d\langle v_f\rangle}{dt} = -C(T)\,\frac{\langle v_f\rangle^2}{v^*}\,e^{-Q_a/kT}\,e^{-\gamma v^*/\langle v_f\rangle} \qquad (7.2.3)$$

where $C(T) = \dfrac{\dot{\eta}(T)}{T(\text{const.})}$

which is equation (7.1.3), the basis of the free-volume model.

The arguments described above apply to metallic glasses in a steady state of homogeneous flow well below the glass transition temperature. The proposal of van den Beukel and Radelaar is that the decay of $\langle v_f\rangle$ which evidently occurs in these conditions also occurs in any annealing treatment, independent of whether or not the ribbon is being stressed, and therefore that $\langle v_f\rangle$ can be regarded as a structural parameter, decaying as structural relaxation proceeds.

Most metallic glasses do not exhibit a conventional glass transition because, upon heating, crystallisation intervenes before T_g can be reached (Huizer 1987, Leake, to be published). The extension of equation (7.1.3) by van den Beukel and Radelaar (1983) to temperatures close to T_g is therefore of little interest to us. They replace $\langle v_f\rangle^2$ with $(\langle v_f\rangle - \langle v_f\rangle_e)^2$, defining the

temperature-dependent equilibrium value $\langle v_f \rangle_e$ of $\langle v_f \rangle$. We emphasize that, at temperatures well below T_g, this is not a mechanism for reversibility; $\langle v_f \rangle$ always decreases.

The parameter α which describes the degree of chemical short-range order in the free-volume model is defined by van den Beukel and Radelaar (1983) as a Warren-Cowley order parameter. It is assumed that ordering is limited to two kinds of atoms, A and B, and that the equilibrium value α_E of a is given by

$$\alpha_E = 1 - \frac{P_{AB}}{C_B}$$

where P_{AB} is the probability that an atom adjacent to a chosen A atom will be of type B and where C_B is the probability that any atom chosen at random will be of type B, i.e. the concentration of B atoms.

Van den Beukel and Radelaar use an explicit expression for α_E in order to estimate the effects of CSRO; however, this approach based on the idea of a single relaxation time for all CSRO contributions implicit in equation (7.1.12), has been found to be over-simple and has been replaced in the free volume model by the idea of a spectrum of relaxation times, as described in section 7.4.

We consider in the next section microscopic interpretations of the AES model. As an introduction to the activation energy treatment of structural relaxation processes, we summarise the method used by Spaepen (1977) to model thermal activation over a potential barrier. It is this method which is the basis of equation (7.1.3) and therefore of the free volume model of kinetics.

Spaepen considers an atom in a square potential well. If v_f, the free volume of this atom, is less than v^*, a constant, then both sides of the well are infinitely high and no structural change can take place. If on the other hand $v_f \geq v^*$, then the well is effectively bounded on one side only, and a jump will certainly occur. The probability that an atom will jump is therefore the probability that $v_f \geq v^*$, in this theory of homogeneous flow.

7.3 Interpretation - The AES Model

The treatment of activation of structural relaxation processes in AES is illustrated in figure 7.3.1. Relaxation processes are of an unspecified nature in AES, but for case of illustration, we consider here a single atom attempting to jump an energy barrier; the "reaction coordinate" is in this case displacement. In contrast to the square well of figure 7.2.2, this potential well is roughly harmonic near its minimum point, and the energy barrier is of fixed height E. The probability that a

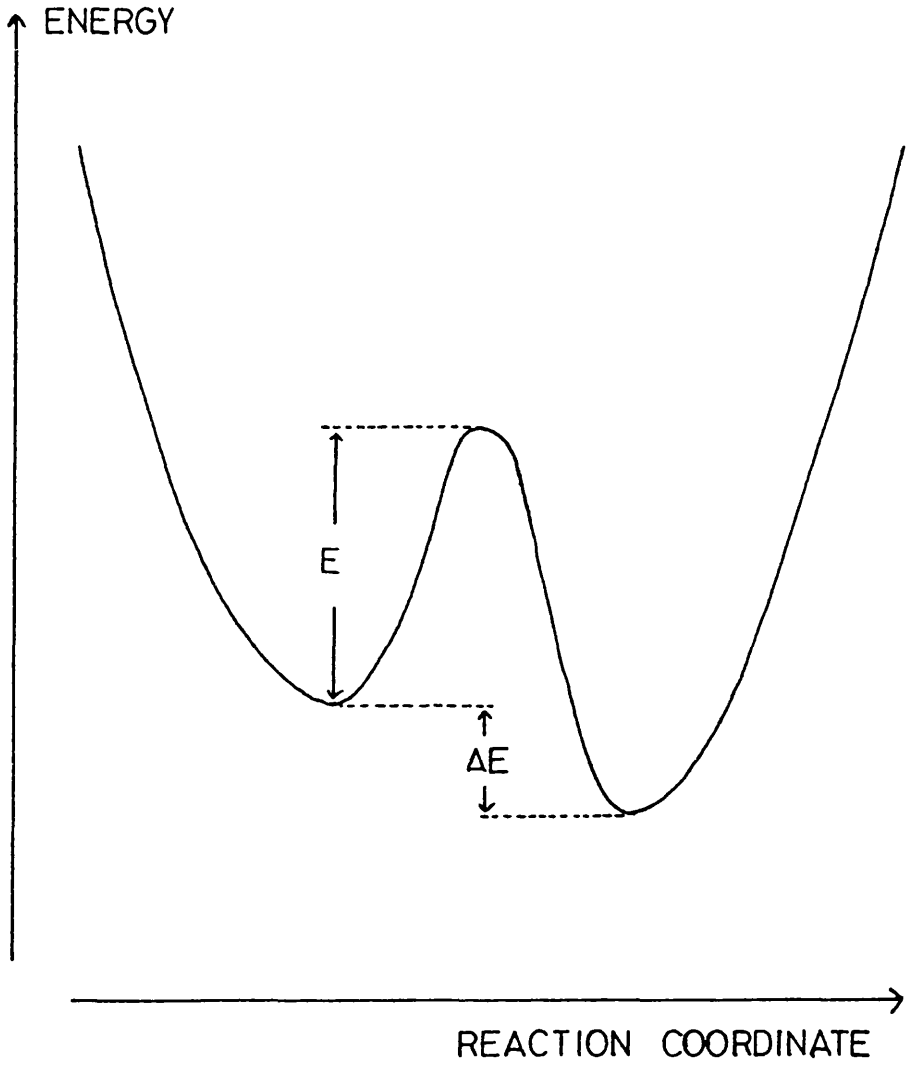

Figure 7.3.1: parameters of the generalised two-level-system

jump will occur is calculated by considering the atom and its neighbours in the amorphous structure to be in equilibrium with a reservoir of heat at temperature T, the annealing temperature. The time it will take for the atom to jump is then the product of this probability and the number of attempts made to cross the barrier per unit time. Equation (7.1.7) expresses this fact; ν is an attempt frequency and the probability p that the jump will occur is given by

$$p = e^{-E/kT} \qquad (7.3.1)$$

In order to find out when (7.3.1) applies, we review a basic thermodynamic argument.

Consider a one-dimensional quantum simple-harmonic oscillator (QSHO) with semiclassical vibration frequency ν. The energy levels of its microstates are given by

$$E_n = (n + 1/2)\, h\nu \qquad n = 0, 1, 2 \qquad (7.3.2)$$

(for a derivation, see Dicke and Wittke (1960), p. 57). Let this QSHO be in thermal equilibrium with a reservoir of heat at temperature T. Then the probability p_i that the QSHO will be in microstate i with energy E_i, measured relative to the bottom of the potential well, is given by Boltzmann's expression

$p_i = (1/Z) \exp -E_i/kT$

where $Z = \Sigma \exp (-E_i/kT)$.

The summation here runs over all microstates. For a derivation of this expression for p_i, see e.g. Waldram (1985) p. 30. The probability that the QSHO will be in a state with energy E or greater is given by

$$p(E_i > E) = \frac{\sum_{i=n}^{\infty} \exp(-E_i/kT)}{\sum_{i=1}^{\infty} \exp(-E_i/kT)} \quad \text{---------- (7.3.3)}$$

where n is the label of the lowest-energy microstate with energy greater than E. Equation (7.3.3) simplifies to

$$p(E_i > E) = e^{-E_n/kT} \frac{\sum_{i=n}^{\infty} e^{-(E_i-E_n)/kT}}{\sum_{i=1}^{\infty} e^{-E_i/kT}} \quad \text{---------- (7.3.4)}$$

and can then be reduced to (7.3.1) in two steps. The first is trivial; because the spacing of quantum levels will always be small compared with E, we can write $E_n = E$. The second step is to replace $(E_i - E_n)$ with E_{i-n} for all i greater than n in the numerator of (7.3.4), such that it cancels with the denominator term by term, leaving the required expression. This second step is only possible because successive energy levels of a one-dimensional QSHO are equally spaced (equation 7.3.2). This peculiarity is specific both to the one-

dimensionality and to the harmonicity of the model oscillator represented by (7.3.2); in general, and in three dimensions, we expect the density of microstates in energy to be a strong function of energy, and therefore we cannot expect equation (7.3.1) to apply.

The above argument, though not set out explicitly by Gibbs et al. (1983), does appear to be implicit in their use of equation (7.1.7).

Reworking the argument with a generalised density of energy levels in place of the constant density in energy implied by (7.3.2) soon becomes intractable. We can write, as a generalisation of equation (7.3.4),

$$p(E_i > E) = e^{-E/kT} \frac{\int_{\varepsilon}^{\infty} g(E') \exp\left[-(E' - E)/kT\right] dE'}{\int_{0}^{\infty} g(E') \exp\left[-(E' - E)/kT\right] dE'} \quad (7.3.5)$$

wherin we would set

$$g(E') = \text{constant}$$

in the one dimensional QSHO case, and obtain (7.3.4). Equation (7.3.5) is of no practical value unless we know the form of g(E).

At this point, a way forward is offered by the chemical reaction rate theory of Eyring (1935). This theory, proposed originally to account for observations of the rates of chemical reactions in the gas phase, is based on

the idea of equilibrium between the initial state of a reaction and a higher-energy 'activated state' or 'activated complex'.

There is no analogue of the activated state in the QSHO model and this is an important shortcoming. We can see why by considering again a single atom jumping from one local potential minimum to another (figure 7.3.2). En route from its initial position (dashed circle) to a new position, the mobile atom, shown shaded, finds itself at a saddle point in potential energy. It is stable with respect to small displacements along the line X_2X_2 as it was to displacements along X_1X_1 in its initial state, but along YY, the potential energy is maximised in the activated state. In Eyring's theory, the probability that the jump will occur is calculated from the equilibrium constant of the reversible reaction between initial and activated states. The stability of the activated state with respect to oscillations along X_2X_2 tilts the equilibrium in favour of the formation of the activated complex, making the jump more likely than it would otherwise have seemed.

Before stating Eyring's results, we must clarify the meaning of the word 'energy' when applied to microscopic states of a system. By activated state and by initial state we mean a macrostate, i.e. a region of local minimum potential, or a saddle point; each macrostate comprises many microstates, as did the QSHO analysed

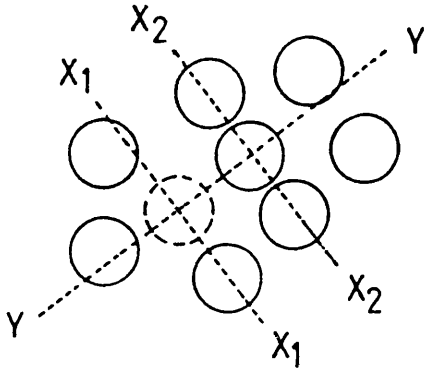

Figure 7.3.2:
(a) the activated state during a single-atom jump

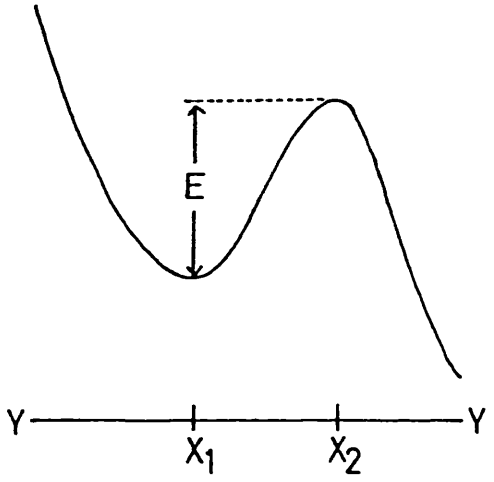

(b) potential energy along YY

(c) potential energy along X_1X_1

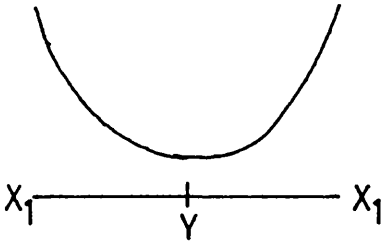

(d) potential energy along X_2X_2

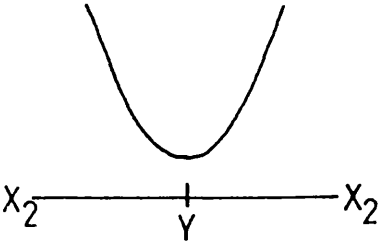

above. By the energy of a macrostate (e.g. E, the energy of the activated state with respect to the initial state) we mean the energy at the point of local minimum potential. This is the energy of the occupied macrostate at zero temperature. At non-zero temperatures, the system also contains extra energy with respect to the local minimum energy level; we will denote this thermal energy by ε. Figure 7.3.3 shows two macrostates with their minimum energy levels separated by E. Macrostates 1, 2 contain thermal energies ε_1, ε_2 repectively. The energy flow ΔU from the reservoir of heat to the system when the system changes from state 1 to state 2 is given by

$$\Delta U = E + \varepsilon_2 - \varepsilon_1 \qquad (7.3.6)$$

In Eyring's theory, the initial and activated states are treated as two macrostates; figure 7.3.4 is the potential energy graph of figure 7.3.3 applied to the geometry of figure 7.3.2. Equation (7.3.5) can now be rewritten

$$p(E_i > E) = e^{-E/kT} \frac{\int_0^\infty g_2(E)\ e^{-E/kT}\ dE}{\int_0^\infty g_1(E)\ e^{-E/kT}\ dE} \qquad (7.3.7)$$

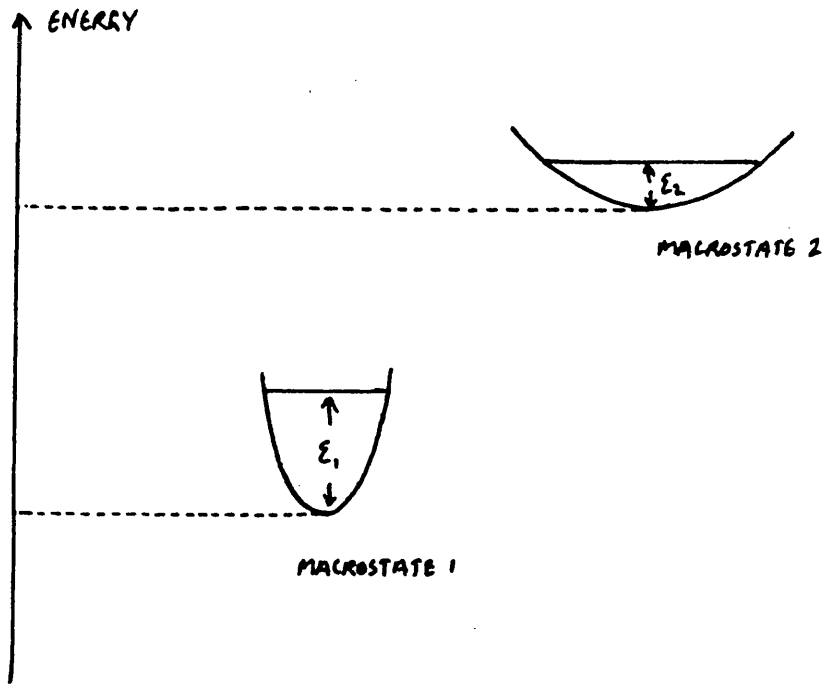

Figure 7.3.3: energies of macrostates

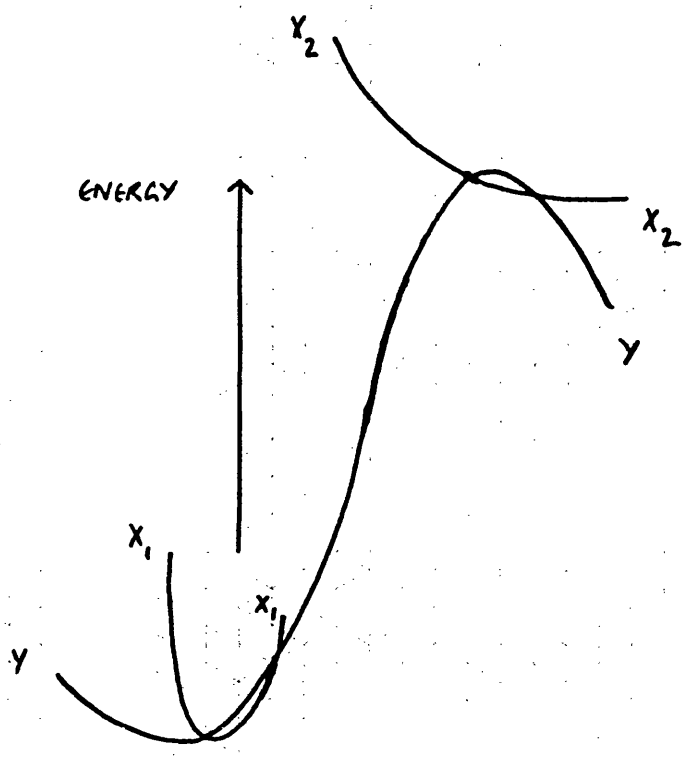

Figure 7.3.4: energy diagram showing activated and initial states (seen from above)

where $g_1(E)$ and $g_2(E)$ are now defined with respect to the local minimum (or saddle point) in potential energy. Waldram (1985, p. 216) has simplified this expression to

$$p(E_i > E) = (\sigma^*/\sigma^\cdot)\, e^{-E/kT} \qquad (7.3.8)$$

where $\sigma^\cdot, \sigma^*$ represent the widths of the two-dimensional potential wells X_1X_1 and X_2X_2 respectively. We can show that this is reasonable by imagining that the energy curves X_1X_1 and X_2X_2 are perfectly harmonic; the more highly curved potential well (X_2X_2 in the diagram) is characterised by a higher semiclassical vibration frequency ν and therefore (equation 7.3.2) by a lower density of microstates in energy. The numerator of (7.3.7) will then be smaller than the denominator in this case; setting $\sigma^* < \sigma^\cdot$ in (7.3.8) has the same effect.

The result then is that the forces on the diffusing atom at right angles to its path as it crosses the barrier affect the kinetics of the jump. If the two-dimensional potential well in which the activated complex finds itself, X_2X_2, is stiffer than the parallel one constraining the initial state, X_1X_1, then $\sigma^* < \sigma^\cdot$ in (7.3.8) and the probability of transition is lower than would be expected from equation (7.3.1); if it is less stiff, the transition probability is higher.

The next step must be to estimate the sign and magnitude of this effect in a real solid. Wert and Zener (1949), in a study of interstitial atomic diffusion coefficients in crystalline metals, point out that the strain energy of the solid is increased when the diffusing atom is in the activated state. They draw on a theoretical result due to Zener (1949), which states that the presence of residual strain energy necessarily results in a lowering of the overall tensile and shear moduli, and conclude that $\sigma^* > \sigma^\cdot$ (our notation), and thus that our estimate of the probability of a diffusive event is always increased by invoking Eyring's result. A lower bound on $(\sigma^*/\sigma^\cdot)$ is therefore 1. Wert and Zener estimate an upper bound on $(\sigma^*/\sigma^\cdot)$, for each of a variety of metal-interstitial combinations, by comparing the strain imposed during an atomic jump with the strain produced in a static measurement of the shear modulus. Using experimentally determined values of the temperature coefficient of the shear modulus, they arrive at maximum estimates for $(\sigma^*/\sigma^\cdot)$ of between 10 and 60.

We can incorporate these results into the AES model by rewriting equation (7.1.7)

$$\frac{1}{\tau} = \frac{\sigma^*}{\sigma^\cdot} \nu_0 e^{-E/kT} \qquad (7.3.9)$$

and interpreting it as follows. E is the

difference between the energy level at the saddle point through which the structure passes and the energy level at the minimum point where it started. The fraction $(\sigma^*/\sigma^\cdot)$ can be regarded as the ratio of the widths of the potential wells normal to the coordinate along which structural relaxation occurs; these widths are defined more precisely by

$$\sigma = \int_0^\infty g(E)\ e^{-E/kT}\ dE$$

where g(E) is the density of microstates accessible to the initial $(\sigma^\cdot)$ or activated (σ^*) configurations of the systems, referred to the local minimum or saddle point in energy. The frequency at which attempts are made to cross the barrier is ν_0 (the Debye frequency in the case of a single atom jumping).

An important shortcoming of AES remains; how to interpret the temperature-dependence of the equilibrium number $q_s(E)$ of processes, with activation energy E, still to occur. The fact that $q_s(E)$ can increase during an anneal after a lower-temperature preanneal implies that some of the relaxation processes must be returning, from their relaxed states, to their initial states, or to some similar equilibrium position of relatively high energy.

This raises a question: what happens after the system has passed through the activated state? In the language of

figure 7.3.4: what happens to the line YY beyond its intersection with X_2X_2?

Gibbs et al. (1983, appendix) proposed that a third microstate exists, beyond the activated state (figure 7.3.5). This is the relaxed state; initial and relaxed configurations of the system comprise a two-level system (TLS). In the TLS model, reversibility is the re-activation at a high annealing temperature of some of the TLSs from their relaxed states (attained during a low-temperature preanneal) over the barrier to their initial states.

Accordingly, Gibbs et al. set up the kinetic model with the following differential equation for n_1, the probability that level 1, the initial state, will be occupied:

$$\frac{dn_1}{dt} = \nu(n_2 e^{-E_2/kT} - n_1 e^{-E_1/kT}) \quad \text{---------- (7.3.10)}$$

where the probability that level 2 will be occupied is $n_2=1-n_1$ and where E_1 and E_2 are defined in figure 7.3.5. The symbol ν replaces ν_0 from here on; it stands for $(\sigma^*/\sigma^\cdot)\ \nu_0$ in equation (7.3.9).

At this point, Gibbs et al. introduce the approximation

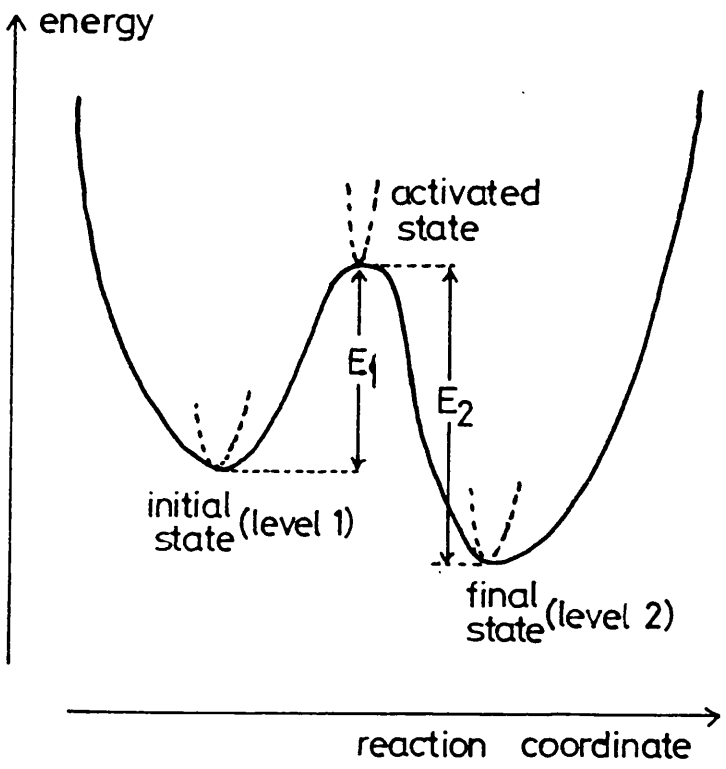

Figure 7.3.5: two-level system of Gibbs et al. (1983)

$E_1 - E_2 >> kT$

with which equation (7.3.10) simplifies to

$$\frac{dn_1}{dt} = -n_1 \nu e^{-E_1/kT} \quad \text{---------- (7.3.11)}$$

The shortcoming here is a lack of self-consistency in the model, which is subsequently developed on the basis of equation (7.3.11). The term representing backflux (from state 2 to state 1) has been dropped from equation (7.3.10), therefore there can be no reactivations from state 2 to state 1, and likewise no reversibility.

Solving equation (7.3.10) without precluding the possibility of reversible structural changes is the subject of chapter 8. It is shown there that a consistent model can be constructed on the basis of this equation and that its description of the kinetics of irreversible structural relaxation is not too different from that described in section 7.1, provided that reversibility is a small effect. A natural distinction between reversible processes and the remaining majority of processes which do not contribute to reversibility is found, in terms of TLS parameters, in chapter 8.

7.4 Towards a Unified Model

Applications of the free volume model and of AES to several sets of experimental results have brought the two approaches closer together. In summary: the free volume

model, while retaining a sharp distinction between the irreversible elimination of free volume and other, "non-TSRO" components, makes use, in its present state, of the idea of a spectrum of activation energies to describe these "non-TSRO" relaxation processes. Meanwhile, recent work with AES has made a phenomenological distinction between reversible and irreversible proceses, assigning to each a spectrum of activation energies and a coupling function.

Free Volume Model

Van den Beukel, van der Zwaag and Mulder (1984) analysed their measurements of changes in length and velocity of sound in amorphous $Fe_{40}Ni_{40}B_{20}$ by fitting isothermal data from preannealed samples to equation (7.1.4) and then using the values of the fitting parameters obtained to calculate the contribution of TSRO (decay of free volume) during more complicated thermal treatments.

They assume here that equilibrium chemical short range order is attained during the preanneal; this is assured by preannealing for so long that a long-term property value has been attained. This method of analysis allows the contributions of CSRO to be derived; in any thermal treatment, the difference between the observed property change and that calculated on the basis of TSRO alone is due to CSRO.

By fitting equation (7.1.4) to isothermal data from preannealed samples, van den Beukel et al. (1984) obtain a single set of adjustable parameters which is adequate to describe TSRO at all the annealing temperatures they used. They point out though that the values of the fitting parameters are of little interest in themselves, because the same set of experimental data can, within the experimental accuracy, be described by different sets of parameters. In other words, a satisfactory set of fitting parameters need not be unique.

This procedure for calculating the effect of TSRO in the free-volume model is still used in its most recent applications. Interpretations of the remaining, non-TSRO, contributions have changed considerably, however, from the original idea of a simple decay process with single activation energy due to van den Beukel and Radelaar (1983).

Figure 7.4.1 shows a typical result of van den Beukel et al. (1984). The isothermal change in the square v^2 of the magnitude of the velocity of sound in as-received $Fe_{40}Ni_{40}B_{20}$ is shown by black spots in figure 7.4.1. The solid line labelled T represents the calculated contribution of TSRO; the remainder (dashed line) is ascribed to CSRO by van den Beukel et al. By comparing curves like figure 7.4.1 for a variety of isothermal annealing temperatures, and by applying the same technique to results from preannealed samples, van den Beukel et al. were able to obtain both the

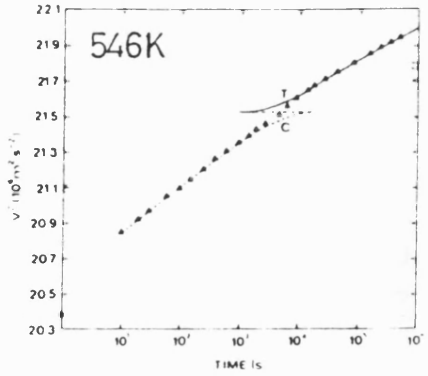

Figure 7.4.1: TSRO and CSRO in $Fe_{40}Ni_{40}B_{20}$ (van den Beukel et al. 1984)

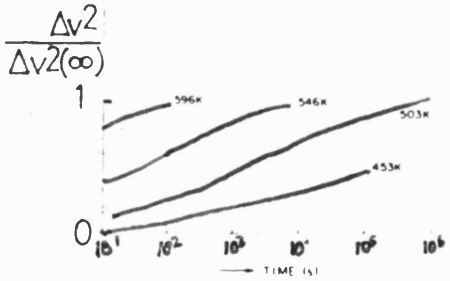

Figure 7.4.2: evolution of fractional change in v^2 due to CSRO in $Fe_{40}Ni_{40}B_{20}$ (van den Beukel et al. 1984)

temperature-dependence (due to CSRO) of the equilibrium value of v^2, and graphs of the kinetics of fractional reversible change in v^2 due to CSRO.

Figure 7.4.2 shows the evolution of the change in v^2, expressed as a fraction of the total change, due to CSRO, according to van den Beukel et al. (1984). To explain this kinetic behaviour, van den Beukel et al. employed the idea of a spectrum of activation energies for CSRO, after Gibbs et al. (1983). They do not, in this paper, explicitly construct an activation energy spectrum; however, their departure from the original idea (van den Beukel and Radelaar 1983) of a single activation energy, itself a function of free volume, is significant.

The nomenclature of the free volume model might be thought to imply that CSRO itself does not involve a change in topology. However, van den Beukel et al. (1984) make it clear that this is not the case; they ascribe much of the length change seen in isothermal anneals of $Fe_{40}Ni_{40}B_{20}$ to CSRO.

AES is used to model CSRO within the free volume model by van den Beukel (1986). It has long been recognised that the range of temperatures and times over which the effects of structural relaxation can be observed is too wide to be accounted for by a process with a single activation energy, as van den Beukel points out; CSRO can be described by a box spectrum of activation energies as shown in figure 7.4.3(a), according to van den Beukel.

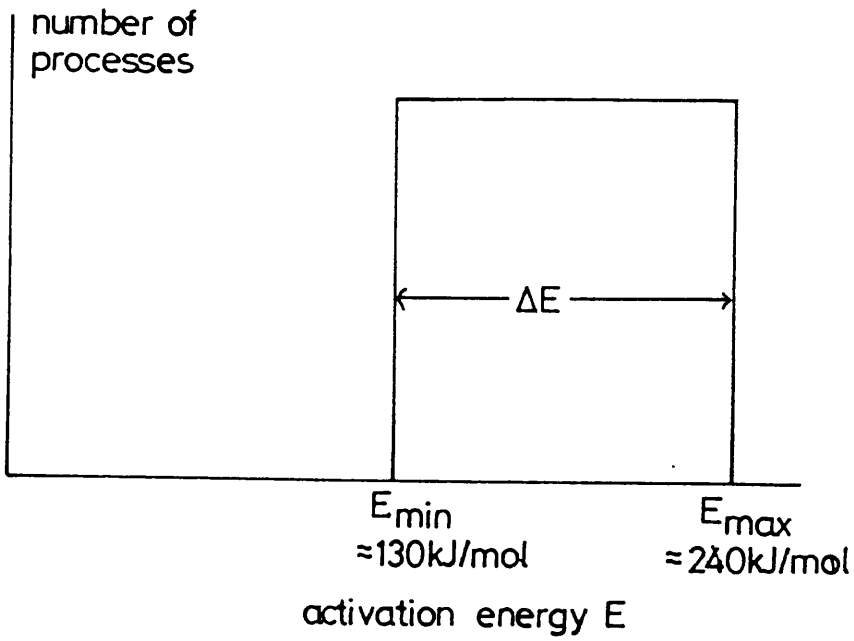

Figure 7.4.3:

(a) the box spectrum of activation energies used by van den Beukel (1986) to model CSRO

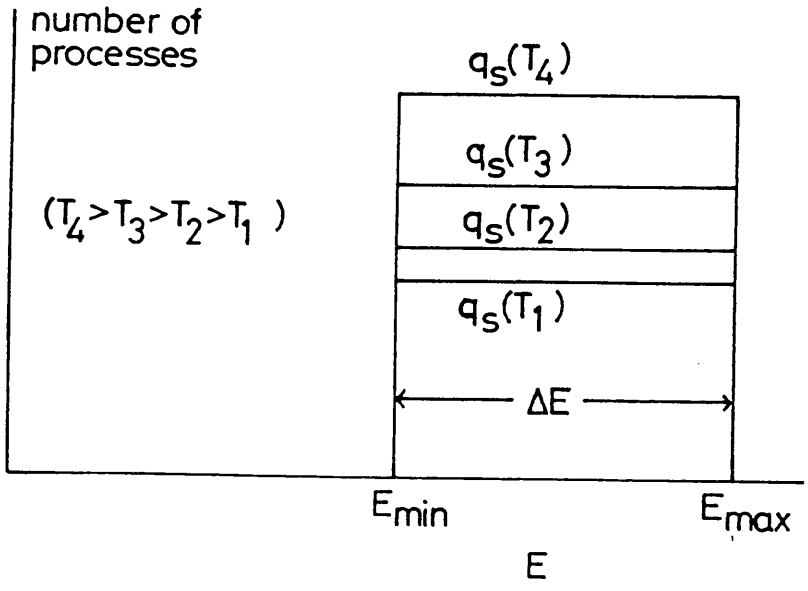

(b) as (a), modified to include explicitly the temperature dependence of the equilibrium state

The number of structural relaxation processes with activation energy E between E_{MIN} (≈130kJ/mol) and E_{MAX} (≈240kJ/mol) is constant, and the number outside these limits is zero. The approximate linearity in log-time of the reversible component over a range of logt (e.g. figure 7.4.2) is explained, using the conventional AES analysis of section 7.1, on the basis of the box spectrum. Although van den Beukel does not state it explicitly, the height of the spectrum of figure 7.4.3 is a function of temperature; this has to be true to account for reversibility at all. With this modification (figure 7.4.3(b)), the free volume account of CSRO begins to resemble AES analysis very closely. It must be remembered though that in addition to the spectra of figure 7.4.3(b), there is a group of processes which take place more slowly than CSRO, and which are irreversible in that their equilibrium number is zero at all temperatures. These processes represent mechanisms for the decay of free volume.

Very recent work (Kokmeijer, Huizer, Thijsse and van den Beukel 1987) suggests that still further modifications of the free volume model are necessary in the light of further experimental results obtained using $Fe_{40}Ni_{40}B_{20}$. Kokmeijer et al. suggest that the non-TSRO component of structural relaxation (i.e. the difference between the observed property change and that calculated on the basis of TSRO alone) comprises contributions from two simultaneous, probably connected sets of processes spanning a similar range of activation energies. One of

these (CSRO) is reversible; the other is irreversible. The irreversible process is not identified by Kokmeijer et al., but they do separate it clearly from the reversible component by determining the effect of changes in annealing temperature on what are in effect two different properties: the resistance measured at the anneal temperature and the resistance measured at 77K. They find that the dependence of long-term resistance value on annealing temperature is opposite in sign for the two different measuring temperatures, but that an irreversible *decrease* in resistance, not accounted for by TSRO and superposed on CSRO, is seen at both measurement temperatures. Two physical properties are coupled with opposite signs to the reversible structural changes and with the same sign to irreversible (but non TSRO) structural changes. Reversible and irreversible processes are therefore distinct.

Although Kokmeijer et al. choose to regard the new, relatively fast irreversible component of property change they have seen as part of the non-TSRO processes, it could be regarded as a fast contribution to the irreversible change which, at longer times, fits the free-volume decay equation. An AES approach to their results would consider the fast irreversible process and the slower irreversible change, ascribed to TSRO by Kokmeijer et al., as the low-energy and high-energy parts of a broad spectrum of activation energies.

Experimental facts seem to have disproved one of the axioms of the free volume model as proposed by van den

Beukel and Radelaar (1983): that the structural change remaining after TSRO has been subtracted-off is reversible and due to CSRO.

Before reviewing the progress of AES in its own right, let us examine more carefully the use of AES to describe CSRO within the free volume model. Van den Beukel (1986) plots the change in the square of the speed of sound in $Fe_{40}Ni_{40}B_{20}$ as a function of change in free volume for isothermal anneals of as-received samples at six different temperatures (figure 7.4.4). The data lie on straight lines at each temperature apart from the fastest contributions which are ascribed to CSRO. Van den Beukel takes the intercept of each straight line with the Δv^2-axis to be the long term change in v^2 due to CSRO alone at that temperature. By subtracting from each experimental trace the corresponding straight-line values of Δv^2, van den Beukel was able to plot the fractional change $f = \Delta v^2/\Delta v^2(\infty)$ in v^2 due to CSRO alone against annealing time at each temperature (figure 7.4.5).

Van den Beukel then calculates values of the AES attempt frequency ν for a range of values of f. This is done using a method almost identical to that developed in chapter 8 for application to irreversible structural relaxation results. The argument is as follows.

The isotherms of figure 7.4.5 are straight lines apart from the 453K curve which shows upward curvature in its early stages. The activation energy spectrum is

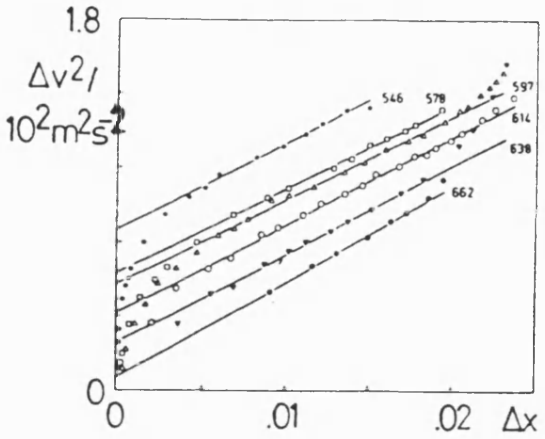

Figure 7.4.4: change Δv^2 in square of speed of sound in $Fe_{40}Ni_{40}B_{20}$ vs. the calculated change Δx in reduced free volume (van den Beukel 1986)

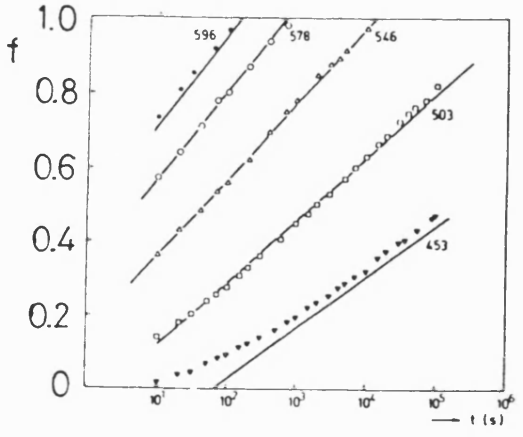

Figure 7.4.5: fractional change f - $\Delta v^2/\Delta v^2(\infty)$ in v^2 due to CSRO alone vs. time at a series of temperatures (van den Beukel 1986; $Fe_{40}Ni_{40}B_{20}$)

therefore approximately flat over the range of energies spanned. Suppose that the spectrum is of box form (figure 7.4.3(a)). Then a fraction f of the total CSRO will be achieved when

$$E = E_{MIN} + f\,\Delta E \qquad (7.4.1)$$

at each temperature. Since $E = kT\ln\nu t$, we can write

$$\ln t = -\ln\nu + E/(kT)$$

for each chosen value of f. For a given choice of f, a graph of lnt vs. 1/T should yield a straight line with gradient E/k and intercept $-\ln\nu$.

Straight line graphs are obtained by van den Beukel for eight values of f between 0.2 and 0.9. From the gradients of these lines E is obtained as a function of f and then, by applying equation (7.4.1), estimates of E_{MIN} and ΔE are made. The intercept of each line yields a value of ν; van den Beukel finds that ν increases as f increases.

The range of values of ν obtained is wide: from $3.10^{12}s^{-1}$ (f = 0.2) to $3.10^{18}s^{-1}$ (f = 0.9). This is an important result because it applies not only to the use of AES to model CSRO within the free volume model, but also to any

straightforward application of AES to the results on reversible changes in $Fe_{40}Ni_{40}B_{20}$ presented by van den Beukel.

A major weakness in van den Beukel's analysis, however, is the use of single box spectrum to describe reversible relaxation at a variety of temperatures. The box function is simple to work with analytically but its sharp edges are not readily interpretable in physical terms. Moreover, the results of this analysis rely heavily on the simple form (7.4.1) of the relation between fractional degree of order attained, f, and E; this equation in turn is specific to a box spectrum with E_{MIN} and ΔE the same at all temperatures. Even with some realistic blurring of its edges, the single box function remains a very special case.

Van den Beukel tries to fit pairs of values of activation energy E and attempt frequency ν to the equation

$$\nu = \nu' \exp(\alpha E/k)$$

but the result is a very poor fit (figure 7.4.6); a line through the data shows consistent curvature throughout the ranges of E and ν investigated.

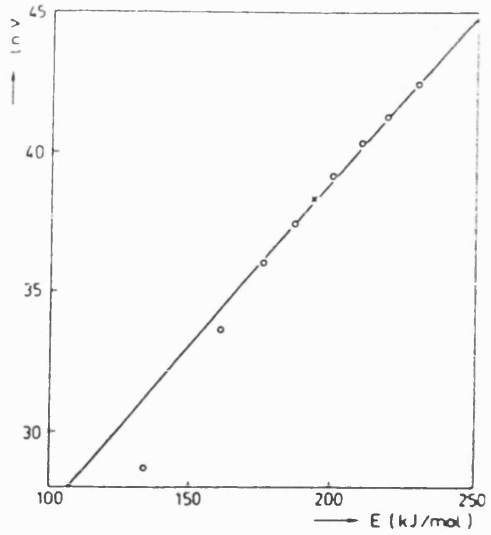

Figure 7.4.6: $\ln \nu$ plotted against activation energy E (van den Beukel 1986)

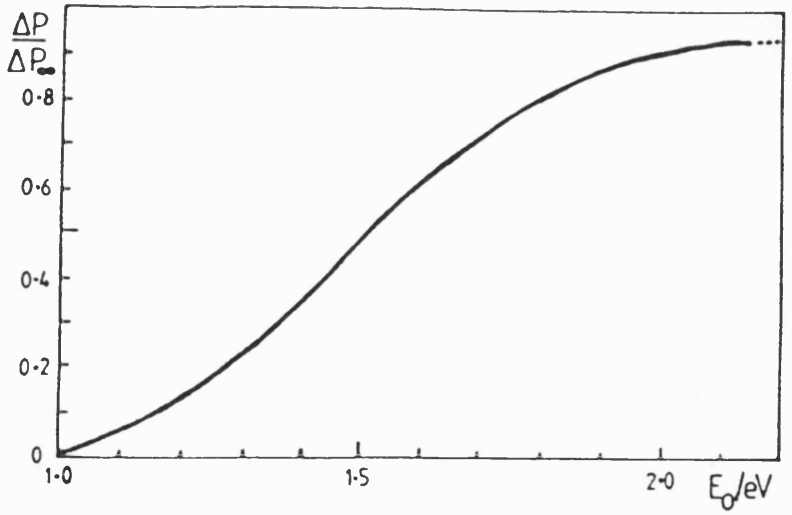

Figure 7.4.7: fractional property change as a function of t_0 in AES using a gaussian spectrum, the exact annealing function and a single coupling constant (Leake et al. 1988)

AES Model

The use by van den Beukel (1986) of a wide range of values of ν to model reversible structural relaxation suggests that the assumption that ν is constant in AES might have to be abandoned. However, recent work shows that the large variations in ν found necessary by van den Beukel can be ascribed to the analytically over-simplified choice of a box spectrum of activation energies. We review this development of AES next, and then turn to the question of the distinction between reversible and irreversible structural relaxation within AES.

Leake, Woldt and Evetts (1988) found that much of the need for variation in ν suggested by van den Beukel (1986) can be eliminated by choosing a Gaussian trial form for the activation energy spectrum. They used the temperature-independent form

$$q(E) = q_0 \exp\{-(E - \bar{E})^2/(2\sigma^2)\}$$

where q_0 is a constant, $\bar{E} = 1.5\text{eV}$ and $\sigma = 0.3\text{eV}$. They used the exact form of the annealing function $\theta(E,T,t)$ in equation (7.1.8) and assumed that the coupling function $\overline{c(E)}$ is constant over all E. With values of 10^{12}s^{-1} for

ν and 500K for T, they obtained the fractional isothermal property change $\Delta p(t)/\Delta p(\infty)$ as a function of E_0, where $E_0 = kT\ln\nu t$ (figure 7.4.7). By replotting this master curve as a series of isotherms $\Delta p(t)$, Leake et al. demonstrated that this more realistic choice of spectrum accounts for the log-time kinetics observed by van den Beukel (1986) at high temperatures, the deviations from linearity in log-time at low temperatures and the increase in slope of the linear parts of the log-time plots (figure 7.4.5) with increasing temperature. Leake et al. point out that some variation of ν might have to be invoked in order to fit a given set of data optimally; their main point is that a physically reasonable choice of spectrum can obviate the variations, spanning several orders of magnitude, in ν invoked by van den Beukel.

Equation (7.1.8) applies to isothermal anneals but can be extended to anisothermal treatments in numerical predictions by treating each step in time as a brief isothermal anneal and demanding continuity of $\Delta p(T,t)$ between steps. Leake et al. (1988) modelled constant heating-rate d.s.c. results obtained by Majewska Glabus and Thijsse (1982) and optimised the parameters of the Gaussian spectrum. The best values were found to be

$\bar{E} = 2.40$ eV,

$\sigma = 0.51$ eV.

Optimisation was by trial and error; a systematic method for optimising the parameters of a Gaussian spectrum will be outlined in chapter 9, below.

We conclude from this work that much of the need for variation in v reported by van den Beukel (1987) is due to the rectangular shape of the trial form of activation energy spectrum used.

Turning now to the question of the distinction between reversible and irreversible processes, within AES, we begin by noting that Leake et al. (1988) found that their optimised Gaussian spectrum was temperature-dependent. This implies that this property will change reversibly upon thermal cycling, according to AES analysis, as outlined in section 7.1.

Recent work suggests however that the AES account of reversibility presented above is over-simplified. van den Beukel and Huzier (1985) analyse the much-used results of van den Beukel et al. (1984), which show the square of the speed of sound in pre-annealed $Fe_{40}Ni_{40}B_{20}$ decreasing, passing through a minimum and then increasing during isothermal anneals. The preanneal was for $2.5.10^5$s at 541K; the annealing temperatures T_A and the times t_m at which minima in v^2 were observed are set out in table 7.4.1.

According to AES, the value of E_0 at the end of the preanneal is equal, in the step approximation, to the value of E_0 attained at t_m during the anneal itself.

$$kT_p \ln \nu t_p = kT_A \ln \nu t_m \quad \text{---------- (7.4.2)}$$

where T_p denotes pre-annealing temperature and t_p is the length of the preanneal. The right-hand side of equation (7.4.2) refers only to reversible processes; the left hand side refers to all relaxation processes, but is dominated by the large contribution of irreversible ones.

Van den Beukel and Huizer point out that equation (7.4.2) provides a means of testing the internal consistency of AES analysis as outlined above. Rearranging it:

$$\ln t_m = -\ln \nu + (T_p/T_A) \ln(\nu t_p) \quad \text{---------- (7.4.3)}$$

shows that a graph of $\ln t_m$ against $1/T_A$ provides two estimates of ν; the intercept on the $\ln t_m$-axis is $-\ln \nu$ and the gradient is $T_p \ln \nu t_p$, in which term all the quantities except ν are known.

The values of $\ln t_m$ and $(1/T_A)$ are included in table 7.4.1, and shown graphically in figure 7.4.8. Gibbs

Table 7.4.1 Minima in $v^2(t)$ for $Fe_{40}Ni_{40}B_{20}$ preannealed at 541K for $2.5 \cdot 10^5$s.

T_A anneal temperature
t_m time of minimum

T_A(K)	t_m(s)	$(1/T_A)/10^{-3}K^{-1}$	$\ln(t_m/s)$
568	5000	1.76	8.52
591	900	1.69	6.80
620	120	1.61	4.79
638	40	1.57	3.69
662	10	1.51	2.30

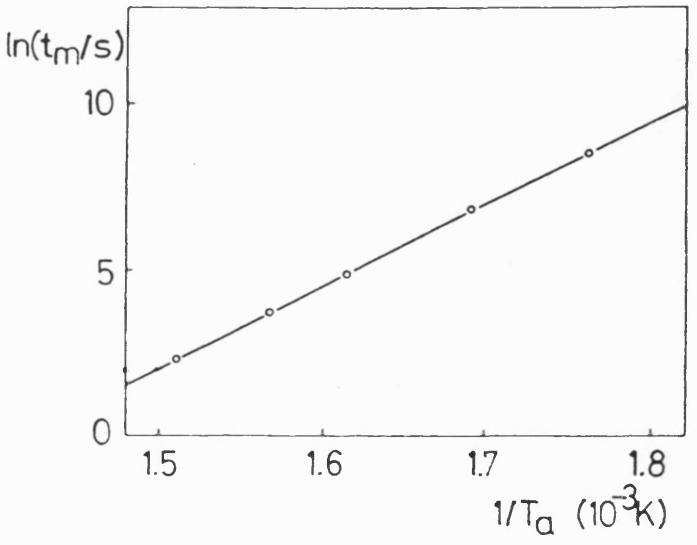

Figure 7.4.8: testing AES by plotting $\ln t_m$ vs. $1/T_A$

(1985) measured the gradient of the best straight line through the five points and arrived at an estimate of $2.5.10^{14}s^{-1}$ for ν. However, the intercept of this straight line with the $\ln t_m$ axis, obtained by extrapolating figure 7.4.8, is -35 ± 0.5, yielding for ν the estimate $1.0.10^{15}s^{-1} < \nu < 2.6.10^{15}s^{-1}$. There appears to be an internal inconsistency here.

At first sight, the extrapolation necessary to reveal this inconsistency might appear unrealistic but in fact it is not. Extrapolation to the $\ln t_m$ axis is a geometrical convenience; ν is determined by both the vertical position and the gradient of the straight line on the graph and the two determinations conflict.

It might be objected that equation (7.4.2) is itself too approximate for a proper test of AES because it is derived using the step function approximation to $\theta(E,T,t)$. However, any inaccuracy ΔE_0 in the expression for E_0 due to the rise of the step approximation will be the same, to a very good approximation, during the preanneal and during the anneal itself because the width of the steep portion of $\theta(E,T,t)$ varies only very weakly with temperature at a given value of E (figure 7.4.9). The approximation is therefore much improved by replacing $kT_A\ln(\nu t_m)$ with $kT_A\ln(\nu t_m) + \Delta E$ and by replacing

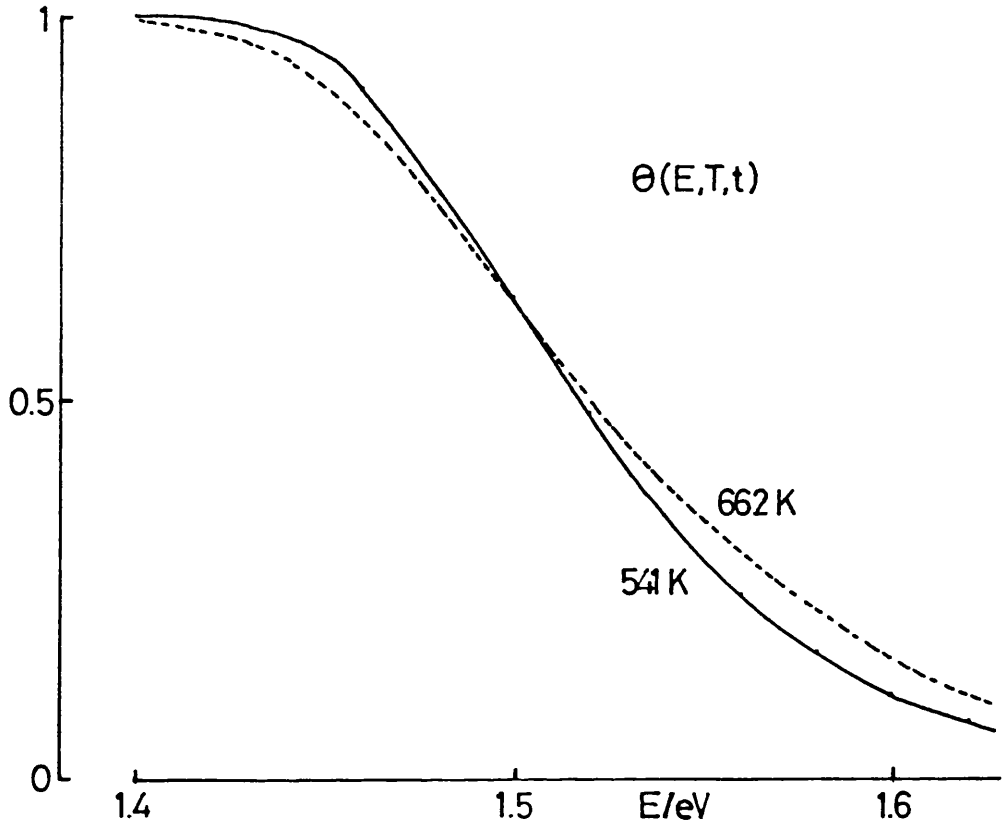

Figure 7.4.9: $\theta(E,T,t)$ at two widely different temperatures with νt chosen such that E_0 = 1.5eV for both curves. The area under the two curves is almost equal

$kT_p \ln(\nu t_p)$ with $kT_p \ln(\nu t_p) + \Delta E$ in equation (7.4.1), leaving it unchanged.

It seems that the symbol ν in equation (7.4.2) represents one quantity when it appears on the left hand side and another when it appears on the right. This fact has a straight-forward interpretation within AES: the reversible and the irreversible processes are characterised by different attempt frequencies ν. A comparison of equations (7.4.2) and (7.4.3) reveals that the value of ν determined from the gradient of the straight line in figure 7.4.8 refers mostly to irreversible processes, and that this other value of ν, obtained from the intercept, refers to reversible processes only. The calculations of van den Beukel and Huzier can therefore be interpreted as follows:

ν (irreversible) = $2.5 \times 10^{14} s^{-1}$,

$1.0 \times 10^{15} s^{-1} < \nu$ (reversible) $< 2.6 \times 10^{15} s^{-1}$.

This interpretation confirms qualitatively the universally observed difference in kinetics between (fast) reversible and (slow) irreversible structural relaxation.

Further evidence for the distinctions of reversible and irreversible contributions to $\Delta p(t)$ is provided by the results of Huizer, Mulder and van den Beukel (1985), who

subjected an FeMnBSi alloy to thermal treatments similar to those summarised in table (7.4.1). Samples were preannealed for a range of times at 525K and then annealed at the higher temperature of 578K. As in the experiments of van den Beukel and Huizer (1985), a minimum is observed in $\Delta p(t)$ in each case. Huizer et a. measured both Curie temperature T_c and the square, v^2, of the speed of sound during identical sets of thermal treatments. They found that $T_c(t)$ scaled linearly with $v^2(t)$ both before and after t_m in each anneal, but that the two scaling constants (pre-t_m and post-t_m) were different. Since AES ascribes the existence of a minimum to the competition between reversible structural relaxation (before t_m) and irreversible structural relaxation (almost all after t_m), we are bound to conclude that the ratio of the functions $\overline{c(E)}$ coupling structural change to T_c and to v^2 is different for reversible and for irreversible processes. The alternative explanation, that one or both of the functions $\overline{c(E)}$ changes sign at the value of E corresponding to the minimum point in $\Delta p(t)$ is most unlikely to be correct because, as Leake (1987) has pointed out, the position of the minimum is arbitrary, being dictated by the length of the preanneal and the ratio of the annealing and preannealing temperatures.

Leake (1987) suggests the following modification to AES in response to this result:

$$\Delta p(t) = C_r \int_0^\infty q_r(E,T)\ \theta(E,T,t)\ dE + C_i \int_0^\infty q_i(E,T)\ \theta(E,T,t)\ dE \quad (7.4.4)$$

where the subscripts r and i refer to reversible and irreversible structural processes respectively. Leake has assumed that $C_r(E)$ and $C_i(E)$ can be regarded as constants rather than functions of E because there is no direct evidence that functions, rather than constants, are required. We now consider two respects in which equation (7.4.4) might be modified.

Firstly, in the light of the findings of van den Beukel and Huizer (1985) and of Huizer et al. (1985), it appears to be necessary to introduce a difference between the expressions for the annealing function $\theta(E,T,t)$ in the two integrands of equation (7.4.4). In the former integral on the right hand side of the equation, $\theta(E,T,t)$ should be replaced with

$$\theta_r(E,T,t) = 1 - \exp(-\nu_r e^{-E/kT})$$

where ν_r is the value of ν pertinent to reversible structural relaxation, obtained for example from the intercept of a graph like figure 7.4.8. Correspondingly, in the latter integral we write

$$\theta_i(E,T,t) = 1 - \exp(-\nu_i\ e^{-E/kT})$$

where ν_i refers to irreversible processes, and can be obtained from the gradient of a graph of $\ln t_m$ against $(1/T_A)$.

Secondly, we propose that $q_i(E,T)$ be made temperature-independent. All the temperature-dependence of the equilibrium glassy strucutral state has been subsumed into the temperature-dependent quantity $q_r(E,T)$. If $q_i(E,T)$ was different at different annealing temperatures, then it would be possible, by successively annealing at two different temperatures, to obtain a reversible contribution to $\Delta p(t)$ from the latter (irreversible) integral alone.

An equation of the same form as (7.4.4) seems to be needed instead of equation (7.1.8) if AES is to be reconciled with the experimental results discussed above.

The distinction made in equation (7.4.4) between reversible and irreversible processes is empirical; there is no microscopic basis for it in terms of the parameters of AES. Moreover, there is a fundamental difficulty in accounting for the existence of reversible changes at all on the basis of equation (7.1.7), as pointed out in section (7.3).

We now show that this difficulty can be overcome, and that a physical basis for the distinction implicit in

equation (7.4.4) exists within AES, by re-working the AES model on the basis of the equation (7.3.10) rather than its approximate form (7.1.7).

8. NEW WORK ON THE AES MODEL

Chapter 8 New Work on the AES Model

This chapter describes new work on the AES model of isothermal property changes $\Delta p(t)$ associated with structural relaxation. We regard $\Delta p(t)$ as the sum of the effects of a large number of discrete relaxation processes, each modelled as a two level system (TLS) in thermal contact with a reservoir of heat at constant temperature. The energy parameters of the TLSs are treated as continuously distributed and we assume that the TLSs are independent, in the sense that the probability of a change in state of each TLS is unaffected by changes of state of the others. We assume that each TLS attempts to change its state with frequency ν, where ν is the same for all the TLSs.

In these respects the model developed here is identical to the treatment on which it is based, by Gibbs et al. (1983) (AES). We now address one of the shortcomings of AES which has been noted in chapter 7 above. We show how the approximation $\Delta E >> kT$, which was made at a very early stage in AES, restricts the validity of the model so severely that no consistent description of reversible changes is possible; we reconstruct the AES model without restricting the TLS energy parameters at all, and demonstrate that AES is a limiting case of our more general model. Without using any fitting parameters or functions, we show that only TLSs with energy level splittings ΔE of order a few kT can contribute significantly to reversible structural change. This

result, which is a direct consequence of the mathematical form of the solution of equation (7.3.10), implies that, for alloys showing large reversible effects, a significant fraction of the TLSs must have ΔE of order a few kT.

We retain the two major assumptions of AES, that each TLS behaves independently of the others and that the attempt frequencies ν of all the TLSs are the same. Without these assumptions the analysis would contain too many unknown functions to allow it to be properly tested against experimental results. The aim of this chapter is to show how a model based on these assumptions has been developed to a testable state in a new direction.

(8.1) Exact Solution of the Occupancy Equation

We require the exact solution of the ordinary differential equation

$$\frac{dn_1}{dt} = \nu\{ e^{-E_2/kT} - n_1(e^{-E_2/kT} + e^{-E_1/kT})\} \text{ ------- (8.1.1)}$$

subject to the initial boundary condition

$$\left.\begin{array}{l} n_1 = n_1(0) \\ \text{when } t = 0 \end{array}\right\} \text{ ---------- (8.1.2)}$$

Equation (8.1.1) is of the form

$$dx/dt = \alpha + \beta x \text{ ---------- (8.1.3)}$$

where $x \equiv n_1$

$\alpha \equiv \nu \exp(-E_2/kT)$

$\beta \equiv -\nu \exp(-E_2/kT) \quad -\nu \exp(-E_1/kT)$.

and can be integrated immediately:

$$\int_{xo}^{x} \frac{d\tilde{x}}{\alpha + \beta\tilde{x}} = \int_{o}^{t} d\tilde{t}$$

$$[(1/\beta) \ln(\alpha + \beta x)]_{x_o}^{x} = t$$

$$\ln\left[\frac{\alpha + \beta x}{\alpha + \beta x_o}\right] = \beta t$$

$$\alpha + \beta x = (\alpha + \beta x_o) e^{\beta t}$$

$$x = (1/\beta)\ (\alpha(1-e^{-\beta t}) + \beta x_o)\ e^{\beta t} \text{ ---------- (8.1.4)}$$

In order to compare equation (8.1.4) with the equivalent result in AES, we temporarily expand the abbreviations:

$$n_1(E_1, \Delta E, T, t) = n_1(o) \exp\{-\nu t (e^{-E_1/kT} + e^{-E_2/kT})\}$$

$$+ \frac{e^{-E_2/kT}\ (1-\exp(-\nu t (e^{-E_1/kT} + e^{-E_2/kT})))}{e^{-E_2/kT} + e^{-E_1/kt}} \text{ -------- (8.1.5)}$$

Equation (8.1.5) is visibly less tractable than the equivalent expression in AES, which reads, in our notation,

$$n_1(E_1, T, t) = n_1(0)\ \exp\ (-\nu t e^{-E_1/kT}) \text{ .---------- (8.1.6)}$$

It is clear that by setting

$$\exp(-E_2/kT) = 0 \quad \text{---------- (8.1.7)}$$

in equation (8.1.5), we can obtain equation (8.1.6) exactly, but this condition implies that the deeper well of the TLS is infinitely deep. Condition 8.1.7 therefore represents the most extreme case of the limit in which ΔE, the splitting in energy, becomes large compared with kT. This limit can, however, be approached more gradually; let

$$(\Delta E/kT) \gg 1$$

Then

$$(E_2-E_1)/kT \gg 1$$

$$\exp(-E_2/kT) \ll \exp(-E_1/kT) \quad \text{---------- (8.1.8)}$$

a less drastic condition than (8.1.7).

The solution (8.1.6) derived in AES is a zeroth order approximation to (8.1.5), in that no terms in $\exp(-E_2/kT)$ appear in it. This happened in AES because the approximation $\Delta E \gg kT$ was introduced into the differential equation (8.1.1) rather than into the exact solution (8.1.5). We are now able to examine the limit $\Delta E \gg kT$ more carefully by allowing $\Delta E/kT$ to become large in the solution (8.1.5) and we do so below, in this section and in section 8.2. First, we examine the structure of the solution (8.1.5) in more detail; this structure is most easily seen if we rewrite it in terms of E_1 and ΔE, instead of E_1 and E_2, so that the ΔE-dependence is explicit:

$$n_1(t) = (1 + e^{\Delta E/kT})^{-1} + [n_1(o) - (1+e^{\Delta E/kT})^{-1}] \times$$

$$\exp[-\nu t e^{-E_1/kT} (1 + e^{-\Delta E/kT})] \text{ ---------- (8.1.9)}$$

$$\Delta n_1 (t) = [(1 + e^{\Delta E/kT})^{-1} - n_1(o)] \theta (E_1, \Delta E, T, t) \text{ ---- (8.1.10)}$$

where $\Delta n_1(t) = n_1(t) - n_1(0)$

and $\theta (E_1, \Delta E, T, t) = 1 - \exp\{-\nu t e^{-E_1/kT} (1 + e^{-\Delta E/kT})\}$

Equation (8.1.10) represents simple exponential decay of the occupancy n_1 of the upper level towards an equilibrium value $(1+\exp(\Delta E/kT)^{-1}$. In these respects it is identical to the solution obtained by Kronmüller (1983, eq. 12) to the equivalent problem of a magnetic TLS in a metallic glass.

In the form (8.1.10), this solution is easy to interpret. Consider first the term in square brackets. This represents the total available change in occupancy; its full effect is seen as $t \rightarrow \infty$. We can identify the term $(1 + e^{\Delta E/kT})^{-1}$ with the final value of the occupancy n_1 by the following argument.

The condition for equilibrium is

$dn_1/dt = 0$.

Substituting this condition into equation (8.2.1) tells us that, in equilibrium,

$$n_1 = (1 + e^{\Delta E/kT})^{-1} \text{ ---------- (8.1.11)}$$

The term $\theta(E_1, \Delta E, T, t)$ is a function of time with a value between 0 and 1. It tells us what fraction of the total available occupancy change has occurred, on average, by the time t. Since $\theta(E_1, \Delta E, T, t)$ contains all the time-dependence of the right hand side of equation (8.1.10), the functional form of θ will determine the kinetics of the contribution to the property change of each TLS in this model. In the remainder of this section we examine the effects of the TLS parameters E_1 and ΔE on kinetics through the E_1- and ΔE- dependence of θ.

The full form (equation (8.1.10)) of θ is

$$\theta\ (E_1,\ \Delta E,\ T,\ t) = 1 - \exp\ (-\nu t\ (1 + e^{-\Delta E/kT})\ e^{-E_1/kT})$$

In the limit $\Delta E >> kT$, we can write

$$\theta = 1 - \exp\{-\nu t e^{-E_1/kT}\} \quad (\Delta E >> kT) \text{ ---------- } (8.1.12)$$

which is identical to the $\theta(E_1, T, t)$ of AES. In the opposite limit, $\Delta E = 0$, we find

$$\theta = 1 - \exp\ (-2\nu t e^{-E_1/kT}) \text{ ---------- } (8.1.13)$$

We can see by comparison of equation (8.1.12) and equation (8.1.13) that for any given value of E_1, the evolution of Δn is identical in form in these two cases, but that when $\Delta E = 0$, everything happens at twice the rate as when $\Delta E >> kT$. Moreover, since ΔE occurs in $\theta(E_1, \Delta E, T, t)$ only as a multiplicative factor of t, the entire effect on kinetics of departures from the condition $\Delta E >> kT$ is to increase the rate of evolution of n_1 by a factor between one and two. The mathematical form of the E_1-, T- and t- dependence of θ is unchanged.

Figure (8.1.1) shows θ as a function of E_1/kT for a single fixed value of νt and a range of values of ΔE. The effect of varying ΔE from $\Delta E >> kT$ to $\Delta E = 0$ is to shift the curve along the E_1/kT axis by an amount $\ln 2$. The form of the curve is unchanged, and we define a characteristic point at a value E_0 of E_1 by the condition

$$\theta(E_1, \Delta E, T, t) = 1 - (1/e)$$

E_0 can therefore be regarded as a function of ΔE, T and t; it takes the value $kT \ln \nu t$ when $\Delta E >> kT$ and $kT \ln 2\nu t$ when $\Delta E = 0$.

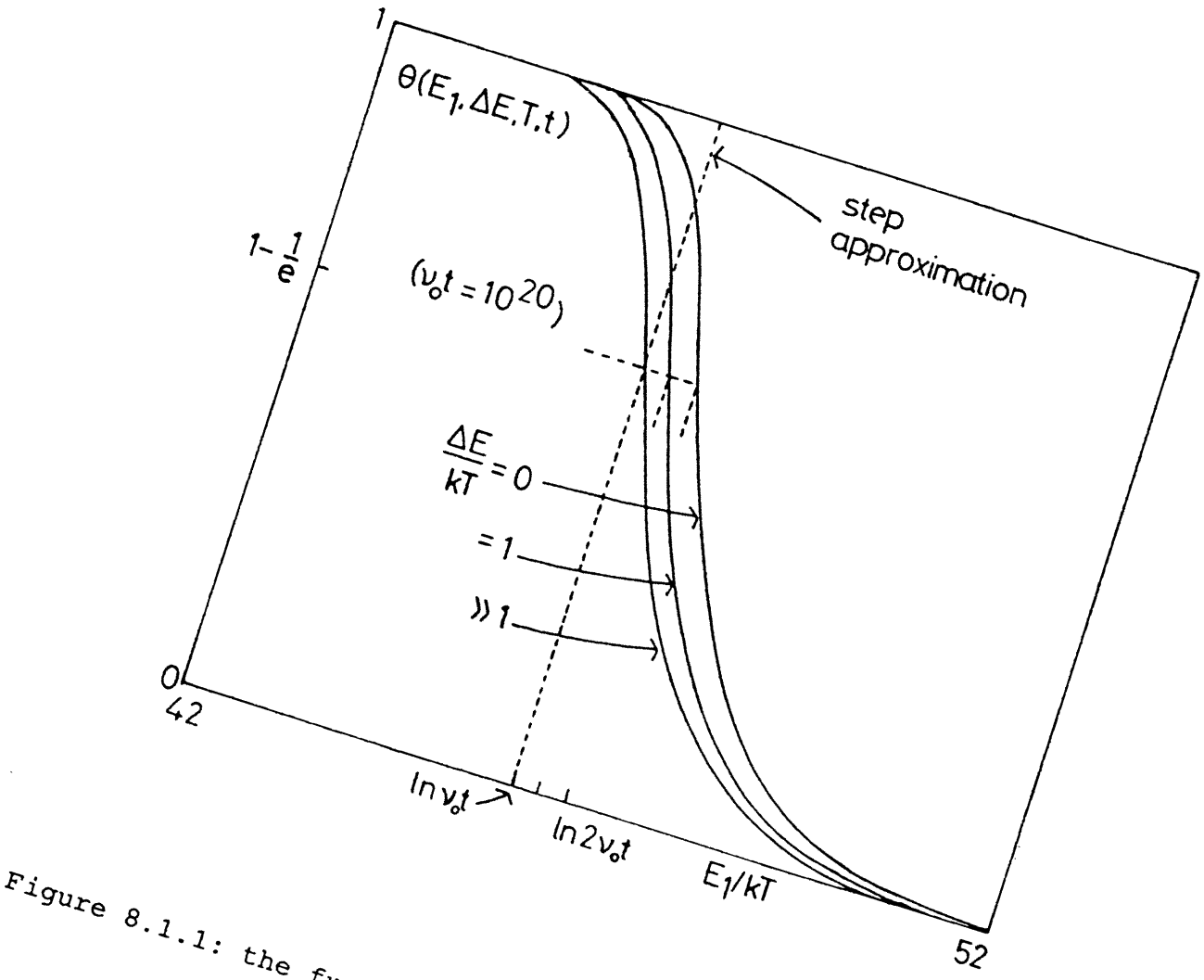

Figure 8.1.1: the function $\theta(E_1, \Delta E, T, t)$

We can conclude from the above analysis that the kinetic function $\theta(E_1, \infty, T, t)$ of AES is a good approximation to the full kinetic function $\theta(E1, \Delta E, T, t)$; it is exact provided that $\Delta E >> kT$; otherwise it predicts evolution of Δn_1 at a slower rate than would be predicted using the full kinetic function. Time appears to run artificially slowly by a factor varying between 1/2, for TLSs with $\Delta E = 0$, and 1, for TLSs with $\Delta E >> kT$.

It will therefore sometimes be a good approximation to use in place of the full kinetic function $\theta(E_1, \Delta E, T, t)$ the AES form, which from here on we denote $\theta_0(E_1, T, t)$.

What AES cannot tell us, however, is how the TLS parameters affect the temperature dependence of the long term value, in an isothermal anneal, of the occupancy n_1. The equilibrium occupancy is given by equation (8.1.11), but in AES the only possible equilibrium state is $n_1 = 0$ for all TLSs, whatever the parameters E_1 and ΔE, because of the explicit exclusion of the term representing TLS transitions from state 2 to state 1 in equation (8.1.6). This clearly cannot be reconciled with the many observations of non-zero temperature coefficient of long term property value.

We now reconstruct the activation energy spectrum model, based on equation (8.1.9) instead of on equation (8.1.6); since equation (8.1.9) contains information about the equilibrium occupancy function, the model we now build will predict how the distribution of TLSs over E_1 and ΔE affect the long term property value, considered as a function of temperature.

8.2 A better two level systems model

Consider an assembly of TLSs, each with fixed energy parameters E_1 and ΔE. We define a distribution function $q(E_1, \Delta E)$ such that the number dN of TLSs with barrier height within dE_1 of E_1 and with energy level splitting within $d\Delta E$ of ΔE is

$$dN = q(E_1, \Delta E)\, dE_1\, d\Delta E$$

(We emphasize here that in AES, the symbol q was used differently, to represent how many TLSs are still in state 1 at a given time. In the present treatment, q is a time-independent function.)

Of this number dN, the fraction which will be in state 1 is $n_1(E_1, \Delta E, T, t)$, so the number dN_1 of TLSs with these values of E_1 and ΔE which are in state 1 is

$$dN_1 = n_1(E_1, \Delta E, T, t)\, q(E_1, \Delta E)\, dE_1 d\Delta E$$

We are interested in isothermal changes in some physical property p caused by structural changes. We assume that the total property change seen during structural relaxation is the sum of independent contributions from each TLS, weighted linearly by a function $\overline{c(E_1, \Delta E)}$, representing how effectively, on average, all the TLSs with barrier height within dE_1 of E_1 and energy level splitting within $d\Delta E$ of ΔE are coupled to the physical property p. We call $\overline{c(E_1, \Delta E)}$ the average coupling function or average weighting function and it is defined such that the TLSs with these values of E_1 and ΔE contribute

$$d(\Delta p) = \overline{c(E_1, \Delta E)}\ q(E_1, \Delta E)\Delta n_1(E_1, \Delta E, T, t)\ dE_1 d\Delta E \text{ ------ (8.2.1)}$$

to the total property change $\Delta p(t)$. Processes represented by TLSs with identical energy parameters may couple quite differently to the physical property p in question; $\overline{c(E_1, \Delta E)}$ is an average of the coupling factors $c(E_1, \Delta E)$ of all the TLSs with a given E_1, ΔE. As far as equation (8.2.1), the analysis is formally equivalent to AES, except for our explicit reference to the parameter ΔE. We now however use equation (8.1.10) for $\Delta n_1(E_1, \Delta E, T, t)$ in (8.2.1) and integrate over all E_1 and all ΔE.

$$\Delta p(t) = \int_0^\infty dE_1 \int_0^\infty d\Delta E\ [(1 + e^{\Delta E/kT})^{-1} - n_1(0)]\ \theta(E_1, \Delta E, T, t)\ x$$
$$\overline{c(E_1, \Delta E)}\ q(E_1, \Delta E) \text{ ---------- (8.2.2)}$$

where θ is defined in equation (8.1.10) and $n_1(0)$ must in general be regarded as a function of both E_1 and ΔE. Equation (8.2.2) is an exact statement of the relation between the distribution function q, the coupling function c, the initial occupancy function $n_1(0)$ and the isothermal property change $\Delta p(t)$. Its analogue in AES is

$$\Delta p(t) = \int_0^\infty dE_1 \, \overline{c(E_1)} \, (q_0(E_1) - q_s(E_1) \, \theta_0 \, (E_1, T, t) \quad \text{------} \quad (8.2.3)$$

where $\bar{c}$, q_0 and q_s are unknown functions of E_1. Equation (8.2.2) contains fewer unknown functions than equation (8.2.3), since our equivalent of $q_s(E_1)$ is the known function $(1 + \exp(\Delta E/kT))^{-1}$, but our functions are in principle more complicated because they each have two arguments instead of one.

The four elements of the integrand of equation (8.2.2) can each be interpreted physically:

1 The number of TLSs with given values of E_1, ΔE is $q(E_1, \Delta E)$ and does not change with time.

2 The average coupling function between all the TLSs with given values of E_1, ΔE is $\overline{c(E_1, \Delta E)}$.

3 The maximum change in average occupancy function n_1 is

$(1 + \exp(\Delta E/kT))^{-1} - n_1(0)$

which is the difference between final and initial occupancies. This maximum occupancy change is attained when the TLSs in question have had time to reach equilibrium with the rest of the solid at temperature T.

4 The time taken for this equilibration to occur depends strongly on E_1 but only weakly on ΔE, as can be seen in figure 8.1.1, showing the form of $\theta(E_1, \Delta E, T, t)$. Using the crude step function approximation to θ sketched in figure 8.1.1,

$$\theta = \begin{cases} 1, & E_1 \leq kT\ln\nu t \\ 0, & E_1 > kT\ln\nu t, \end{cases}$$

equation (8.2.2) becomes

$$\Delta p(t) \approx \int_0^{kT\ln\nu t} dE_1 \int_0^{\infty} d\Delta E \, [(1 + e^{\Delta E/kT})^{-1} - n_1(0)] \, \overline{c(E_1, \Delta E)} \times q(E_1, \Delta E)$$

and we can now obtain from it directly an estimate of the equilibration time as follows: all the TLSs with $E_1 < kT\ln\nu t$ have equilibrated, and all those with

$E_1 > kT\ln 2t$ have not yet begun to equilibrate. The equilibration time is therefore given by $t = (1/\nu) \exp(E_1/kT)$ in this zeroth order approximation. The annealing function θ sweeps through the TLSs according to their E_1 value; the only effect of the value of ΔE on kinetics is to modify the effective value of E_1 (by less than kT1n2) for each TLS.

We now outline the implications of equation (8.2.2) for practical modelling of experimental results using the AES model; we find that the model embodied in equation (8.2.2) is applicable to reversibility experiments and to as-received anneals. In the former case, the present treatment produces new results; in the latter case, we show that analysis in the literature, based on the model of Gibbs et al. (1983), can readily be interpreted in the terms of the present model.

8.3 Long term property value

Consider an idealised experiment comprising successive very long isothermal anneals at different temperatures, in which the initial structural state for each isothermal anneal is the equilibrium state characteristic of the previous temperature. In the analysis of such an

experiment, we can write for the initial value $n_1(0)$ of the occupancy n_1 of state 1

$$n_1(0) = (1 + \exp(\Delta E/kT_0))^{-1} \quad \text{----------} \quad (8.3.1)$$

where T_0 is the temperature of the previous long anneal, called the pre-annealing temperature from now on. Equation (8.3.1) asserts that the equilibrium state attained at temperature T_0 has become the initial state for the anneal at temperature T.

Herein lies an important difference between the analysis of results on as-received and on preannealed metallic glasses. In the as-received state, the occupancy function is unknown. After a long preanneal it is defined by equation (8.3.1). Only the time-invariant functions $\overline{c(E_1, \Delta E)}$ and $q(E_1, \Delta E)$ are then unknown. Equation (8.3.1) is equivalent to having a known form for $q_s(E_1, T)$ in AES.

Equation (8.3.1) now reads

$$\Delta p(t) = \int_0^\infty dE_1 \int_0^\infty d\Delta E \; \overbrace{[(1 + e^{\Delta E/kT})^{-1} - (1 + e^{\Delta E/kT_0})^{-1}]}^{\text{"A"}} \times \theta(E_1, \Delta E, T, t)\, \overline{c(E_1, \Delta E)}\, q(E_1, \Delta E) \quad -- \quad (8.3.2)$$

The term "A" is a function of ΔE only so we can rewrite equation (8.3.2)

$$\Delta p(t) = \int_0^\infty d\Delta E \; [(1 + e^{\Delta E/kT})^{-1} - (1 + e^{\Delta E/kT_0})^{-1}] \; g_t(\Delta E) \quad \text{--- (8.3.3)}$$

where

$$g_t(\Delta E) = \int_0^\infty dE_1 \; \theta(E_1, \Delta E, T, t) \; \overline{c(E_1, \Delta E)} \; q(E_1, \Delta E).$$

Again we can interpret simply the role of $g_t(\Delta E)$ by using the approximate step form for θ

$$g_t(\Delta E) = \int_0^{kT\ln vt} dE_1 \; \overline{c(E_1, \Delta E)} \; q(E_1, \Delta E) \quad \text{(approximate form)}$$

Sketches of the exact and approximate evaluations of $g_t(\Delta E)$ for a single value of ΔE are shown in figure 8.3.1. The step function appears to be a good approximation because the width of the rapidly falling part of the exact curve is small, being of order kT, or about one twentieth of an electron-volt at typical annealing temperatures. The important feature of $g_t(\Delta E)$, which is common to the exact and the approximate treatments, is that as $t \to \infty$, the position of the steep portion of θ on the E_1 axis becomes very slowly varying. More precisely, the rate of progress along the E_1- axis of the "step" is given by

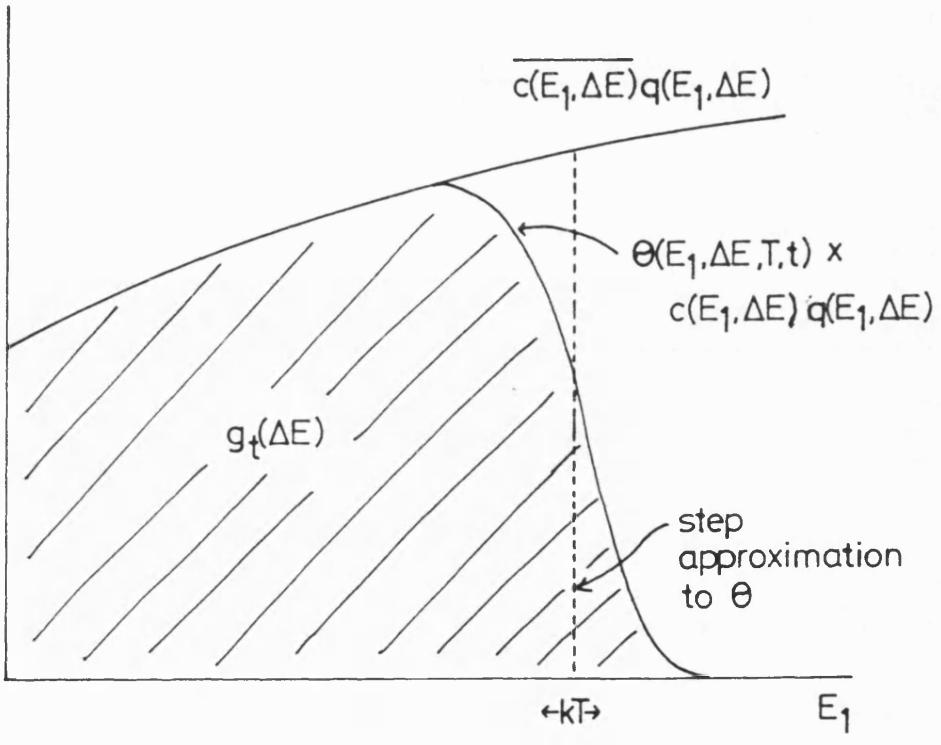

Figure 8.3.1: evaluation of $g_t(\Delta E)$ from $\overline{c(E_1,\Delta E)}\,q(E_1,\Delta E)$ for a given value of ΔE

$$\frac{dE_0}{dt} = \frac{d\ kT\ln\nu t}{dt} = \frac{kT}{t}$$

and therefore declines as 1/t. We now write in place of equation (8.3.2) in the limiting case of a very long anneal

$$\Delta p(\infty) = \int_0^\infty d\Delta E\ [(1 + e^{\Delta E/kT})^{-1} - (1 + e^{\Delta E/kT_0})^{-1}]\ g_\infty(\Delta E) \quad \text{---} \quad (8.3.4)$$

where

$$g_\infty\ (\Delta E) = \lim_{t \to \infty} g_t\ (\Delta E).$$

The term $g_\infty(\Delta E)$ in equation (8.3.4) therefore tells us how many TLSs with a given value of ΔE have been able to contribute, weighted according to their degree of coupling to the property p, given that the preanneal and anneal were both very long. The integral of $g_\infty(\Delta E)$ over ΔE is weighted by the term "A" which tells us how much each TLS can contribute to the total occupancy change.

The weighting effect of the term "A" in equation (8.3.2) is such that only the portion

$$0 < \Delta E < \text{a few } kT$$

of the integral is significant, as we can see by examining the functional form of "A".

Figure (8.3.2) is a sketch of the term

$$(1 + \exp(\Delta E/kT))^{-1} - (1 + \exp(\Delta E/kT_0)^{-1}$$

in the integrand of equation (8.3.2), as a function of ΔE and with $T/T_0 = 4/5$. This value of T/T_0 has been chosen as a minimum estimate; in typical experiments the ratio of the absolute annealing and preannealing temperatures is much closer to unity. The graph has a peak at $\Delta E \approx kT$ and most of the area under the curve lies in the region $0 < \Delta E <$ a few kT. Its effect in equation (8.3.2) is therefore to weight the integration over ΔE of the function

$$\overline{c(E_1, \Delta E)}\ q(E_1, \Delta E)$$

towards small values of ΔE, in the range 0 to a few kT.

TLSs with ΔE much bigger than a few kT simply cannot contribute to Δp in a reversibility experiment, even if they are many and strongly coupled to p. The importance of this result is that kT is very small ($\approx$ .05eV at 580K); we expect on the basis of the arguments put forward in chapter 7 that TLSs representing structural rearrangements will have splitting energies ΔE spread over a large range from 0 to $\Delta E \gg kT$. We therefore expect relatively few of the TLSs, those which happen to be nearly symmetric in energy, to be able to contribute to

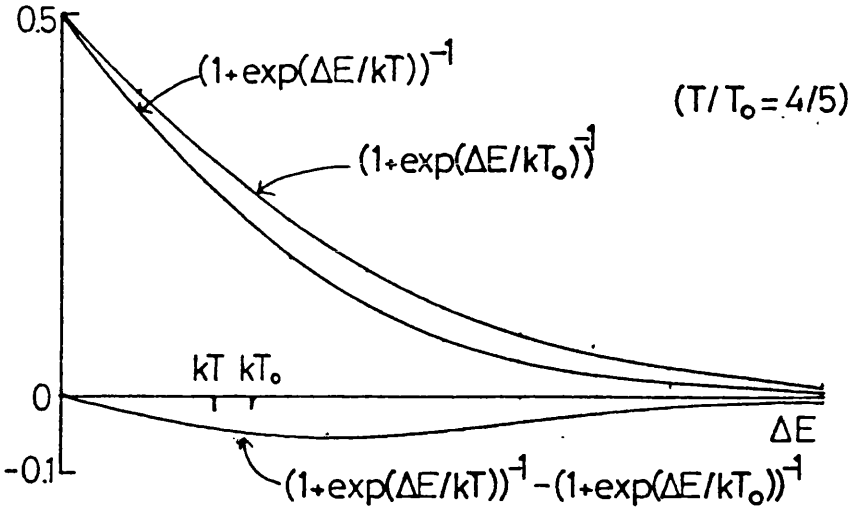

Figure 8.3.2: difference between two curves

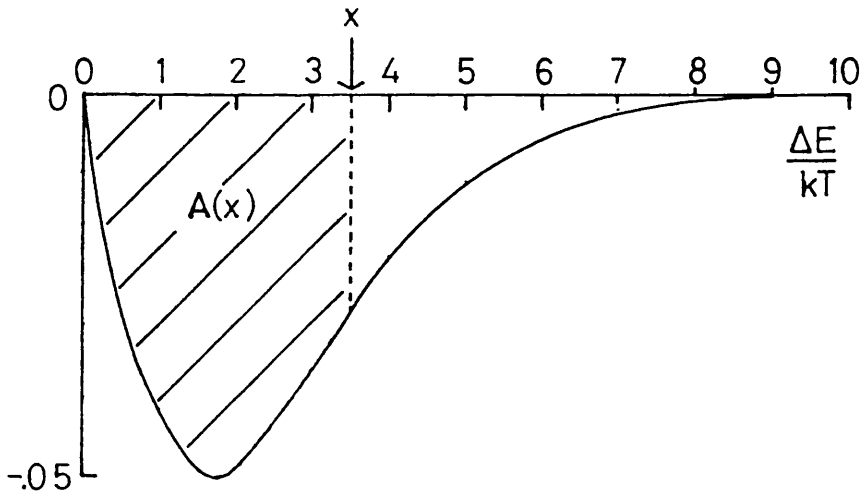

Figure 8.3.3: evaluation of integral

the long term temperature dependence of the structure, and therefore of properties related to the structure.

We have shown that in a TLS model the difference between reversible and irreversible processes is one of degree and need not also be one of kind. An event involving a change in chemical order which results in an overall energy change ΔE of magnitude much greater than kT is necessarily irreversible; conversely, the migration of an atom from a region of dense packing to one of relatively loose packing will be reversible if the energy change associated with it happens to be very small, of order kT.

The assertion that most of the area under the difference curve in figure 8.3.2 lies between $\Delta E = 0$ and a few times kT can be made more precisely by evaluating the area under the graph of figure 8.3.2 between the vertical axis $\Delta E = 0$ and some arbitrary abscissa $\Delta E = xkT$, as shown figure 8.3.3. The area A is given by the integral

$$A(x) = \int_0^{xkT} [(1 + e^{\Delta E/kT})^{-1} - (1 + e^{\Delta E/kT_0})^{-1}] \, d\Delta E$$

It is shown in appendix 3 that an exact algebraic expression for A is

$$A(x, T, \alpha) = kT \left\{ \ln \frac{e^x}{1 + e^x} - \frac{1}{\alpha} \ln \frac{e^{\alpha x}}{1 + e^{\alpha x}} \right\} - kT(1/\alpha - 1) \quad -- \quad (8.3.5)$$

where $\alpha = T/T_0$. The values of A at $x = 0$ and as $x \to \infty$ follow immediately from (8.3.5).

$$A(x = 0, T, \alpha) = 0$$

$$\lim_{x \to \infty} A(x, T, \alpha) = -k(T-T_0) \ln 2$$

The value of A is sketched as a function of x in figure 8.3.4, for a single value of $(T-T_0)$ and for two values of α. The graph shows that the maximum value of A, as $x \to \infty$ is determined by $(T-T_0)$ alone, and that the steepness of descent towards this limiting value is determined by α.

In order to put on a firm quantitative footing the assertion made above that most of the area under the curve of figure 8.3.3 lies between $\Delta E = 0$ and a few kT, we define x_0 to be a value of x such that $A(x_0)$ is some fraction f, $0<f<1$, of its limiting value.

$$A(x_0, T, \alpha) = f \lim_{x \to \alpha} A(x, T, \alpha)$$

We then have to show that, even when f is very close to 1, x_0 is not much greater than 1, whatever the value of α. On the horizontal axis of figure 8.3.4 the two values

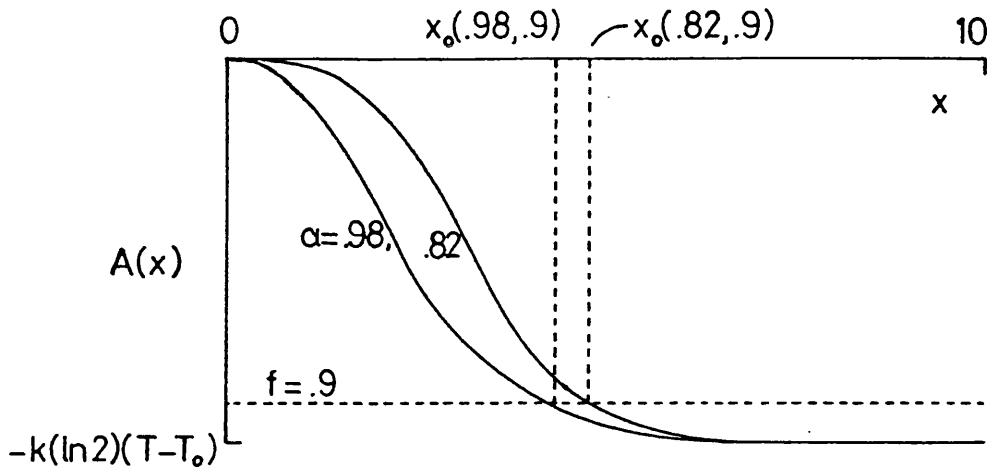

Figure 8.3.4: the function A(x)

of x_0 for the case f = 0.9 are shown, one for each value of α.

The number x_0 is a function of α and of f. We can regard $x_0(\alpha, f)kT$ as an effective upper limit in the integral for A(x). By cutting off the infinite integration at the value x_0kT of ΔE, we exclude from the estimation of Δp only those TLSs in the tail of the curve of figure 8.3.4. These TLSs by definition cannot contribute much to the integral. The higher the value of f we choose, the better approximation it is to use x_0kT as the upper limit in the integral (8.3.2).

In appendix (3), we investigate in detail the dependence of x_0 on α for various values of f. The results are summarised in figure 8.3.5. We conclude from figure 8.3.5 that for T within 20% of T_0 (where both temperatures are absolute), only TLSs with ΔE less than about 5kT can contribute significantly to the temperature dependence of the long-term property value.

We now examine the effect on the temperature-dependence of long-term property value of the form of the function $g_\infty(\Delta E)$ over the significant range of ΔE, ie 0 to a few times kT, with a view to finding $g_\infty(\Delta E)$ by comparing our

Figure 8.3.5: x_0 as a function of α for three values of f

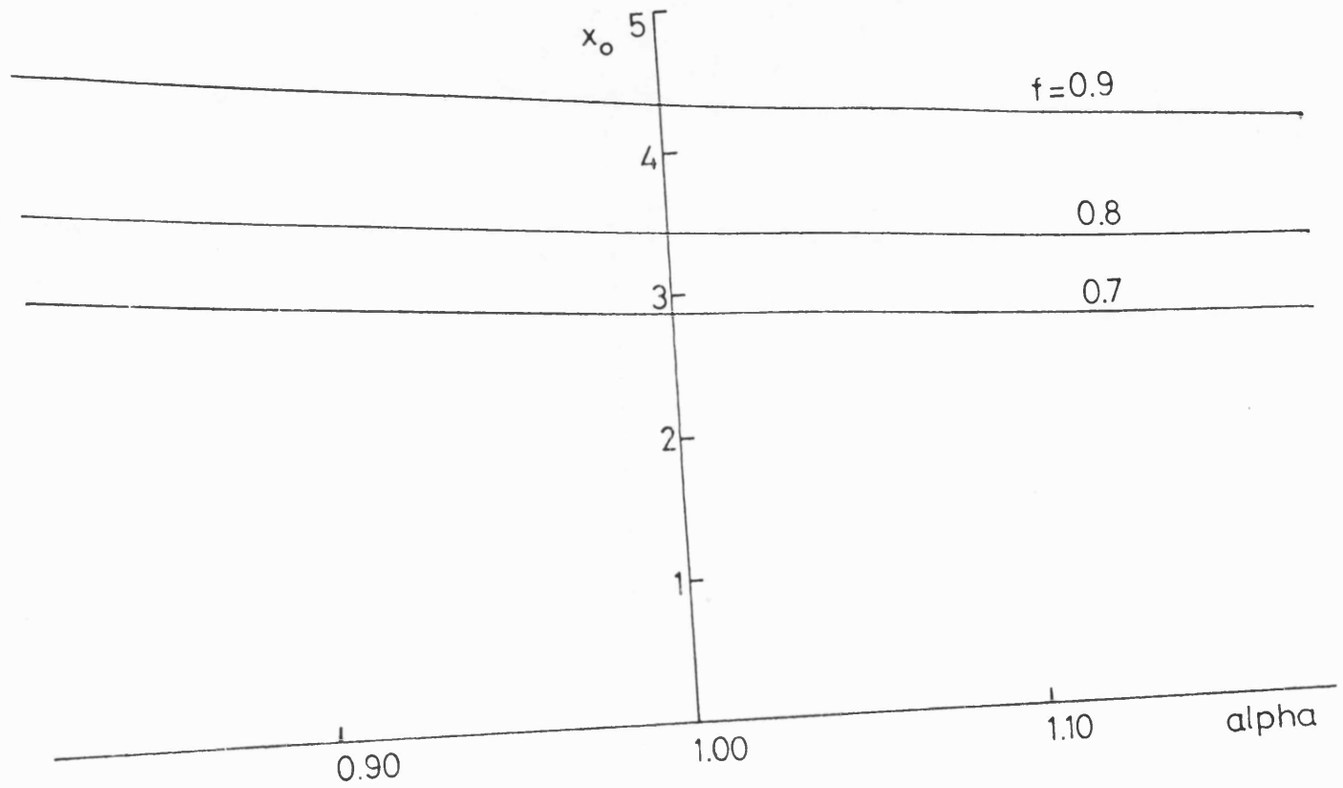

predictions with experimental observations of the temperature dependence of long-term value.

Now that the importance of the term "A" in equation (8.3.2) as a weighting function has been established, it is no longer necessary to consider explicitly the term $(1 + \exp(\Delta E/kT_0))^{-1}$ representing the initial occupancy function. For our present purpose of investigating the temperature dependence of the equilibrium structural state and its effect on the property p, it will suffice to consider a single annealing temperature. We rewrite (8.3.4)

$$p_\infty(T) = \int_0^\infty d\Delta E \; (1 + \exp(\Delta E/kT))^{-1} \; g_\infty(\Delta E) + \text{const} \text{ -------- } (8.3.7)$$

where $p_\infty(T)$ represents the limiting value as $t \to \infty$ of the property p, corrected for any isostructural temperature dependence of p. From now on we omit the constant term representing the initial state, since it is independent of T.

Equation (8.3.7) is an integral transform. The task of inverting the transform in order to obtain the function $g_\infty(\Delta E)$ from an observed form of $p_\infty(T)$ is addressed in the next section. The most important result of this work is easy to justify analytically though; it is the following:

We assume for a moment that $g_\infty(\Delta E)$ can be written

$$g_\infty(E) = g_0 \text{ (for all } \Delta E)$$

where g_0 is a constant. Equation (8.3.7) then becomes

$$p_\infty(T) = g_0 \int_0^\infty d\Delta E \ (1 + \exp(\Delta E/kT))^{-1}$$

$$= g_0 kT \int_0^\infty \frac{dx}{1 + e^x}$$

$$= g_0 kT \ln 2$$

$$= g_0 T \times (9.572 \text{ E-24 J/K}) \quad \text{---------- (8.3.8)}$$

We therefore predict that if $g_\infty(\Delta E)$ is a constant of magitude g_0 over the range of ΔE from 0 to a few kT, then the equilibrium property value will be a linear function of annealing temperature; the ratio of $dp_\infty(T)/dT$ to g_0 is 9.572 E-24 J/K, as given by equation (8.3.8).

There is no good reason to believe that $g_\infty(\Delta E)$ is a constant, of the form of equation (8.3.6). The purpose of using this trial form is to show that the magnitude of $g_\infty(\Delta E)$ around $\Delta E = kT$ determines to first order the gradient of the 'equilibrium line', as defined in section 3.2. We will now derive a method for quantitatively

fitting $g_0(\Delta E)$ to a given $p_\infty(T)$ by examining equation (8.3.7) in more detail.

8.4 Modelling Long-term Temperature Dependence

We now address the problem of inverting the integral transform

$$p_\infty(T) = \int_0^\infty d\Delta E \; (1 + e^{\Delta E/kT})^{-1} \; g_0(\Delta E) \quad \text{---------- (8.4.1)}$$

with a view to being able to derive, given a function $p_\infty(T)$ obtained in a reversibility experiment, the corresponding function $g_0(\Delta E)$.

If $p_\infty(T)$ can be expressed as a power series in T, this inversion can be accomplished in a straightforward manner. Let us express the distribution function $g_0(E)$ as a power series in ΔE

$$g_0(\Delta E) = a_0 + a_1 \Delta E + a_2 (\Delta E)^2 + \ldots$$

We can now write out equation (8.4.1) term by term.

$$p_\infty(T) = a_o(kT) \int_0^\infty \frac{dx}{1 + e^x}$$

$$+ a_1(kT)^2 \int_0^\infty \frac{xdx}{1 + e^x}$$

$$+ a_2(kT)^3 \int_0^\infty \frac{x^2dx}{1 + e^x}$$

$$+ \ . \ . \ .$$

$$+ a_n(kT)^{(n+1)} \int_0^\infty \frac{x^n dx}{1 + e^x}$$

The first integral can be evaluated analytically:

$$\int_0^\infty \frac{dx}{1 + e^x} = \left[\frac{e^x}{1 + e^x} \right]_0^\infty$$

$$= \ln 2$$

The higher order integrals cannot be expressed algebraically but a general expression for them can be derived in terms of the Riemann zeta function.

$$I_n \equiv \int_0^\infty \frac{x^n dx}{1 + e^x}$$

$$= (1 - 1/2^n) \ \Gamma(n + 1) \ \xi \ (n + 1) \qquad (n > 0)$$

This equation is derived from the list of representations of the Riemann zeta function given by Abramowitz and Stegun (1965), p. 807, by setting

$$n = s - 1$$

in their equation 23.2.8. We can now evaluate the I_n, making use of the table of values of the Riemann zeta function $\xi(n)$ given by Abramowitz and Stegun (1965), p. 811. The I_n, including I_0 as evaluated above are set out in table (8.4.1).

We have arrived at a power series in T for $p_\infty(T)$.

$$\begin{aligned} p_\infty(T) = & 0.6931\ a_0(kT) \\ & + 0.8225\ a_1(kT)^2 \\ & + 1.8032\ a_2(kT)^3 \\ & + \ldots \end{aligned}$$

Conversely then if we start with $p_\infty(T)$ in the form

$$p_\infty(T) = c_0 + c_1T + c_2T^2 + c_3T^3 + \ldots$$

then we can write down immediately the power series in ΔE for $g_\infty(\Delta E)$:

$$g_\infty(\Delta E) = \frac{c_1}{0.6931\ k} + \frac{c_2\Delta E}{0.8225\ k^2} + \frac{c_3(\Delta E)^2}{1.8032\ k^3} + \ldots$$

$$= (1.674 \times 10^4)c_1 + (1.636 \times 10^8)c_2\Delta E + (8.675 \times 10^{11})c_3\ (\Delta E)^2 + \ldots$$

Table 8.4.1 Values of the integrals I_n

n	$1-1/2^n$	$\Gamma(n+1)$	$\zeta(n+1)$	I_n
0	---- not applicable ----			0.6931
1	0.5	1	1.6449	0.8225
2	0.75	2	1.2021	1.8032
3	0.875	6	1.0823	5.6821
4	0.9375	24	1.0369	23.3302
⋮	⋮	⋮	⋮	⋮
$\to\infty$	1	n!	1	n!

where in the last line all energies have been measured in eV.

Once the linear, quadratic, cubic (etc.) coefficients of an equilibrium line $p_\infty(T)$ obtained experimentally have been found, they can be transformed into, respectively, the constant, linear, quadratic (etc.) coefficients in the power series for $g_\infty(\Delta E)$ by multiplying them by the appropriate factor.

Table (8.4.1) shows that as n gets large, the value of the definite integral I approaches n!. This method of inversion is therefore applicable in principle to any function $p_\infty(T)$ which can be expressed as a power series, however long the series. Given the poor resolution available in long term reversibility experiments though, it is likely that the first few terms in the power series will be sufficient to fit results.

8.5 Kinetic Analysis

Above we have seen how the distribution of TLSs over the parameter ΔE affects the temperature dependence of the long term property value in this model by considering the limiting case $t \to \infty$. we now consider the time dependence of structural change.

For the evolution of the physical property p during the anneal we have equation (8.2.2):

$$\Delta p(t) = \int_0^\infty dE_1 \int_0^\infty d\Delta E \; [(1 + e^{\Delta E/kT})^{-1} - n_1(0)] \; \theta(E_1, \Delta E, T, t) \; X \; \overline{c(E_1, \Delta E)} \; q(E_1, \Delta E)$$

We know from the brief consideration of kinetics in section 8.1 that a good approximation to the function

$\theta(E_1, \Delta E, T, t)$ is the function

$$\theta_0(E_1, T, t) = 1 - \exp(-\nu t e^{-E_1/kT})$$

which is independent of ΔE. We now introduce this approximation to equation (8.2.2), bearing in mind that its effect is to distort the kinetic analysis by allowing time to run at between half and full speed for those TLSs with ΔE of order kT, as discussed in section 8.2.

$$\Delta p(t) \propto \int_0^\infty dE_1 \; \theta_0(E_1, T, t) \; h(E_1) \qquad \text{---------- (8.5.1)}$$

where $h(E_1) = \int_0^\infty d\Delta E \; [(1 + e^{\Delta E/kT})^{-1} - n_1(0)] \; \overline{c(E_1, \Delta E)} \; q(E_1, \Delta E)$

Equation (8.5.1) is a useful rearrangement because it is of exactly the form of the modelling equation of the AES model (Gibbs et al. 1983), bearing in mind our redefinition of the symbol q. Activation energy spectra derived from experimental results using the AES model can be interpreted within the model presented here using equation (8.5.1). We now examine in turn the cases of well preannealed and as-received samples.

Consider a sample which has been preannealed at temperature T_0 for so long that the irreversible structural changes characteristic of the as-received state have become negligibly slow. We then have

$$n_1(0) = (1 + e^{\Delta E/kT_0})^{-1}$$

ie

$$h(E_1) = \int_0^\infty d\Delta E \; [(1 + e^{\Delta E/kT})^{-1} - (1 + e^{\Delta E/kT_0})^{-1}] \; \overline{c(E_1, \Delta E)} \; q(E_1, \Delta E) \qquad \text{------ (8.5.2)}$$

The function $h(E_1)$, derived as a spectral function over some range of E_1 as part of an AES analysis, contains a great deal of information. At each value of E_1 for which h is known, the numerical value of the integral in (8.5.2) is known. Integrals of this form, as already discussed in section 8.3 (equations 8.3.4 et seq.) are heavily weighted towards the region $\Delta E \lesssim kT$ by the square-bracketed term. At each value of E_1 considered, the size of h is approximately proportional to the magnitude of the function $\overline{c(E_1, \Delta E)} \; q(E_1, \Delta E)$ with that same value of E_1 and with ΔE in the range from 0 to a few kT.

$$h(E_1) \approx [\overline{c(E_1, \Delta E)}\ q(E_1, \Delta E)]_{\Delta E \approx kT} \int_0^{\infty} [(1 + e^{\Delta E/kT})^{-1} - (1 + e^{\Delta E/kT_0})^{-1}]\, d\Delta E$$

$$= k(T_0 - T)\ [\overline{c(E_1, \Delta E)}\ q\ (E_1, \Delta E)]_{\Delta E \approx kT}$$

by letting $x \to \infty$ in equation A3.2

Analysis of the kinetics of reversible property changes will therefore yield directly the weighted number density of TLSs with small ΔE as a function of barrier height E_1. However, there will be an uncertainty of kTln2 along the E_1 axis of the function $h(E_1)$ because the TLSs involved in reversible changes, having ΔE of order kT, are those for which the approximate form θ_0 of θ is least appropriate.

Results of experiments on as-received samples are more common in the literature and generally show better fractional resolution than those for reversibility experiments because of the comparative ease of observation of irreversible effects and their relatively large magnitudes.

Kinetic analysis of such results using equation (8.2.2) is more complicated because $n_1(0)$ is not known. We must regard $n_1(0)$ as a function of E_1, of ΔE and of all the parameters which characterise the degree of order of the

as-received state. It is emphasized here that $n_1(0)$ is the probability that a particular TLS will be found in its upper state at time zero. It is therefore an indicator of structural order unlike the function $\overline{c(E_1,\Delta E)}q(E_1, \Delta E)$ which is time-invariant because the TLSs are regarded as non-interacting.

To proceed further we must consider separately those TLSs which can contribute to reversible changes and those which cannot. This distinction is a natural one in this model because it divides the TLSs with ΔE of order kT from all the others. All TLSs contribute to the large irreversible property change seen in the annealing of an as-received sample but we know that the total contribution of those with small ΔE is small because experiment shows that reversible changes are commonly much smaller in magnitude than irreversible ones (for references, see chapter 3). We can therefore model the as-received change by neglecting all TLSs with ΔE of order kT, using the methods of the AES model, provided that the TLSs able to contribute to temperature dependence of the structural state are sufficiently small in number and sufficiently weakly coupled to the physical property in question. This AES analysis is therefore particularly appropriate to a glass like $Pd_{82}Si_{18}$, in which reversible structural effects appear to be very small (as shown for example by the annealing experiments described in chapter 3).

We now simply set $n_1(0)$ equal to 1 for all the TLSs. This is in effect what Gibbs et al. (1983) have done by considering only the TLSs which are initially in state 1. The effect of considering only the unrelaxed TLSs is that we will derive by this analysis not the total weighted number density of states in E_1 and ΔE, but the density of those TLSs which were in state 1 in the as-received glass. It is clear that irreversible property change measurements must always be limited in this way, because the TLSs which are already in their lower energy states at t = 0 can contribute nothing to the observed property change. The only way to investigate the total density of TLSs is a reversibility experiment, and then the results will be limited to those TLSs with ΔE of order kT.

The function $h(E_1)$ derived from irreversible property change data can now be identified as follows

$$h(E_1) = \int_0^\infty d\Delta E \; [(1 + e^{\Delta E/kT})^{-1} - 1] \; \overline{c(E_1, \Delta E)} \; q(E_1, \Delta E) \quad ---(8.5.3)$$

This relation can be rewritten in approximate form by neglecting the term $(1 + \exp(\Delta E/kT))^{-1}$ altogether, as illustrated in figure (8.5.1)

$$h(E_1) \approx - \int_0^\infty \overline{c(E_1, \Delta E)} \; q(E_1, \Delta E) \; d\Delta E \quad ---------- \quad (8.5.4)$$

provided that the contribution of the TLSs with ΔE small is sufficiently small, i.e., provided that reversible

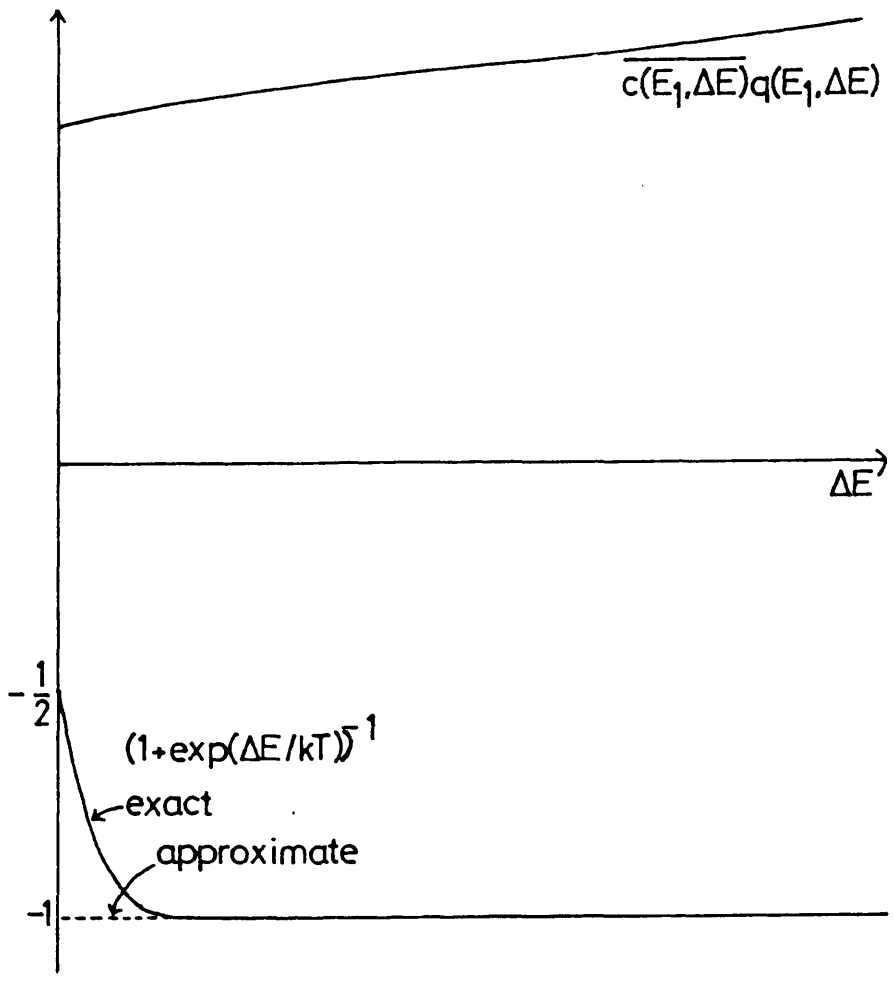

Figure 8.5.1: the integral of equation 8.5.3

effects are sufficiently unimportant in the glass in question.

The methods of kinetic analysis now at our disposal can be summarised as follows. The first step is to find a function $h(E_1)$ such that

$$\Delta p(t) = \int_0^\infty dE_1 \, \theta_0(E_1, T, t) h(E_1)$$

In the case of a reversibility experiment (i.e. with a well preannealed sample), we can then deduce the magnitude of the weighted number density function $c(E_1,\Delta E)q(E_1, \Delta E)$ in the region $\Delta E \approx kT$ using the equation

$$h(E_1) \approx k(T - T_0) \, [\overline{c(E_1, \Delta E)} \; q(E_1, \Delta E)]_{\Delta E \approx kT}$$

wherein we must accept an uncertainty of size kTln2 in E_1. In the as-received case, $h(E_1)$ can be identified with the density in E_1 of the TLSs which are initially in the excited state, provided that reversibility has been shown to be a small effect.

$$h(E_1) \approx - \int_0^\infty \overline{c(E_1, \Delta E)} \; q(E_1, \Delta E) \; d\Delta E$$

There are some practical problems with the application of these techniques to real experimental data; these will be considered in the next section.

8.6 Kinetic Modelling of Experimental Results

In order to analyse experimental data using the techniques outlined above, we need to know exactly when the isothermal anneal began and we need a working value for the attempt frequency ν.

The problem of locating the origin in time of an isothermal annealing treatment arises because real anneals are never truly isothermal; the change from room temperature T_R to the anneal temperature T_A always takes place over a significant period of time because the sample and its holder must have an appreciable thermal mass if the temperature is to remain stable during the anneal. In an idealised experiment, the temperature would change instantaneously from T_R to T_A at time $t = 0$. In real experiments we must start the experimental clock at some moment during the warming-up period. We call this point t_0, so that the hypothetical experimental clock reads $t-t_0$. Two questions now arise: first, can we find a time t_0 such that the effects of the real thermal treatment on the sample are equivalent to the effects of

an idealised isothermal anneal beginning at t_0, and second, how do we estimate t_0.

The methods of kinetic analysis outlined above provide answers to these questions.

Consider the thermal treatment shown in figure 8.6.1; the sample, which is at room temperature T_R at time t=0, is heated and reaches a steady annealing temperature T_A by the time $t=t_H$. If we can define t_0 at all, it is clearly greater than zero because the temperature is lower than it would be in an idealised isothermal anneal starting at time t=0 throughout the period $0<t<t_H$. It is also clear that t_0 if it exists at all must be less than t_H because an isothermal anneal beginning at time $t=t_H$ would provide less treatment at elevated temperatures than the real thermal treatment does. We therefore define t_0, between t=0 and $t=t_H$, such that the effects of the thermal treatment are equivalent, at all times $t>t_H$, to the effects of an isothermal anneal at temperature T beginning at time $t=t_0$ (figure 8.6.2).

In order to find an expression for t_0, we consider the effects of the real thermal treatment on an ensemble of

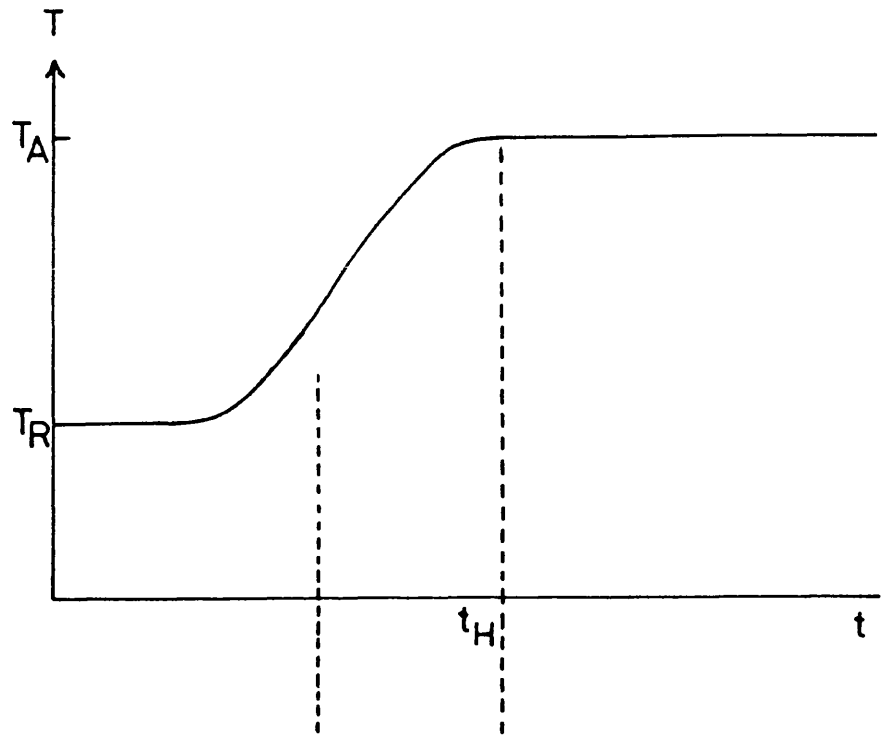

Figure 8.6.1: real thermal treatment

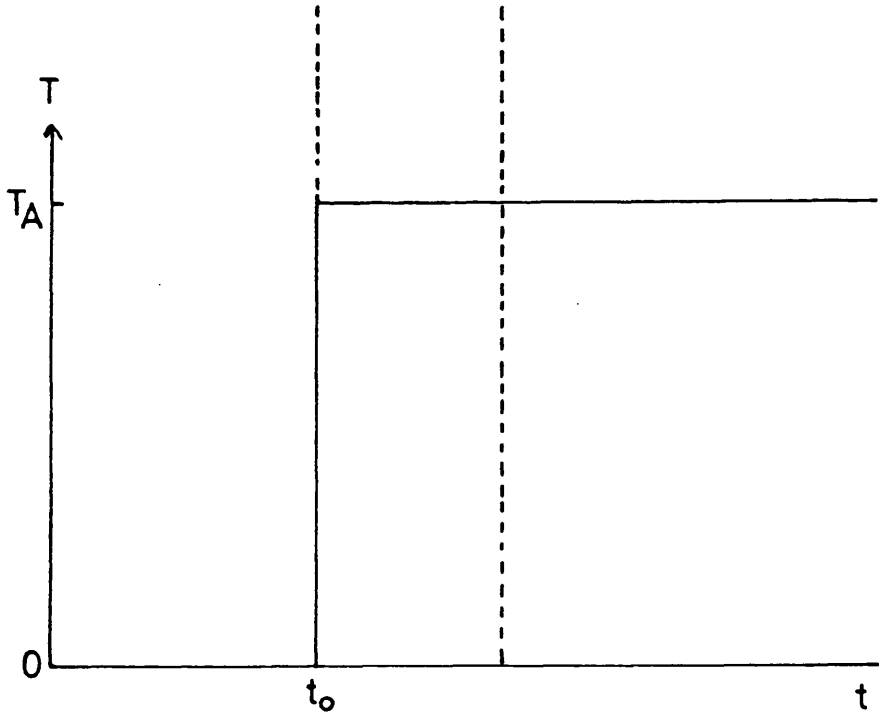

Figure 8.6.2: equivalent ideal thermal treatment

TLSs, all with the same barrier heights E_1 and with $\Delta E >> kT$. The occupancy function $n_1(t)$ satisfies equation (7.3.11):

$$\dot{n}_1 = -n_1 \exp(-E_1/kT)$$

because we are working in the limiting case of no reversible structural change. The solution of this kinetic equation for the case of constant temperature is simply

$$n_1(t) = n_1(0) \exp\ (-\nu t e^{-E_1/kT})$$

as derived by Gibbs et al. (1983). When T is a function of t, as it is between t=0 and $t=t_H$, the solution is

$$n_1(t) = n_1(0) \exp(-\nu \int_0^t e^{-E_1/kT(t')}\ dt')$$

The only modification to the equations of Gibbs et al. (1983) necessary to generalise them from the isothermal case to a general thermal treatment is to rewrite the annealing function $\theta_0(E_1, T, t)$

$$\theta(E_1, T, t) = 1 - \exp(-\nu \int_0^t e^{-E_1/kT(t')}\ dt') \quad ----- \quad (8.6.1)$$

That equation (8.6.1) is a generalisation of the AES expression for θ_0 can be seen by setting T(t) to T_A for all t in (8.6.1); the more familiar expression for θ_0 is obtained.

Remembering that t_0 is a value of t chosen such that the effect of an anneal at T_A starting at $t=t_0$ is the same as the effect of the real thermal treatment, with temperature given by T(t), we can use the more general annealing function defined in equation (8.6.1) to define t_0 for this ensemble of identical TLSs. We require of t_0 that, for all $t>t_H$,

$$\theta_0(E_1,\ T_A, t-t_0) = \theta_0(E_1,\ T(t),\ t)$$

i.e. that

$$e^{-E_1/kT_A}\ (t - t_0) = \int_0^t e^{-E_1/kT(t')}\ dt' \qquad \text{----------} \quad (8.6.2)$$

$$t_0 = t - e^{E_1/kT_A} \int_0^t e^{-E_1/kT(t')}\ dt'$$

It is reassuring to note at this point that setting T(t′) equal to T_A for all t′ yields the expected result $t_0=0$.

Given the real experimental function $T(t)$, $t<t_H$, we can therefore employ equation (8.6.2) to calculate t_0. Figure (8.6.3) illustrates the integrals of equation (8.6.3) graphically. The area OABCD under the curve represents the integral

$$\int_0^t e^{-E_1/kT(t')}\, dt'$$

which must, according to equation (8.6.2), be equal to the term

$$e^{-E_1/kT_A}\,(t - t_0)$$

which is represented in the figure by the area of the rectangle CDEF. In other words, the figures OAE and BAF are required to be equal in area.

To solve equation (8.6.2) we rewrite it

$$t_0 = e^{E_1/kT_A}\,(te^{-E_1/kT_A} - \int_0^t e^{-E_1/kT(t')}\, dt')$$
$$= e^{E_1/kT_A} \int_0^{t_H} (e^{-E_1/kT_A} - e^{-E_1/kT(t')})\, dt'$$

The upper limit t has been changed to t_H because for $t>t_H$ the integrand is, by the definition of t_H, identically equal to zero. We now make the substitution

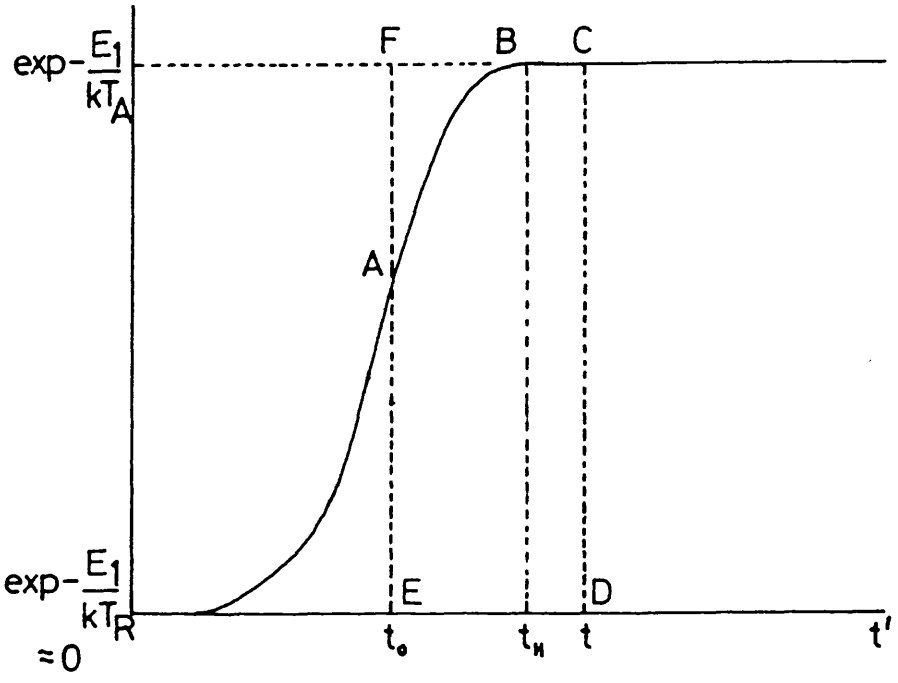

Figure 8.6.3: the integrals of equation 8.6.2

$$x(t) = (T_A - T(t))/T_A$$

in the second term of the integrand.

$$\exp\left(\frac{-E_1}{kT(t)}\right) \equiv \exp\left(\frac{-E_1}{kT_A(1-x)}\right)$$

Provided that the absolute temperature T never exceeds $2T_A$, the binomial expansion

$$(1-x)^{-1} = 1 + x + x^2 + x^3 + \ldots \quad (0<x<1)$$

is valid in the denominator of the above expression:

$$\exp\left(\frac{-E_1}{kT(t)}\right) = \exp\left\{\left(\frac{-E_1}{kT_A}\right)(1 + x + x_2 + \ldots)\right\}$$

yielding for t_0 the equation

$$t_0 = \int_0^{t_4} (1 - \exp(-\underline{E_1}(x + x^2 + x^3 + \ldots))) \, dt \text{ --------- } (8.6.3)$$
$$\qquad\qquad kT_A$$

This series expansion of the integrand is computationally useful, as can be seen by estimating the magnitude of the term E_1/kT. Taking E_1 = 1eV and T = 500K as typical values, we find that

$$\underline{E_1} \approx 20$$
$$kT$$

The second of the two terms in the integrand is therefore appreciable compared to the first only when

$$\left| \sum_{n=1}^{\infty} x^n \right| \lesssim \frac{1}{4}$$

because for values of the series sum greater in magnitude than about one quarter, the second term in the integrand will be less than one percent the size of the first term:

$$\exp\left\{ -\frac{E_1}{kT_A} (x + x^2 + x^3 + \ldots) \right\} < e^{-20(1/4)} = 0.0067 << 1$$

We can therefore ignore any errors in our summation of the series, provided that the result of the summation is greater than about one quarter. Figure (8.6.4) shows as functions of x the full series sum and two approximations to it, one using only the first two terms and the other using the first three. Over the range $-1<x<0.7$. From the graph of the full series sum we see that the condition that the sum be smaller in magnitude than one quarter is satisfied by x in the range

$$-(1/3) < x < (1/5).$$

The approximate curves compare very well with the exact curve over this range of values of x. For $x>0$ ($T<T_A$), the error introduced by omitting all but the first three terms in the summation is never bigger than 1 percent. The error is worse for negative x, reaching a maximum of 4 per cent at $x = -(1/3)$, because convergence is

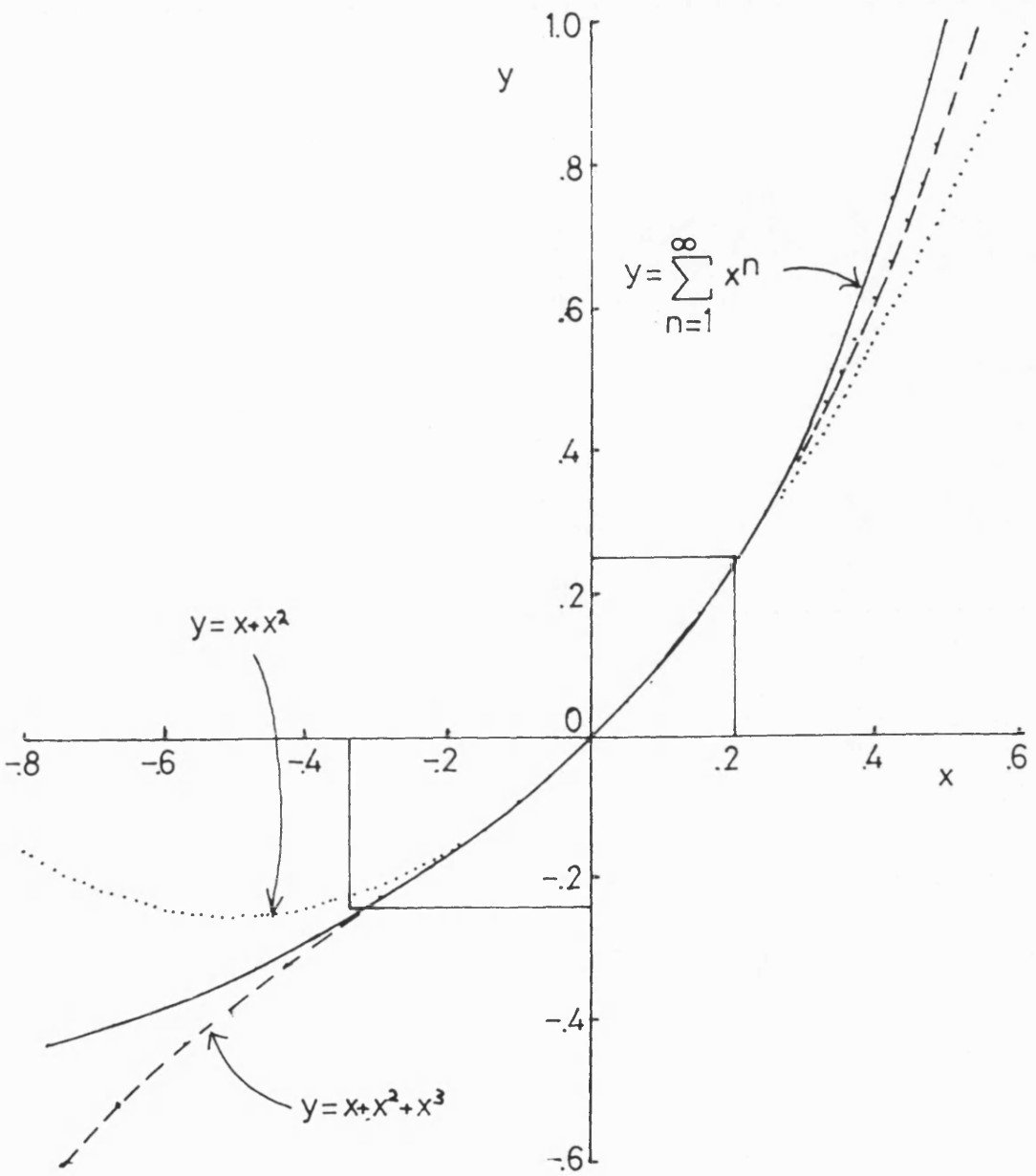

Figure 8.6.4: power series in x

oscillatory in this region but it would be unusual to allow T to exceed T_A by more than a few degrees in an experiment, so the region $x<-.01$ is of little practical interest.

An adequate approximation to equation (8.6.3) for t_0 is therefore:

$$t_0 = \int_0^{t_H} (1 - \exp (- \frac{E_1}{kT_A} (x + x^2 + x^3))) \, dt$$

This expression can be evaluated much more quickly than the exact one without significant loss of accuracy, and is therefore to be preferred as the basis of a numerical evaluation of t_0 from experimental data.

So far we have been considering an ensemble of identical TLSs, and we have found that a unique t_0 exists such that at times $t>t_H$, the effect on the occupancy function of the TLSs of the thermal treatment T(t) is identical to that of an isothermal anneal beginning at t_0. However, t_0 is a function of E_1, the barrier height, so we cannot define a single t_0 for an ensemble of TLSs with a spread of barrier heights E_1. The idea of defining t_0 is therefore of questionable value. If t_0 were a strong function of E_1 then the method of modelling a real

thermal treatment as if it were an ideal isothermal anneal would be restricted to those experimental results in which the warming-up period, and therefore the thermal mass of the sample holder, are small. This is not the case though; t_0 is a weak function of E_1, and it can be defined, typically to within a few hundred seconds, for a wide range of barrier heights E_1.

The weak dependence of t_0 on E_1 is exemplified by the results shown in table (8.6.1), taken from one of the sets of experimental data analysed in the next chapter. The table shows for the values 1.0, 1.5 and 2.0 eV of E_1, the values of t_0 obtained from a typical experimental heating curve. The t_0 values derived span 530s. This example gives a pessimistic estimate of the uncertainty in the values of t_0 to be expected in general because this experiment, designed with thermal stability in mind and therefore incorporating a sample holder of large thermal mass, is characterised by longer warming up times than others reported in the literature.

Various other methods of calculating the effective starting time of isothermal anneals have been reported. Woldt and Leake (1985) use a simple graphical technique. They draw a tangent to the curve T(t) at about the point of inflection of the curve (Woldt 1986), and define t_0 as

Table 8.6.1 Values of t_0 obtained using three different values of E_1 on a typical experimental heating curve.

Value of E_1 used in eV	t_0/s
1.0	2750
1.5	3058
2.0	3285

the time coordinate of the intersection of this tangent with the horizontal straight line $T=T_A$ (figure 8.6.5).

Woldt (1986) uses a second method of estimating t_0 in some experiments; t_0 is defined as the moment at which the heating rate falls below 10% of the maximum heating rate encountered during the warming up period. Woldt found that the values of t_0 obtained this way, measured relative to the moment at which heating began, were a simple function of the temperature difference T_A-T_R. By fitting all the pairs of values of t_0 and T_A-T_R to a single equation, Woldt was able to estimate t_0, given a value of T_A-T_R.

Given an estimate of t_0, we are in a position to analyse real experimental data as if it had been generated in an ideal isothermal annealing experiment. The change Δp in physical property can therefore be plotted as a function of time or as a function of log time. To go further with the method of analysis outlined in section 8.5, we need to use the technique of Gibbs et al. (1983) to find the function $h(E_1)$. Since $h(E_1)$ is related to $\Delta p(t)$ through the function $\theta(E_1, T, t)$ (equation 8.6.1) we need a working value of the parameter ν which occurs in θ.

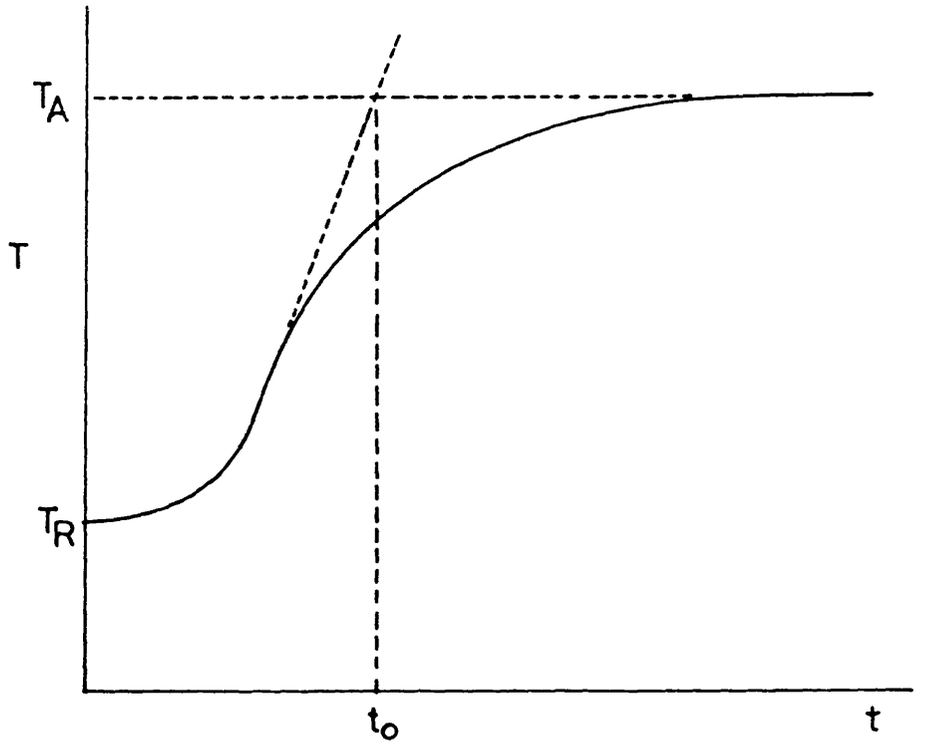

Figure 8.6.5: method of estimating t_0 used by Woldt and Leake (1995)

The parameter ν is not simply an attempt frequency; it is the product of an attempt frequency and a factor which depends on the entropy of activation, as discussed in section 7. Any *a priori* calculation of ν would therefore depend on detailed knowledge of the nature of the initial state of the TLS and of its activated state. Such an approach to the estimation of ν may be of much importance in later work as a test of specific microscopic description of TLSs, but for the purposes of phenomenological analysis of kinetic data we only need to derive from the results themselves an estimate of ν consistent with an independent TLS model.

Gibbs (1985) and Bothe and Neuhäuser (1982) have addressed this problem. Their method is an analysis of the crossover effect; it makes use of the experimental fact that at some time t_m during the anneal at temperature T_A of a sample preannealed at temperature T_0 for some time t_p, $\Delta p(t)$ may attain a maximum or minimum value. The temperatures and durations of the preanneal and the anneal are related by the equation

$$kT\ln\nu t_m = kT_0\ln\nu t_p$$

and this equation is used to derive ν given a set of

values (T, T_0, t_m, t_p). There are two respects in which this analysis might be unreliable.

Firstly, the term $kT\ln\nu t$ is an estimate of E_0 for a group of processes which are all reversible, so the value of ν derived will be an overestimate by a factor of between 1 and 2 because the approximate annealing function $\theta_0(E_1,T,t)$ has been used in place of $\theta(E_1,\Delta E,T,t)$. (This conclusion is justified by the discussion of equations 8.1.12 and 8.1.13 in section 8.1 above.) This objection is relatively unimportant however in view of the large range of values, spanning several orders of magnitude, proposed for ν.

Secondly, and more importantly, the value of ν is derived from a single experimental measurement of T, T_0, t_m, and t_p.

A different empirical method of deriving ν which avoids these two shortcomings has been developed as part of the present study and is outlined below. It involves the analysis of the results of a set of isothermal anneals at different temperatures of samples of a metallic glass showing little or no reversible effect, all in the as-received state.

The isothermal data are plotted on a graph of Δp versus kTlnt. A schematic graph of this type is shown in figure (8.6.6). A value p_0 of Δp is chosen such that the straight line $\Delta p = p_0$ cuts as many of the curves as possible. The abscissas of the intersections of the line $\Delta p = p_0$ with the curves obtained at temperatures T_1, T_2, T_3, ... ($T_1 < T_2 < T_3$ ...) we label $\varepsilon(T_1)$, $\varepsilon(T_2)$, $\varepsilon(T_3)$, ... respectively.

We now apply the AES model in its step function approximation form to these points of intersection. If reversible effects are absent or negligibly small, it is clear that the value of E_1 reached by the characteristic point E_0 of the approximate annealing function $\theta_0(E_1, T, t)$ must be the same at all the intersections because the same amount of structural change has occurred at each of them. Moreover, this value of E_0 is given at each temperature T by the equation

$$E_0 = kT\ln\nu t.$$

A simple manipulation yields the prediction of a linear relationship between the values of E(T) read off on the kTlnt-axis and T.

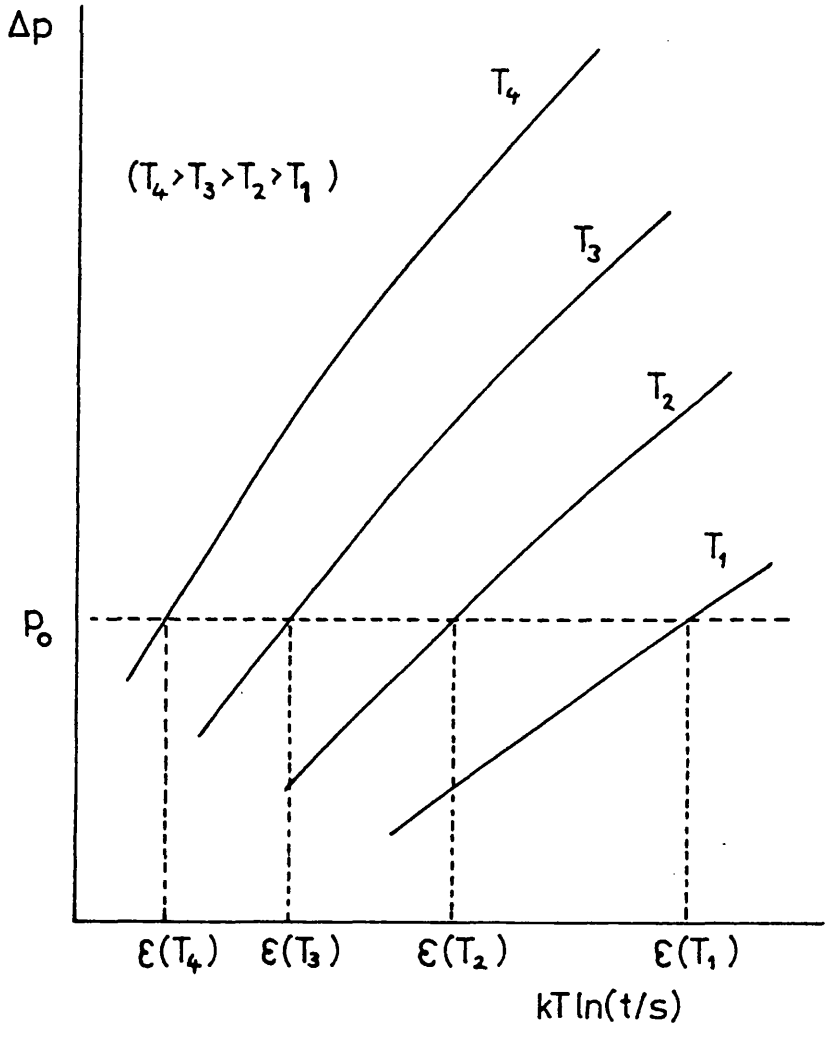

Figure 8.6.6: schematic graph of results of a set of as-received anneals plotted against kTlnt

$$E_0 = kT\ln\nu + kT\ln t$$

(ν in s^{-1}, t in s)

$$kT\ln t = E_0 - kT\ln\nu$$

$$\varepsilon(t) = E_0 - (k\ln\nu)\ T$$

We therefore predict that a graph of $\varepsilon(T)$ against T will be a straight line with gradient $-k\ln\nu$ and intercept on the $\varepsilon(T)$-axis E_0. If the graph turns out to be highly non linear then the present model, with its constant value of ν is inapplicable; if the graph is a straight line within reasonable error limits, then the independent TLS analysis is appropriate, and we will have arrived at an estimate of ν within these error limits. This procedure therefore provides a test of the present model. The crossover analysis could be extended similarly by applying equation (8.7.4) to several separate crossover experiments using different pairs of temperatures T and T_0 and the same source of metallic glass ribbon. Only if they all yield roughly the same value of ν can the model as presented so far be considered successful.

We are now in a position to apply the analytical methods of section 8.5 to experimental data presented in this thesis and to results published by other experimenters.

9. APPLICATIONS OF THE EXTENDED AES MODEL

Chapter 9 Applications of the Extended AES Model

It has been established that a two-level-systems model (the 'extended AES model') can account for both reversible and irreversible structural relaxation without introducing a sharp distinction between reversible and irreversible processes. Reversible structural relaxation is simply the effect of changes in state of those two-level-systems (TLSs) with splitting energy ΔE of order kT, according to the arguments presented in the previous chapter.

Analytical techniques have been proposed to allow information about the distribution of TLS over the parameters E_1 and ΔE to be obtained from the results of kinetic analysis of isothermal property changes and from the temperature dependence of the long-term property value in reversibility experiments. These techniques are now applied to the results of the experiments described in chapter 3 and to one set of results from the literature.

9.1 Kinetic Analysis

The isothermal changes in resistance of separate lengths of as-received $Pd_{82}Si_{18}$ were measured as a function of time at annealing temperatures of 253°C, 239°C, 211°C, 187°C and 150°C. In each case, the results, stored on a flexible disc by a microcomputer, were in the form of a table giving the time, temperature and resistance at

intervals of about 40 seconds, lengthening to several minutes once the set temperature had been attained. The first task with each set of results was to estimate t_0, the time at which a truly isothermal anneal at the set temperature, having the same effects after a long time as the real treatment, would have begun.

A computer program implementing equation (8.6.4) as a summation was written. The data points themselves were used as the steps in the summation. The value of t_0 obtained is insensitive to the value of E_1 used in equation (8.6.4) as argued in section 8.6; the estimate E_1 = 1.5eV was used throughout.

Each set of data was plotted on a single graph of the relative resistance change $\Delta R/R_0$ against $kT_A \ln(t-t_0)/s$, following the method outlined in section 8.6. This graph is reproduced as figure 9.1.1; the vertical arrows indicate the time at which each set temperature was attained to within 1K. The curves vary systematically, the trend being towards the zero of $\Delta R/R_0$ for decreasing anneal temperature T_A.

The horizontal line in figure 9.1.1 was chosen to intersect as many of the five curves as possible. The projections on to the $kT_A \ln(t-t_0)$ axis of the intersections of this line with curves drawn through the

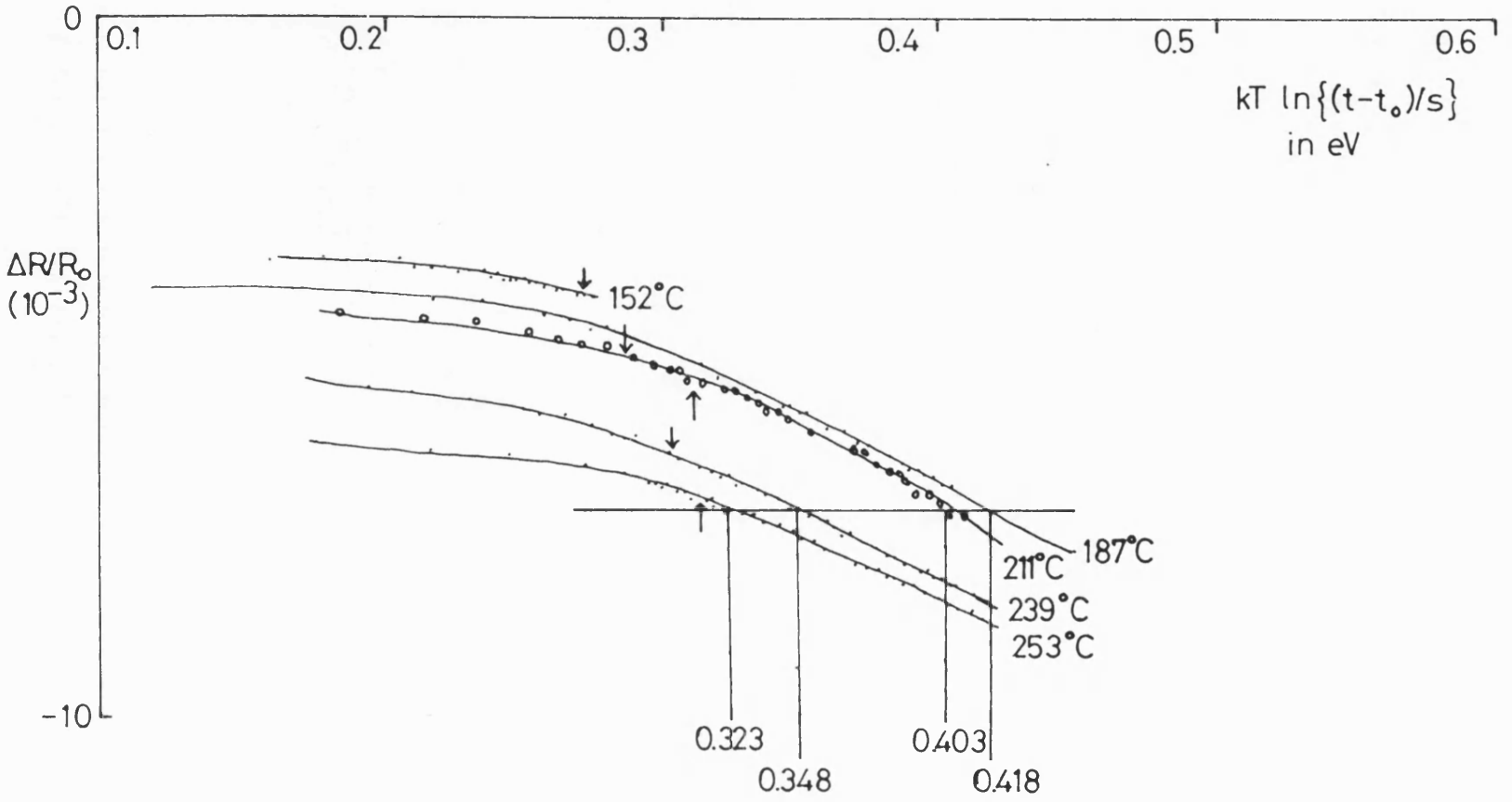

Figure 9.1.1: $Pd_{82}Si_{18}$: kinetic analysis (first step)

data obtained at 187°C, 211°C, 239°C and 253°C are given as $\varepsilon(187°C)$, $\varepsilon(211°C)$, $\varepsilon(239°C)$ and $\varepsilon(253°C)$ respectively in table 9.1.1.

According to the arguments set out in the latter half of section 8.6, we expect $\varepsilon(T)$ to be a linear function of T with gradient $-k\ln\nu$ according to the AES model in its step-function approximation. This test of the AES model is applied in figure 9.1.2, a graph of $\varepsilon(T)$ vs. T. The four points do not suggest curvature in either direction. There is therefore no systematic deviation from linearity and we can conclude that the AES model has passed this experimental test, within the limits of the random scatter of the points in figure 9.1.2. We obtain an estimate of ν by drawing the best straight line and straight lines of maximum and minimum gradient (shown dashed) through the points. The best straight line yields

$$k\ln\nu = 1.6 \times 10^{-3} \text{ eV/K}$$

$$\nu = 1.2 \times 10^{8} s^{-1}.$$

The lines of maximum and minimum gradient yield

$$5.6 \times 10^{6} s^{-1} < \nu < 3.7 \times 10^{9} s^{-1}.$$

Table 9.1.1

Kinetic Analysis: Second Step

T/°C	187	211	239	253
$\mathcal{E}$(T)/eV	0.418	0.403	0.348	0.323

Figure 9.1.2: $Pd_{82}Si_{18}$: kinetic analysis (third step)

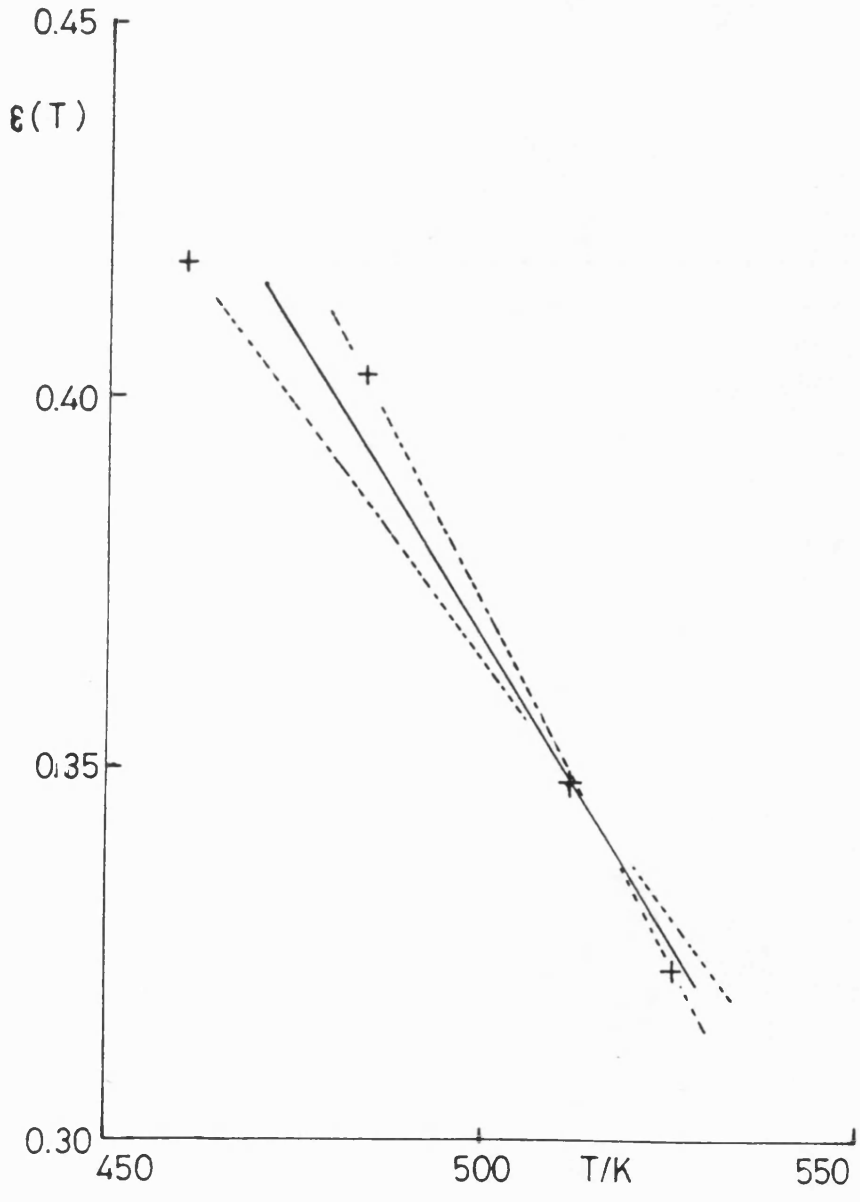

Thus the maximum value of n is three or four orders of magnitude less than a typical Debye frequency. Since

$$\nu = \frac{\sigma^*}{\sigma_0} \nu_0$$

where ν_0 is the TLS attempt frequency (Debye frequency in the case of a single atom jumping) according to equation (7.3.9), this low value of ν implies either that the ratio of the widths, as defined in section 7.3, of the saddle and the minimum of the TLS is of order 10^{-3} or that the attempt frequency is much lower than a typical Debye frequency. It is hard to imagine a configuration of atoms in which the width of the window through which the activated complex must pass is orders of magnitude less than the width of the potential well representing the initial state; the result suggests that ν_0 is indeed much smaller than a typical Debye frequency.

Using the best value, $1.2 \times 10^8 s^{-1}$, of ν, we can plot all five sets of data on a single graph of $\Delta R/R_0$ vs. $kT_A \ln\nu(t-t_0)$ (figure 9.1.3). The method used to obtain ν guarantees that the five curves will coincide at at least one point - the point with the value of $\Delta R/R_0$ used to extract the values of $\varepsilon(T)$ from figure 9.1.2. In fact the curves, of which only the portions obtained with T within 1K of the set temperature are shown in figure

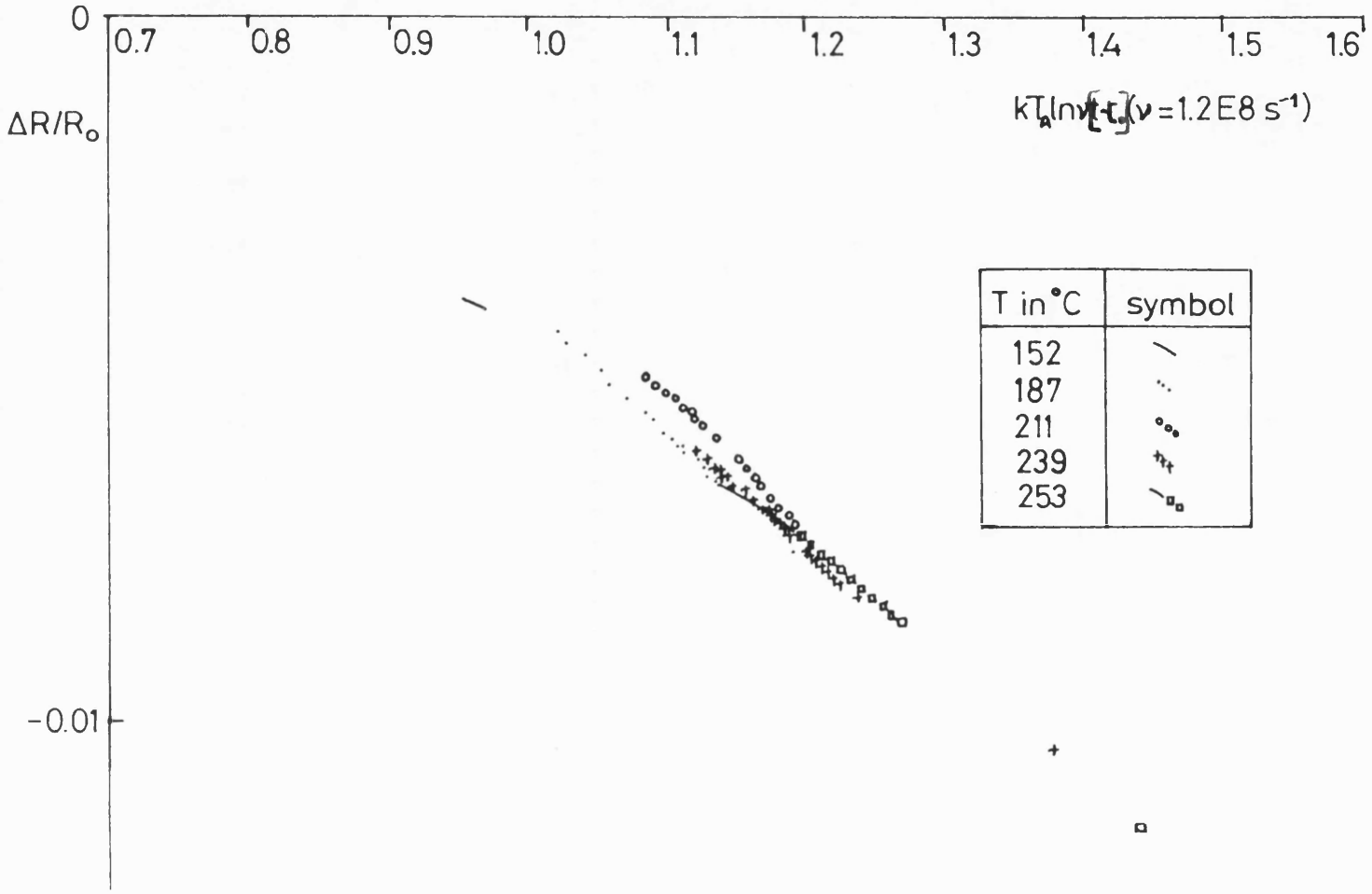

Figure 9.1.3: $Pd_{82}Si_{18}$: kinetic analysis (fourth step)

9.1.3, lie remarkably well on a single straight line. Because of the wide range of anneal temperatures used in these experiments, the straight line extends over about 0.4 eV.

Turning now to the interpretation of the results, we apply equation (8.5.1), writing $\Delta R/R_0$ for Δp and find that a trial form

$$h(E_1) = A \qquad (E_1 \geq 1eV)$$

where A is a constant, yields in the step function approximation to $\theta(E_1,T,t)$,

$$\frac{\Delta R}{R_0} = \int_0^{1eV} dE_1 \; kT_A \ln\nu(t-t_0)h(E_1) + A[kT_A\ln\nu(t-t_0) - 1eV]$$

$$= AkT_A\ln\nu(t-t_0) + B \qquad \text{---------- (9.1.1)}$$

where B is a constant. Equation 9.1.1 describes the coincident straight lines of figure 9.1.3 well, and allows us to extract from figure 9.1.3 a value for A, the height of the function $h(E_1)$. This value is

$$h(E_1) = -1.8 \times 10^{-2}\ eV^{-1} \qquad (1eV \leq E_1 \leq 1.4eV).$$

The interpretation of $h(E_1)$ is now straightforward. Since reversibility is a small effect in $Pd_{82}Si_{18}$

(section 3.4), we apply equation (8.5.4), to find that

$$\int_0^\infty \overline{c(E_1,\Delta E)}\, q(E_1,\Delta E)\, d\Delta E = 1.8 \times 10^{-2} eV^{-1} \quad (1eV \leq E_1 \leq 1.4eV).$$

The irreversible structural relaxation of $Pd_{82}Si_{18}$ is an example of log-time kinetics and is well described by a constant number density of TLSs in E_1 over the range 1eV to 1.4eV.

Gaussian Spectra

The trial form $h(E_1)$ = constant is successful when Δp is a linear function of log-time. A gaussian form for $h(E_1)$ can be used to simulate non-log-time kinetics, as discussed in section 7.4. Equation (8.5.1) then needs to be evaluated numerically; this was done using a computer simulation program for a series of gaussians $h(E_1)$ centred at 1.9eV and with various widths. The results are shown in figure 9.1.4, a graph of Δp vs. $\log_{10}\nu t$.

The full analytic form for $\theta_0(E_1,T,t)$ was used in these simulations. The full width at half height (FWHH) of the gaussian used is indicated, in eV, next to each curve. Integration was from 0 to 5eV in steps of 0.001eV. It was shown that the step size was sufficiently small, and the upper limit sufficiently large, to avoid significant computational errors.

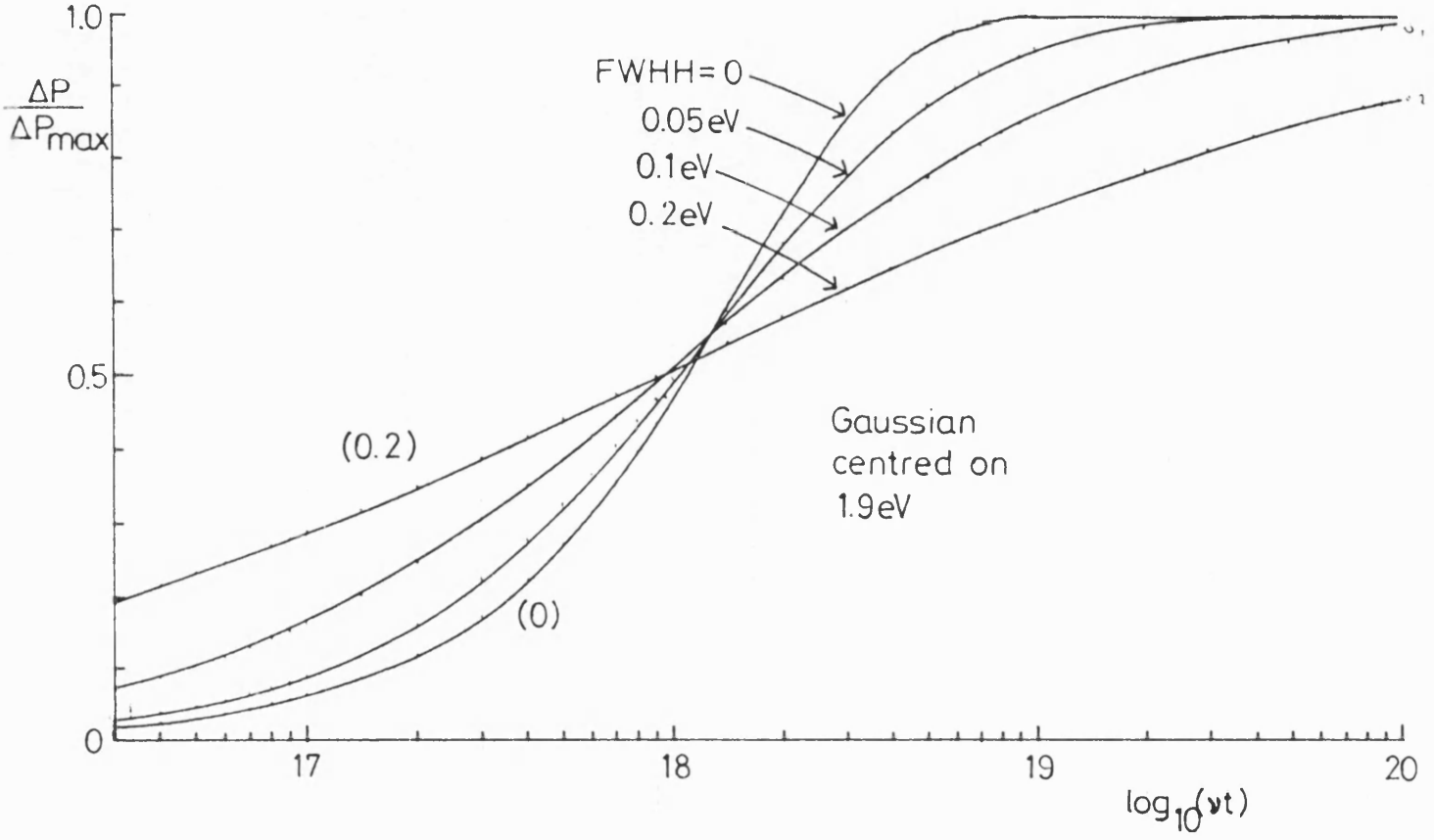

Figure 9.1.4: numerical simulations;

$p(\nu,t) = \int_0^\infty q(E)\theta(E,T,t)dE$, T = 526K. Numbers indicate width of gaussian q(E) in eV

A broad gaussian, with a large FWHH of 0.2eV, produces a curve $\Delta p(\log_{10}\nu t)$ which is very nearly linear over the range $16 < \log_{10}\nu t < 20$. As FWHH decreases, the curve becomes more sigmoidal in form, acquiring an easily identifiable point of inflection. In the limit of zero FWHH (a delta function) Δp is highly non-linear in log-time.

With a view to fitting experimental curves $\Delta p(\log t)$ to gaussian functions $h(E_1)$, the interquartile range of each curve in figure 9.1.4 is recorded, together with the FWHH of the corresponding gaussian, in table 9.1.2. The pairs of values are plotted in figure 9.1.5; an experimental curve $\Delta p(\log t)$ with a prominent point of inflection can be fitted to the gaussian function $h(E_1)$ with FWHH obtained by interpolation in figure 9.1.5.

For example, the data of Cost and Stanley (1982) on reversible isothermal resistance change in $Fe_{40}Ni_{40}P_{14}B_6$ has an interquartile range (when plotted as a function of $\log_{10}$time) of 3.0 (figure 9.1.6). According to figure 9.1.5, a gaussian trial form for $h(E_1)$ will be optimised in its fit to the data if it has a FWHH of 0.10eV.

The interpretation of $h(E_1)$ in the case of a reversible change is, according to tbe analysis of section 8.5,

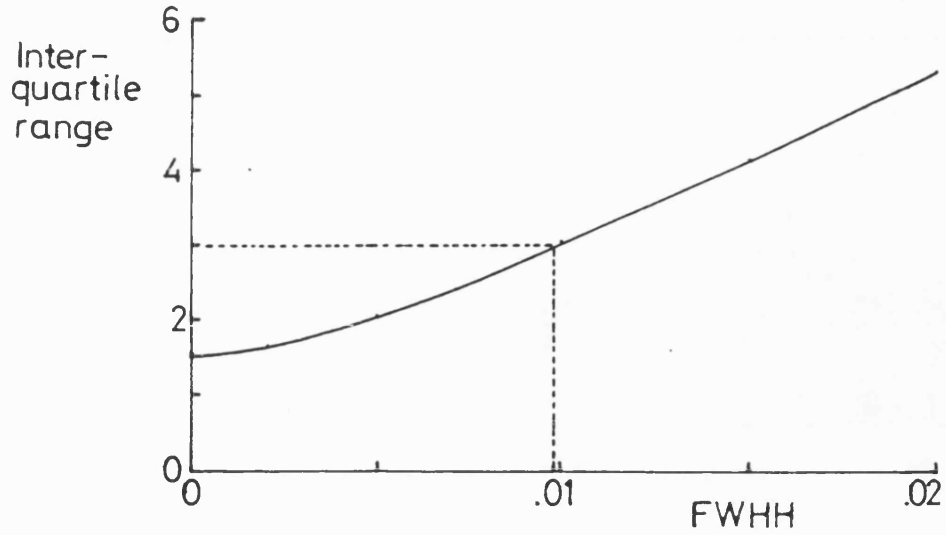

Figure 9.1.5: fitting gaussian spectra

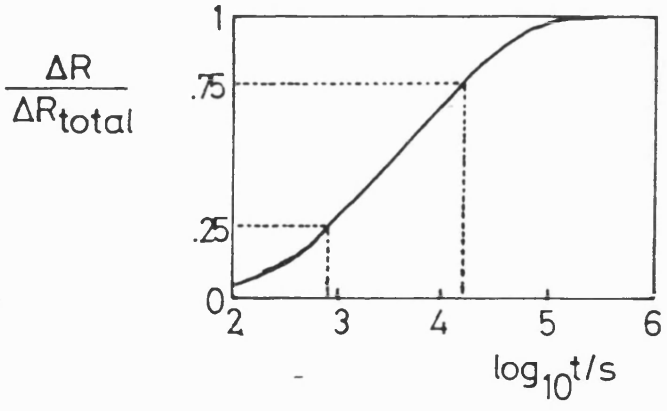

Figure 9.1.6: reversible isothermal resistance change in $Fe_{40}Ni_{40}P_{14}B_6$ (Cost and Stanley 1982)

Table 9.1.2

Fitting Gaussian Spectra

Gaussian FWHH/eV	Δp ($\log_{10}$ vt) interquartile range
0	1.54
0.02	1.65
0.05	2.07
0.1	3.04
0.15	4.13
0.2	5.31

$$h(E_1) \approx k(T_0 - T_A)\ [\overline{c(E_1,\Delta E)q(E_1,\Delta E)}]_{\Delta E \approx kT}$$

when T_0 is the temperature of the long preanneal.

9.2 Long-term Temperature Dependence

Reversible isothermal resistance changes in the $Pd_{82-x}V_xSi_{18}$ glasses are very small (section 3.4), and the resolution obtained was not sufficient to allow quantitative kinetic analysis. However, we can still obtain some information from the observed values of the temperature dependence of long term property value, $P_\infty(T)$, which is given in the case of resistance measurements by

$$\frac{dp_\infty(T)}{dT} = \frac{1}{R}\frac{d\Delta R}{d\Delta T_A}$$

Because the reversible effect is small, the functional dependence of p_∞ on T was not determined. The methods of section 8.4, therefore, cannot be applied; instead we can obtain an estimate, using equation (8.3.8), of g_0, the limiting value of the function $g_\infty(\Delta E)$ as ΔE becomes small. The function $g_\infty(\Delta E)$ (equation 8.3.3) is the total number density in ΔE, weighted by a coupling function, of those TLSs which are able, kinetically, to contribute to structural relaxation during a very long anneal. If we

knew the form of $p_\infty(T)$ in detail, we could predict how $g_\infty(\Delta E)$ varies with increasing ΔE, using the methods of section 8.4; in the present case, with only the gradient of $p_\infty(T)$ to work with, we can obtain only its limiting value as $\Delta E \rightarrow 0$.

Using equation (8.3.8),

$$p_\infty(T) = g_0 T \ (9.572 \times 10^{-24} J/K) + \text{constant}$$

and the values of $(1/R)d\Delta R/d\Delta T_A$ summarised in table 3.4.2, we obtain the values of g_0 given in table 9.2.1. In each case, g_0 is a negative quantity of order 0.1eV.

In summary, we have determined two integrals of the function $\overline{c(E_1,\Delta E)}q(E_1,\Delta E)$ in $Pd_{82}Si_{18}$. This is a weighted number density function, defined such that, if all the TLSs with barrier weights in the narrow range (E_1,E_1+dE_1) and with splitting energies in the narrow range $(\Delta E,\Delta E+d\Delta E)$ were to change state, the corresponding relative resistance change, measured at about 253°C, would be $\overline{c(E_1,\Delta E)}q(E_1,\Delta E)dE_1 d\Delta E$. The two integrals obtained are

Table 9.2.1

Limiting Values g_0 of the Function $g_\infty(\Delta E)$ for $Pd_{82-x}V_xSi_{18}$

Composition	$Pd_{82}Si_{18}$	$Pd_{81}V_1Si_{18}$	$Pd_{80}V_2Si_{18}$
$(1/R)d\Delta R/d\Delta T_A/10^{-6}K^{-1}$	-10	-5	-8
$g_0/10^{18}J^{-1}$	-1.0	-0.5	-0.8
g_0/eV^{-1}	-0.17	-0.08	-0.13

$$\int_0^{\infty} \overline{c(E_1,\Delta E)}\, q(E_1,\Delta E)\, d\Delta E = 0.018\text{eV}^{-1} \quad (1\text{eV} \leq E_1 \leq 1.4\text{eV})$$

$$\int_0^{E_{MAX}} \overline{c(E_1,\Delta E)}\, q(E_1,\Delta E)\, dE_1 = -0.17\text{eV}^{-1} \quad (0 < \Delta E \leq 5kT)$$

where E_{MAX} is the highest value of E_1 kinetically accessible, of order 2eV.

The substitution of vanadium for palladium decreased the magnitude of the value of the latter integral, but no trend with vanadium concentration was identified.

These two estimates would be rather difficult to show on a single graph and the information they provide about $\overline{c(E_1,\Delta E)}\, q(E_1,\Delta E)$ is very far from complete, but from this information alone we can identify the difference in sign, noted in the last paragraph of chapter 3, between the effect of reversible and irreversible ordering on high-temperature electrical resistance in $Pd_{82}Si_{18}$. (The lower estimate tells us that the reversible processes, those represented by TLSs with ΔE of order kT, increase the resistance when they change from state 1 to state 2. The higher estimate tells us that the combined effect of such a change of state in the TLSs with any value of E_1 in the range 1 to 1.4eV is to decrease the resistance; most of these processes are irreversible.)

The incompleteness of the information obtained about $\overline{c(E_1,\Delta E)}\, q(E_1,\Delta E)$ is largely a result of the lack of a kinetic analysis of the very small reversible effect in

$Pd_{82}Si_{18}$. A similar study of a metallic glass showing a larger reversible effect, and therefore more suitable for kinetic analysis, would produce a more complete set of integrals of the weighted number density function; it is suggested that such a study would be a good way to further the work on AES analysis developed and applied in chapter 8 and in this chapter.

10. SUMMARY OF FINDINGS

Chapter 10 Summary of Findings

Two themes of this work were indentified in the introduction to this thesis: the relation of structural changes to changes in electrical resistance and the microscopic mechanisms underlying structural relaxation. Progress in these two areas is summarised below.

10.1 The Link between Structural Change and Resistance Change

Resistance changes measured during structural relaxation cannot readily be transformed to resistivity changes because the accompanying changes in dimension are anisotropic and poorly understood. The difference is significant, however, according to a comparison of resistometric and dilatometric studies of relaxation in a single metallic glass. No direct measurements of changes in resistivity during relaxation have been made.

Resistometric studies of structural relaxation show that low temperature (4.2K) and high temperature resistance are different physical properties, in that identical annealing treatments may affect them in opposite senses. R(T) is best considered as a function which itself depends on structural order.

The many theoretical approaches to conduction in amorphous metallic solids and liquids are of little use in linking resistance changes to specific structural changes, either because structural parameters do not yet

figure in usable formulations of the theories or (in the case of Ziman's nearly free electron model) because too much of the content of the theory is lost in the approximations introduced on the way to obtaining verifiable predictions.

We are therefore obliged to make use of empirical generalisations. The experiments on the PdVSi glasses showed that there is a correspondence between irreversible structural relaxation and the effects, primarily densification, of hydrostatic pressure. Densification is an important component of irreversible structural relaxation in the PdVSi group, but not in all metallic glasses, as a literature survey has shown.

Irreversible structural relaxation reduces the sensitivity of the resistance of $Pd_{82}Si_{18}$ to hydrostatic pressure significantly; this effect has not been properly understood.

10.2 Microscopic Modelling of Structural Relaxation

Kinetic analysis has been applied to the results of many experiments involving reversible and irreversible structural relaxation. An illustration of the utility of analysing the rates of property changes is provided by a simple qualitative example which sheds some further light on one of the findings listed above. Cost and Stanley (1982) and Balanzat (1981) subjected $Fe_{40}Ni_{40}P_{14}B_6$ to thermal cycling treatments in the same temperature range.

Cost and Stanley measured the high-temperature resistance and found a repeatedly reversible change with a time constant of order 10^4s. Balanzat measured the resistance at 4.2K and found a reversible change which was not only in the opposite direction to that found by Cost and Stanley (as pointed out in section 10.1) but which was also characterised by a much smaller time constant, of less than 600s. The structural parameters linked to reversible changes in low-temperature and high-temperature resistance seem to be distinct. Thus kinetic considerations provide an extra way of distinguishing one relaxation process from another.

The AES model of structural relaxation has been extended in two directions. The first development is the application of Eyring's theory of absolute reaction rates to the two level system model. This has resulted in a new expression for the apparent attempt frequency in the AES model which is the product of the real attempt frequency and a dimensionless factor determined by the relative stiffness of vibrational modes of the activated complex and corresponding vibrational modes of the TLS in its initial state.

The second development involved a reworking of the mathematics of the AES model. In its original form, the TLS occupancy equation on which the model is based specifically prohibited the reversal of structural ordering; the probability that a TLS in state 2 (lower energy) might return to state 1 (higher energy) had been set to zero by Gibbs et al. (1983). As a result, kinetic

analysis of reversible effects were meaningless within the terms of the original model.

Removing this restriction and allowing back-flux from state 2 to state 1 has extended the scope of the AES model such that it can provide a unified description of reversible and irreversible effects. Reversible processes are represented by TLSs with splitting energy ΔE of order kT.

In its present, extended form, the AES model can be used to analyse the long-term temperature dependence of structural state and the kinetics of reversible and irreversible relaxation in terms of a single distribution function.

Techniques for applying the AES model to experimental data have been developed where necessary, most importantly by establishing a systematic and computationally inexpensive method of calculating, for a given real thermal treatment, t_0, the time at which a truly isothermal anneal having the same effects in the long term as the real anneal would have begun. This is necessary because the AES model is applied most readily to isothermal anneals.

An experimental test of the self-consistency of the AES model in describing irreversible changes in a property which shows little or no reversible behaviour has been devised and it has been shown, using experimental results

on $Pd_{82}Si_{18}$, that, for this metallic glass at least, the model is indeed self-consistent.

Appendix 1 Specifications

The specifications, details and manufacturers of the electrical equipment referred to in this thesis are as follows.

1 Current calibrator (constant current source)

manufacturer: Time Electronics Ltd.
Botany Industrial Estate
Tunbridge, Kent
(0732) 355993

model: 609 direct current calibrator

output stability limits

with temperature: 30ppm/K

with time at constant temperature: 10ppm/hour
75ppm over 6 months

2 Nulling Microvoltmeter

manufacturer: Keighley Instruments Ltd.
1, Boulton Road
Reading, Berks. RG2 0NL
(0734) 861287

model: 155 null detector microvoltmeter

accuracy: 1% full scale, i.e. 10μV

zero drft: less than 0.5μV over 24 hours (long term drift non cumulative) typically less than 0.1μV/K temperature dependence

input resistance: 1MΩ

3 Vernier Potentiometer

manufactured by the Cambridge Instrument Co. Ltd.

resolution: 1μV

resistance seen by battery: 100Ω

4 Battery

manufacturer: Chloride Power Storage
PO Box 5
Clifton Junction
Swinton
Manchester M27 2LR
061-794-4611

type of cell: FAP 17 HBF

nominal voltage: 2V

capacity: 64 ampere hours

discharge rate: 150μV/hour at 130 mA (this is the lowest discharge rate for which Chloride provide information)

5 Standard Resistors

supplier: R.S. Components Ltd.

stock number: 158-058

temperature coefficient of resistance: 0±3ppm/K

thermal e.m.f. 0.2μV/K

6 Relays

supplier: R.S. Components Ltd.

stock numbers: 348-627 (4 pole, 2 throw)

348-661 (2 pole, 2 throw)

7 Analogue to Digital Converter

manufacturer: C.I.L. Electronics

model: PCI 6380

stability with respect to temperature fluctuations:

0.01%/K

long term stability: 0.01%/month

resolution (limited by random digital noise): 15 bits,

equivalent to .05%.

Appendix 2: Anharmonicity and Compression

The manner in which anharmonicity contributes to p.c.r. can be illustrated by a simple argument. A harmonic potential well can be represented by the equation

$$V = a(x - x_0)^2$$

where x is the interionic separation, x_0 is its mean value, and V is the contribution of the pair of ions under consideration to the potential energy of the solid. The application of hydrostatic pressure to the solid can be represented by a force, F, causing a decrease δ in the mean interionic separation:

$$V' = a(x - x_0)^2 + F(x - x_0)$$

$$= a(x - (x_0 - \delta)^2) - \delta^2$$

where $\delta = F/2a$. The coefficient a of the quadratic term is unchanged, although the mean separation is reduced by δ. In a perfectly harmonic solid, the compressibility would be determined by the coefficient a of the harmonic term in the expression for V(x). This coefficient a, and therefore the mean square amplitude of small thermal vibrations of the ions about their mean positions, would be unchanged in a perfectly harmonic solid undergoing isothermal compression.

Anharmonicity is the presence of an additional, non-zero term in $(x - x_0)^3$ in the zero-pressure potential:

$$V = a(x - x_0)^2 + b\ (x - x_0)^3.$$

Again, we represent the effect of pressure by adding a term $F(x - x_0)$ to the above expression for V:

$$V' = a(x - x_0)^2 + b\ (x - x_0)^3 + F(x - x_0)$$

The compressed potential V′ has a minimum point at the value of x given by

$$dV'/dx = 0$$

$$(x - x_0)^2 + (2a/3b)(x - x_0) + F/3b = 0$$

which has a root $x = x_0 - F/2a$, provided that the anharmonic coefficient b is small compared with $a^2/3F$. Writing $x_0' = x_0 - F/2a$, we find that V′ can be re-expressed:

$$V' = a\left(1 - \frac{3bF}{2a^2}\right)(x - x_0')^2 + b(x - x_0')^3 + 0(x) + \text{const.}$$

The anharmonic coefficient in this expansion about the new minimum point is unchanged, but the harmonic coefficient a is decreased by a factor $3bF/2a^2$, provided that b is small compared with $a^2/3F$. Generalising this

argument to three dimensions, we can predict that the restoring force on an ion in a slightly anharmonic potential well will decrease linearly with applied pressure, to a first order approximation, at a rate proportional to the anharmonicity.

A metal in which the interatomic potential wells are slightly anharmonic will therefore exhibit pressure dependence of that component of the room temperature resistance which is due to thermal disruption of the ions from their mean positions.

Appendix 3

Consider the integral

$$A = \int_0^\infty [1 + e^{\Delta E/kT})^{-1} - (1 + e^{\Delta E/kT_0})^{-1}] d\Delta E \quad \text{----------} \quad (A3.0)$$

Let $y = \Delta E/kT$. Then

$$A = kT \int_0^\infty [(1 + e^{y})^{-1} - (1 + e^{\alpha y})^{-1}] dy \quad \text{----------} \quad (A3.1)$$

where $\alpha = T/T_0$, a constant close to 1.

Invoking the identity

$$\frac{d}{dy} \ln \frac{e^y}{1 + e^y} \equiv \frac{1}{1 + e^y}$$

we can integrate (A3.1) to give

$$A(x,T,\alpha) = kT\left[\ln \frac{e^x}{1 + e^x} - \frac{1}{\alpha} \ln \frac{e^{\alpha x}}{1 + e^{\alpha x}}\right] - kT \ln 2 \left(\frac{1}{\alpha} - 1\right) \quad (A3.2)$$

which is equation (8.3.5)

Equation (A3.2) can be further simplified to

$$A(x,T,\alpha) = kT\left[\ln \frac{(1 + e^{\alpha x})^{1/\alpha}}{1 + e^x} - \ln 2 \left(\frac{1}{\alpha} - 1\right)\right]$$

We wish next to calculate $x_0(\alpha, f)$ such that

$$A(x_0,T,\alpha) = f \lim_{x\to\infty} A(x,T,\alpha) \quad \text{---------- (A3.3)}$$

where f is a constant lying in the range $0<f<1$. Since

$$\lim_{x\to\infty} A(x,T,\alpha) = -kT\ln 2 \left(\frac{1}{\alpha} - 1\right)$$

an equation for x_0 is

$$kT\left[\ln\frac{(1 + e^{\alpha x_0})^{1/\alpha}}{1 + e^{x_0}} - (1/\alpha - 1)\ln 2\right] = -fkT(1/\alpha - 1)\ln 2$$

i.e.

$$\frac{(1 + e^{\alpha x_0})^{1/\alpha}}{1 + e^{x_0}} = \exp\left[(1 - f)(1/\alpha - 1)\ln 2\right] \quad \text{--------- (A3.4)}$$

We introduce here the notation

$$g(x_0) \equiv (1 + e^{\alpha x_0})^{1/\alpha} \;/\; (1 + e^{x_0})$$

Figure A3.1 shows g(x) for various values of α. The dashed lines are drawn through the points at which each curve reaches the value

$$\exp[(1 - f)(1/\alpha - 1)\ln 2]$$

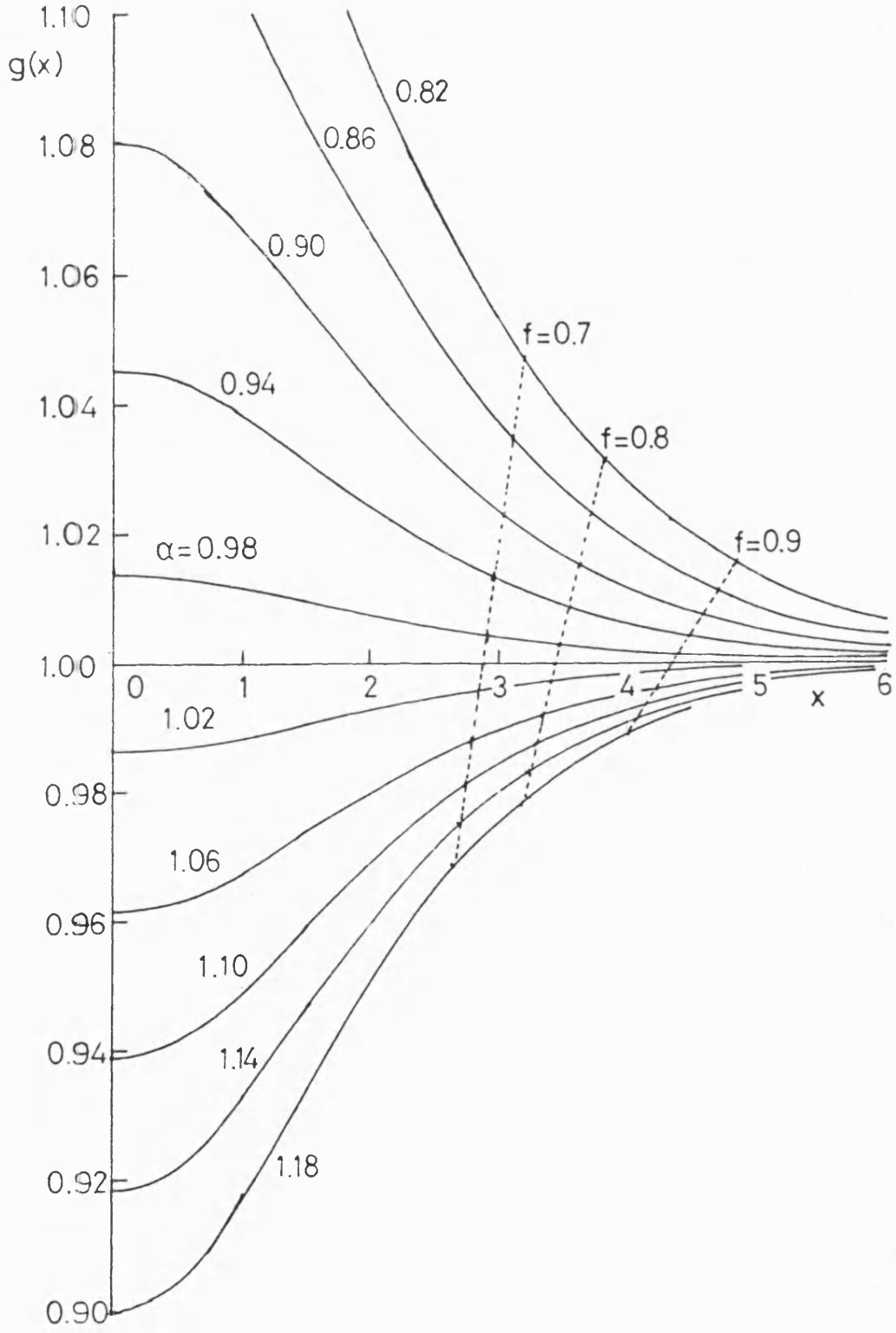

Figure A3.1: g(x)

Each corresponds to a single value of f. The dashed lines therefore represent solutions of equation (A3.4) for a range of values of α and f. Figure A3.1 was used to obtain graphical estimates of the set of roots $x_0(\alpha,f)$ of equation (A3.3) by projecting the intersections of the solid lines and the dashed lines onto the horizontal axis. Table A3.1 shows the results of this procedure for each pair of values (α,f).

The roots obtained by this method are rough estimates, but they are good enough to be used as the starting points for Newton-Raphson numerical solutions of equation (A3.3).

The principle of the Newton-Raphson method is well known. Given an estimate x_n of x, an improved estimate is

$$x_{n+1} = x_n + \frac{\exp[1/\alpha - 1)(1 - f)\ln 2] - g(x_n)}{g'(x_n)}$$

where $g'(x)$ is g differentiated with respect to x. For convergence, both the root and the initial guess need to be well away from any stationary points or points of inflection of g(x). Inspection of figure A3.1 reveals that the root is usually close to a point of inflection; the method will therefore not converge unless the first guess is a good one. This is why graphical estimates were needed as starting points.

Table A3.1 Graphical solutions of the equation

$$g(x) = \exp\left[(1/\alpha - 1)(1-f)\ln 2\right]$$

for a range of values of α and f.
g(0) calculated using $g(0) = 2^{(1/\alpha)} / 2 = \exp\left[(1/\alpha - 1)\ln 2\right]$

α	g(0)	f=0.9		f=0.8		f=0.7	
		$g(x_o)$	x_o	$g(x_o)$	x_o	$g(x_o)$	x_o
0.82	1.1643	1.0143	4.85	1.0309	3.85	1.0467	3.20
0.86	1.1195	1.0113	4.65	1.0228	3.75	1.0344	3.10
0.90	1.0801	1.0077	4.50	1.0155	3.60	1.0234	3.00
0.94	1.0452	1.0044	4.35	1.0089	3.50	1.0134	2.95
0.98	1.0142	1.0014	4.2	1.0028	3.50	1.0043	2.85
1.02	0.9865	0.9986	4.20	0.9973	3.50	0.9959	2.90
1.06	0.9615	0.9961	4.25	0.9922	3.40	0.9883	2.85
1.10	0.9389	0.9937	4.15	0.9875	3.30	0.9813	2.75
1.14	0.9184	0.9915	4.10	0.9831	3.25	0.9748	2.70
1.18	0.8997	0.9895	4.05	0.9791	3.25	0.9688	2.65

A simple fortran program was used to implement the Newton-Raphson method. The results, set out in table A3.2, show that rapid convergence was obtained in all cases. P.T. Squire (private communication) has pointed out that inverse tabulation offers a faster route to these answers. Equation (A3.3) can be rearranged

$$f = 1 - \ln\left[\frac{(1 + e^{\alpha x_0})^{1/\alpha}}{1 + e^{x_0}}\right] \Big/ \left[(1/\alpha - 1)\ln 2\right]$$

from which f can be plotted as a function of x_0 for arbitrary values of α. The curves obtained can alternatively be regarded as graphs of x_0 as a function of f; $x_0(\alpha, f)$ can therefore be obtained graphically or by linear interpolation from a family of such curves, to any desired degree of accuracy.

There is a case in which equation (A3.3) breaks down; this is when $\alpha = 1$. The area A(x) under the graph of figure 8.3 shrinks to zero for all x, even as $x \to \infty$, when $\alpha = 1$. However the ratio of the finite integral A(x) to the infinite integral $A(\infty)$ has a finite limit as α approaches 1 from above or below. This is represented by the continuity of the dashed lines in figure A3.1 as they cross the line $g(x) = 1$, which is also the locus of $\alpha = 1$.

Table A3.2 Results of Newton - Raphson method

alpha	f	guess 1	guess 2	...	
0.82	0.7	2.90000	3.17216	3.19186	3.19196
0.82	0.8	3.40000	3.77109	3.81632	3.81694
0.82	0.9	4.30000	4.73754	4.81366	4.81568
0.86	0.7	2.90000	3.10049	3.11125	3.11128
0.86	0.8	3.40000	3.69075	3.71855	3.71879
0.86	0.9	4.30000	4.64178	4.68790	4.68866
0.90	0.7	2.90000	3.03280	3.03756	
0.90	0.8	3.40000	3.61434	3.62946	3.62953
0.90	0.9	4.30000	4.54940	4.57371	4.57392
0.94	0.7	2.90000	2.96864	2.96991	
0.94	0.8	3.40000	3.54142	3.54799	3.54800
0.94	0.9	4.30000	4.45993	4.46980	4.46983
0.98	0.7	2.90000	2.90759	2.90760	
0.98	0.8	3.40000	3.47156	3.47323	
0.98	0.9	4.30000	4.37299	4.37503	
1.02	0.7	2.90000	2.84932	2.85002	
1.02	0.8	3.40000	3.40445		
1.02	0.9	4.30000	4.28833	4.28839	
1.06	0.7	2.90000	2.79352	2.79662	
1.06	0.8	3.40000	3.33977	3.34094	
1.06	0.9	4.30000	4.20565	4.20890	
1.10	0.7	2.90000	2.73995	2.74697	2.74698
1.10	0.8	3.40000	3.27729	3.28214	
1.10	0.9	4.30000	4.12480	4.13576	4.13580
1.14	0.7	2.90000	2.68839	2.70066	2.70070
1.14	0.8	3.40000	3.21681	3.22751	3.22755
1.14	0.9	4.30000	4.04563	4.06816	4.06836
1.18	0.7	2.90000	2.63864	2.65735	2.65745
1.18	0.8	3.40000	3.15815	3.17662	3.17674
1.18	0.9	4.30000	3.96805	4.00543	4.00600

The roots $x_0(\alpha, f)$ are therefore physically meaningful in the limit $\alpha \to 1$, and they can be evaluated by setting

$$\alpha = 1 - \delta$$

in the expression A3.0 for A(x) and letting δ become small. We again use y as a dummy variable to avoid confusion between x and x_0,

$$A = \int_0^x \left[\frac{1}{1 + e^y} - \frac{1}{1 + e^y e^{-\delta y}} \right] dy$$

$$= \int_0^x \frac{e^y (e^{-\delta y} - 1)}{(1 + e^y)(1 + e^y e^{-\delta y})}$$

Now let $\delta \to 0$ and retain only terms in order 1 or less in δ

$$A(x) \to -\delta \int_0^x \frac{y e^{-y} dy}{(1 + e^y)^2}$$

Equation A3.3 for x_0 now becomes independent of δ:

$$\int_0^{x_0} \frac{y e^y}{(1 + e^y)^2} \, dy = f \int_0^{\infty} \frac{y e^y dy}{(1 + e^y)^2} \qquad \text{(A3.5)}$$

Integrate by parts:

$$\int_0^{x_0} \frac{y e^y}{(1 + e^y)^2} = \left[\frac{y e^y}{1 + e^y} \right]_0^{x_0} - \int_0^{x_0} \frac{e^y}{1 + e^y} \, dy$$

$$= \frac{x_0 e^{x_0}}{1 + e^{x_0}} - \ln \frac{1 + e^{x_0}}{2}$$

Equation (A3.5) now becomes

$$\frac{x_0 e^{x_0}}{1 + e^{x_0}} - \ln \frac{1 + e^{x_0}}{2} = f\left[\lim_{x_0 \to \infty} \{x_0 - \ln e^{x_0} + \ln 2\}\right]$$

$$= f \ln 2$$

$$x_0 = (1 + e^{-x_0})[\ln(1 + e^{x_0}) - (1 - f)\ln 2] \text{ --------- (A3.6)}$$

Equation (A3.6) is in a convenient form for solution by binary chopping, that is, guessing a value for x_0 and using the right hand side of (A3.6) to generate the next estimate, and so on until convergence is achieved. A fortran program was used to solve (A3.6) in this way for the values 0.7, 0.8, 0.9 of f.

In all cases, convergence was monotonic but very gradual, so it is not obvious during the iterative process how close to the root the current estimate is. In order to make sure that enough iterations had been made, the method was applied three times for each value of f, starting from widely different initial guesses in each of the three attempts. For each value of f, convergence was to the same point, to within a margin much less than the required accuracy, in all three attempts. At least one of the guesses was above the root, and at least one below, for each value of f. The output from the program makes tedious reading and is not reproduced here, but the results $x_0(\alpha = 1, f)$ are set out in table A3.3 and were

Table A3.3 Results of binary chopping procedure.

($\alpha = 1$)

f	$x_0(1,f)$
0.7	2.8783
0.8	3.4381
0.9	4.3307

used in the construction of the dashed lines in figure A3.1.

P.T. Squire (private communication) has pointed out that of the three possible algebraic arrangements of equation (A3.3) of the form $x_0 = h(x_0)$, equation (A3.3) itself is not the best choice for rapid convergence. Much quicker convergence can be obtained using the form

$$x_0 = -\ln \left[\frac{x_0}{\ln(1 + e^{x_0}) - (1 - f)\ln 2} - 1 \right]$$

The results confirm table (A3.3) at much less cost in computing time.

REFERENCES

The following abbreviations for the proceedings of conferences are used in the list of references below.

RQ4 Proceedings of the Fourth International Conference on Rapidly Quenched Metals, ed. T. Masumoto and K. Suzuki, The Japan Institute of Metals 1982

LAM5 Proceedings of the Fifth International Conference on Liquid and Amorphous Metals, ed. C.N.J. Wagner and W.L. Johnson, Journal of Non-Crystalline Solids **61&62** (1984)

RQ5 Proceedings of the Fifth International Conference on Rapidly Quenched Metals, ed. S. Steeb and H. Warlimont, North Holland Physics Publishing 1985

MSG Proceedings of the International Conference on Metallic and Semiconducting Glasses, Hyderabad, India, 1986, ed. A.K. Bhatnagar, in Key Engineering Materials **13-15** (1987)

RQ6 Proceedings of the Sixth International Conference on Rapidly Quenched Metals, Montreal 1987, to appear in Materials Science and Engineering

Abramowitz M. and Stegun I.A. (eds.) 1985 "Handbook of Mathematical Functions" U.S. Govt. Printing Office, Washington

Allia P., Andreone R., Sato Turtelli R., Vinai F. and Riontino G. 1982 J. Appl. Phys. 53, 8798

Ashcroft N.W. and Mermin N.D. 1976 "Solid State Physics" publ. Saunders College, Philadelphia

Ast D.G. and Krenitsky D.J. 1976 Scripta Metall. **10**, 247

Balanzat E. 1980 Scripta Metall. **14**, 173

Balanzat E., Halbwachs M., Hillairet J., Mairy C., Guyot P. and Simon J.P. 1983 Acta Metall. 31, 883

Balanzat E. and Hillairet J. 1981 J Phys. F **11**, 1977

Balanzat E., Stanley J.T., Mairy C. and Hillairet J. 1985 Acta Metall. 33, 785

Barnard R.D. 1972 "Thermoelectricity in Metals and Alloys" Taylor and Francis, London

Bradley C.C., Faber T.E., Wilson E.G. and Ziman J.M. 1962 Phil. Mag. 7, 865

Brady G.S. 1963 "Materials Handbook" McGraw, London

Bridgman P.W. 1958 "The Physics of High Pressure" G. Bell, London

Bothe K. and Neuhauser H. 1982 Scripta Metall. **16**, 1053

Cahn R.W., Pratten N.A., Scott M.G., Sinning H.-R. and Leonardsson L. 1984 Materials Society Research Symp. vol. 28, Rapidly Solidified Metastable Materials ed. B.H. Kear and B.C. Giessen, Elsevier, Amsterdam, 241

Chason E., Kelton K.F., Pershan P.S., Sorenson L., Spaepen F. and Weiss A.H. 1985 RQ5, 683

Chou C.P., Davis L.A. and Hasegawa R. 1979 J. Appl. Phys. **50**, 3334

Chen H., Croxon A.A.M. and Greig D. 1986 J. Non-Crystalline Solids **86**, 94

Cochrane R.W., Strom-Olsen J.O., Rebouillat J.P. and Blanchard A. 1980 Solid State Comm. **35**, 199

Cochrane R.W., Destry J., Brebner J.L., Baibich M.N. and Muir W.B. 1981 Physica **107B**, 131

Cohen M.H. and Turnbull D. 1959 J. Chem. Phys. **31**, 1164

Cost J.R. and Stanley J.T. 1981 Scripta Metall. **15**, 407

Cost J.R. and Stanley J.T. 1982 RQ4, 491

Cote P.J. and Meisel L.V. 1982 Phys. Rev. B **25**, 2138

Dicke R.H. and Wittke J.P. 1960 "Introduction to Quantum Mechanics" Addison-Wesley, Reading, Massachusetts

Egami T. 1978 J. Mat. Sci. **13**, 2587

Evans R., Greenwood D.A. and Lloyd P. 1971 Phys. Letters **35A**, 57

Eyring H. 1935 J. Chem. Phys. **3**, 107

Faber T.E. 1972 "An Introduction to the Theory of Liquid Metals" Cambridge University Press

Faber T.E. and Ziman J.M. 1965 Phil. Mag. **11**, 153

Fritsch G., Dyckhoff W., Pollich W. and Luscher E. 1985 J. Phys. F **15**, 1537

Gaefvert U. 1976 Physica Srcipta **14**, 257

Gaskell P.H. 1987 MSG, 71

Gibbs M.R.J. 1985 RQ5, 643

Gibbs M.R.J., Evetts J.E. and Leake J.A. 1983 J. Mat Sci. **18**, 278

Gibbs M.R.J. and Hygate G. 1986 J. Phys. F **16**, 809

Gibbs M.R.J. and Sinning H.-R. 1985 J Mat. Sci. 20, 2517

Gibbs M.R.J., Stephens D.W. and Evetts J.E. 1984 LAM5, 925

Gudmundsson H., Rao K.V., Astrom H.V. and Chen H.S. in "Amorphous Metallic Alloys", ed. F.E. Luborsky, Butterworth, London, 1983

Halder N.C., North D.M. and Wagner C.N.J. 1969 Phys. Rev. **177**, 47

Hernando A., Nielsen O.V. and Madurga V. 1985 J. Mat. Sci. **20**, 2093

Hillairet J., Balanzat E., Derradji N.E. and Chamberod A. 1984 LAM5, 781

Huizer E. 1987 PhD. thesis, Delft Technical University

Huizer E., Mulder A.L. and van den Beukel A. 1985 RQ5, 639

Inque A., Matsuzaki K., Toyota N., Chen H.S., Masumoto T. and Fukase T. 1985 J. Mat. Sci. **20**, 2323

Kelton K.F. and Spaepen F. 1982 RQ4, 527

Kelton K.F. and Spaepen F. 1984 Phys. Rev. B 30, 5516

Keupers A., De Schepper L., Knuyt G. and Stals L.M. 1985 J. Non.-Crys. Sol. **72**, 267

Kokmeijer E., Huizer E., Thijjse B.J. and van den Beukel A. 1988, to appear in RQ6

Komatsu T. and Matusita K. 1986 J. Mat. Sci. **21**, 1693

Komatsu T., Matusita K. and Yokota R. 1985 J. Mat. Sci. **20**, 3271

Komatsu T., Sato S. and Matusita K. 1986 Acta Metall. 34, 1899

Komatsu T., Yokota R., Shindo T. and Matusita K. 1984 J. Non.-Crys. Sol. **65**, 63

Kronmuller H. 1983 phys. stat. sol. b **118**, 661

Lazarus D. 1979 Solid State Comm. 32, 175

Leake J.A. 1987 MSG, 151

Leake J.A. to be published in Proc. Symp. Magnetic Properties of Amorphous Materials, Benalmádena, Spain, 1987 (North-Holland)

Leake J.A., Woldt E. and Evetts J.E. 1988 to appear in RQ6

Leonardsson L. PhD. thesis, Chalmers University of Technology, Goteborg, Sweden, 1984

Lin C.-H., Bevk J. and Turnbull D. 1979 Solid State Comm. 29, 641

Majewska-Glabus I. and Thijjse B.J. 1985 RQ5, 635

Marcus M.A. 1979 Acta Metall. **27**, 879

Marton L. (ed.) 1973 "Methods of Experimental Physics" vol. 6B "Solid State Physics" Academic Press, New York

Masumoto T. and Maddin R. 1971 Acta Metall. **19**, 725

McNeil L.E. 1983 PhD. thesis, University of Illinois

Mizutani U. 1983 Progress in Mat. Sci. **28**, 97

Mogro-Campero A. and Walter J.L. 1980 J. de Phys. Colloque C8 **41**, 497

Mooij J.H. 1973 phys. stat. sol. (a) **17**, 521

Morgan G.J., Howson M.A. and Paja A. 1987 MSG, 377

Mott N.F. 1972 Phil. Mag. **26**, 1249

Mott N.F. 1987 "Conduction in Crystalline Metals" Clarendon Press, Oxford

Mulder A.L., Drijver J.W. and Radelaar S. 1981 Proc. Conf. on Metallic Glasses, Science and Technology, Budapest 1980, ed. C. Hargitai et al., Kultura, Budapest, 299

Nagel S.R. 1978 Phys. Rev. Lett. **41**, 990

Naugle D.G. 1984 J. Phys. Chem. Solids **45**, 367

Omar M.A. 1975 "Elementary Solid State Physics: Principles and Applications" Addison-Wesley

Pierron-Bohnes V., Mirebeau I., Balanzat E. and Cadeville M. C. 1984 J. Phys. F **14**, 197

Primak W. 1955 Phys. Rev. **100**, 1677

Rayne J.A. and Levy R.A. 1977, Proc. 2nd Int. Symp. on Amorphous Magnetism, Troy, New York in "Amorphous Magnetism II", ed. R.A. Levy and R Hasegawa, Plenum Press, New York, 319

Riontino G., Allia P. and Vinai F. 1984 LAM5, 1365

Riontino G. and Marino F. 1984 Scripta Metall. **18**, 13

Samara G.A. and Giardini A.A. 1964 The Review of Scientific Instruments **35**, 989

Schiff L.I. 1968 "Quantum Mechanics" McGraw-Hill

Schulz R., Mehra M. and Johnson W.L. 1985 J. Phys. F **15**, 2109

Sinha A.K. 1970 Phys. Rev. B **1**, 4541

Sonius M.E., Thijjse B.J. and van den Beukel A. 1983 Scripta Metall. **17**, 545

Spaepen F. 1977 Acta Metall. **25**, 407

Squires G.L. 1985 "Practical Physics" Cambridge University Press

Taub A.I. and Spaepen F. 1980 Acta Metall. **28**, 1781

van den Beukel A. 1986 Proc. ASM Conf. on Rapidly Solidified Materials, San Diego 1986 in "Rapidly Quenched Materials", ed. P.W. Lee and S. Carbonara, ASM

van den Beukel A. and Huizer E. 1985 Scripta Metall. **19**, 1327

van den Beukel A. and Radelaar S. 1983 Acta Metall. **31**, 419

van den Beukel A., van der Zwaag S. and Mulder A.L. 1984 Acta Metall. **32**, 1902

Vassilou J.K. 1986 J. Appl. Phys. **59**, 482

Waldram J.R. 1985 "The Theory of Thermodynamics" Cambridge University Press

Wang C.-Y. 1967 The Review of Scientific Instruments **38**, 24

Waseda Y and Egami T. 1979 J. Mat. Sci. **14**, 1249

Weiss R.J. 1963 "Solid State Physics for Matallurgists" Pergamon, Oxford

Wert C. and Zener C. 1949 Phys. Rev. **76**, 1169

Woldt E. 1986 PhD. thesis, University of Cambridge

Woldt E. and Leake J.A. 1985 RQ5, 687

Yokota R., Tanaka Y., Komatsu T. and Matusita K. 1985 J. Non-Crys. Sol. **76**, 313

Zener C. 1949 Acta Cryst. 2, 163

Ziman J.M. 1961 Phil. Mag. **6**, 1013